



MONASH University

The Pathological Role of *Cell Division Autoantigen 1* (CDA1) in renal fibrosis

Pacific Huynh

Bachelor of Science (Honours)

A thesis submitted for the degree of *Doctor of Philosophy* at
Monash University in 2018
Faculty of Medicine, Nursing and Health Sciences

Copyright notice

© Pacific Huynh (2018).

I certify that I have made all reasonable efforts to secure copyright permissions for third-party content included in this thesis and have not knowingly added copyright content to my work without the owner's permission.

To my late grandmother, Diem Le (04/12/1946-23/02/2017).

Abstract

Background:

Cell Division Autoantigen 1 (CDA1) plays a role in the development of *chronic kidney disease* (CKD) by enhancing *transforming growth factor-beta* (TGF β)-mediated profibrotic processes. CDA1 deficiency resulted in the attenuation of renal fibrosis in a mouse model of diabetic nephropathy. Whether the inhibition of CDA1 activity after the onset of diabetic kidney disease, as well as in non-diabetic kidney injury, can attenuate renal fibrosis has yet to be experimentally investigated. Thus, I examined the effect of the induced genetic deletion of CDA1, at two different timepoints of disease progression, on the development of renal fibrosis in a mouse model of *streptozotocin* (STZ)-induced diabetic nephropathy. I also examined the effect of the absence of CDA1 on renal fibrosis development in two models of *acute kidney injury* (AKI); *unilateral ureteric obstruction* (UUO) and *ischaemia/reperfusion* (IR) injury.

Methods/Results:

In the diabetic nephropathy studies, genetic deletion of CDA1 was induced by tamoxifen administration to CDA1 flox /ERCre mice at 5 or 10 weeks after STZ-induced diabetes and kidneys were harvested for analysis after an additional 5 or 10 weeks, which represents early and delayed intervention against CDA1 activity, respectively. Tamoxifen administration to CDA1 flox /ERCre mice reduced CDA1 gene expression by ~70-80%, irrespective of diabetic status or duration of study. Early intervention against CDA1 activity resulted in the attenuation of renal fibrosis development in diabetic mice, as seen by the reductions in diabetes-associated profibrotic gene expression, such as fibronectin and collagen I, and collagen IV accumulation. In contrast, delayed intervention against CDA1 activity had minimal effect on diabetes-associated renal fibrosis.

In the UUO study, male CDA1 wildtype (WT) and CDA1 *knockout* (KO) mice had their left ureter ligated and kidneys were collected for analysis 5, 10 and 14 days post-UUO. In the IR study, left renal artery of CDA1 WT and CDA1 KO male mice were ligated for 45 mins before being released to restore blood flow. Kidneys were collected for analysis 4 and 8 days post-IR injury. There was robust upregulation of TGF β expression, >4-fold compared to Sham mice, and related profibrotic gene expression, such as fibronectin and collagens I and III, as well as increases in *extracellular matrix* (ECM) deposition, particularly of collagens, in response to renal injury in both models. CDA1 deficiency failed to attenuate the development of renal fibrosis in either AKI model, despite evidence of reduced TGF β signalling activation in CDA1 KO mice at 4 days after IR injury. Interestingly, however, CDA1 deficiency appears to exacerbate proinflammatory gene expression, with increases in TNF α , iNOS, and IL6 expression at 4 days post-IR injury compared to CDA1 WT mice. The differences in transcriptional changes in these genes between CDA1 WT and CDA1 KO mice, however, were not seen at 8 days after IR injury nor in the more severe UUO model.

Conclusions:

Targeting CDA1 activity at early stages of disease development leads to the attenuation of diabetes-associated renal injury, while delayed intervention was less effective. Thus, targeting CDA1 represents a relatively non-aggressive approach to retard renal disease via the attenuating TGF β signalling activity.

Declaration

This thesis contains no material which has been accepted for the award of any other degree or diploma at any university or equivalent institution and that, to the best of my knowledge and belief, this thesis contains no material previously published or written by another person, except where due reference is made in the text of the thesis.

Signature: *Pacific*.....

Print Name: PACIFIC HUYNH

Date:30/4/18.....

Acknowledgements

It would be remiss of me if I did not first thank my supervisors, Dr Zhong-Lin Chai and Prof Mark Emmanuel Cooper, for without them I would not be here today. I'd like to express my deepest gratitude to Chai, who saved me from obscurity and allowed me to work under his guidance. Always willing to hear my hair-brained ideas, Chai has allowed me the opportunity to work in such a great department, which provided me with the opportunity to further develop into the scientist I am today. I must thank them again for their patience, particularly at the end of my candidature, for they were able to handle a wretch like me.

My thanks to my colleagues within the now former Proliferation and Fibrosis Laboratory, Aozhi Dai and Tieqiao Wu. Aozhi, in particular, took the time to teach me everything I have used as a foundation of PhD studies, ranging from surgeries and animal handling to histological analyses, and I must not neglect to thank her for the groundwork she's done in establishing the acute kidney injury models which I have used for my thesis. Truly, without her, my PhD studies would have been bland.

I'd like to thank the members of the Department of Diabetes, particularly the members of the former Diabetic Complications department, whom I've learned a lot from. The post-doctoral scientists within the department, Dr Gavin Clive Higgins, Dr Raelene Pickering and Dr Carlos Rosado and many others, who were always willing to lend an ear to my troubles, as well as assisting me with any queries I had on a particular experiment. I must acknowledge the assistance I received from our animal technical staff, Samantha Sacca, Elisha Lastavec and Megan Haillay, who helped with experimental procedures performed on the mice utilised in this study. I'd also like to thank Dr Phillip Kantharidis and Alex Dimitropoulos, who took the time out of their busy schedule to proof-read drafts of my thesis. I thank them for the patience and sage advice I have received from them.

I must single out two post-doctoral fellows in my department, Dr Bryna Chow and Dr Jay Jha, for without them I would not have had made the first steps to investigate a particular study in this thesis. Almost serendipitously, I was able to obtain fascinating results and insight into a key part of this thesis and I thank them for such an outcome.

I express my deepest gratitude to my friend and mentor, Dr Stephen Gray, who has helped me during our time at the Baker IDI. Always willing to lend an ear to my troubles, I truly believe the advice he provided at a particular point in my first year was the turning point of my PhD studies. Indeed, if it were not for that and his continued mentorship, I do not believe I would have been able to progress any further from that point.

Lastly, I thank all the people who've helped push me this far, particularly the friends I've made throughout my PhD candidature, as well as my family. They know who they are.

Table of Contents

Abstract	iv
Declaration	vi
Acknowledgements	vii
List of Figures	xiii
List of Tables	xvi
List of Abbreviations	xvii
Chapter 1. Introduction	1
Chapter 2. Literature Review	4
2.1. Wound Repair in the kidney, Chronic Kidney Disease and Fibrosis.....	4
2.1.1. Wound Repair in the kidney	4
2.1.2. Diabetic Nephropathy: The leading cause of End-Stage Renal Disease.....	7
2.1.3. Diabetic Nephropathy: Structural and Functional Correlations.....	7
2.1.4. Diabetic Nephropathy and progression towards <i>End-Stage Renal Disease</i> (ESRD).....	12
2.2. Fibrosis in the kidney	13
2.2.1. Fibrosis in CKD: Downward spiral to the end.....	13
2.2.2. Mediators of Fibrosis	14
2.2.3. <i>Transforming growth factor beta</i> (TGF β).....	15
2.2.3.1. An overview of TGF β	15
2.2.3.2. TGF β signalling pathway.....	15
2.2.4. TGF β in CKD and Fibrosis	18
2.2.4.1. Pathological roles of TGF β in DN	18
2.2.4.2. Promotion of ECM deposition.....	18
2.2.4.3. Inhibition of matrix turnover	19
2.2.4.4. Activation of matrix-producing cells.....	19
2.2.4.5. Amplification of proinflammatory and profibrotic signals.....	19
2.2.5. Targeting the TGF β signalling pathway	21
2.2.5.1. Inhibition of the TGF β signalling pathway.....	21
2.2.5.2. Exploring the TGF β signalling pathway.....	22
2.3. <i>Cell Division Autoantigen 1</i> (CDA1)	27
2.3.1. Cell Division Autoantigen 1: An introduction.....	27
2.3.2. CDA1 and disease	28
2.3.3. CDA1 and TGF β : A synergistic relationship.....	28
2.3.4. CDA1 and <i>in vivo</i> models of diabetic nephropathy	28

2.4. Hypothesis	34
2.5. Aims	34
Chapter 3. Methodology	35
3.1. Materials	35
3.1.1. General Chemicals	35
3.1.2. Buffers and solutions.....	37
3.1.2.1. General Buffers and Solutions.....	37
3.1.2.2. Buffers for ELISAs.....	38
3.1.2.3. Composition of buffers for hydroxyproline analysis.....	38
3.1.2.4. Composition of buffers for protein analysis	39
3.1.2.5. Composition of buffers for histological stains.....	39
3.1.2.6. Composition of buffers for Periodic acid/Schiff's staining.....	40
3.1.2.7. Composition of buffers for Masson's trichrome staining.....	40
3.2. General Methods	43
3.2.1. Genotyping of genetically modified mice.....	43
3.2.1.1. Isolation of genomic DNA.....	43
3.2.1.2. Genotyping of mice using polymerase chain reaction.....	43
3.2.1.3. Agarose Gel Electrophoresis	43
3.2.2. Animal studies and measurements of metabolic parameters	43
3.2.2.1. Induction of diabetes with streptozotocin (STZ).....	43
3.2.2.2. Monitoring of animals in diabetic studies.....	44
3.2.2.3. Unilateral Ureteric Obstruction (UUO) and Ischaemia/Reperfusion (IR) injury	44
3.2.2.4. Euthanasia of animals and tissue collection	44
3.2.2.5. Measuring albuminuria.....	44
3.2.2.6. Measuring creatinine levels	45
3.2.2.7. Measuring glycated haemoglobin.....	45
3.2.2.8. Urinary kidney injury molecule-1 (KIM1) ELISA.....	45
3.2.3. Isolation of <i>ribonucleic acids</i> (RNA) from tissues	46
3.2.3.1. Isolation of RNA using phenol/chloroform/water extraction	46
3.2.3.2. Deoxyribonuclease (DNase) treatment of RNA	46
3.2.3.3. Reverse transcription of RNA into cDNA.....	46
3.2.3.4. Quantitative Real Time PCR (qRT-PCR).....	47
3.2.4. Quantification of total collagen content.....	49
3.2.4.1. Acid Hydrolysis of tissue.....	49
3.2.4.2. Hydroxyproline Assay	49
3.2.5. Protein Analysis	50
3.2.5.1. Extraction of proteins from tissue.....	50

3.2.5.2. Determination of protein concentration using bicinchoninic acid (BCA) assay	50
3.2.5.3. Sodium Dodecyl Sulfate Polyacrylamide Gel Electrophoresis (SDS-PAGE).....	50
3.2.5.4. Western Blot	50
3.2.6. Histological stains	51
3.2.6.1. Periodic Acid Schiff (PAS) Staining	51
3.2.6.2. Massons' trichrome staining.....	51
3.2.6.3. Immunohistochemical staining.....	51
3.2.6.4. Quantification of histological stains	52
3.2.7. Statistical Analysis	52
Chapter 4. Optimisation of conditions to induce the genetic deletion of CDA1 in	
CDA1^{flox}/ERCre mice.....	53
4.1. Background.....	53
4.2. Method.....	54
4.2.1. Generation of CDA1 ^{flox} /ERCre mice	54
4.2.2. Optimization of tamoxifen dosage to delete CDA1 gene in CDA1 ^{flox} /ERCre mice.....	54
4.3. Results	54
4.3.1. Genotyping of CDA1 ^{flox} /ERCre mice.....	54
4.3.2. Tamoxifen decreases renal CDA1 mRNA levels in a dose-dependent manner.....	55
4.4. Discussion and Conclusion.....	58
Chapter 5. Induced genetic deletion of CDA1 in Diabetic Nephropathy: Early Intervention	
Study.....	60
5.1. Background.....	60
5.2. Methods	60
5.2.1. CDA1 ^{flox} /ERCre mice, induction of diabetes and induced genetic deletion of CDA1 ...	60
5.3. Results	61
5.3.1. Reduced renal CDA1 gene expression in tamoxifen-treated CDA1 ^{flox} /ERCre mice	61
5.3.2. CDA1 deficiency does not affect diabetes-associated metabolic parameters	63
5.3.3. CDA1 deficiency attenuates diabetes-associated renal injury and fibrosis	63
5.3.4. Renoprotective effect of CDA1 deficiency is myofibroblast independent.	68
5.4. Discussion.....	69
Chapter 6. Induced genetic deletion of CDA1 in Diabetic Nephropathy: Delayed Intervention	
Study.....	71
6.1. Background.....	71
6.2. Methods	71
6.2.1. CDA1 ^{flox} /ERCre mice, induction of diabetes and induced genetic deletion of CDA1 ...	71
6.3. Results	72

6.3.1. CDA1 deficiency does not affect diabetes-associated metabolic parameters	72
6.3.2. Reduced renal CDA1 mRNA levels in tamoxifen-treated CDA1flox/ERCre mice	75
6.3.3. Delayed intervention against CDA1 activity does not affect development of diabetes-associated renal fibrosis	75
6.4. Discussion.....	81
Chapter 7. Genetic deletion of CDA1 in non-diabetic renal fibrosis.....	85
7.1. Background.....	85
7.2. Methods	86
7.2.1. <i>Unilateral Ureteral Obstruction (UUO)</i>	86
7.2.2. <i>Ischemia/Reperfusion (IR) Injury</i>	87
7.3. Results	87
7.3.1. CDA1 and Unilateral Ureteral Obstruction.....	87
7.3.1.1. Morphological changes in obstructed kidneys of CDA1 WT and KO mice	87
7.3.1.2. UUO-induced upregulation of profibrotic markers in CDA1 WT mice.....	88
7.3.1.3. Genetic deletion of CDA1 does not affect UUO-induced renal fibrosis	89
7.3.1.4. The effect of CDA1 deficiency on complement and inflammatory markers	90
7.3.2. CDA1 and Ischaemia/Reperfusion Injury.....	100
7.3.2.1. IR-associated activation of TGFβ signalling and changes in profibrotic and proinflammatory gene expression.....	100
7.3.2.2. Effect of CDA1 deficiency on the gene expression of TGFβ signalling components in renal IR injury	100
7.3.2.3. Effect of CDA1 deficiency on IR-associated profibrotic and proinflammatory gene changes.....	101
7.3.2.4. The effects of CDA1 deficiency in IR-associated ECM accumulation.....	101
7.3.2.5. The effects of CDA1 deficiency on transcriptional changes concerning cell cycle regulation and apoptosis	102
7.4. Discussion.....	113
Chapter 8. Discussion & Conclusion	118
8.1. Summary of major findings.....	118
8.1.1. Overview	118
8.1.2. Induced genetic deletion of CDA1 and its effects on the progression of diabetic nephropathy	118
8.1.2.1. Inducible CDA1 KO mice	118
8.1.2.2. The effect of early versus delayed intervention against CDA1 in diabetic nephropathy	119
8.1.3. Global CDA1 KO and its effect on renal fibrosis in mouse models of AKI	119
8.2. The pathological role of CDA1 in renal disease.....	120
8.2.1. Renal disease is associated with an elevation in CDA1 expression.....	120

8.2.2. Speculated mechanisms behind CDA1 ability to enhance TGF β signalling	121
8.2.3. The inhibition or absence of CDA1 activity affects TGF β signalling and subsequent renal fibrosis development in a time and context-dependent manner	122
8.3. Questions left unanswered, study limitations and future directions	123
8.4. Conclusions	125
References	126
Appendix	153
Supplementary Figures	153
Publications during enrolment	159

List of Figures

Figure 2.1. Nephron, the functional unit of the kidney.....	6
Figure 2.2. Traditional view of disease progression in diabetic nephropathy.	9
Figure 2.3. Pathological features of diabetic nephropathy.....	10
Figure 2.4. Histological changes in diabetic nephropathy.	11
Figure 2.5. Induction of the canonical Smad-dependent pathway by TGF β 1 in renal fibrosis.	17
Figure 2.6. The pathological role of TGF β in CKD, particularly diabetic nephropathy.	20
Figure 2.7. CDA1 is conserved in mammals.	32
Figure 2.8. The pathological role of CDA1 in renal fibrosis.	33
Figure 4.1. Detection of the genetic deletion of CDA1 in CDA1flox/ERCre mice treated with tamoxifen.....	56
Figure 4.2. Detection of CDA1 deletion from CDA1flox/ERCre mice treated with tamoxifen.	57
Figure 5.1. Timeline of the 10-week STZ-induced diabetic study	61
Figure 5.2. Induced genetic deletion of CDA1 in renal cortex of 10-week diabetic CDA1flox/ERCre mice.	62
Figure 5.3. Induced CDA1 deficiency does not affect diabetes-associated albuminuria but may reduce urinary KIM-1 excretion.....	65
Figure 5.4. Induced genetic deletion of CDA1 attenuates diabetes-associated profibrotic gene expression in mice.....	66
Figure 5.5. Induced genetic deletion of CDA1 attenuates diabetes-associated Collagen IV deposition in mice.	67
Figure 5.6. Induced genetic deletion of CDA1 does not affect diabetes-associated α SMA upregulation in mice.....	68
Figure 6.1. Timeline of the 20-week STZ-induced diabetes study.....	71
Figure 6.2. Delayed induced CDA1 deficiency does not affect diabetes-associated albuminuria, nor urinary KIM1 excretion.....	74
Figure 6.3. Induced genetic deletion of CDA1 in renal cortex of 20-week diabetic CDA1flox/ERCre mice.....	77
Figure 6.4. Induced genetic deletion of CDA1 does not affect diabetes-associated profibrotic gene expression in mice.....	78
Figure 6.5. Delayed induction of CDA1 genetic deletion attenuates diabetes-associated collagen III deposition.	79
Figure 6.6. Delayed induction of CDA1 genetic deletion does not affect diabetes-associated collagen IV deposition.	80
Figure 7.1. Timeline of UO model.....	86

Figure 7.2. Timeline of IR injury model.....	87
Figure 7.3. Upregulation of CDA1 gene expression in UUO.....	91
Figure 7.4. Genetic deletion of CDA1 does not affect UUO-associated upregulation in TGF β gene expression, nor its receptor.	91
Figure 7.5. Genetic deletion of CDA1 does not affect UUO-associated changes in profibrotic gene expression.....	92
Figure 7.6. The effect of CDA1 deficiency on UUO-associated activation of inflammatory and complement pathways.....	93
Figure 7.7.a. UUO-associated ECM deposition in mice is not affected by CDA1 deficiency.....	94
Figure 7.7.b. UUO-associated ECM deposition in mice is not affected by CDA1 deficiency. Continued from previous page.....	95
Figure 7.8.a. UUO-associated collagen deposition is unchanged in CDA1 KO mice after 5 days of obstruction.....	96
Figure 7.8.b. UUO-associated collagen deposition is unchanged in CDA1 KO mice after 5 days of obstruction.....	97
Figure 7.9.a. UUO-associated collagen deposition is affected by CDA1 deficiency after 10 days of obstruction.....	98
Figure 7.9.b. UUO-associated collagen deposition is affected by CDA1 deficiency after 10 days of obstruction.....	99
Figure 7.10. Gene expression of CDA1 in IR injury.....	103
Figure 7.11. Activation of TGF β signalling in IR injury.....	104
Figure 7.12. IR-associated activation of the TGF β signalling pathway is attenuated by CDA1 deficiency early in disease development.....	105
Figure 7.13. Effects of CDA1 deficiency on profibrotic gene expression in response to renal ischaemic/reperfusion injury in mice.....	106
Figure 7.14. Effects of CDA1 deficiency on proinflammatory gene expression in response to renal ischaemic/reperfusion injury in mice.....	107
Figure 7.15. ECM deposition and renal morphology in a mouse model of renal IR injury.....	108
Figure 7.16. CDA1 deficiency does not affect total collagen content in response to renal ischaemic/reperfusion injury in mice.....	109
Figure 7.17.a. CDA1 deficiency does not affect collagen deposition in response to renal ischaemic/reperfusion injury in mice.....	110
Figure 7.17.b. CDA1 deficiency does not affect collagen deposition in response to renal ischaemic/reperfusion injury in mice.....	111

Figure 7.18. Effects of CDA1 deficiency on gene expression related to apoptosis, cell cycle regulation and proliferation in response to renal ischaemic/reperfusion injury in mice.	112
Figure 8.1. Deletion of exons 2-5 of the mouse CDA1 gene leads to a non-functional gene product.	122
Supplementary Figure 1. Total collagen content progressively increases with time in the UUO model.	153
Supplementary Figure 2. Induced genetic deletion of CDA1 attenuates diabetes-associated ECM accumulation in mice.	154
Supplementary Figure 3. Tamoxifen administration induces genetic deletion of CDA1 in aortic tissue of CDA1 ^{flox} /ERCre mice.	155
Supplementary Figure 4. Delayed CDA1 genetic knockout does not attenuate diabetes-associated ECM deposition.	156
Supplementary Figure 5. Mesangial expansion is not significantly increased in STZ-induced diabetic mice.	157
Supplementary Figure 6. Confirmation of genetic deletion of CDA1 in UUO study.	158
Supplementary Figure 7. UUO-associated collagen content in mice is not affected by CDA1 deficiency.	158

List of Tables

Table 2.1. Genetic and pharmacological studies on TGF β signalling in renal disease.....	23
Table 3.1. General chemicals and compounds utilised in this thesis.....	35
Table 3.2. Sequence of primers and probes used for quantitative real time PCR.....	41
Table 3.3. Primer sets used for genotyping.....	42
Table 3.4. Reaction mix used for reverse transcription	47
Table 3.5. Reaction mix used for TaqMan reactions	48
Table 3.6. Reaction mix used for SYBR reactions	48
Table 5.1. Metabolic parameters of mice at 4 weeks after STZ-induced diabetes induction	62
Table 5.2. Metabolic parameters of mice from the 10-week diabetic study.....	64
Table 6.1. Metabolic parameters of mice at 10 weeks after STZ-induced diabetes induction	72
Table 6.2. Metabolic parameters of mice from the 20-week diabetic study.....	73
Table 7.1. Kidney-to-Body Weight ratio of CDA1 WT and KO mice undergoing UUO	88

List of Abbreviations

A	ampere(s)
ACE	angiotensin-converting enzyme
AGE	advanced glycation end-product
AKI	acute kidney injury
ALK1	activin receptor-like kinase 1
AngII	angiotensin II
ApoE	apolipoprotein E
α SMA	smooth muscle actin, alpha
ATP	adenosine triphosphate
BAK	BCL2-antagonist/killer 2
BAX	BCL2-associated X protein
BCA	bicinchoninic acid
BCL2	B-cell CCL/lymphoma 2
BMP	bone morphogenetic protein
BW	body weight
C	complement component, suffixes: 3, 5
CASK	calcium/calmodulin-dependent serine protein kinase
CDA1	cell division autoantigen-1
CDK	cyclin-dependent kinases
cDNA	complementary DNA
CKD	chronic kidney disease
Cre	cyclic recombinase
CTGF	connective tissue growth factor
DENTT	differentially expressed nucleolar TGF β 1 target
dKO	double KO
DM	diabetes mellitus
DNA	deoxyribonucleic acid
DNase	deoxyribonuclease
ECM	extracellular matrix
ELISA	enzyme-linked immunosorbent assay
EMT	epithelial-mesenchymal transition
EndoMT	endothelial-mesenchymal transition
eNOS	endothelial nitric oxide synthase/NOS3
ERCre	estrogen receptor cyclic recombinase

ERK	extracellular signal-regulated kinase 2
ESRD	end-stage renal disease
GBM	glomerular basement membrane
GFR	glomerular filtration rate
GLUT1	glucose transporter 1
g	gram(s), prefixes: <i>nano</i> (n), <i>micro</i> (μ), <i>milli</i> (m), <i>kilo</i> (k)
Hbx	human hepatitis B virus X protein
hr	hour(s)
HRP	horse-radish peroxidase
ICAM1	intracellular adhesion molecule 1
IHC	immunohistochemistry
IL	interleukin
I κ B α	inhibitor of kappa B
iNOS	inducible nitric oxide synthase/NOS2
IR	ischaemia/reperfusion
KIM1	kidney injury molecule 1
KO	knockout
L	litre(s), prefix: <i>micro</i> (μ), <i>milli</i> (m)
LAP	TGF β -latency-associated peptide
LTBP	latent-TGF β binding proteins
m	metre(s), prefixes: <i>nano</i> (n), <i>micro</i> (μ)
MAPK	mitogen activated protein kinase
MCP1	monocyte chemotactic protein 1
min	minutes(s)
miRNA	microRNA
MMP	matrix metalloproteinase
mRNA	messenger ribonucleic acid
MSR1	macrophage scavenger receptor 1
mTOR	mammalian target of rapamycin
NADPH	nicotinamide adenine dinucleotide phosphate
NAP	nucleosome assembly protein
NF κ B	nuclear factor of kappa light-chain-enhancer in activated B cells
NLS	nuclear localisation sequence
NO	nitric oxide
NOX4	NADPH oxidase 4

P3K	phosphatidylinositol-3-kinase
PAI1	plasminogen activator inhibitor-1
PAS	periodic acid-Schiff
PCR	polymerase chain reaction
PDGF	platelet-derived growth factor
PEST	proline/glutamic acid/serine/threonine-rich
PKC	protein kinase C
pSmad3	phosphorylated Smad3
qRT-PCR	quantitative real-time PCR
RAAS	renin-angiotensin-aldosterone system
rcf	relative centrifugal force
REST/NRSF	repressor element 1-silencing transcription factor/neuron-restrictive silencer factor
RNA	ribonucleic acid
ROS	reactive oxygen species
RT-PCR	reverse transcriptase PCR
SBE	Smad-binding elements
SDS-PAGE	sodium dodecyl sulfate polyacrylamide gel electrophoresis
sec	second(s)
shRNA	short hairpin RNA
siRNA	small interfering RNA
Ski	Sloan-Kettering Institute proto-oncogene
SnoN	Ski-related novel gene, non Alu-containing
STZ	streptozotocin
TGFβ	transforming growth factor beta
TGIF	transforming growth interacting factor
TIMP	tissue inhibitors of MMPs
TβRI	TGFβ receptor type 1
TβRII	TGFβ receptor type 2
TNFα	tumour necrosis factor alpha
TSPYL2	testis-specific Y-encoded protein like 2
UUO	unilateral ureteral obstruction
V	volt(s)
VCAM	vascular adhesion molecule 1
VEGF	vascular endothelial growth factor
WT	wildtype

Chapter 1. Introduction

Fibrosis is the common final pathological event in most chronic organ diseases. Excessive fibrogenesis, the prominent feature in fibrosis, is observed in most *chronic kidney diseases* (CKD), particularly diabetic nephropathy where it is progressive in nature. Indeed, regardless of aetiology, the extent of fibrotic lesions in the kidney generally correlates with the severity of renal injury.¹ Unhindered progression of renal fibrosis eventually leads towards *End Stage Renal Disease* (ESRD), a leading cause of mortality in diabetic patients.² There is currently no effective treatment which directly targets renal fibrosis, with the use of current therapeutic treatments, which work through lowering blood pressure and/or achieving proper glucose control, shown to slow but cannot halt the progression of diabetic nephropathy towards ESRD. This is due, in part, to an incomplete understanding of these disease processes. Therefore, further research is required to elucidate key factors driving the progression of fibrosis in diabetic nephropathy and other chronic renal diseases.

The studies presented in this thesis attempts to examine the pathological role of *Cell Division Autoantigen 1* (CDA1) in various experimental mouse models of renal disease. CDA1, initially characterised as an antiproliferative nuclear phosphoprotein, has since been implicated in the development of fibrosis through its ability to enhance *transforming growth factor beta* (TGF β) signalling. Prior studies in our laboratory have demonstrated that the inhibition or absence of CDA1 led to the attenuation of TGF β signalling activity in mouse models of diabetic nephropathy and diabetes-associated atherosclerosis, which consequently attenuated the development of fibrosis in these models. Thus, my thesis was determined to examine the therapeutic potential of CDA1 inhibition utilising a unique inducible CDA1 knockout mouse strain in a mouse model of diabetic nephropathy. In addition, I further examined the pathological role of CDA1 in the development of non-diabetic renal fibrosis using the global CDA1 knockout mouse strain in two mouse models of acute kidney injury.

The first two chapters serves as the introduction and literature review (**Chapter 1**, which you are reading right now, and **Chapter 2**), which collectively cover the topics which provide a basic understanding to the research presented in this study. First, a basic explanation of renal physiology and the typical wound healing process in the kidney is briefly described. Next, diabetic nephropathy, which is the current leading cause of ESRD worldwide, is discussed, with topics covering the progression of disease and current challenges associated with treatment. Next, significance of fibrosis in renal pathology, the mechanisms driving the fibrotic processes towards renal failure, and current research in development towards the treatment of renal fibrosis is outlined, with emphasis placed on the TGF β signalling pathway due to its importance in driving the fibrotic process. Lastly, CDA1, which is known for its ability to enhance TGF β signalling, is introduced, with topics covering

mechanistic aspects of CDA1 activity, its roles in fibrosis development and our hypothesis of the renoprotective effects associated with the absence or inhibition of CDA1 activity in renal disease.

The succeeding chapters describe the experimental outcomes of my investigations into the pathological role of CDA1. Many of the experimental protocols utilised in studies presented in this thesis are detailed in **Chapter 3**, with experimental details of procedures specific to certain studies included within their respective chapters. The studies presented in this thesis were aimed to further examine the pathological role of CDA1 in renal fibrosis through the use of conventional and inducible genetic knockout mouse strains in experimental models of non-diabetic and diabetic kidney disease, respectively.

To address the first part of my thesis, I utilised a unique inducible CDA1 knockout mouse strain, the CDA1^{flox}/ERCre mouse, to examine the effect of induced genetic deletion of CDA1 on the development of renal fibrosis in a mouse model of diabetic nephropathy (**Chapters 4-6**). The genetic deletion of CDA1 was induced in these mice through the administration of tamoxifen. Preliminary studies were performed to determine an appropriate dose of tamoxifen required to induce the significant reduction of CDA1 gene expression, while avoiding any potential side-effects associated with high doses of tamoxifen (**Chapter 4**). From these studies, a dose of 1.5 mg tamoxifen/mouse/day for 3 consecutive days was found to induce ~70-80% reduction of renal CDA1 expression in CDA1^{flox}/ERCre mice. Thus, this dose was used for subsequent diabetic studies.

Induced genetic deletion of CDA1 was performed to mimic the therapeutic intervention against CDA1 activity in a mouse model of *streptozotocin* (STZ)-induced diabetic nephropathy. In these studies, genetic deletion of CDA1 was induced by the administration of tamoxifen to CDA1^{flox}/ERCre mice at 5 or 10 weeks after STZ-induced diabetes onset, and kidneys were harvested for analysis after an additional 5 or 10 weeks, respectively. The former and latter represents early and delayed intervention against CDA1 activity (**Chapter 5 and 6**), respectively. Early intervention against CDA1 activity resulted in the attenuation of renal fibrosis development in diabetic mice, as seen by the reduction in diabetes-associated profibrotic gene expression, such as fibronectin and collagen I, and collagen IV accumulation (**Chapter 5**). In contrast, in the delayed intervention study, induced genetic deletion of CDA1 had little, if any, effect on diabetes-associated renal fibrosis (**Chapter 6**). Collectively, these findings suggest that targeting CDA1 at early stages of diabetic nephropathy development was more effective than if treatment was delayed.

To address the second part of my thesis, I examined the effect of global genetic *knockout* (KO) of CDA1 in two mouse models of acute kidney injury (AKI), the *unilateral ureteric obstruction* (UUO) and *ischaemia/reperfusion* (IR) injury models (**Chapter 7**). In the UUO study, CDA1 *wildtype* (WT) and CDA1 KO mice had their left ureter ligated and kidneys were collected for analysis 5, 10 and 14 days post-UUO. In the IR study, left renal artery of CDA1 WT and CDA1 KO male mice were ligated for 45 mins before being released to restore blood flow and kidneys were

collected for analysis 4 and 8 days post-IR injury. Although there was evidence of enhanced TGF β signalling activity, as seen by the robust upregulation of profibrotic gene expression and subsequent accumulation of *extracellular matrix* (ECM) components, in both AKI models, CDA1 deficiency was unable to prevent the development of renal fibrosis in either AKI model. Interestingly, CDA1 KO mice exhibited profound transcriptional changes in genes related to inflammation, cell cycle control and apoptosis, which was also associated with reduced TGF β signalling activity at early stages of IR injury development. These transcriptional changes, however, are not seen at later stages of IR injury development nor in the UUO model. Collectively, these results suggest that CDA1 may play a role in the modulation of TGF β -mediated pathological processes at early stages of disease development and that inhibition of CDA1 activity becomes increasingly redundant, possibly compensated by other profibrotic processes, as the renal disease develops.

In conclusion, the work presented in this thesis was an attempt towards gaining a more thorough understanding of the role of CDA1 in various forms of renal disease. Indeed, while it is clear that CDA1 plays a role in the disease development, in both non-diabetic and diabetic forms of renal disease, it appears that the effects of the absence or inhibition of CDA1 activity on the TGF β signalling pathway and subsequent fibrosis development are time and context-dependent. Nonetheless, these studies further validate that targeting CDA1 in renal disease represents a relatively non-aggressive approach toward the inhibition of the TGF β -mediated fibrosis development and thus may be viable in the therapeutic intervention of renal fibrosis in chronic kidney disease, particularly diabetic nephropathy.

Chapter 2. Literature Review

2.1. Wound Repair in the kidney, Chronic Kidney Disease and Fibrosis

The kidney is a critical organ that performs essential homeostatic functions in vertebrates, arguably enabling the versatility required for these animals to survive in a number of aquatic and terrestrial environments. The human adult kidney comprises of approximately 0.8-1.5 million nephrons, the basic functional unit in the kidney, which is comprised of many discrete cell types. Blood supplied to the kidneys is filtered, to allow the reabsorption of small molecules, such as ions, water and nutrients, back into the bloodstream, while also expelling metabolic waste products by secretion (**Figure 2.1**). Through these processes, the main homeostatic functions performed by the kidney include the maintenance of electrolyte, water and acid-base balance, hormonal secretion, regulation of blood pressure and excretion of metabolic waste products.

2.1.1. Wound Repair in the kidney

The ability to repair damaged tissue in response to injury is a fundamental process to ensure the functionality and survival of any vascularised tissue. The kidney is no different which, with the high metabolic demands of renal cells, requires rapid replacement of injured cells and restoration of normal renal function to maintain homeostasis.³ Failure to repair damaged tissues can lead to kidney dysfunction and failure, which itself is associated with comorbidities due to the physiological importance of continued kidney function in the maintenance of body homeostasis. While our initial understanding of wound repair and regeneration in the kidney stems from investigations from non-mammalian renal systems,⁴ it is expected that the cellular and molecular responses in wound repair would be similar amongst all vertebrates. Indeed, initial characterisation of wound healing processes have since been verified in mammals, particularly in mice and humans.

Although most renal cells in mammals are able to undergo similar processes in response to renal injury, kidney tubular epithelium, in particular, possesses a great capacity to repair and regenerate in order to restore normal epithelial integrity.⁵⁻⁷ Under normal physiological conditions, the rate of renal tubular cell turnover to maintain homeostasis is low.⁸ Upon injury, the rate of proliferation of these cells increases exponentially.⁹ Damaged epithelial and endothelial cells release a plethora of growth factors, cytokines/chemokines and other bioactive molecules leading to the activation of various components of the coagulation cascade, inflammatory pathways and the immune response.^{10, 11} An initial inflammatory response, characterised by the influx of leukocytes, such as neutrophils, monocytes and macrophages, results in and is aided by neovascularisation, angiogenesis, vasodilation and basement membrane remodelling, leading to the establishment of new supply routes to the centre of the wound.¹² The further release of cytokines/chemokines by macrophages recruits and activates fibroblasts, allowing their migration to the site of injury. Fibroblasts deposit *extracellular matrix* (ECM) components which assists in cell orientation and provides docking sites

for various factors, molecules and cells, thus laying the foundation required to restore original tissue architecture. The ECM is actively remodelled through a combination of synthesis, degradation and contraction by activated fibroblasts known as myofibroblasts.¹³ Once the site is fortified with sufficient matrix production, damaged or lost cells are replaced through proliferation and/or hypertrophy of remaining surrounding cells, restoring tissue function. However, if regeneration is not possible, ECM components, such as collagen, will be deposited to fill the void, with the resulting scar serving to re-establish the anatomical continuity of the damaged tissue albeit with a diminished functional capacity. Whether an injurious event progresses towards complete regeneration or repair consisting of fibrogenesis largely depends on the initial inflammatory response. More often than not in adult kidney, a dysregulation of innate and adaptive immune systems drives processes that favour the latter. Regardless, once tissue homeostasis has been achieved, inflammatory processes subside, with all recruited cells undergoing apoptosis and/or exiting the site through the lymphatic system.

The above outlines a typical wound healing response to a single episode of *acute kidney injury* (AKI). In these cases, the initial insult is cleared by the response initiated by wound repair processes, which are scaled down once tissue homeostasis has been achieved. However, unregulated and/or continuous activation of wound repair processes in response to persistent injury may consequently lead to further injury. Indeed, progressive loss of nephrons and the associated reduction in renal function occur when the degree of injury exceeds the rate of repair, as is often seen in cases of *chronic kidney diseases* (CKD), particularly diabetic nephropathy.

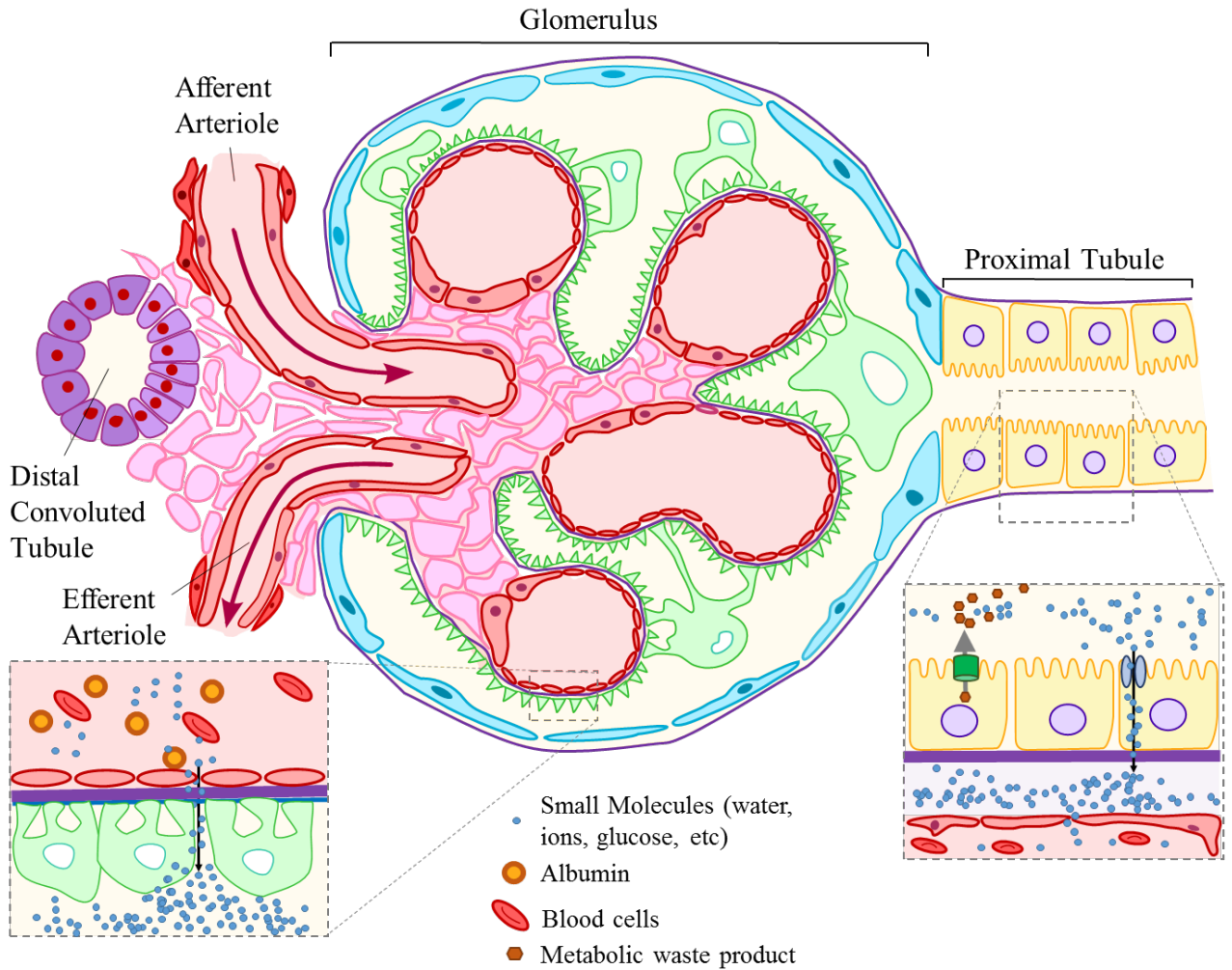


Figure 2.1. Nephron, the functional unit of the kidney. Blood is filtered through the kidney as it flows through the glomerulus from and out of the afferent and efferent arterioles, respectively (Arrows). The combination of podocytes (light green), basement membrane (purple) and endothelial cells (red) make up the filtration barrier which prevents the entry of large molecules, such as albumin (orange circles) and blood cells (red disks), while allowing small molecules (blue circles), such as ions, water, sugar, and nitrogenous waste, to pass through and enter into the Bowman's capsule to produce glomerular filtrate. As the glomerular filtrate passes through the tubules (yellow), ions and water are reabsorbed back into the bloodstream. In addition, tubular epithelial cells secrete metabolic waste products, which facilitates the removal of excessive amounts of dissolved substances (brown hexagon) from the circulation into the tubular fluid, as well as maintains the pH of blood to $\sim 7.4 \pm 0.05$. Adapted from M. Komorniczac, Wikimedia Commons (2009).

2.1.2. Diabetic Nephropathy: The leading cause of End-Stage Renal Disease

Diabetic Nephropathy is a microvascular complication of diabetes mellitus, the most common form of CKD and the current leading cause of *End-Stage Renal Disease* (ESRD) in the United States,¹⁴ if not worldwide.^{2, 15, 16} Diabetic patients with kidney disease, which amount to approximately a third of all diabetic cases,^{17, 18} are generally associated with a greater mortality risk, in both Type 1,^{19, 20} and Type 2 diabetic patients,²¹ than those without kidney disease. Despite a majority of diabetic patients succumbing to cardiovascular diseases²², particularly before the development of severe CKD,²³ ESRD is becoming a more prevalent disorder in diabetic patients due to changes in interventions resulting in increases in survival rates.²⁴ With prevalence of diabetes in the global adult population expected to increase from 8.8% in 2015 to 10.4% in 2040,²⁵ the impact of diabetic nephropathy is expected to be an increasingly prominent global health issue.

2.1.3. Diabetic Nephropathy: Structural and Functional Correlations

Traditionally, the progression of diabetic nephropathy was described as the presence of persistent and progressive albuminuria, followed by the gradual and steady decline in *glomerular filtration rate* (GFR) (**Figure 2.2**).²⁶ As the disease develops, the associated loss in renal function is generally accompanied by hypertension, as well as the occurrence of other microvascular diabetic complications, such as retinopathy. However, it is now understood that diabetic nephropathy is a far more complex pathological process,²⁷ with noted differences in disease progression between Type 1 and 2 diabetic individuals.²⁸ In addition, improvements in diabetes management, including increased use of *renin-angiotensin-aldosterone system* (RAAS) inhibitors, as well as improved blood pressure and intensive glycaemic control, have challenged the two paradigms of the traditional view of diabetic nephropathy. Firstly, that albuminuria inevitably progressively increases in diabetic nephropathy and secondly, the decline of GFR occurs after development of albuminuria. Indeed, in addition to reported cases of diabetes-associated albuminuria regressing in diabetic patients, decline of GFR can occur in the absence of microalbuminuria (<30 mg/day).²⁹ Furthermore, diabetic nephropathy is typically diagnosed after an extended period of time after the onset of diabetes, approximately 10 years in Type 1 diabetic patients,³⁰ while being highly variable in Type 2 diabetic patients.³¹ By the time when clinical signs of CKD have appeared, generally when GFR is <60 mL/min/1.73m² and/or albuminuria is present at >30 mg/day,²⁷ renal lesions have already developed in these patients. In fact, clinical features of diabetic nephropathy may never present in some diabetic patients, despite histologically proven diabetic lesions.³² Nonetheless, these clinical manifestations are generally associated with advanced diabetic glomerulosclerosis, with worsening clinical presentations being reflective of more severe renal lesions.³³⁻³⁵

The characteristic hyperglycaemia in diabetic individuals leads to changes in many metabolic and haemodynamic factors which drive the development of diabetic nephropathy. Among the many pathological processes activated by prolonged exposure to the diabetic milieu, the initiation of

diabetic nephropathy can be largely attributed to the formation of *advanced glycation end products* (AGEs), oxidative stress and the activation of the polyol pathway.³⁶⁻³⁹ In diabetic nephropathy, all renal cells are exposed to the diabetic milieu, with different renal cell types varying in the degree and response to this high glucose environment. Mesangial cells, in particular, are stimulated by the diabetic milieu to secrete cytokines and deposit ECM components, such as fibronectin and collagens. This leads to the first observable histological changes in diabetic nephropathy; thickening of the glomerular basement membrane followed by mesangial area expansion.^{33, 40} Further pathological changes in the glomeruli, such as loss of podocytes by detachment, apoptosis and/or effacement, and enhanced endothelial-mediated capillary permeability, leads to a disruption in the glomerular filtration barrier and subsequent proteinuria (**Figure 2.3**). Indeed, the extent of podocyte loss and mesangial expansion have been predictive of clinical manifestations of diabetic nephropathy, noticeably albuminuria.^{41, 42} Eventually, the combination of these pathological changes will lead to the development of glomerulosclerosis (**Figure 2.4**), which will further drive renal injury through the narrowing and compression of glomerular capillaries leading to decreased hydraulic permeability of the glomerular filtration barrier and decrease in GFR.³³ In addition to glomerular changes, early stages of diabetic nephropathy progression are characterised by renal hypertrophy, primarily due to the proliferation and hypertrophy of tubular epithelial cells, as well as thickening of the tubular basement membrane. Increased reabsorption of the glomerular filtrate by tubular cells contributes towards hyperfiltration, a temporary increase in GFR, as observed at the initial period of diabetic nephropathy progression.⁴³ The increased levels of glucose, lipids, proteins and cytokines in the diabetic glomerular filtrate induce the activation of many pathological processes, particularly inflammation, which lead to further tubular injury.⁴⁴ In response to these insults, injured tubular cells secrete cytokines and other modulators, which further stimulate the activation of important pathological processes, such as inflammatory cell infiltration, apoptosis and atrophy of tubules, and tubulointerstitial fibrosis. The development of tubulointerstitial fibrosis, a relatively late phenomenon in diabetic nephropathy which correlates with sustained reduction in GFR in diabetic patients,^{45, 46} is associated with vascular dysfunction,⁴⁷ glomerular hypertension, increased susceptibility towards ischaemic injury and, eventually, loss of tubular cells. The combination of these pathological processes in all compartments of the nephron, unhindered, leads to the progressive loss of renal function and progression towards ESRD.

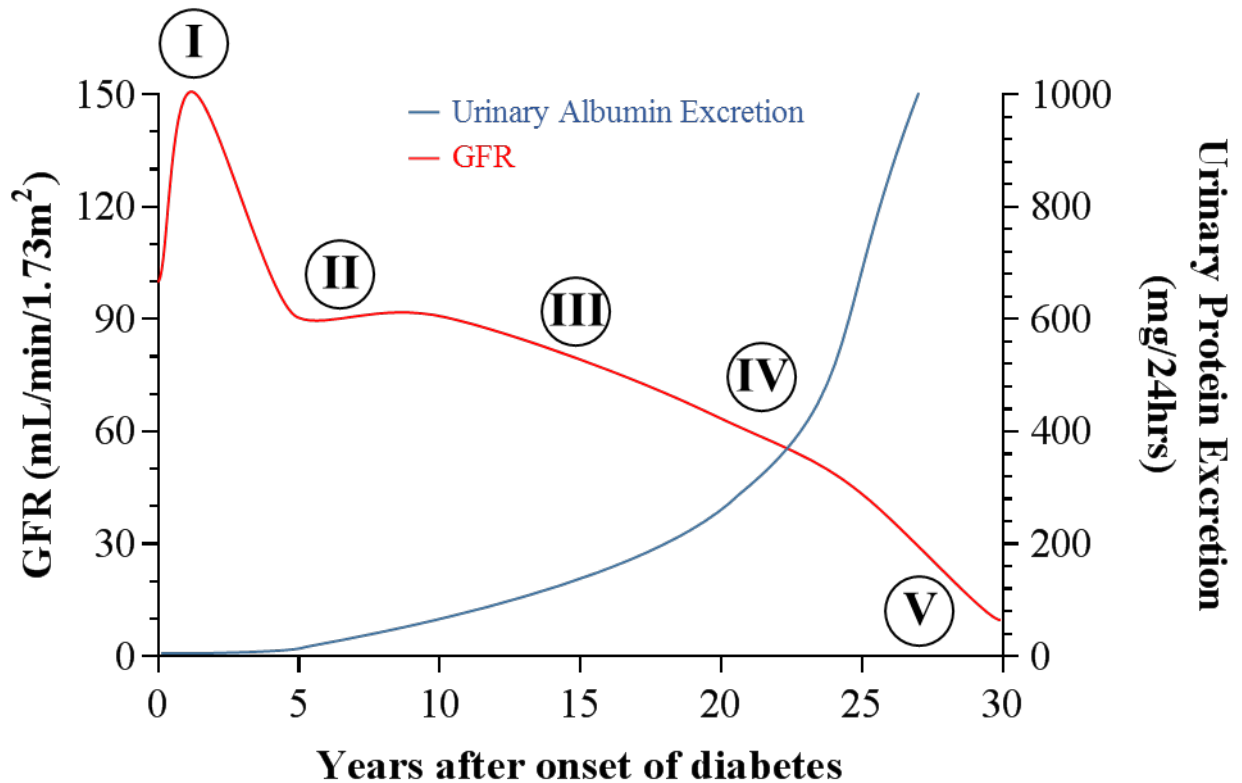


Figure 2.2. Traditional view of disease progression in diabetic nephropathy. Based on initial observations by Mogensen, CE., et al,²⁶ diabetic nephropathy progresses through five stages; Stage I: Pre-nephropathy, with an initial period of hyperfiltration but generally, no other signs of disease; Stage II: silent nephropathy, where GFR and urinary albumin levels are normal (>60 mL/min/1.73 m² and <30 mg/day, respectively); Stage III: incipient nephropathy, where there is a progressive decrease in GFR and progressive increase in albuminuria (microalbuminuria to macroalbuminuria); Stage IV: overt nephropathy with pronounced macroalbuminuria and Stage V: end-stage renal disease. Traditionally, development of diabetic nephropathy is thought to be the progressive reduction in renal function with accompanying increase in urinary albumin excretion. However, this paradigm is not only complicated by the differences in rate of progression between Type 1 and Type 2 diabetic patients, but also by the observation that decline in GFR and presence of albuminuria can occur independently from each other. Adapted from Pugliese, G. (2014).²⁹

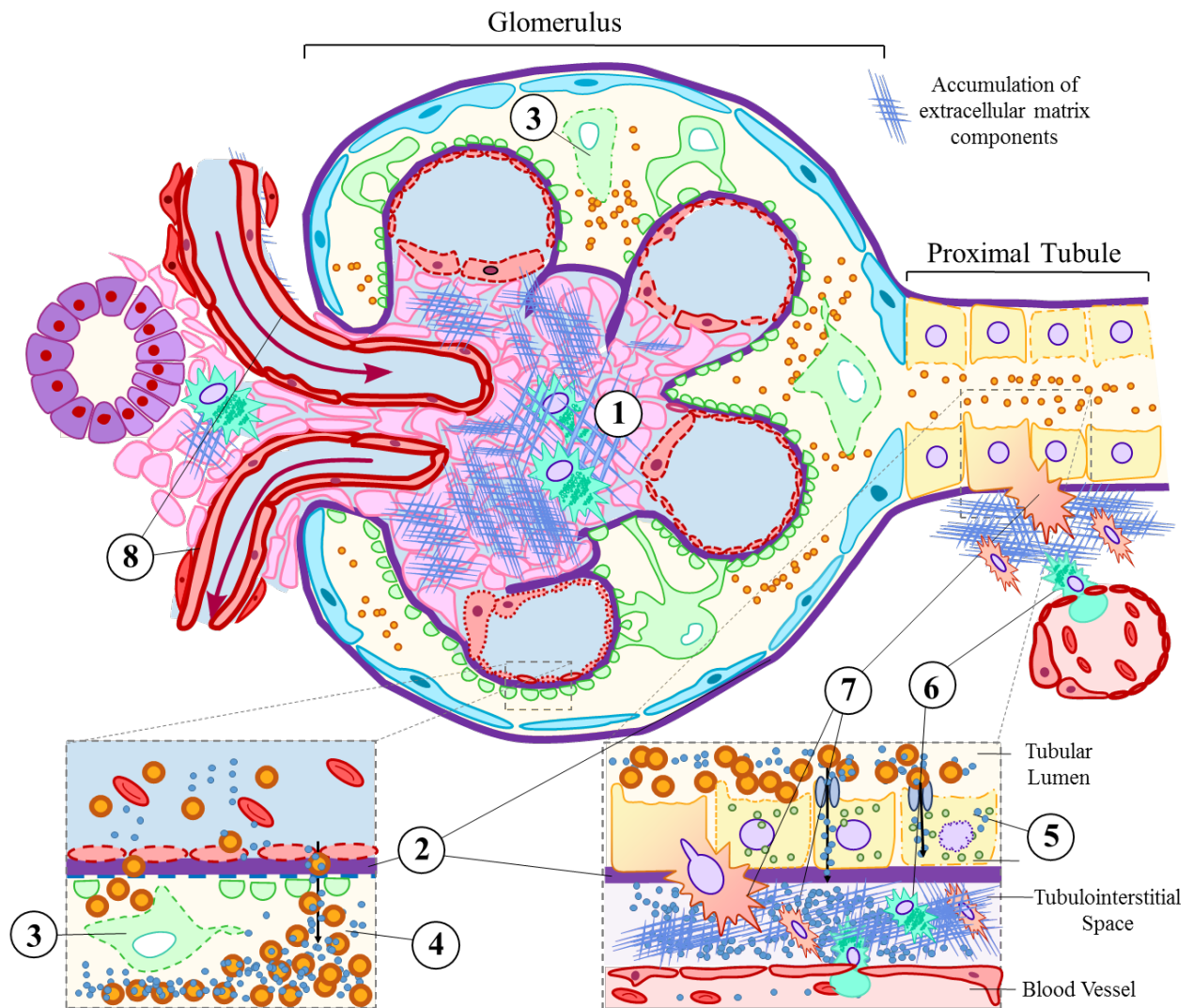


Figure 2.3. Pathological features of diabetic nephropathy. As a result of exposure to chronic hyperglycaemia, mesangial cells undergo hypertrophy, as well as secreting ECM components, leading to the expansion of the mesangial area (1). In addition, the deposition of ECM components also leads to the thickening of the basement membrane in the glomerular and tubulointerstitial space (2). The combination of chronic hyperglycaemia, production of *reactive oxygen species* (ROS) and cytokine release by mesangial cells leads to injury to podocytes (3). Morphological changes of podocytes in response to injury leads to effacement of foot process, podocyte detachment and apoptosis which subsequently leads to increased glomerular permeability of large molecules, such as albumin, into the tubular fluid (4). Collectively, these glomerular changes make up the hallmarks of diabetic glomerulosclerosis. The aforementioned glomerular changes result in tubular injury (5). Increased uptake of glucose, increase production of AGEs, ROS and release of cytokines by injured tubular cells results in the infiltration of inflammatory cells, particularly macrophages (6). Further injury will eventually lead to the promotion of fibrotic processes, which is characterised by the activation/differentiation of fibroblasts into myofibroblasts from a variety of sources, including tubular epithelial cells (7). Arteriosclerosis may also occur (8). Adapted from M. Komorniczac, Wikimedia Commons (2009).

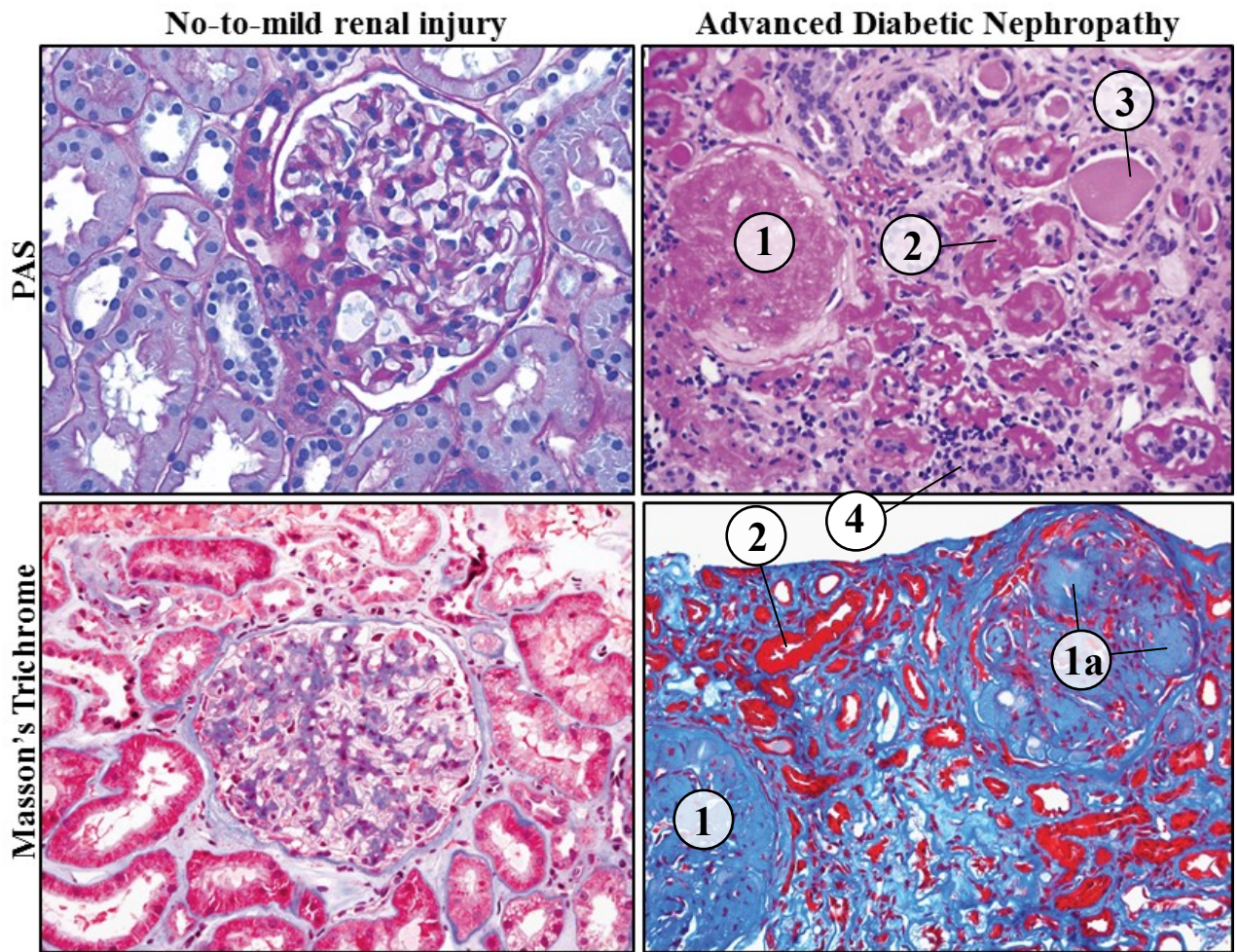


Figure 2.4. Histological changes in diabetic nephropathy. Representative images of *Periodic Acid Schiff* (PAS) (top panels) and Masson’s Trichrome (bottom panels) stains of human renal biopsies with no-to-mild renal injury and advanced diabetic nephropathy. Some key morphological changes can be observed in advanced diabetic nephropathy sections (right-hand side), including glomerulosclerosis (1) with the formation of nodular lesions at more advanced stages of disease (1a), tubular atrophy (2) and formation of protein casts (3). Note: The increased presence of ECM accumulation in the tubulointerstitial area, as represented by the “waxy” appearance of the space between tubules in PAS-stained section (top-right panel) and the blue staining in Masson’s trichrome stained section (bottom-right panel), as well as increased infiltration of inflammatory cells (4). Adapted from Zhou, X., Laszik, Z., Nadasdy, T., & D’Agati, V. (Eds.). (2017). *Silva's Diagnostic Renal Pathology*. Cambridge: Cambridge University Press.⁴⁸

2.1.4. Diabetic Nephropathy and progression towards *End-Stage Renal Disease (ESRD)*

The mechanisms that drive the progression of diabetic nephropathy towards ESRD is similar to those seen in other forms of CKD. The persistent infiltration of inflammatory cells, development of advanced glomerulosclerosis and tubulointerstitial fibrosis, among other pathological processes, are the result of the persistent and chronic injury in diabetic nephropathy, with all compartments of the kidney ultimately affected, in one way or another. Although most renal cells are theoretically able to proliferate to replace their injured counterparts, complete regeneration of nephrons is highly improbable, despite extensive research, due in part to the complex architectural structure, as well as the many different specialised cell types, of the kidney.⁴⁹ Podocytes, in particular, have limited regenerative capacity and are particularly prone to dying off if not attached to the glomerular basement membrane.⁵⁰ Thus, it is assumed that once there is sufficient loss of podocytes, and subsequent breakdown of the glomerular filtration ability within that nephron, the damage is irreversible. While the remaining functional nephrons will undergo compensatory changes to maintain renal homeostasis, the stress placed on the remaining nephrons as the disease progresses will increase, thus leading to further nephron loss at later stages of CKD.⁵¹ The progressive loss of kidney function, which is associated with increased risk of comorbidities,⁵² eventually leads to azotaemia, systemic organ failure and death.

The treatment of diabetic nephropathy generally involves the management of diabetes, particularly by controlling blood pressure and/or maintaining normal blood glucose levels. Although care must be taken with the use of combined therapies,⁵³ the use of conventional therapies, such as the use of *angiotensin-converting enzyme* (ACE) inhibitors, have been proven to slow the progression of diabetic nephropathy.⁵⁴⁻⁵⁶ Furthermore, pancreatic transplantation in Type 1 diabetic patients was associated with regression of glomerulosclerosis and tubulointerstitial fibrosis after an extended period of sustained normoglycaemia.^{57, 58} However, these treatments, while alleviating and/or eliminating the initial injurious agent in diabetes, do not directly target the pathological processes, particularly inflammation and fibrosis, which drive the progressive loss of nephrons in diabetic nephropathy. Furthermore, by the time diabetic nephropathy is clinically diagnosed, generally after an extended period of time after the onset of diabetes, the development of severe renal lesions, as well as a significant loss of functional nephrons, would have already occurred. As adult kidneys have limited regenerative capacity, management of diabetes may not be adequate to prevent the progression to ESRD. Indeed, while intensive glucose control early in diabetes has been shown to prevent the development of diabetic complications, it has not been shown to be as effective at reducing the risk of diabetic nephropathy, nor improve clinical outcomes, if intensive glucose control is initiated after the development of diabetic complications or after an extended period after diabetes onset.²³ Currently, the only options available for patients who have reached ESRD involve lifelong dialysis or transplantation to replace the non-functional organ. Thus, direct treatments which prevent,

retard and/or reverse the pathological processes which drive progressive loss of nephrons in CKD are highly desired, especially in the face of an increasing number of diabetic patients as a result of the worldwide Type 2 diabetes epidemic.

2.2. Fibrosis in the kidney

2.2.1. Fibrosis in CKD: Downward spiral to the end

Fibrosis is widely considered to be the final common pathological feature of most CKD, including diabetic nephropathy. Fibrosis is characterised by the excessive deposition of ECM components, primarily collagens, as well as the presence and proliferation of ECM producing cells, particularly fibroblasts and their activated counterparts, myofibroblasts.^{59, 60} In fact, the degree and extent of fibrosis generally correlates with decline in renal function and progression towards ESRD.^{1, 61, 62} Although glomerular pathology is the primary source of injury in DN, it is the progressive development of fibrosis within the tubulointerstitial area which drives progression towards ESRD.^{63, 64} Indeed, the diabetes-associated decline in renal function has been shown to correlate better with tubulointerstitial fibrosis than with glomerular pathology,⁶⁵ with the extent of tubulointerstitial fibrosis being predictive of disease progression in Type 2 diabetic patients.^{66, 67} Furthermore, tubulointerstitial disease has been reported to occur independent of glomerular disease in Type 1 diabetics patients.³³

Despite its role in the progression of CKD, fibrogenesis, which is the deposition of ECM components, is intrinsically a self-limiting process that restricts injury and a beneficial response, at least initially, to injury. The consequences of fibrosis generally depend on the extent and spatial location of ECM deposition, as well as the intrinsic function of the given tissue. In the event when regeneration is limited, deposition of ECM is required to maintain tissue integrity, despite the subsequent scar tissue having a reduced functional capacity compared to the original pre-injured tissue. Not only is ECM dynamically maintained to ensure tissue homeostasis, fibroblasts are extensively modulated by a plethora of signalling molecules and cues, which lead to the modifications to genetic and epigenetic programs, to proliferate and produce ECM, as well as undergoing apoptosis once scar tissue formation is adequate.^{68, 69} However, this response may prove to be maladaptive in advanced stages of renal disease development. As is often seen in the cases of CKD, persistent and/or extensive injury sustains the local levels of growth factors and cytokines, creating a microenvironment which promotes the ongoing activation and proliferation of inflammatory cells. In particular, the persistent infiltration of macrophages in CKD leads to the activation of many intrinsic renal cells, as well as promoting the activation and infiltration of other inflammatory and immune cells, through the further release of growth factors, cytokines and *reactive oxygen species* (ROS). Indeed, it is generally accepted that persistent and/or dysregulated activation of inflammatory processes drives fibroblasts to produce and deposit ECM components.⁷⁰ In addition, cross-linking of the ECM by fibroblasts leads to altered biochemical and biomechanical matrix properties, making

them more resistant to degradation. Thus, with interstitial collagen deposition interfering with healthy parenchymal architecture and functionality,^{71, 72} fibrosis drives the progression of CKD by subjecting the remaining nephrons to an increased workload, which subsequently drives further nephron loss.

2.2.2. Mediators of Fibrosis

Although a number of different renal cells are known to synthesise and deposit ECM, such as fibroblasts, mesangial and tubular epithelial cells,⁷³ the main contributors to ECM deposition in fibrosis are myofibroblasts.^{59, 60} While virtually non-existent in normal physiological states in the kidney, elevated levels of myofibroblasts have been reported in cases of CKD, including diabetic nephropathy.⁷⁴ Like fibroblasts, myofibroblasts are involved in the synthesis and deposition of ECM components, as well as remodelling of ECM with the production of proteolytic enzymes, after injury. Furthermore, the *de novo* expression of *alpha-smooth muscle actin* (α SMA) allows for the contraction of the wound, facilitating the wound healing process. As expected, their persistence in CKD leads to the dysregulation of the ECM, where the extent of myofibroblast infiltration generally correlates with decline in renal function,⁷⁵ promoting the excessive accumulation of ECM components, while reducing its turnover. Despite its importance in the development of fibrosis, the source of myofibroblasts *in vivo* remains controversial.⁷² While it is undisputed that myofibroblasts can be derived from a number of different sources and processes, there is no general consensus on the relative contribution of each source with respect to the development of renal fibrosis *in vivo*.⁷⁶ Myofibroblasts have been proposed to be activated by the following; proliferation/activation of residential fibroblasts,⁷⁷ recruitment of bone-marrow derived cells,^{78, 79} transdifferentiation from tubular epithelial cells,⁸⁰ endothelial cells,⁸¹ pericytes,⁸² and macrophages.⁸³ The complex nature of the fibrotic process is not only complicated by the ability of myofibroblasts to arise from a variety of different sources but also the observation that activated myofibroblasts from these sources can undergo partial transdifferentiation and not necessarily acquire a complete set of mesenchymal-like traits.^{59, 84} The latter has made the validation of the relevance of myofibroblasts activation from these sources *in vivo* in renal disease development difficult. Nonetheless, it is generally accepted that myofibroblasts are the key ECM producing cells in renal fibrosis, with the investigation into pathways involved with the regulation of myofibroblast activity and/or activation garnering great interest.

As mentioned above, the actions of fibroblasts, as well as their activation/differentiation into myofibroblasts, are regulated by a combination of factors, including cytokines and other soluble mediators, ECM components and mechanical stress.⁶⁹ Injured renal cells, as well as infiltrating inflammatory cells, release a plethora of cytokines and other molecules which contribute towards the development of renal disease. Among the many cytokines which have been implicated in the fibrotic process, including *platelet-derived growth factor* (PDGF),⁸⁵ *connective tissue growth factor* (CTGF),⁸⁶ and angiotensin II,^{87, 88} the most extensively studied and, arguably, the most important profibrotic cytokine is *transforming growth factor beta* (TGF β).

2.2.3. Transforming growth factor beta (TGFβ)

2.2.3.1. An overview of TGFβ

Transforming growth factor beta (TGFβ), a member of the larger TGFβ superfamily, is a multifunctional cytokine with many physiological roles including angiogenesis, cell cycle control, chemotaxis, differentiation, immunomodulation, haematopoiesis and ECM formation.⁸⁹⁻⁹¹ Indeed, TGFβ is recognised as a key profibrotic cytokine involved with progression of fibrotic disease, particularly in the vasculature and kidney.⁹²⁻⁹⁵ While there are three isoforms of TGFβ present in mammals and they all elicit similar responses *in vitro*,⁹⁶ the most notable and extensively studied isoform implicated in fibrosis is TGFβ1. Elevated levels of TGFβ1 have been reported in many forms of human CKD, including chronic glomerulosclerosis and diabetic nephropathy suggesting a role for TGFβ1 in the progression of fibrosis in these diseases.^{97, 98} Indeed, this was subsequently demonstrated in a number of different animal studies. Specifically, spontaneous development of fibrotic lesions, particularly in the kidney, has been reported in mice overexpressing TGFβ1, as well as one of its receptors, leading to constitutive activation of the TGFβ signalling pathway.⁹⁹⁻¹⁰³

2.2.3.2. TGFβ signalling pathway

TGFβ1 is virtually expressed by all cell types, including many residential renal cells, such as mesangial and tubular epithelial cells, with infiltrating leukocytes, with macrophages in particular, being a major source of many cytokines, including TGFβ1, in renal disease.¹⁰⁴⁻¹⁰⁶ Transcription of the TGFβ1 gene can be stimulated by a variety of different factors, including glucose at high concentrations,¹⁰⁷⁻¹¹⁰ oxidative stress,¹¹¹ and cytokines, such as TNFα and *interleukin* (IL)-1β.¹¹² In addition, TGFβ1 is known to be able to stimulate its own expression,¹¹³ with autoinduction of TGFβ1 in proximal tubular epithelial cells being suggested to contribute towards the sustained and/or amplified TGFβ signalling observed in CKD.¹¹⁴

TGFβ1 is initially synthesised and secreted into the ECM as part of a biologically inactive complex, non-covalently bound to *TGFβ-latency-associated peptide* (LAP) and *latent-TGFβ binding proteins* (LTBP).¹¹⁵ Activation of TGFβ1 can be induced by proteolytic cleavage, interactions with integrins or the presence of *reactive oxygen species* (ROS),^{111, 116, 117} allowing TGFβ1 to bind to the *TGFβ Type II receptor* (TβRII). The recognition of the ligand leads to a conformational change of the TβRII, allowing for the formation of a heteromeric complex with the *TGFβ Type I receptor* (TβRI). TβRII subsequently transphosphorylates TβRI, allowing TGFβ-induced intracellular signalling to take place. Intracellular TGFβ signalling is largely mediated by the Smad family of proteins, through the canonical Smad-dependent pathway.^{13, 94, 118} The activated TβRI/TβRII complex phosphorylates receptor-specific Smads, Smad2 and Smad3, which are then incorporated into a complex with a common mediator Smad, Smad4 (**Figure 2.5**).¹¹⁸ The resultant phosphorylated Smad2/3/4 complex translocates into the nucleus and modulates the transcription of target genes.^{119, 120} While the Smad2/3/4 complex recognises and binds specific sequences, such as *Smad-binding*

elements (SBE), within the promoter of target genes, interactions with other transcription factors are generally required for high-affinity binding and subsequent transcription of target genes.¹²¹ In addition to these roles in transcription, Smad2/3 is also involved in the post-transcriptional regulation/processing of *microRNAs* (miRNA). After the translocation of the activated Smad3 into the nucleus, it facilitates the production of mature miRNA through the Drosha complex, in a seemingly Smad4-independent manner.^{122, 123} Therefore, by signalling through the canonical Smad-dependant pathway, TGF β exerts its physiological and pathological actions through the transcriptional and posttranscriptional modulation of gene expression.¹²⁴

TGF β signalling also utilises a number of different intracellular signalling pathways to confer its many physiological roles. Indeed, in addition to the canonical Smad-dependent pathway, the activated TGF β receptor complex is also known to activate the *mitogen-activated protein kinase* (MAPK), Rho-like GTPase and *phosphatidylinositol-3-kinase* (P3K)/Akt/*mammalian target of rapamycin* (mTOR) pathways.^{77, 125-128} While the physiological actions of TGF β 1 are highly diverse and generally context-dependent, it is the dynamic interaction among these intracellular pathways, as well as the cross-talk with many other signalling pathways, which enables the diverse cellular response associated with TGF β signalling. For example, regulation of the canonical Smad pathway has been identified to occur in a number of ways. The transcription of Smad7, which can be induced by Smad3,¹²⁹ allows for the inhibition of TGF β signalling activity through a number of different ways, such as degradation of the T β RI or inhibition of Smad2/3/4 activity.^{130, 131} In addition, ras signalling through the MAPK pathway has been shown to attenuate Smad2/3 nuclear accumulation,¹³² while transcriptional corepressors, such as *Sloan-Kettering Institute proto-oncogene* (Ski), *Ski-related novel gene, non Alu-containing* (SnoN) and *transforming growth interacting factor* (TGIF), modulate the effects of Smad signalling.^{133, 134}

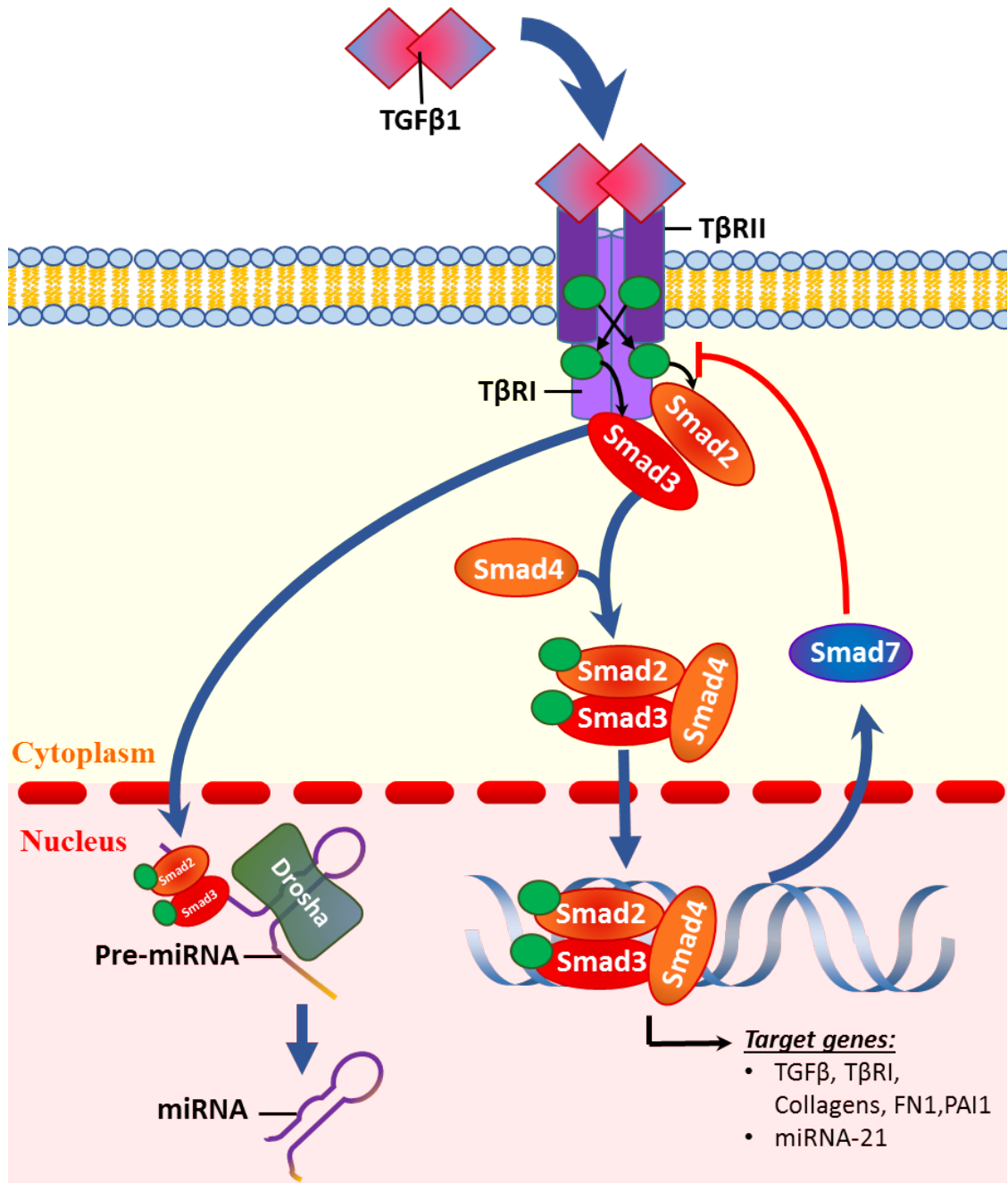


Figure 2.5. Induction of the canonical Smad-dependent pathway by TGFβ1 in renal fibrosis. Upon activation, TGFβ1 dimers activates TβRII, which subsequently induces the formation of heteromeric complex with TβRI. TβRII then transphosphorylates TβRI, leading to the phosphorylation of Smad2 and Smad3, which subsequently complexes with Smad4 and then translocates into the nucleus. The Smad2/3/4 complex, which can be aided by interactions by wide-range of transcription factors, then modulates the transcription of target genes, particularly profibrotic genes, such as collagens, fibronectin (FN1) and αSMA, as well as several miRNA species, such as miRNA-21 and miRNA-192. Smad2/3 is also involved in the post-transcriptional processing of miRNA, which could ultimately promote the development of renal fibrosis. While the expression of inhibitory Smads, like Smad7, is induced by Smad2/3/4, which would otherwise allow for the self-regulation of TGFβ signalling, Smad7 expression and/or activity is often reduced in CKD. Adapted from Meng, X-M., Nikolic-Paterson, DJ., and Lan, HY. (2016).⁷⁶

2.2.4. TGF β in CKD and Fibrosis

2.2.4.1. Pathological roles of TGF β in DN

As mentioned above, TGF β has been implicated as a key cytokine in the progression of CKD, with enhanced activation of the TGF β signalling pathway commonly observed in human diabetic nephropathy.^{135, 136} In fact, short periods of hyperglycaemia are sufficient enough to induce elevated levels of renal TGF β 1 in humans,¹³⁷ and a positive association has been reported between serum levels of TGF β 1 and increased risk of renal disease in African-American men.¹³⁸ Furthermore, overexpression of TGF β 1 has been associated with an exacerbation of diabetes-associated renal injury in mice.¹³⁹

The effect of TGF β signalling in CKD is largely context-dependent, as manifested by the differences in resultant effects in various specific renal cells (**Figure 2.6**).¹⁴⁰ In podocytes, TGF β 1 may induce their detachment from the GBM,¹⁴¹ as well as subsequent apoptosis, which will ultimately lead to podocyte effacement and loss.¹⁴² While TGF β 1 has shown to induce the proliferation of mesangial cells,¹⁴³ it has also been shown to suppress proliferation,¹⁴⁴ as well as inducing autophagy and potentiating pro-apoptotic signals in tubular epithelial cells.^{102, 145, 146} Further demonstrating the complex nature of TGF β signalling, TGF β may also afford opposing effects on vascular cells through different pathways, such as inducing or inhibiting angiogenesis through an *activin receptor-like kinase 1* (ALK1)/Smad1/5-dependent mechanism or a Smad2/3-dependent pathway, respectively.^{90, 147} TGF β activity has also been implicated in a number of pathological processes commonly associated with diabetic nephropathy, such as induced expression of *vascular endothelial growth factor* (VEGF) in podocytes,¹⁴⁸ as well as *Glucose transporter 1* (GLUT1) expression in mesangial cells.¹⁴⁹

The critical pathological role of TGF β in chronic diseases is, undoubtedly, to promote profibrotic processes, as evident by its involvement with the development of glomerulosclerosis and tubulointerstitial fibrosis.^{140, 150} Although TGF β signalling may be self-regulated through a negative feedback loop via the production of inhibitory Smads or the interactions with other signalling pathways, the presence of persistent and/or extensive injury drives TGF β -mediated processes towards overall increased production and reduced turnover of ECM components.

2.2.4.2. Promotion of ECM deposition

TGF β signalling is able to promote the deposition of ECM components via various means. The transcription of many ECM components, including fibronectin and collagens,^{107, 151-153} is directly induced by TGF β 1.¹⁵⁴ In fact, the transcription of procollagen is considered to be the rate-limiting step in collagen synthesis.¹⁵⁵ Although the transcription of each matrix gene may be regulated by certain TGF β -binding partners,¹⁵⁶ many are Smad3-dependent, particularly collagen I,^{157, 158} with the presence of certain sequences, such as SBE, in their promoter regions.^{13, 119, 120, 153, 159} In addition, TGF β has also been demonstrated to be involved in the transcriptional and post-transcriptional

modulation of several miRNA species, with the upregulation of miRNA-21, as well as downregulation of miRNA-29 and miRNA-200, observed in renal disease.¹⁶⁰⁻¹⁶² TGF β signalling may also induce or inhibit the transcription of genes involved with the post-translational modification of histones, thereby indirectly modulating the expression of target genes, particularly ECM components.¹⁶³

2.2.4.3. Inhibition of matrix turnover

In addition to stimulation of fibrotic genes, TGF β has been reported to reduce matrix turnover by a number of mechanisms. Firstly, TGF β induces the downregulation of *matrix metalloproteinases* (MMP)/collagenase expression.^{164,165} Indeed, it has been previously demonstrated that inflammatory cytokine-induced MMP1 transcription is inhibited by TGF β 1 in a Smad3/4 dependent manner.¹⁶⁶ Secondly, this may be complemented with an associated upregulation of *tissue inhibitors of MMPs* (TIMPs) or *plasminogen activator inhibitor-1* (PAI1).^{105,167,168} Lastly, TGF β has also been known to induce the expression of lysyl oxidases,¹⁶⁹ which may result in abnormal matrix crosslinking and increased resistance of the ECM to proteolytic degradation.

2.2.4.4. Activation of matrix-producing cells

A large body of *in vitro* data have implicated TGF β as a major activator of myofibroblasts in fibrosis.^{79,83} Stimulation of cultured cells with TGF β 1 has been shown to induce the acquisition of mesenchymal-like traits, such as enhanced migratory capacity, elevation in apoptosis resistance and production of ECM components, with a concomitant loss of some of their original cell lineage traits.^{84,170,171} Although many of the changes seen in TGF β -dependent mesenchymal transition appear to be Smad3 dependent, such as the induction of α SMA in epithelial cells,¹⁷² other effectors and signalling pathways are also known to be involved in the activation of myofibroblasts.⁸⁴

2.2.4.5. Amplification of proinflammatory and profibrotic signals

In addition to the mechanisms outlined above, TGF β may contribute towards the progression of renal disease through the propagation and amplification of proinflammatory and profibrotic signals. Constitutive TGF β signalling in tubular epithelial cells has been shown to induce acute tubular injury, accompanied by interstitial inflammation.¹⁷³ In addition to profibrotic cytokines, TGF β has also been shown to stimulate the production of proinflammatory cytokines, such as IL8 and *monocyte chemoattractant protein 1* (MCP1), in proximal tubular cells,¹⁷⁴ as well as accessory proteins, such as endoglin and integrins, which facilitate cell-to-matrix adhesion.¹⁷⁵⁻¹⁷⁷ As a result, the release of these cytokines leads to the persistent infiltration of activated macrophages and increased accumulation of myofibroblasts, which subsequently sustains the high levels of TGF β observed in CKD.¹⁷⁸ The activation of the macrophages, in particular, leads to a positive feedback loop, whereby increased production and secretion of cytokines leads to the activation of residential renal cells, which stimulates the release of more cytokines, thus contributing to a vicious self-perpetuating cycle which, ultimately, results in the development of progressive CKD.

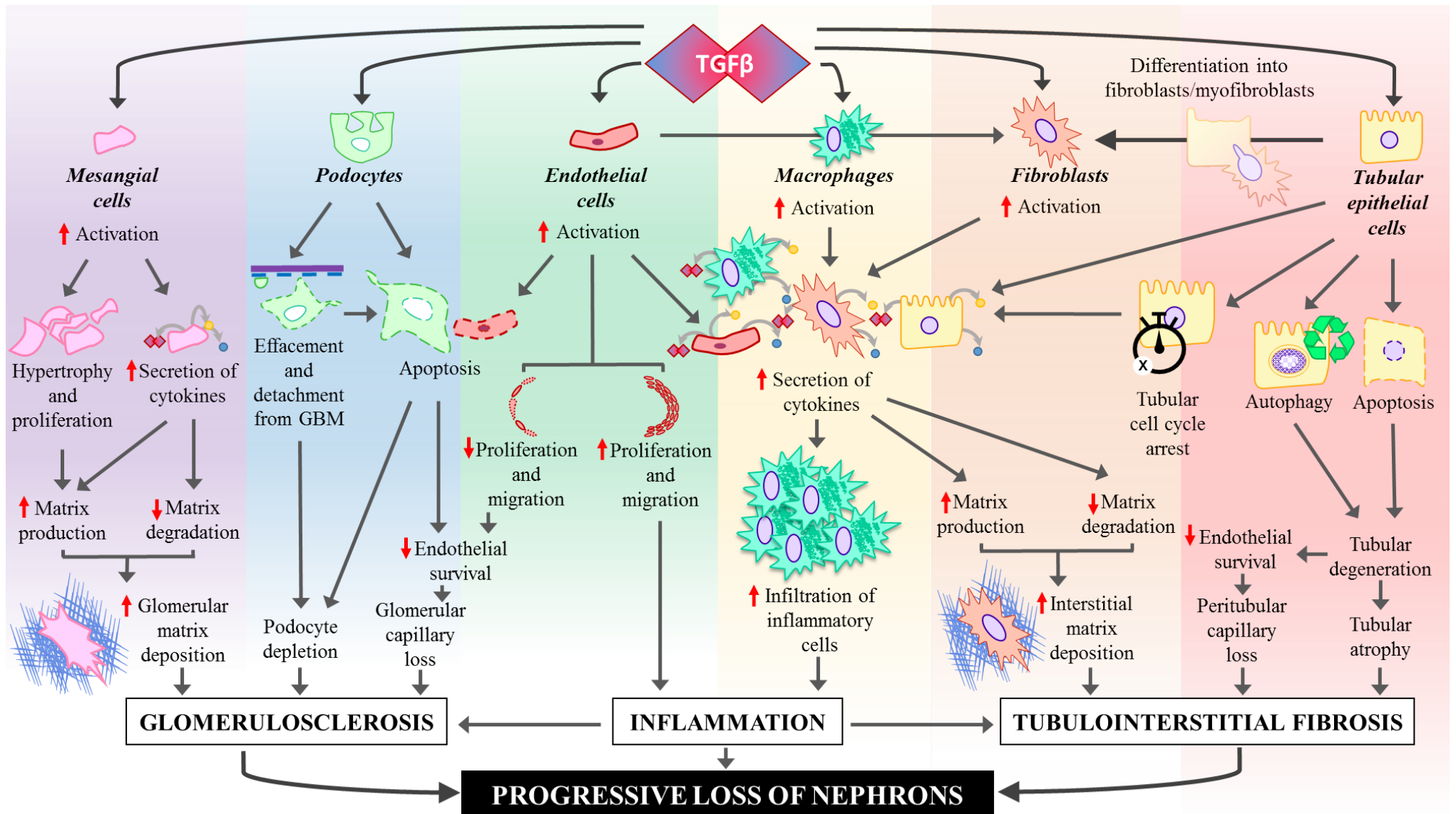


Figure 2.6. The pathological role of TGFβ in CKD, particularly diabetic nephropathy. TGFβ is able to produce a wide variety of effects, which is usually cell-type and context dependant. Ultimately, the net effect of all these processes contribute towards the progressive loss of nephrons in CKD.

2.2.5. Targeting the TGF β signalling pathway

2.2.5.1. Inhibition of the TGF β signalling pathway

Our understanding of the TGF β signalling pathway has been elucidated by a combination of genetic and pharmacological studies (**Table 2.1**). Not only have these studies revealed the relevance of the intrinsic components of the TGF β signalling pathway in the context of fibrosis, they also provide the theoretical basis for therapeutic strategies to combat the progression of fibrosis in human disease.^{124, 179, 180} Inhibition of TGF β signalling has frequently been demonstrated to ameliorate renal fibrosis in a number of animal studies. The use of TGF β neutralising antibodies, in particular, were shown to be effective in attenuating renal fibrosis in a number of animal models, such as diabetic nephropathy,¹⁸¹⁻¹⁸³ and obstructive nephropathy.^{184, 185} In addition, an engineered TGF β neutralising monoclonal antibody, fresolimumab (GC1008), has been used in human clinical trials, particularly in focal segmental glomerulosclerosis.¹⁸⁶ Pharmacological agents, such as pirfenidone, designed to inhibit TGF β signalling have also been demonstrated to attenuate fibrosis in mouse models of glomerulonephritis,¹⁸⁷ diabetic nephropathy,¹⁸⁸ and obstructive nephropathy.¹⁸⁹ The success of these animal studies prompted their use in human patients with focal segmental glomerulosclerosis,¹⁹⁰ as well as in diabetic nephropathy.¹⁹¹

Complete blockade of TGF β signalling activity, however, has been associated with undesirable side-effects. As mentioned above, TGF β is a pleiotropic cytokine with many regulatory roles. The physiological importance of this pathway is emphasised by animal studies with genetic deletion of either TGF β receptor being associated with embryonic lethality.¹⁹²⁻¹⁹⁴ More importantly, although TGF β signalling promotes fibrosis progression in chronic disease, TGF β is also known to be involved in the modulating the inflammatory response, emphasised by the severe and spontaneous inflammatory phenotype observed in TGF β 1 deficient mice,^{54, 195} as well as in inducible T β RII knockout mice.¹⁹⁶ In addition to its modulatory roles on circulating inflammatory and immune cells,¹⁹⁷ TGF β is known to modulate the activation of vascular smooth muscle cells,¹⁹⁸ and macrophages,¹⁹⁹ as well as contributing towards the inhibition of renal inflammation through an *inhibitor of kappa B* (I κ B α)/Smad7-dependent mechanism.^{200, 201} These effects are not limited to the kidney, as increases in aortic rupture susceptibility due to angiotensin II-induced aortic aneurysm development has been seen with the use of TGF β neutralising antibodies.²⁰² In addition, despite promising results in animal studies, the use of TGF β neutralising antibodies have proven fruitless in human clinical studies. Administration of metelimumab (CAT-192) in a clinical trial of systemic sclerosis ended with no evidence of efficacy,²⁰³ while a recent phase II clinical trial was ended prematurely due to alleged ineffectiveness of TGF β neutralising antibodies (LY2382770) in diabetic nephropathy.²⁰⁴ Granted, the failure of the latter clinical study may have been due to the low dose of TGF β inhibitor used out of concern of likely side-effects associated with more rigorous inhibition of

the TGF β signalling pathway. However, in the case of the former agent, the administration of metelimumab was associated with the development of severe adverse events, although these were not more frequent in patients receiving higher doses.

Nonetheless, the TGF β signalling pathway remains an attractive target to combat fibrosis progression in CKD. Not only is the renoprotective efficacy of conventional therapies against diabetic nephropathy, particularly ACE inhibitors, associated with reduced TGF β levels and subsequent attenuation of signalling activity,²⁰⁵⁻²⁰⁹ the effectiveness of anti-TGF β strategies in various forms of organ fibrosis demonstrates the critical pathological role of TGF β in fibrosis and the therapeutic potential of modulating this signalling pathway. Thus, an ideal therapeutic strategy would be to attempt to prevent the profibrotic actions of TGF β , while avoiding the deleterious effects associated with complete inhibition of TGF β signalling.

2.2.5.2. *Exploring the TGF β signalling pathway*

Complete inhibition of TGF β signalling can lead to broad biological effects, particularly substantial deleterious effects. Inhibition of downstream components of the TGF β signalling pathway, however, may provide a safer alternative to afford renoprotective effects, while minimising the possibility of adverse effects. Investigations into specific components of the TGF β signalling pathway, while being informative, demonstrate the complexity of this pathway. As mentioned above, the main effectors in the TGF β signalling pathway are the Smad family of proteins. The contributions of the receptor-mediated Smads, Smad2 and Smad3, in the progression of fibrosis are of particular interest. Interestingly, despite both Smads being activated upon TGF β 1 stimulation, Smad2 and Smad3 appear to possess differential effects on TGF β signalling. Indeed, absence of either Smad2 or Smad3 expression *in vitro* and *in vivo* has revealed different roles for each Smad in development, as well as under pathological conditions. Indeed, the global genetic deletion of Smad2 in mice is embryonically lethal,²¹⁰ and tubule-specific Smad2 deficient mice have exhibited an exacerbation of renal fibrosis development in a mouse model of obstructive nephropathy.²¹¹ On the other hand, Smad3 deficient mice, while embryonic viable, have been associated with an increase in mortality in a number of independent studies.²¹²⁻²¹⁴ In addition, these Smad3 deficient mice were also observed to exhibit an impaired inflammatory response in the skin.²¹⁵ Nonetheless, the absence of Smad3 has been associated with an attenuation of renal fibrosis in experimental murine models of obstructive nephropathy,²¹⁶ diabetic glomerulosclerosis,²¹⁷ and acute ischaemic renal injury.²¹⁸ These findings demonstrate that targeting downstream components of TGF β signalling represents a more reliable and safer approach to retard renal fibrosis in CKD. Thus, our laboratory has investigated the pathological role of a potent enhancer of the TGF β signalling pathway.

Table 2.1. Genetic and pharmacological studies on TGF β signalling in renal disease

Target	Method	Major Findings
Inhibition or Absence		
<i>TGFβ</i>	Neutralising antibody	<ul style="list-style-type: none"> Attenuation of renal fibrosis in rodent models of Type 1,^{181, 219} and Type 2 diabetic nephropathy,^{182, 220} obstructive nephropathy,^{184, 185, 221} and ischaemia/reperfusion injury.²²²
	Genetic Knockout	<ul style="list-style-type: none"> Macrophage-specific TGFβ-knockout did not attenuate renal fibrosis in acute renal injury models of obstructive nephropathy and ischemic/reperfusion injury.²²³ Exacerbation of renal inflammation in a mouse model of ischaemic/reperfusion injury with contralateral nephrectomy.²²⁴
	Anti-sense oligonucleotides	<ul style="list-style-type: none"> Attenuation of renal fibrosis in a model of obstructive nephropathy.²²⁵
<i>TGFβ Receptors</i>	Pharmacological Inhibitor	<ul style="list-style-type: none"> Oral administration of GW788388 attenuates renal fibrosis in db/db mice.²²⁶
<i>TβRI</i>	Pharmacological Inhibitor	<ul style="list-style-type: none"> Administration of IN-1130 suppresses renal fibrosis in rats,²²⁷ as well as adult mice in obstructive nephropathy.²²⁸ SB431542 administration attenuates <i>unilateral ureteric obstruction</i> (UUO)-induced renal fibrosis.²²¹
<i>TβRII</i>	Genetic Knockout	<ul style="list-style-type: none"> Attenuation of HgCl₂-induced proximal tubular injury in proximal tubule-specific/γ-glutamyl transferase-promoter driven TβRII knockout mice.²²⁹ Attenuation of UUO-induced renal fibrosis, associated with impairment of TGFβ/Smad3 signalling, but also an exacerbation of UUO-induced renal inflammation in tubule-specific/Cadherin 16-promoter driven TβRII knockout mice.²³⁰

		<ul style="list-style-type: none"> Induced knockout of TβRII prior to disease initiation in matrix-producing (COL1A2 and Tenascin-C promoter driven) interstitial cells was unable to prevent renal fibrosis in UUO and aristolochic acid renal injury models.²³¹ However, αSMA-promoter driven knockout of TβRII attenuates UUO-associated renal fibrosis and inflammatory cell infiltration.⁷⁸
<i>Smad3</i>	Genetic Knockout	<ul style="list-style-type: none"> Attenuation of UUO-associated renal fibrosis, inflammation and tubular apoptosis in Smad3 KO mice.^{212, 216} Attenuation of aristolochic acid-induced renal fibrosis in Smad3 KO mice.²³² Attenuation of <i>streptozotocin</i> (STZ)-induced diabetic glomerulosclerosis,²³³ without affecting albuminuria.²¹⁷ Smad3 deficiency was associated with reductions in renal injury and IL6 expression in a model of bilateral renal ischaemic/reperfusion injury.²¹⁸
	Pharmacological Inhibitor	<ul style="list-style-type: none"> Administration of SIS3 was able to attenuate diabetes-associated renal fibrosis, without affecting albuminuria.²³⁴ Administration of GQ5 selectively inhibited Smad3 phosphorylation, and subsequently led to attenuation of renal fibrosis in a rat model of obstructive nephropathy.²³⁵
<i>Smad2</i>	Genetic knockout	<ul style="list-style-type: none"> Kidney-specific/Cadherin 16-promoter driven Smad2 knockout exacerbates UUO-associated renal fibrosis.²¹¹

<i>Smad4</i>	Genetic knockout	<ul style="list-style-type: none"> • Kidney-specific/Cadherin 16-promoter driven Smad4 mutant mice exhibited an exacerbation of renal inflammation, as seen by increased inflammatory cell infiltration and upregulation of inflammatory markers (TNFα, IL1β, MCP1 and ICAM1), in a model of UUO. In addition, UUO-induced renal fibrosis was attenuated in these animals, by disrupting Smad3/4 promoter activity.²⁰¹
<i>Smad7</i>	Genetic knockout	<ul style="list-style-type: none"> • Exacerbation of renal fibrosis and inflammation in mouse models of UUO,²³⁶ and aristolochic acid-induced nephropathy.²³⁷
<i>miRNA-21</i>	Silencing	<ul style="list-style-type: none"> • Ultrasound-mediated gene transfer of inducible miRNA-21 <i>short hairpin RNA</i> (shRNA) plasmids attenuates renal fibrosis progression in mouse models of UUO,¹⁶² and Type 1,²³⁸ and 2 diabetic nephropathy.²³⁹
	Genetic knockout	<ul style="list-style-type: none"> • miRNA-21 deficiency attenuated renal fibrosis induced by UUO and ischaemia/reperfusion injury.²⁴⁰
<i>miRNA-214</i>	Combination	<ul style="list-style-type: none"> • Genetic deletion or pharmacological inhibition of miRNA-214 attenuates UUO-associated renal fibrosis.²⁴¹
<i>Non-Smad pathways</i>	Pharmacological Inhibitor	<ul style="list-style-type: none"> • Administration of U0126 or LY-294002, Erk1/2 and PI3K inhibitors, respectively, attenuated renal fibrosis in a mouse model of UUO.²⁴² • Administration of U0126 exacerbated ischaemia/reperfusion-associated renal injury and fibrosis.²⁴³ • Administration of LY33353, a Protein kinase C-β inhibitor, attenuates diabetes-associated albuminuria and glomerulosclerosis in db/db mice.²⁴⁴

Enhancement

TGFβ

Genetic
overexpression

- Dose-dependent increase of TGFβ1 expression exacerbates diabetes-associated renal injury in Akita mice.¹³⁹
- Overexpression of TGFβ was associated with an attenuation of UUO-associated renal inflammation.²⁰⁰

TβRI

Genetic
Overexpression

- Inducible tubular epithelial cell-specific/Pax 8-promoter driven TβRI overexpression mouse strain spontaneously presents with pathological features reminiscent of AKI, including tubular injury, oxidative stress and infiltration of inflammatory cells.¹⁷³

Latent TGFβ

Genetic
overexpression

- Overexpression of latent TGFβ protein attenuates renal fibrosis in models of UUO,²⁴⁵ and crescentic glomerulonephritis.²⁴⁶

Smad7

- Ultrasound-mediated gene transfer of inducible Smad7 overexpression plasmids attenuates UUO-induced renal fibrosis.²⁴⁷

2.3. Cell Division Autoantigen 1 (CDA1)

2.3.1. Cell Division Autoantigen 1: An introduction

Cell Division Autoantigen 1 (CDA1) is a nuclear phosphoprotein and a member of the *nucleosome assembly protein* (NAP) family of proteins.²⁴⁸⁻²⁵¹ Encoded by the gene *Testis-specific Y-encoded-like protein 2* (TSPYL2) located on the X-chromosome,²⁴⁹ CDA1 is expressed in most mammals, with expression reported in rodents,^{252, 253} monkeys,²⁵⁴ and humans.^{255, 256} Studies investigating CDA1 have predicted several structural regions within the CDA1 protein, many of which are highly conserved among mammals. This includes a proline-rich amino-terminal domain, an arginine/lysine rich domain, a NAP domain and a carboxyl-terminal bipartite acidic tail domain (**Figure 2.6**).^{248, 257} The presence of the NAP domain suggests that CDA1 may be involved with chromatin remodelling and nucleosome assembly, as seen with other members of the NAP protein family.²⁵⁸ Indeed, CDA1 has been previously shown to be able to bind to histones and *deoxyribonucleic acid* (DNA),²⁵¹ and subsequently modulate the transcription of target genes, such as neuronal genes involved in development, particularly *Grin2a* and *Grin2b*, by directly binding to their promoters.²⁵⁹ In addition, CDA1 has also been shown to repress transcriptional activity through direct binding to proteins such as *calcium/calmodulin-dependent serine protein kinase* (CASK),²⁵¹ and the androgen receptor.²⁶⁰ Thus, it appears that CDA1 may act as a transcription factor to either induce or repress the transcription of target genes and that this may involve interactions with other transcription factors. Collectively, CDA1 has been speculated to possess many physiological and pathological roles, including cell cycle regulation, synaptic gene regulation and tumour-suppression, as well as enhancing TGF β signalling.^{250, 251, 255, 259-264}

Initially characterised as an antiproliferative protein,²⁴⁸ investigations into actions of CDA1, through a number of gene mutation and domain deletion studies, have unveiled possible mechanisms to explain its activity in physiology and pathology. The antiproliferative ability of CDA1 may be dependent on the activation of the CDA1 protein by *cyclin-dependent kinases* (CDK), with an initial investigation mapping two potential CDK phosphorylation sites, Ser20 and Thr340, within the human CDA1 protein.²⁴⁸ The latter CDK phosphorylation site may be functionally important given that, in addition to its high conservation among mammals, it is located within the NAP domain of the CDA1 protein (**Figure 2.7**). While the NAP domain has been speculated to be responsible for the interactions of some proteins to CDA1, such as p53,²⁶⁵ and the androgen receptor,²⁶⁰ with experimental data demonstrating binding with cyclin B,²⁶⁶ the presence of the acidic carboxyl tail has been proposed to be responsible for the antiproliferative abilities of CDA1. In addition to an initial investigation where an amino-terminal portion of human CDA1 (residues 2-452) was unable to arrest cell growth,²⁴⁸ an independent group utilised genetic deletion and domain swapping studies to demonstrate that the acidic carboxyl tail of CDA1 was required for the suppression of cyclin B/CDK1 activity and subsequent cell cycle arrest at the G2/M phase.²⁶⁶ The acidic carboxyl tail has also been proposed to

be responsible for other functions of CDA1 including repression of androgen receptor transcriptional activity,²⁶⁰ and degradation of *human hepatitis B virus X protein* (Hbx) through a ubiquitin-proteasome dependent pathway.²⁶⁷ The direct mechanisms of how these structural domains influence the actions of CDA1 and their relevance in disease development *in vivo* remain to be investigated.

2.3.2. CDA1 and disease

CDA1 has been proposed to play important roles in the development of chronic disease, particularly those associated with fibrosis. Lowly expressed in most tissues under normal physiological conditions,^{252-254, 268} elevated levels of CDA1 expression have been observed in diabetes-associated atherosclerosis and diabetic nephropathy in rodents and humans.^{255, 256, 262} The upregulation of CDA1 in these diseases coincide with elevated TGF β expression levels and signalling activity. Conversely, in pathologies associated with reduced TGF β activity, such as cancer and aortic aneurysm, CDA1 expression is downregulated as seen in human biopsy samples of malignant lung,²⁶¹ kidney,²⁵⁶ and liver tissue,²⁶⁹ as well as in human abdominal aortic aneurysm biopsy samples.²⁷⁰ Furthermore, it has been reported that human glioma patients with reduced levels of CDA1 had a poorer prognosis.²⁷¹

2.3.3. CDA1 and TGF β : A synergistic relationship

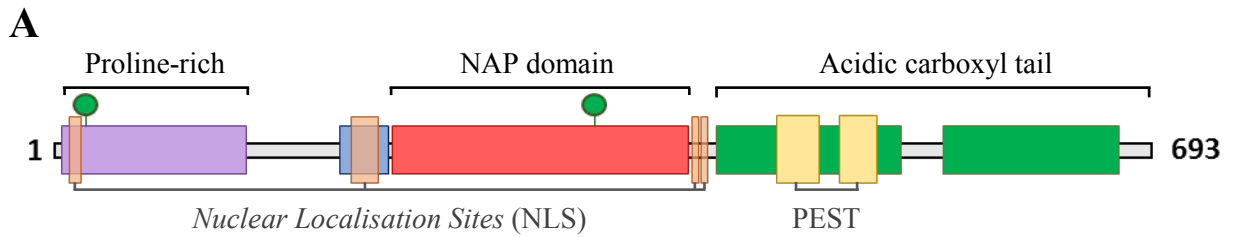
Initial studies on CDA1 reported that it was a potential target gene in the TGF β signalling pathway. Human lung cancer cell lines treated with TGF β 1 induced the expression of a gene designated as *Differentially Expressed Nucleolar TGF β 1 Target* (DENTT),²⁵⁰ which was later revealed to be CDA1.²⁶¹ This response to TGF β treatment was also observed in vascular smooth muscle cells and renal proximal tubule cells.^{255, 262} Subsequent studies, however, demonstrate that CDA1 is not just a downstream target gene of TGF β but also a critical enhancer of the profibrotic actions of TGF β signalling.^{255, 262} Overexpression of CDA1, through adenoviral infection, led to the enhanced activation of Smad and MAPK signalling pathways and consequent upregulation of profibrotic genes, such as CTGF, collagens and fibronectin, in a dose-dependent manner. These effects were further amplified by the addition of exogenous TGF β 1 and found to occur in a T β RI-dependent manner.²⁷² Conversely, silencing CDA1 had an ameliorating effect on TGF β signalling. Indeed, the use of CDA1-specific *small interfering RNAs* (siRNA) decreased but did not completely block the phosphorylation and consequent activation of Smad3. Indeed, the expression of the aforementioned TGF β -stimulated profibrotic genes, particularly collagens and CTGF, were ultimately blocked with the introduction of these CDA1-specific siRNA.²⁵⁵

2.3.4. CDA1 and *in vivo* models of diabetic nephropathy

Due to the modulatory role of CDA1 on TGF β signalling *in vitro*, as well as the *in vivo* observations of CDA1 upregulation in human fibrotic diseases, it has been proposed that targeting CDA1 might have therapeutic potential in fibrosis (**Figure 2.8**). This hypothesis was examined through the use of global genetic deletion of the CDA1 encoding gene, *Tsply2*, in a mouse model of

diabetic nephropathy.²⁵⁶ Utilising the loxP/Cre recombination system, deficiency of CDA1 did not appear to cause any abnormal phenotypes, when compared to wild type mice.²⁵⁶ This finding has also been observed by other independent groups,^{257, 264} despite a suggested role for CDA1 in tumour-suppression. The lack of adverse effects in CDA1 knockout mice further suggests that TGF β signalling is not completely blocked by the absence of functional CDA1, which would be otherwise embryonically lethal and/or have severe side-effects.

CDA1 deficiency, however, had a renoprotective effect in mouse models of *streptozotocin* (STZ)-induced diabetic nephropathy.²⁵⁶ In the two mouse strains examined, C57BL6 and *apolipoprotein E* (ApoE) *knockout* (KO), the latter being more susceptible to glomerulosclerosis,²⁷³ diabetes-associated profibrotic gene expression, such as TGF β 1 and collagens, was attenuated in CDA1 KO mice. These transcriptional changes correlated with a reduction in renal injury indices, as well as a reduction in ECM deposition, in both the tubules and glomeruli. These reductions occurred despite there being no significant differences in metabolic parameters between CDA1 KO and wildtype diabetic mice. Interestingly, these renoprotective effects were more pronounced in ApoE KO mice, as seen by the reduction in diabetes-associated albuminuria, as well as renal hypertrophy, in diabetic CDA1/ApoE *double KO* (dKO) mice when compared to diabetic ApoE KO mice.²⁵⁶ The renoprotective effect of CDA1 deficiency was demonstrated to be due to an amelioration of the TGF β signalling response, as shown by reduced *phosphorylated Smad3* (pSmad3) immunostaining in diabetic CDA1/ ApoE dKO mouse kidneys, as well as the ameliorated response of primary renal cells isolated from CDA1 KO mice towards exogenous TGF β . These findings suggest that CDA1 is a potential molecular candidate to target against renal diseases associated with enhanced TGF β activity, such as diabetic nephropathy.



B

human	1	MDRPDEGPPAKTRRLSSSESPQRDP PPPP	-----	PPPPLRLPLP	40		
chimpanzee	1	MDRPDEGPPAKTRRLSSSESPQRDP PPPP	-----	PPPPLRLPLP	40		
mouse	1	MDRPDEGPPAKTRRLSSSESPQRDLPP	-P	-----	PPPPLRLPLP	39	
cat	1	MDRQDEGPPAKARRLSSSEPAQHDQL	PPPPPPPPPP	PPPLRLPLP	50		
cattle	1	MDRADEGPPAKARRLSGSEPPQSE	LLPPPPPPPP	-----	PPPPLRLPLP	46	
deer	1	MDRPDEGPPAKARRLSGSEPLSEL	-----	PPPPPP	-----	PPPPLRLPLP	41
beaver	1	MDRPDEGPPAKTRRLSSPEPPQRDP	PPPP	-----	PPPPLRLPLP	40	
seal	1	MDRQDEGPPAKARRLSSSEPSQHDQL	LPLPPPPPP	-----	PPLLRLPLP	43	
NLS							
human	41	PPQQRPRLQEETEAAQVLADMRGV	GLGPALPPPPYV	ILEEGGIRAYFTL	90		
chimpanzee	41	PPQQRPRLQEETEAAQVLADMRGV	GLGPALPPPPYV	ILEEGGIRAYFTL	90		
mouse	40	PPQQRPRPQEETEAAQVLADMRGV	-GPTLPPPLPYV	ILEEGGIRAYFTL	87		
cat	51	PPEQRPRLQEETEAAQVLADMRGV	GLGPALPPPPYV	ILEEGGIRAYFTL	100		
cattle	47	PPQQRPRLQEETEAAQVLADMRGV	GLGPALPPPPYV	ILEEGGIRAYFTL	96		
deer	42	PPQQRPRLQEETEAAQVLADMRGV	GLGPALPPPPYV	ILEEGGIRAYFTL	91		
beaver	41	PPQQRPRLREETEAAQVLADMRGV	GLGPTLPPPPYV	ILEEGGIRAYFTL	90		
seal	44	PPEQRPRLREETEAAQVLADMRGV	GLGPALPPPPYV	ILEEGGIRAYFTL	93		
NLS							
human	91	GAECPGWDSTIESGYGEAPPPTES	LEALPTPEASGG	SLEIDFQVQSSSF	140		
chimpanzee	91	GAECPGWDSTIESGYGEAPPPTES	LEALPTPEASGG	SLEIDFQVQSSSF	140		
mouse	88	SAESPGWDHAMESGFGEAP-STG	IMETLPSSEISGG	SLEIDFQVAEPSSL	136		
cat	101	GSGGPGWEPPEMESGYGEAPPPTES	LETYSPSEASGG	SVEIDFQVVEPGSF	150		
cattle	97	GAGGPGWEPAVESGYGESPLAES	LETLSPSEVSGE	SLEIDFQVTEPSSF	146		
deer	92	GAGGPGWEPAVESGYGGSSPPVES	LETLSPSEVSGG	SLEIDFQVTEPSSF	141		
beaver	91	GAGGPGWDPAIESGYGEAPPPTGS	LETLPPSESSGG	SLEIDFQVAESSL	140		
seal	94	GAGSPGWEPAMESGYGGAPPPTES	LETFSPSEASGG	SLEIDFQVIEPSSF	143		
NLS							
human	141	GGEGALETCSAVGWAPQRLVDPKS	KEEAIIIVEDEDE	DERESMRSRRRR	190		
chimpanzee	141	GGEGALETCSAVGWAPQRLVDPKS	KEEAIIIVEDEDE	DERESMRSRRRR	190		
mouse	137	-GEKALETCSLGGWGPQMLVGPKR	KEEAIIIVEDEDE	DDKESVRRRQRRR	185		
cat	151	AGENVLETCSAGHWAYQRLTGPGG	KEEAIIIVEDDDE	DEKESVRKRR	197		
cattle	147	AGEKALETCSAGGRGYQRLAGPRG	REETVIVEDDDE	DEKESVRKRR	193		
deer	142	AGEKALETCSAGGRGYQRLAGPRG	REETVIVEDDDE	DEKESVRKRR	188		
beaver	141	AGEKALETCSAVGWGPQVLVGPKR	KEEAIIIVEDEDE	ENVKESVRR	188		
seal	144	AGEKALETCSAGEWGYQRLAGPRG	KEEAIIIVEDDDE	DEKESVRKRR	190		
NLS							
human	191	RRRRRKQRKVKRESRERNAERM	ESILQALEDIQLD	LEAVNIKAGKAF	LRL	240	
chimpanzee	191	RRRRRKQRKVKRESRERNAERM	ESILQALEDIQLD	LEAVNIKAGKAF	LRL	240	
mouse	186	RR--RRKQRKAKESRERSAQRME	ESILQALESIQMD	LEAVNIKAGKAF	LRL	233	
cat	198	RRRKRKQRKVKKESK-KNAEKI	ECILQALENIQLD	LEAVNIKAGKAF	LRL	246	
cattle	194	RRRKRKPRKVKRESPEKNAEKI	ECILQALENIQLD	LEAVNIKAGKAF	LRL	243	
deer	189	RRRKRKPRKVKRESPEKNAEKI	ECILQALENIQLD	LEAVNIKAGKAF	LRL	238	
beaver	189	RRRRKQRKVKKESKERNARME	ESILQALESIQMD	LEAVNIKAGKAF	LRL	238	
seal	191	RRRKRKQRKMKKESKERNARME	ESILQALENIQLD	LEAVNIKAGKAF	LRL	240	
NLS							
human	241	KRKF IQMRRPF LERRDL IQH	IPGFVVKAF LNHP	RISIL INRRDED	IFRY	290	
chimpanzee	241	KRKF IQMRRPF LERRDL IQH	IPGFVVKAF LNHP	RISIL INRRDED	IFRY	290	
mouse	234	KRKF IQMRRPF LERRDL IQH	IPGFVVKAF LNHP	RISIL INQRDRD	IFRY	283	
cat	247	KRKF IQMRRPF LERRDL IQH	IPGFVVKAF LNHP	KISIL INRRDED	IFRY	296	
cattle	244	KRKF IQMRRPF LERRDL IQN	IPGFVVKAF LNHP	KISIL INQRDED	IFRY	293	
deer	239	KRKF IQMRRPF LERRDL IQH	IPGFVVKAF LNHP	KISIL INQRDED	IFRY	288	
beaver	239	KRKF IQMRRPF LERRDL IQH	IPGFVVKAF LNHP	RISIL INQRDED	IFRY	288	
seal	241	KRKF IQMRRPF LERRDL IQH	IPGFVVKAF LNHP	KISIL INRRDED	IFRY	290	
Potential hydrophobic core							

human	291	LTNLQVQDLRHISMGYKMKLYFQTNPYFTNMVIVKEFQRNRSGLVSHST	340
chimpanzee	291	LTNLQVQDLRHISMGYKMKLYFQTNPYFTNMVIVKEFQRNRSGLVSHST	340
mouse	284	LTNLQVQDLRHISMGYKMKLYFQTNPYFTNMVIVKEFQRNRSGLVSHST	333
cat	297	LTNLQVQDLRHISMGYKMKLYFQTNPYFTNMVIVKEFQRNRSGLVSHST	346
cattle	294	LTNLQVQDLRHISMGYKMKLYFQTNPYFTNMVIVKEFQRNRSGLVSHST	343
deer	289	LTNLQVQDLRHISMGYKMKLYFQTNPYFTNMVIVKEFQRNRSGLVSHST	338
beaver	289	LTNLQVQDLRHISMGYKMKLYFQTNPYFTNMVIVKEFQRNRSGLVSHST	338
seal	291	LTNLQVQDLRHISMGYKMKLYFQTNPYFTNMVIVKEFQRNRSGLVSHST	340

Potential hydrophobic core

human	341	PIRWHRGQEPQARRHGNQDASHSFFSWFSNHSLPEADRIAEIKNDLWVN	390
chimpanzee	341	PIRWHRGQEPQARRHGNQDASHSFFSWFSNHSLPEADRIAEIKNDLWVN	390
mouse	334	PIRWHRGQEPQAYNRRSHDTRESFFNWFVSNHSLPEADRIAEIKNDLWVN	383
cat	347	PIRWHRGQEPQARRHRNQDTSHSFFSWFSNHSLPEADRIAEIKNDLWVN	396
cattle	344	PIRWHRGQEPRAHRHGNQDANHSFFSWFSNHSLPEADRIAEIKNDLWVN	393
deer	339	PIRWHRGQEPQARRHGNQDASHSFFSWFSNHSLPEADRIAEIKNDLWVN	388
beaver	339	PIRWHRGQEPQAHNRRNQDASHSFFSWFSNHSLPEADRIAEIKNDLWVN	388
seal	341	PIRWHRGQEPQARRHRNQDTHSFFSWFSNHSLPEADRIAEIKNDLWVN	390

human	391	PLRYYL-RERGSRIKRKKQEMKKRKTGRGCEVVMEDAPDYYAVEDIFSE	439
chimpanzee	391	PLRYYL-RERGSRIKRKKQEMKKRKTGRGCEVVMEDAPDYYAVEDIFSE	439
mouse	384	PVRYYM-RRGGYRSSRKKQHGKE-RAKNQYEMVIMEDAHDHYAIEDILSD	431
cat	397	PLRYYMMGEGGYRANRKKQEKESKNRDCEVVMEDSDDYHIMEDIISE	446
cattle	394	PVRYYMMGEGGYRTSRKKQEKESKNDKEYEVVIMDDSDYHIMEDIIGE	443
deer	389	PVRYYMMGEGGYRTSRKKQEKESKNDKEYEVVIVEDSDDYHIMEDIIGE	438
beaver	389	PLRYYM-REGGYRANRKKQEKESKARNEYEMVIMEDAHDYYGMEDILSE	437
seal	391	PLRYYMMGEGGYRANKKKQEKESKNRDKCEVVILEDSDDYHVMEDIISE	440

NLS NLS

human	440	ISDIDE-----TIDHIKISDFMETTDYFETTDNEITDINENICDSENPDH	484
chimpanzee	440	ISDIDE-----TIDHIKISDFMETTDYFETTDNEITDINENICDSENPDH	484
mouse	432	ISEIDEITDNETIHDIKISDFMETTDYFETTDNEVTDANENLCDSENPDH	481
cat	447	TSDSDDITDNETIHDIKISDFMETTDCFETTDNEITDISESLCDSESPDH	496
cattle	444	TSDSDGITDNETIHDVKISDFMETTDCFETTDNEITDISESLCDSECPGH	493
deer	439	TSDSDGITDNETIHDVKISDFMETTDCFETTDNEITDISESLCDSECPGH	488
beaver	438	ISDIDETTDNETIYDIKISDFMETTDYFETTDNEITDINESLCDSENPDH	487
seal	441	TSDSDGITDNETIHDVKISDFMETTDCFETTDNEITDISESLCDSESPDH	490

human	485	NEVPNNETTDNNE SADDHETT-D-----NNE SADDNNE-----	516
chimpanzee	485	NEVPNNETTDNNE SADDHETT-D-----NNE SADDNNE-----	516
mouse	482	SEGYNTKITDNKGSVAAA-----NPDDNSD-----	505
cat	497	NESPDNETTDNNE SPDDHETT DNNE SDDNETTDNNE SADDNNE NPDD-E	545
cattle	494	NET-----TDNNE SPDNNETTDNNE SADDKESTND-----NSENPE---	529
deer	489	NET-----TDNNE SPDNNETTDNNE SADDKESTDD-----NTENPE---	524
beaver	488	NEGPNNETTDESTDDETTDESAN-----DNESPVNNE-----	520
seal	491	NESPDNETTDNNE SPDDNETTDNNE SDDNETTDNNE SADDNNE NPDNNE	540

human	517	-----NPE DNNKNTDDNEENPNNN-ENTYGNFFFKGG	547
chimpanzee	517	-----NPE DNNKNTDDNEENPNNN-ENTYGNFFFKGG	547
mouse	506	-----DPE--EKNTYDSEDS-NSE-KADGDNTTLRDN	533
cat	546	NPDDNSENPE DNTDDNEENPD DNEENTDDNDENPDGDENPNS-AENPKGG	594
cattle	530	-----DDNTDENEENPD DND-----NADENPNGD-ENPKDG	560
deer	525	-----DENTDENEENPD DND-----NADENPIGDENPKGG	556
beaver	521	-----NLE--NKNTYDNE-----NDDGDNKNLEGS	543
seal	541	NPDENSENPE DNTDDNEENPD DNEENTDD-DENPDGDENPDGDDENPKGG	589

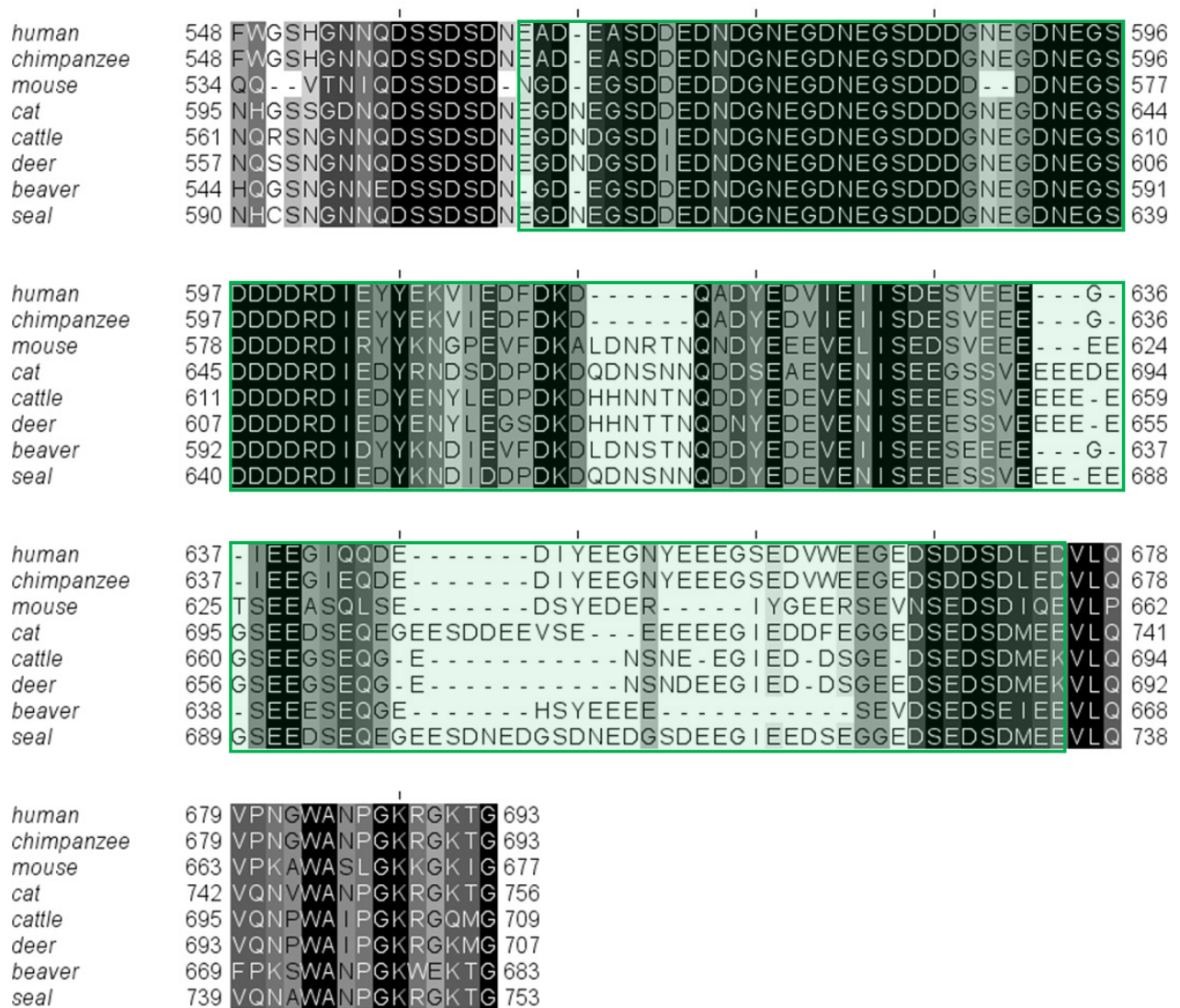


Figure 2.7. CDA1 is conserved in mammals. Schematic diagram of structural regions within the human CDA1 protein (A) and multiple sequence alignment of CDA1 protein in mammals using Clustal Omega,²⁷⁴ and visualised using Jalview (v2.10.3),²⁷⁵ with conserved sequences shaded in grayscale (B). Predicted structural regions, based on previous reports, are boxed/highlighted as follows; proline-rich region (purple), arginine/lysine-rich region (blue), NAP domain (red) and a carboxyl-terminal bipartite acidic domain (green). In addition, green circles denote potential *cyclin-dependent kinases* (CDK) phosphorylation sites, while *nuclear localisation sequences* (NLS) and *proline/glutamic acid/serine/threonine-rich* (PEST) sequences, which are potential recognitions sites for protein degradation,²⁵¹ are also shaded (orange and yellow, respectively). Accession numbers for CDA1 protein from human (NP_071400.1), chimpanzee (JAA20211.1), mouse (NP_084112.1), cat (XP_023104601.1), cattle (JAB84492.1), deer (XP_020741441.1), beaver (XP_020008021.1) and seal (XP_021554369.1).

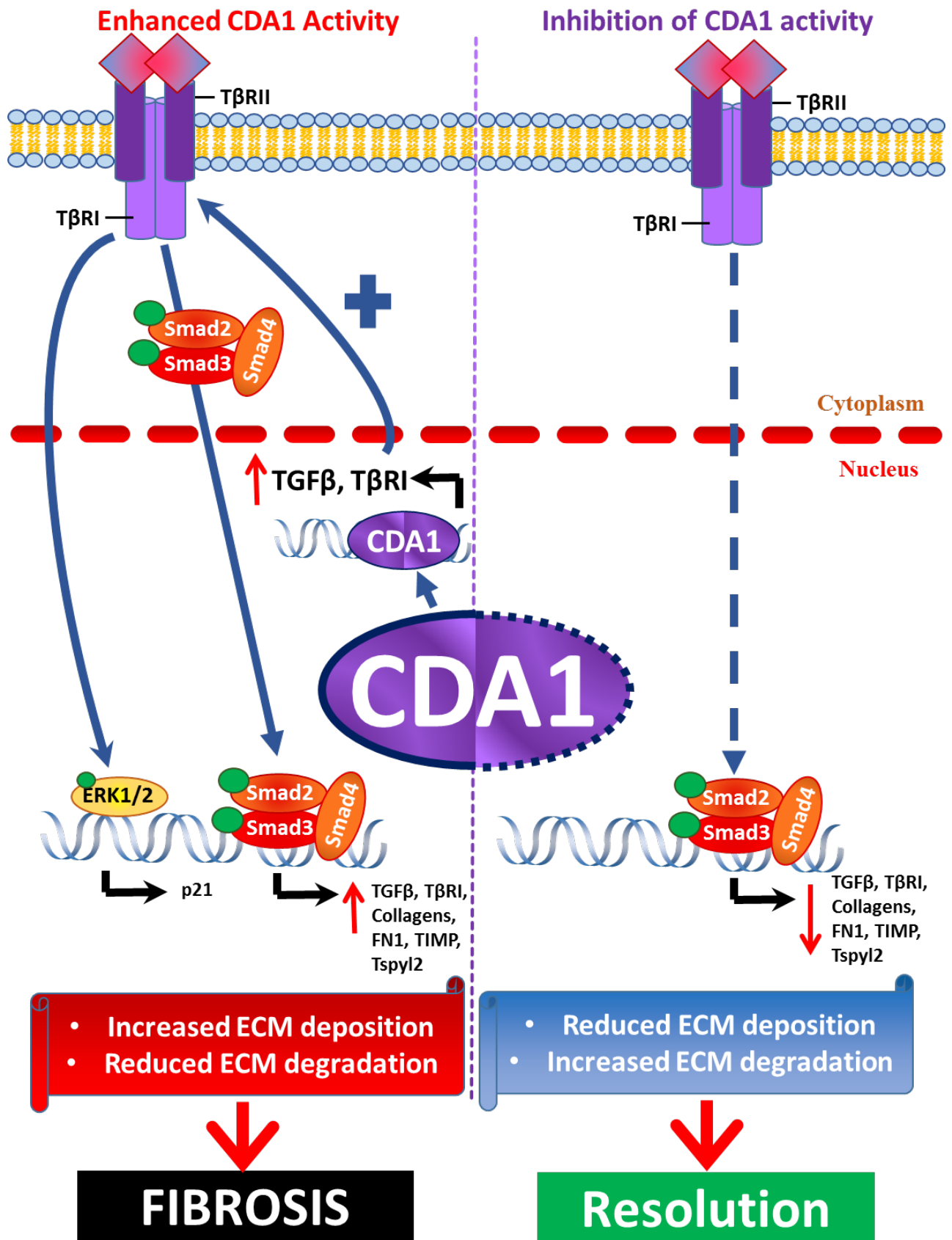


Figure 2.8. The pathological role of CDA1 in renal fibrosis. The upregulation of CDA1 expression in renal disease has been attributed to the activation of the TGFβ signalling pathway. In turn, CDA1 synergistically enhances TGFβ signalling, leading to increased profibrotic gene expression and subsequent ECM accumulation. Thus, it is expected that the absence or inhibition of CDA1 activity would attenuate the development of renal fibrosis via reduced TGFβ signalling in disease.

2.4. Hypothesis

CDA1 has been implicated to play a pathological role in fibrosis through its ability to enhance TGF β signalling in disease. As seen in *in vitro* studies, the inhibition of CDA1 activity was observed to lead to the attenuation of TGF β signalling and subsequent reduction in fibrosis progression (**Figure 2.8**). Indeed, complete genetic deletion of CDA1 was associated with an attenuation of renal fibrosis in a mouse model of diabetic nephropathy. However, due to the nature of the global genetic knockout method, CDA1 is not present at any time during the development nor during the adolescent life of these CDA1 KO mice. Thus, to demonstrate the therapeutic potential of targeting CDA1 in fibrosis, it is imperative to inhibit its actions in a scenario where CDA1 is present prior to our specific interventions. To that end, in lieu of a pharmacological inhibitor of CDA1, I have utilised an inducible genetic knockout approach to examine the effect of induced CDA1 deficiency on the progression of diabetes-associated renal fibrosis. This approach, which is more clinically relevant, allows for the development of disease in the presence of CDA1, which can be deleted at a later selected timepoint. I hypothesised that the deletion of CDA1 at early and later stages of induced renal disease will mimic the therapeutic inhibition of CDA1, leading to the prevention and attenuation of the development of renal fibrosis, respectively, as a result of an attenuation of TGF β signalling.

In addition to the aforementioned studies, I have also examined the effect of CDA1 deficiency on the progression of fibrosis in two mouse models of non-diabetic renal injury. Pioneering studies in my laboratory demonstrated that silencing CDA1 attenuated TGF β -induced profibrotic gene expression *in vitro*.^{255, 262} Indeed, CDA1 KO mice were associated with an attenuation of diabetes-associated renal fibrosis with no obvious effect observed on diabetes-associated metabolic parameters.²⁵⁶ The effect of CDA1 deficiency in non-diabetic renal fibrosis had yet to be examined experimentally. Due to the acute and aggressive nature of the chosen mouse models, these studies utilised the global CDA1 KO mice. It was hypothesized that CDA1 deficiency would lead to an attenuation of TGF β signalling and subsequent reduction in renal fibrosis in these models.

2.5. Aims

To examine the effect of induced genetic deletion of CDA1 using inducible CDA1 KO mice in a model of *streptozotocin* (STZ)-induced diabetic nephropathy, at two timepoints:

- Early intervention, with induced CDA1 deletion at 5 weeks after STZ-induced diabetes onset
- Delayed intervention, with induced CDA1 deletion at 10 weeks after STZ-induced diabetes onset

To examine the effect of global CDA1 deletion in classical models of non-diabetic renal fibrosis/injury:

- *Unilateral ureteral obstruction* (UUA)-induced fibrosis
- *Ischaemia/reperfusion* (IR) injury

Chapter 3. Methodology

3.1. Materials

3.1.1. General Chemicals

Table 3.1. General chemicals and compounds utilised in this thesis

Name	Supplier	Cat. No.
3,3', 5,5-tetramethylbenzidine	Life Technologies	002023
4-(Dimethylamino) benzaldehyde	Sigma-Aldrich	156477
Acid fuchsin	BDH Chemicals Ltd	34319 2E
Activated charcoal	Sigma-Aldrich	05150
Agarose	Promega	V3125
Aniline blue	BDH Chemicals Ltd	34003 4C
Biebrich scarlet	Sigma-Aldrich	B6008
β -mercaptoethanol	Sigma-Aldrich	M3148
Bromophenol blue	Sigma-Aldrich	B0126
<i>Bovine serum albumin</i> (BSA)	Jackson ImmunoResearch	001-000-173
Chloramine-T hydrate	Sigma-Aldrich	857319
Chloroform	LabServ	BSPCL728.2.5
cis-4-Hydroxy-D-proline	Sigma-Aldrich	H5877
Ethanol	LabServ	BSPEL975
<i>Ethylenediaminetetraacetic acid</i> (EDTA)	Sigma-Aldrich	ED45
<i>Ethylene glycol-bis (β-aminoethyl ether)- N,N,N',N'-tetraacetic acid</i> (EGTA)	Sigma-Aldrich	E4378
Ethidium bromide	BioRad	161-0433
Ferric chloride	Analar	10110
Formaldehyde	Merck	1.04003
Glacial acetic acid	ChemSupply	UN28789
Glycerol	Sigma-Aldrich	G7893
Guanidinium thiocyanate	AMRESCO	0380

Haematoxylin	Sigma-Aldrich	H9627
<i>Hydrochloric acid</i> (HCl)	Scharlau	UN1789
Isoamyl alcohol	Sigma-Aldrich	W205702
Isopropyl alcohol	VWR	20842.323
<i>Magnesium sulphate</i> (MgSO ₄)	Sigma-Aldrich	M1144
Methanol	POCD Healthcare	METHANOL2.5LPTL
Molecular grade <i>water</i> (H ₂ O)	Biosciences	786-293
<i>N-Lauroylsarcosine sodium salt</i> (Sarkosyl)	Sigma-Aldrich	61747
Pararosaniline acetate	Sigma-Aldrich	215945
Perchloric acid	Sigma-Aldrich	311421
Phenol	Sigma-Aldrich	242322
Phosphomolybdic acid	Sigma-Aldrich	221856
Phosphotungstic acid	Sigma-Aldrich	P4006
Picric acid (saturated)	Sigma-Aldrich	P6744
<i>Potassium chloride</i> (KCl)	AMRESCO	0395
Sodium acetate	Sigma-Aldrich	S8750
<i>Sodium bicarbonate</i> (NaHCO ₃)	Univar	A475
<i>Sodium carbonate</i> (Na ₂ CO ₃)	Analar	10240.4H
<i>Sodium chloride</i> (NaCl)	Merck	1.06404
Sodium citrate	Sigma-Aldrich	S1804
Sodium deoxycholate	Sigma-Aldrich	D6750
<i>Sodium dodecyl sulfate</i> (SDS)	Sigma-Aldrich	L5750
<i>Sodium fluoride</i> (NaF)	Sigma-Aldrich	S7920
Sodium iodate	Sigma-Aldrich	S4007
Sodium metabisulphite	BDH Chemicals Ltd	30180
<i>Sodium orthovanadate</i> (Na ₃ VO ₄)	Sigma-Aldrich	450243
<i>Sodium pyrophosphate</i> (Na ₄ P ₂ O ₇)	Sigma-Aldrich	221368
<i>Streptozotocin</i> (STZ)	Sigma-Aldrich	S0130
Sulfuric acid (H ₂ SO ₄)	Analar	102763Y
<i>tris(hydroxymethyl)aminomethane</i> (Tris)	AMRESCO	0497
Tris hydrochloride	AMRESCO	0234
Triton-X 100	LABCHEM	1552
Tween 20	Biochemicals	BIO0777
Xylene	ChemSupply	UN1307

3.1.2. Buffers and solutions

3.1.2.1. General Buffers and Solutions

50x Tris Acetate EDTA (TAE) Buffer

2 M Tris

~5.71% (v/v) Glacial acetic acid

50 mM EDTA

20x Tris-buffered saline (TBS), pH 7.4

200 mM Tris

3 M NaCl

1x TBS with Tween 20, pH 7.4

10 mM Tris

150 mM NaCl

0.05-0.1% (v/v) Tween 20

RNASolD

~40% (w/v) Phenol

1.8 M Guanidinium thiocyanate

11.25 mM Sodium citrate (pH 7.0)

0.09-0.225% (v/v) Sarkosyl

0.2 M sodium acetate (pH 4.0)

3.1.2.2. *Buffers for ELISAs*

Coating Buffer

0.16% (w/v) Na₂CO₃

0.29% (w/v) NaHCO₃

10x Assay Buffer, pH 8.0

1.08% (w/v) Tris

64.8% (w/v) Tris hydrochloride

8.06% (w/v) NaCl

0.2% (w/v) KCl

1x Wash Solution

1x Assay buffer with 0.05% (v/v) Tween 20

1x Post-coat/Blocking Solution

1x Assay buffer with 1% (w/v) BSA

1x Sample/Conjugate Solution

1x Assay buffer with 0.05% (v/v) Tween 20 and 1% (w/v) BSA

3.1.2.3. *Composition of buffers for hydroxyproline analysis*

Acetate/citrate buffer, pH 6.0

3.44% (w/v) Sodium acetate

3.75% (w/v) Tri-sodium citrate

0.55% (w/v) Citric acid in isopropanol

Oxidation buffer (1.4% (w/v) chloramine T in acetate/citrate buffer)

One part 7% (w/v) chloramine T (diluted in dH₂O): Four parts acetate/citrate buffer

Ehrlich's reagent

66.67% (w/v) 4-(Dimethylamino) benzaldehyde in 60% (v/v) Perchloric acid

Analytical isopropanol reagent

Three parts Ehrlich's reagent: Thirteen parts isopropanol

3.1.2.4. Composition of buffers for protein analysis

1x Lysis Buffer, pH 7.4-7.5

10 mM Tris

100 mM NaCl

1 mM EDTA

1 mM EGTA

1 mM NaF

20 mM Na₄P₂O₇

2 mM Na₃VO₄

0.1% SDS

0.5% Sodium deoxycholate

1% (v/v) Triton-X 100

10% (v/v) Glycerol

3x Laemelli's Sample Loading Dye

240 mM Tris, pH 6.8

30% (v/v) Glycerol

6% (w/v) SDS

0.06% (w/v) Bromophenol blue

10% (v/v) β-mercaptoethanol

3.1.2.5. Composition of buffers for histological stains

Scott's Tap Water Substitute

0.35% (w/v) NaHCO₃

2% (w/v) MgSO₄

Mayer's Haemalum

0.5% (w/v) Haematoxylin

5% (w/v) Aluminium ammonium sulphate

0.03% (w/v) Sodium iodate

2% (v/v) Glacial acetic acid

30% (v/v) Glycerol

3.1.2.6. Composition of buffers for Periodic acid/Schiff's staining

Schiff Reagent

8% (w/v) Pararosaniline acetate in 1M HCl

1% (w/v) Sodium metabisulphite

3.1.2.7. Composition of buffers for Masson's trichrome staining

Bouin's Solution

75% (v/v) Picric acid (saturated)

9.25-10% (v/v) Formaldehyde

5% (v/v) Glacial acetic acid

Weigert's Iron Hematoxylin Solution

One part of 1.16% (w/v) Ferric chloride with 1% (v/v) concentrated HCl:

One part of 1% (w/v) Hematoxylin in 95% absolute ethanol

Biebrich Scarlet-acid Fuchsin Solution

0.9% (w/v) Biebrich scarlet

0.1% (w/v) Acid fuchsin

1% (v/v) Glacial acetic acid

Phosphomolybdic-Phosphotungstic acid Solution

2.5% (w/v) Phosphomolybdic acid

2.5% (w/v) Phosphotungstic acid

Aniline Blue Solution

2.5% (w/v) Aniline blue

2% (v/v) Glacial acetic acid

Table 3.2. Sequence of primers and probes used for quantitative real time PCR

Target	Forward (5'→3')	Reverse (5'→3')	FAM labelled Probe (5'→3')
αSMA	GACGCTGAAGTATCCGATAGAACA	GGCCACACGAAGCTCGTTAT	TGCCAGATCTTTTCC
C5	CATAATAGCATGTGCCAGCTACAA	CGATTCCAGTCGGCAGTGAT	CCCATGCAGTAATGGA
CDA1	TGCTGCCGGTCCCAA	TGTTTATCCGATCTTCCCTTTCTT	CTTGGGCCAGCCTG
CDA1KO	TGTACTIONCCAGACAAACCCATACTTT	GCGGTTGCGCTGGAAC	CAAACATGGTGATCGTC
Col I	GACTGGAAGAGCGGAGAGTACTG	CCTTGATGGCGTCCAGGTT	ATCGACCCTAACCAAG
Col III	GGGAATGGAGCAAGACAGTCTT	TGCGATATCTATGATGGGTAGTCTCA	AATATCAAACACGCAAGGC
Col IV α3	ACCACGGCCATTCCCTTCAT	CAAAAAGAAGAGAAAACCCACTATAGAGT	CCCTGAAGGAACACAGC
Fibronectin (Fn1)	ACATGGCTTTAGGCGGACAA	ACATTCGGCAGGTATGGTCTTG	CCCCGTCAGGCTTA
ICAM1	GGAGGTGGCGGGAAAGTT	TCCAGCCGAGGACCATACAG	CCCTGGAAC
IL6	GGGAAATCGTGAAATGAGAAA	AAGTGCATCATCGTTGTTTCATACA	ATTGCCATTGCACAAC
iNOS	GGATCTTCCCAGGCAACCA	CAATCCACAAC	ACCGCCCTGGTGCA
MCP1	GTCTGTGCTGACCCCAAGAAG	TGGTCCGATCCAGGTTTTTA	AATGGGTCCAGACATAC
MMP2	TCACTTTCCTGGGCAACAAGT	GCCACGAGGAATAGGCTATATCC	TGCACCAGCGCCGG
Osteopontin	TCCAATCGTCCCTACAGTCGAT	AGCCCTTCAACATGTCTGTTCA	ATCACCTCGGCCGT
p21	TCCACAGCGATATCCAGACATT	CGGACATCACCAGGATTGG	AGAGCCACAGGCACC
p53	CGTATCCGGGTGGAAGGAA	GGCGAAAAGTCTGCCTGTCT	TTTGTATCCCGAGTATCTG
PAI1	TCTCCAATTACTGGGTGAGTCAG	GCAGCCGGAAATGACACAT	CACTGGTGACTCACTTC
Smad7	CCATCAAGGCTTTTACTATGAGA	CCATGGTTGCTGCATGAACT	CTGCAGCGGCC
TGFβ1	GCAGTGGCTGAACCAAGGA	GCAGTGAGCGCTGAATCGA	AAAGCCCTGTATTCCGT
TβRI	CGTGTGCCAAATGAAGAGGAT	AAGGTGGTGCCCTCTGAAATG	CATCACTAGATCGCCC
TβRII	CAGGTGGGAACGGCAAGATA	GCATTGCAGCGGGACG	ATGTCTACTCCATGGCTCT
TNFα	GGCTGCCCCGACTACGT	TTTCTCCTGGTATGAGATAGCAAATC	TCACCCACACCGTCAG
VCAM1	CTGCTCAAGTGATGGGATACCA	ATCGTCCCTTTTGTAGACATGAAG	CCAAAATCCTGTGGAGCAG
MSR1	GGAGGAGAGAATCGAAAGCATT	TCTGGAAGCGTCCCGTGTCT	
BAK1	TGATACCAGTTCCTGCCAGTCA	GGGCTTGCTGGCTGCTT	
Bcl2	AAGGGCTTACACCCAAATCT	TTCTACGTCTGCTTGGCTTTGA	
C3	TGAGCCAGTCGACTATG	TCATCAAATCATCCAACAGCTCTA	
Caspase 8	CAACTTCCTAGACTGCAACCG	TCCAAC	
Ki67	CAAAGGGCGAAGTGGAGCTT	TGTTTCGCAACTTTCGTTTGTG	
TIMP1	TGATTTCCCCGCCAACTC	GGGCTGCACAGTGGAGAATAA	

Table 3.3. Primer sets used for genotyping

Primer Set	Forward (5'→3')	Reverse (5'→3')
mCDA1 Primer Set 1	ACAGGACCTCAGACATATCTCCAT	TGTGCAAACTAGGTTAGTCTCTG
mCDA1 Primer Set 2	CTGAGCATCAACACCTATAACATGT	TGTGCAAACTAGGTTAGTCTCTG
mCDA1 mRNA	CCTGGAGAGCATTCAAATGGACCT	AGTGAGAATCCTGACCACAGTGAA
Cre	GTCGATGCAACGAGTGATGA	CAGTGAAACAGCATTGCTGT
β-actin	GAGGCCAGAGCAAGAGAG	GGCTGGGGTGTTGGT

3.2. General Methods

3.2.1. Genotyping of genetically modified mice

3.2.1.1. Isolation of genomic DNA

Genomic DNA was isolated from tissue using the REExtract-N-Amp Tissue PCR Kit (Sigma-Aldrich, Castle Hill, NSW, Australia; Cat. No. XNAT) with a modified protocol. In brief, ~5 mg of tissue was incubated in a 50 μ L mixture of Extraction Solution and Tissue Preparation Solution (4:1) at 37°C for 15 min and then heated to 96°C for 3 min. 40 μ L of Neutralisation Solution B was then added to the sample and briefly vortexed. Samples were then stored at 4°C until use.

3.2.1.2. Genotyping of mice using polymerase chain reaction

Polymerase Chain Reaction (PCR) was performed to determine the genotype of mice through the amplification of DNA fragments using gene specific primers (**Table 3.3**). Each PCR was performed using GoTaq Green Master Mix (Promega, Madison, WI, USA; Cat. No. M712) according to the manufacturer's protocol. Amplification was performed in Applied Biosystems Veriti Thermal Cycler (Thermo Fisher Scientific, Waltham, MA, USA), using a standard PCR reaction. Following an initial denaturation step at 96°C for 3 min, reactions underwent 35 cycles of the following thermal cycling conditions; a denaturation step at 96°C for 1 min, annealing step at 55°C for 1 min and extension step at 72°C for 1.5 min. At the end of the 35th cycle, the reaction was incubated at 72°C for a further 7 min and then cooled at 4°C until further analysis.

3.2.1.3. Agarose Gel Electrophoresis

Agarose gels were prepared at 1.2% (w/v) using TAE buffer, with ethidium bromide being added to the molten agarose, to allow for visualisation of DNA bands under UV light, and allowed to cool before PCR samples were loaded into the gel. Electrophoresis was run at 100-120 V for 45-60 min, or until dye front reaches the end of the gel. DNA bands were visualised under UV light and recorded using the BioRad Chemidoc system.

3.2.2. Animal studies and measurements of metabolic parameters

3.2.2.1. Induction of diabetes with streptozotocin (STZ)

To induce diabetes, male mice (6-8 weeks of age) underwent multiple intraperitoneal injections of STZ (55 mg/kg per day for 5 consecutive days), as previously described.²⁷⁶ Animals serving as non-diabetic controls were injected with citrate buffer alone. Blood glucose levels were monitored weekly to confirm the diabetic status of these mice. Animals were housed on a 12-hour light/ dark cycle with free access to water and standard mouse chow. The animal study was approved according to the international guidelines, including the “Principles of Laboratory Animal Care” (National Institutes of Health, 1985) and the “Australian Code of Practice for the Care and Use of Animals for Scientific Purpose, 8th edition” (National Health and Medical Council of Australia, 2013). For more details specific to particular studies, particular the induction of genetic deletion of CDA1, refer to **Chapters 5 and 6**.

3.2.2.2. *Monitoring of animals in diabetic studies*

Mice utilised for the diabetic nephropathy studies (**Chapter 5 and 6**) were monitored regularly, with blood glucose and body weight measured weekly. Metabolic parameters were collected by placing mice individually into metabolic cages (Iffa Credo, L'Arbresle, France), to measure food and water intake, as well as urine output, over a 24-hour period. Blood was collected, with heparin used as an anticoagulant, and centrifuged at 6,000 *relative centrifugal force* (rcf) for 6 min to allow for the separation of plasma and blood cells. After a volume of plasma was aliquoted into a new tube, blood cells were resuspended in an equal volume of 0.09% (w/v) sodium chloride solution. Blood, plasma and urine was stored at -20°C until use for biochemical analysis.

3.2.2.3. *Unilateral Ureteric Obstruction (UUO) and Ischaemia/Reperfusion (IR) injury*

Mice designated for either the UUO or IR studies were housed in an experimental animal facility under controlled conditions, with a 12-hour light/ dark cycle and free access to water and standard mouse chow. Surgeries were performed under aseptic conditions within this facility, with mice placed on top of 37°C heating pad to maintain body temperature. The animal study was approved according to the international guidelines, including the “Principles of Laboratory Animal Care” (National Institutes of Health, 1985) and the “Australian Code of Practice for the Care and Use of Animals for Scientific Purpose, 8th edition” (National Health and Medical Council of Australia, 2013). Refer to **Chapter 7** for more details.

3.2.2.4. *Euthanasia of animals and tissue collection*

At their designated experimental endpoint, mice were humanely euthanised using a lethal injection of sodium pentobarbitone (Lethabarb, 100 mg/kg body weight; Virbac, Milperra, NSW, Australia), followed by cardiac puncture and exsanguination. Reflexes were tested by pinching limbs to ensure mice were unconscious prior to making incisions. Once the mouse is deceased, tissues were collected. The kidney, in particular, was sliced longitudinally, with one half being fixated in 10% neutral-buffered formalin for histological analysis, while the other half was snap-frozen in liquid nitrogen and stored at -80°C until use for biochemical analysis.

3.2.2.5. *Measuring albuminuria*

Urinary albumin was measured using a Mouse Albumin ELISA Quantitation kit (Bethyl Laboratories, Montgomery, TX, USA; Cat. No. E90-134), with slight modifications to the manufacturer's protocol. In brief, 100 µL of albumin-specific capture antibody solution (provided with kit, 1:100 dilution in coating buffer) was coated onto Nunc-Immuno MicroWell 96 well solid plates (Sigma-Aldrich; Cat. No. M9410) overnight at 4°C. The next morning, the solution is decanted and all wells were washed with wash solution at least 5 times. Afterwards, wells were blocked with 300 µL of 1% BSA in assay buffer for 1hr at room temperature. After blocking solution is decanted and wells were washed, 100 µL of standards or samples (diluted with sample/conjugate buffer) were added to wells and incubated for 1hr at room temperature, before contents were discarded and wells

washed. Subsequently, 100 μL of *horseradish-peroxidase* (HRP) conjugated albumin-specific detection antibody (diluted 1:20,000 in sample/conjugate buffer) was added to each well. After an incubation at room temperature for 1 hr, wells were once again washed, before 100 μL of 3,3', 5,5-tetramethylbenzidine was added to each well, which was converted to a blue product by HRP. After an incubation time of 15-30 min, 100 μL of 1.8 M H_2SO_4 was added to each well to stop the reaction. The plate was then read at 450 nm using a spectrophotometer plate reader. Concentration of urinary albumin of samples was subsequently calculated in reference to the standards. The albumin excretion rate over 24 hours was calculated according to the urinary albumin concentration and urine output of each individual animal.

3.2.2.6. *Measuring creatinine levels*

Plasma and urinary creatinine levels were measured using a clinical computerized chemistry analyser (Cobas Integra 400 Plus, Roche Diagnostics, Forrenstrasse, Switzerland), according to the protocol provided by the manufacturer. Briefly, 100 μL of urine or plasma samples were aliquoted into COBAS cups (Roche Diagnostics, Cat. No. 1271758020), then loaded into the Cobas Integra 400 Plus running the Creatinine plus ver.2 kit (Roche Diagnostics, Cat. No. 03263991190). After analysis, creatinine concentrations of samples were calculated as reported previously.²⁷⁷

3.2.2.7. *Measuring glycated haemoglobin*

Blood was analysed for glycated haemoglobin was measured using the Cobas b 101 POC system (Roche Diagnostics), according to the manufacturer's protocol. Briefly, 2 μL of blood was loaded into Cobas Hb1ac test cassettes (Roche Diagnostics, Ref. No. 06378676) and analysed using the Cobas b 101 POC system. As the glycated Hb1ac detection limit was between 4-14%, any sample that was out of this range was designated as 4% for low and 14% for high.

3.2.2.8. *Urinary kidney injury molecule-1 (KIM1) ELISA*

Urinary *kidney injury molecule-1* (KIM1) was measured using a mouse HAVcr-1 ELISA kit (EIAab, Wuhan, China; Cat. No. E0785m) according manufacturer's protocol. As plates are pre-coated by the manufacturer, the kit was ready to use once opened. Briefly, a standard curve was generated using the provided reconstituted KIM1 protein of known concentration in the range of 0-5 ng/mL. 100 μL of standard or undiluted sample was added per well, covered with a plate sealer and incubate at 37°C for 2 hr. After wells were aspirated, 100 μL of Detection Reagent A working solution was added to each well, and incubate at 37°C for 1 hr. After wells were aspirated and washed with provided wash solution at least 3 times, 100 μL of Detection Reagent B working solution was added and incubated at 37°C for 1 hr. After another series of washes, 90 μL of Substrate Solution was added and incubated at 37°C for 15 min away from light. The reaction was terminated with 50 μL of Stop Solution and optical density was measured at 450 nm using a spectrophotometer.

3.2.3. Isolation of ribonucleic acids (RNA) from tissues

3.2.3.1. Isolation of RNA using phenol/chloroform/water extraction

Ribonucleic acid (RNA) was isolated from tissue using a modified protocol routinely used in our lab.^{278, 279} In brief, frozen tissue (~10 mg) was homogenised in 1 mL RNASolD (see **Section 3.1.2.1**) using zirconium oxide beads in a Bullet Blender (Next Advance, Averill Park, NY, USA) at 4°C for 10 min, before 200 µL chloroform:isoamyl alcohol was added (49:1). After being briefly vortexed, samples were then centrifuged at >20,000 rcf at 4°C for 20 min. The top aqueous phase was transferred into a new tube containing 500 µL isopropanol. Samples were briefly vortexed and left at -80°C overnight. The next day, samples were allowed to thaw on ice, before they were centrifuged at 4°C, >20,000 rcf for 20 min. With the nucleic acids precipitated out of solution, the supernatant was discarded and the pellet was washed twice with 75% ethanol, which was prepared with molecular grade water. Samples were briefly vortexed and centrifuged at 4°C, >20,000 rcf for 10 min. After, the ethanol was discarded and tube was air-dried for ~5 min. RNA was dissolved with ~12 µL of molecular grade water and heated to ~55°C for 5 min. Samples were then measured for RNA concentration using a UV/VIS spectrophotometer (QIAXpert; Qiagen, Hilden, Germany).

3.2.3.2. Deoxyribonuclease (DNase) treatment of RNA

To remove any potential residual DNA from the samples, 6 µg of total RNA was incubated with 0.35 U *deoxyribonuclease* (DNase) (Thermo Fisher Scientific; Cat. No. 2238G) with 1 µL of DNase 10x buffer (Thermo Fisher Scientific; Cat. No. 8167G) in a total volume of 10 µl at 37°C for ~30 min. The reaction was stopped with the addition of 1.2 µl of DNase Inactivation Reagent (Thermo Fisher Scientific; Cat. No. 8174G) for 2 min at room temperature. The samples were centrifuged at >20,000 rcf for 2 min and the supernatant transferred to new microcentrifuge tubes without disturbing the inactivation beads. Samples were stored at -80°C until use.

3.2.3.3. Reverse transcription of RNA into cDNA

Total cDNA was synthesised in a final reaction volume of 20 µl containing 1.8 µg DNase-treated RNA. First, 1.8 µg of RNA samples was mixed with 100 ng random primers (Thermo Fisher Scientific; Cat. No. 58875) and molecular grade H₂O, to make a total volume of 10 µl. Samples were then incubated at 70°C for 5 min and cooled on ice. 10 µL of the reaction mix listed in **Table 3.3** was added to each tube, leading to a total volume of 20 µl and then incubated at room temperature for 10 min, followed by 37°C for 1 hr. The reaction was terminated at 70°C for 10 min, chilled on ice before being stored at -20°C until use.

Table 3.4. Reaction mix used for reverse transcription

Reagent	Volume (μL)
First-Strand Buffer (Thermo Fisher Scientific; Cat. No. Y02321)	4.0
10 mM dNTP mix (Thermo Fisher Scientific, dATP R0142, dCTP R0152, dGTP R0162, dTTP R0172)	2.0
0.1 M DTT (Invitrogen; Cat. No. Y00147)	2.0
20 U/ μL RNase inhibitor (New England Biolabs, Ipswich, MA, USA; Cat. No. M0314L or TaNaKa Scientific, Tokyo, Japan; Cat. No. 2313A)	0.1
M-MLV Reverse Transcriptase (200U/ μL , Thermo Fischer Scientific; Cat. No. 28025-021)	1.0
Molecular grade H_2O	0.9
Total Volume:	10

3.2.3.4. Quantitative Real Time PCR (qRT-PCR)

Quantitative Real Time PCR (qRT-PCR) was performed in a MicroAmp Optical Microplate, either a 96-well or 384-well plates (Thermo Fisher Scientific; Cat. No. 4346906 or 4483320, respectively). Multiplex reactions, with reaction mix as listed in **Table 3.4**, was performed if a FAM (6-carboxyfluorescein) dye-labelled probe was available for the target gene of interest using Taqman reagent (Refer to **Table 3.1** for primer sequences). An added advantage of these reactions was the ability to analyse the presence of the housekeeping gene, 18S, in the same reaction mix. Alternatively, in the absence of a gene-specific probe, qRT-PCR was performed using gene-specific primers and SYBR green reagents as listed in **Table 3.5**. In these instances, at least two separate wells were required to measure the presence of the target gene and the housekeeping gene for a particular sample. After loading the reaction mix into the required number of wells for each individual sample, 0.5 μL of cDNA sample was added to each well. The QuantStudio 3 or 5 Real-Time PCR Systems was used to run 96 or 384 samples, respectively, for amplification and signal detection. The thermal cycling conditions started with an initial denaturation step at 95°C for 20 sec, followed by >40 cycles that consisted of a denaturation step at 95°C for 1 sec, annealing and extension step at 60°C for 20 sec. Signals from target specific amplification were normalised to signals from 18S ribosomal-RNA amplification utilising the comparative *threshold cycle* (CT) method.²⁸⁰

Table 3.5. Reaction mix used for TaqMan reactions

Reagent	Volume (μL)
18S ribosomal-RNA primer/probe mix (Thermo Fisher Scientific; Cat. No. 4319413E)	0.175
Forward Primer (10 μM)	0.3125
Reverse Primer (10 μM)	0.3125
Probe (1 μM)	0.3125
TaqMan Universal Master Mix (Thermo Fisher Scientific; Cat. No. 4304437)	3.125
Molecular grade H ₂ O	1.7625
Total Volume	6

Table 3.6. Reaction mix used for SYBR reactions

Reagent	Volume (μL)
Housekeeping gene:	
18S ribosomal-RNA primer/probe mix (Thermo Fisher Scientific; Cat. No. 4319413E)	0.175
TaqMan Universal Master Mix (Thermo Fisher Scientific; Cat. No. 4304437)	3.125
Molecular grade H ₂ O	2.7
Total Volume	6
Target gene:	
Forward Primer (10 μM)	0.3125
Reverse Primer (10 μM)	0.3125
Fast SYBR Green Master Mix (Thermo Fisher Scientific; Cat. No. 4385612)	3.125
Molecular grade H ₂ O	2.25
Total Volume	6

3.2.4. Quantification of total collagen content

Hydroxyproline is a non-proteinogenic amino acid which is derived from the post-translational modification of proline residues by prolyl hydroxylases.²⁸¹ Hydroxyproline is a major component of collagen, often being part of a repeating triplet amino acid sequence within collagen and representing ~14.4% of the amino acid composition of collagen in most mammalian tissues. Total collagen content can be estimated in a particular tissue sample using a colorimetric assay to measure hydroxyproline content.²⁸² Tissue samples were prepared via acid hydrolysis prior to hydroxyproline assay analysis. Extrapolation of the total collagen content in a sample was performed by multiplying hydroxyproline values by a factor of 6.94, based on ~14.4% hydroxyproline content in mammalian collagen. Collagen concentration was then calculated and shown as collagen content in µg/mg dry tissue weight.

3.2.4.1. Acid Hydrolysis of tissue

Approximately 10mg of frozen tissue was lyophilised and dry tissue weight was recorded. 1 mL of 6 M hydrochloric acid was then added and samples were heated to 120°C overnight in air-tight tubes to hydrolyse the tissue. Samples were re-lyophilised and resuspended in 0.1 M hydrochloric acid and used for hydroxyproline assay.

3.2.4.2. Hydroxyproline Assay

Total collagen content was measured according to a modified and scaled down hydroxyproline assay protocol,²⁸² to be performed on a 96-well clear optical microplate. A standard curve was generated using 4-hydroxyproline in the range of 0-100 µg/mL. 100 µL of oxidation buffer in isopropanol (8:92, see **Section 3.1.2.3**) was added to each well. 10 µL of acid hydrolysed tissue sample (**Section 3.2.4.1**) or standards was added to each individual well, performed in duplicate, and incubated at room temperature for 4 min. 100 µL of isopropanol was then added to each well. An adhesive cover was placed over the plate to prevent evaporation and placed on an orbital shaker briefly to mix contents. The plate was then incubated at 60°C for 25 min before being placed in a spectrophotometer and absorbance was measured at 560 nm. Hydroxyproline concentrations for each sample were calculated based on the determined absorbance of samples using the line-of-best-fit equation generated from the standard curve.

To confirm the reliability of the modified protocol used in this thesis, kidney samples at different timepoints from the UUO study were measured for their total collagen content. Indeed, using this modified protocol, I was able to confirm that total collagen content progressively increases with time in the UUO model (**Supplementary Figure 1**).

3.2.5. Protein Analysis

3.2.5.1. Extraction of proteins from tissue

Kidney tissues were homogenized, in Lysis buffer (**Section 3.1.2**) with appropriate protease and phosphatase inhibitors, using magnetic homogenising beads at 4°C for 10 min. Samples were then centrifuged at >20,000 rcf, 4°C for 20 min and the supernatant, containing soluble protein, was transferred into a new tube and stored at -80°C until use.

3.2.5.2. Determination of protein concentration using bicinchoninic acid (BCA) assay

Total protein concentration was measured using Pierce *bicinchoninic acid* (BCA) Protein Assay Kit (Thermo Fisher Scientific; Cat. No. 23225). A standard curve was generated using BSA in the range of 1000 µg/mL to 0 µg/mL. 100 µL of BCA assay buffer was added into each well and then 5µl of standards or protein samples (diluted ~1/20 in lysis buffer) were added in duplicate in clear 96-well microassay plates. Plates were covered with parafilm and incubated at 37°C for 25 min. Absorbance was measured at 562 nm. Protein concentration of samples were calculated based on the determined absorbance of samples using the line-of-best-fit equation generated from the standard curve.

3.2.5.3. Sodium Dodecyl Sulfate Polyacrylamide Gel Electrophoresis (SDS-PAGE)

Samples were mixed with Laemmli's SDS-PAGE sample buffer containing 10% (v/v) β-mercaptoethanol and heated at 96°C for 5 min. Approximately 20 µg/lane of sample was loaded into Bolt 4-12% Bis-Tris Plus Gels (Thermo Fisher Scientific; Cat. No. NW04127BOX). SDS-PAGE was performed at 150 V for 1.5 hr or until the dye front reached the end of the gel.

3.2.5.4. Western Blot

Electrophoresed proteins were then transferred from the polyacrylamide gel onto nitrocellulose membranes using Trans-Blot Turbo Mini nitrocellulose transfer packs (0.2 µm pore size, Bio-Rad, Hercules, CA, USA; Cat. No. 1704156) and BioRad Transblot Turbo Semi-Transfer system (Bio-Rad; Cat. No. 1704155) at 1.3 A for ~14 min. Membranes were blocked with 2% (w/v) BSA in TBS for 1 hr at RT, before being incubated with primary antibody (1:500 dilution, Anti-Smad3 (phospho-S423+S425) antibody [EP823Y]; Abcam, Cambridge, UK; Cat. No. ab52903 or anti-αSMA antibody; Cell Signalling Technology, Danvers, MA, USA; Cat. No. 14968) overnight at 4°C. After several washes with TBS with 0.05% (v/v) Tween-20 (TBS-T), membranes were probed with an appropriate secondary antibody (1:10,000 dilution, IRDye 800CW Goat anti-Rabbit IgG (H + L); LI-COR, Lincoln, NE, USA; P/N 925-32211) for 1 hr at room temperature. Membranes were visualised using Odyssey CLx Infrared Imaging System (LI-COR) after several washes of TBS-T. Protein bands were quantified using ImageStudio and normalised against either β-actin (1:4,000 dilution, anti-β-Actin [8H10D10] antibody, Cell Signalling Technology; Cat. No. 3700) or α-tubulin bands (1:10,000 dilution, anti-α-Tubulin [DM1A] antibody, Cell Signalling Technology; Cat. No. 3873).

3.2.6. Histological stains

3.2.6.1. Periodic Acid Schiff (PAS) Staining

3 μm paraffin sections were dewaxed by immersing slides in xylene twice, for 10 min each, and then in absolute ethanol thrice, for 5 min each. Afterwards, slides were rinsed in running water and then washed in distilled water at least 3 times, with each wash lasting 1 min each. They were then oxidised with 1% (w/v) periodic acid for 5 min and washed once again in distilled water. Sections were placed in Schiff Reagent for ~20 min before being rinsed in distilled water, then left in warm running water for 15 min. They were counter-stained with Mayer's haemalum for 30 sec and Scott's tap water for 10 sec before being dehydrated and coverslips mounted with DPX mounting medium (Sigma-Aldrich; Cat. No. 06522).

3.2.6.2. Masson's trichrome staining

Renal ECM was stained by using the Masson's trichrome staining kit (Australian Biostain P/L; Cat. No. AMT.K). Briefly, sections were dewaxed in several changes of xylene and absolute ethanol (**see Section 3.2.6.1**) and then rinsed with running tap water. Slides were then placed in Bouin's solution for 1 hr at 60°C and rinsed in running tap water for 5-10 min. Slides were then stained in Weigert's iron hematoxylin working solution for 10 min and rinsed in warm running tap water for 10 min, followed by a wash in distilled water. They were then stained with Biebrich scarlet-acid fuchsin solution for 10-15 min, washed briefly in distilled water and then placed in phosphomolybdic-phosphotungstic acid solution for 10-15 min. Sections were transferred into aniline blue solution and stained for 8 min before being rinsed briefly in distilled water and placed in 1% (v/v) acetic acid solution for 2-5 min. Slides were then washed with distilled water, dehydrated and coverslips mounted using DPX.

3.2.6.3. Immunohistochemical staining

Paraffin embedded sections were stained for collagen IV using goat anti-collagen IV (1:250 dilution; SouthernBiotech, Birmingham, AL, USA; Cat. No. 1340-01) or collagen III using goat anti-collagen III antibodies (1:250 dilution; SouthernBiotech; Cat. No. 1330-01) using a modified avidin-biotin-peroxidase compound immunoglobulin enzyme bridge protocol with species matched kits (Vector Laboratories, Burlingame, CA, USA).

Sections were dewaxed as described in **Section 3.2.6.1**. Endogenous peroxidases activity was quenched with 3% (v/v) hydrogen peroxide (Pierce, Rockford, IL) in methanol for 20 min. Following a wash step, consisting of several changes in tap water and distilled water, slides were pre-warmed at 37°C in distilled water, antigen retrieval was performed using 0.4% (w/v) pepsin (Sigma-Aldrich; Cat. No. P6887) in 0.01M HCl solution at 37°C for 10 min, followed by another series of washes. Slides were bathed in 0.5% (w/v) skim milk in TBS solution and left for 10 min. After a wash step with TBS and *TBS with 0.1% Tween-20* (TBS-T), primary antibody solution, prepared in 1% (v/v) normal horse serum (Vector Laboratories; Cat. No. S-2000) in TBS, was added to sections and

incubated overnight in a humidified chamber at 4°C. The following morning, slides were washed in sequence from running tap water, distilled water, TBS then TBS-T. Slides were then further blocked with an Avidin-Biotin blocking kit (Vector Laboratories; Cat. No. SP-2001), with 10 min incubation of each solution followed by another series of washes. Next, an appropriate secondary biotinylated antibody was added for 10 min (1:500 dilution in TBS, Biotinylated Horse Anti-Goat IgG Antibody; Vector Laboratories; Cat. No. BA-9500). After a series of washes, slides were incubated with horseradish peroxidase-conjugated avidin complex (VECTASTAIN Elite ABC-HRP Kit; Vector Laboratories; Cat. No. PK-6100) for 15 min. Following another wash, peroxidase activity was visualised with 3,3'-diaminobenzidine tetrahydrochloride (Sigma-Aldrich; Cat. No. D5905) containing 0.05% (v/v) hydrogen peroxide in TBS. Following a wash in running tap water, slides were counter-stained with Mayer's haemalum for 30 sec and immersed in Scott's tap water for 10 sec before being dehydrated and mounted with DPX.

3.2.6.4. Quantification of histological stains

Twenty images at 200x magnification were taken around the renal cortex of each section, in a blinded-manner, and staining was analysed using the Image-Pro Plus 7.0 software (Media Cybernetics, Bethesda, MD, USA). The histogram-based mode of colour thresholding was used to digitally analyse histological staining and determine the percentage area of positive staining in each image. The three red-green-blue parameters were manually gated between 0 and 255 to exclusively encompass the colour of a specific stain, such as blue for Masson's trichrome staining, magenta for PAS staining or brown for positive immunohistochemical staining. Accuracy of these parameters were confirmed with negative staining and/or a pseudo-colour.

3.2.7. Statistical Analysis

Statistical analysis was performed using GraphPad Prism 7 (GraphPad Software, La Jolla, CA, USA). All data were expressed in mean±SE. Differences in the mean among groups were analysed using one-way ANOVA followed by multiple comparisons between groups using the Holm-Sidak *post-hoc* test. Any value which exceeded two standard deviations from the mean of that group were considered statistical outliers and excluded from that analysis. A difference with $p < 0.05$ was considered to be statistically significant.

Chapter 4. Optimisation of conditions to induce the genetic deletion of CDA1 in CDA1flox/ERCre mice

4.1. Background

CDA1 has been implicated as a potential molecular target to combat fibrosis progression in CKD. Utilising a global CDA1 knockout mouse strain, our laboratory has observed an attenuation in diabetes-associated renal fibrosis in CDA1 deficient mice.²⁵⁶ However, as these mice do not have the functional CDA1 gene during their development, life, and the time span of the experimental disease model, these studies do not accurately represent the clinical scenario observed in humans, where CDA1 is present prior and throughout disease development. Thus, to circumvent this issue, we have generated a tamoxifen-induced CDA1 KO mouse strain, the CDA1flox/ERCre mouse, to mimic a pharmacological inhibitory approach against CDA1 expression.

The CDA1flox/ERCre mouse strain utilises the inducible lox/Cre system of DNA recombination, enabling the induced genetic recombination of a gene of interest with the administration of tamoxifen. The CDA1flox/ERCre mouse strain was generated by crossing two mouse strains, the previously established CDA1flox and ERCre strains. The CDA1flox mouse has LoxP sites, recognition sites for the *cyclization recombination* (Cre) enzyme,²⁸³ inserted to flank exons 2-5 of the CDA1 encoding gene, *Tsyp12*. The ERCre mouse, also known as the CAGGCre-ERTM mice, expresses the recombinant enzyme, ERCre, which is a fusion protein of the mutant *estrogen receptor* (ER) and the Cre DNA recombinase, under the global CAGG promoter.²⁸⁴ This mutant ER is activated with the administration of tamoxifen or its active form, 4-hydroxytamoxifen, and not by endogenous estrogen.²⁸⁵ While ERCre is expressed ubiquitously in the CDA1flox/ERCre mice, in the absence of tamoxifen, ERCre is retained in the cytoplasm and the CDA1 gene is left intact. Upon tamoxifen administration, ERCre will translocate into the nucleus and will excise the region between LoxP sites flanking exons 2-5 of CDA1 gene, *Tsyp12*. Thus, tamoxifen administration in these mice results in the global genetic deletion of CDA1.

Prior to the use of CDA1flox/ERCre mice in subsequent animal studies (**Chapter 5 and 6**), I performed pilot studies to optimise the conditions for the genetic deletion of CDA1 upon tamoxifen administration. In addition, although the tamoxifen-induced loxP/Cre system is commonly used to induce the genetic recombination of a gene of interest, tamoxifen is known to act through the estrogen receptor, with high doses of tamoxifen being associated with offsite effects. Thus, the purpose of this chapter was to determine the optimal dosage of tamoxifen to induce a significant reduction in CDA1 expression in CDA1flox/ERCre mice, while minimising potential side effects.

4.2. Method

4.2.1. Generation of CDA1flox/ERCre mice

CDA1flox/ERCre mice, which were on a C57BL6 background, were bred from CDA1flox and ERCre parents. Tissue from either tail or kidney of each mouse was used for extraction of genomic DNA (see Section 3.2.1). Genotyping analysis was performed using the extracted genomic DNA to confirm the presence of the ERCre gene, as well as to confirm the presence of the floxed CDA1 gene.

4.2.2. Optimization of tamoxifen dosage to delete CDA1 gene in CDA1flox/ERCre mice

Tamoxifen (Sigma-Aldrich; Cat. No. T5648) was dissolved in absolute ethanol, and then mixed with corn oil (Sigma-Aldrich; Cat. No. C8267) to make 1.0 or 1.5 mg of tamoxifen per 250 μ L corn oil mixture. Male CDA1flox/ERCre mice aged 10-12 weeks (~25-35 g BW) were injected with tamoxifen intraperitoneally, once a day for 3-6 consecutive days. Littermate CDA1flox mice without the transgenic ERCre served as genotype controls. Mice designated as treatment controls were injected with corn oil alone. Mice were culled 3-14 days after their final injection, and organs were collected for genotyping and gene expression analysis.

4.3. Results

4.3.1. Genotyping of CDA1flox/ERCre mice

To determine whether knockout of CDA1 upon tamoxifen administration was achieved at the genomic level in CDA1flox/ERCre mice, *polymerase chain reaction* (PCR) analysis using genomic DNA as templates was performed using various combinations of primers (**Table 3.2 and Figure 4.1A**). As illustrated in **Figure 4.1A**, the use of mCDA1 Primer Set 1, which consists of WT-F and KO-R primers, produces a PCR product of ~638 *base pairs* (bp) if exons 2-5 of the CDA1 gene are present. If exons 2-5 are deleted, the WT-F primer is not able to anneal and PCR amplification does not occur. This is seen in **Figure 4.1B**, where a band is present in CDA1 WT mice, while this band is absent in global CDA1 KO mice. Additionally, the use of mCDA1 Primer Set 2, consisting of KO-F and KO-R primers (**Figure 4.1A**), results in ~1165 and/or ~359 bp product(s) depending on whether exons 2-5 of the CDA1 gene are present and/or absent, respectively. Tamoxifen administration at 1.0 mg per day, regardless whether mice received 3 or 6 daily consecutive doses of tamoxifen, resulted in a reduced intensity of the CDA1 band produced by Primer Set 1 in CDA1flox/ERCre mice when compared to CDA1flox/ERCre mice administered vehicle or CDA1flox mice which lacked the ERCre gene (**Figure 4.1C**). These mice were also associated with the presence of a KO band when CDA1 Primer Set 2 was used, indicating that a significant amount of DNA template of the CDA1 gene had exons 2-5 deleted. Of note, CDA1flox/ERCre mice receiving vehicle also showed a faint KO band, indicating that minor background activity of ERCre can occur without tamoxifen administration in these mice. In contrast, gene deletion of CDA1 was not observed in CDA1flox mice,

particularly those receiving tamoxifen (**Figure 4.1C**). The use of these primers demonstrates that deletion of exons 2-5 of the CDA1 gene is only achieved in CDA1flox/ERCre mice. Furthermore, upon tamoxifen administration (1 mg/day) for 3 or 6 consecutive days, the intensity of KO bands is markedly greater than those seen in vehicle-treated CDA1flox/ERCre mice (**Figure 4.1C**). This demonstrates that the genetic deletion of the floxed CDA1 gene can be induced by the tamoxifen administration in CDA1flox/ERCre mice. Genetic deletion of CDA1 was also observed in other tissues, including heart, liver, lung, suggesting that this knockout occurs in most, if not all, tissues examined (**data not shown**).

4.3.2. Tamoxifen decreases renal CDA1 mRNA levels in a dose-dependent manner

As seen in **Figure 4.1**, PCR analysis of genomic DNA confirmed the genetic deletion of the CDA1 gene in CDA1flox/ERCre mice upon tamoxifen administration. Thus, to determine the relative expression of intact CDA1 gene in CDA1flox/ERCre mice administered tamoxifen, total renal RNA was extracted from these mice for *quantitative real-time PCR* (qRT-PCR) analysis. Absence of the mRNA regions corresponding to exons 2-5 of the CDA1 gene was first confirmed by reverse transcription PCR analysis of renal mRNA from these mice (**Figure 4.2A**). Quantitative assessment via qRT-PCR revealed that wild type CDA1 mRNA levels decreased in CDA1flox/ERCre mice receiving tamoxifen in a dose dependent manner (**Figure 4.2B**). CDA1flox/ERCre mice treated with tamoxifen (1 mg/day) for three and six consecutive days led to a ~60% and ~70% reduction in CDA1 gene expression, respectively (**data not shown**). With further optimization of the tamoxifen dosage, a greater reduction in CDA1 gene expression levels was achieved in mice treated with a higher dose of tamoxifen (1.5 mg/day) for 3 consecutive days, with a ~80% reduction in gene expression when compared to controls (**Figure 4.2B**, $p < 0.01$ vs vehicle-treated CDA1flox/ERCre mice). In addition, as renal tissues from these mice were collected 3 days after their final injection, the recombination of the CDA1 gene by tamoxifen administration in CDA1flox/ERCre mice appears to occur relatively quickly.

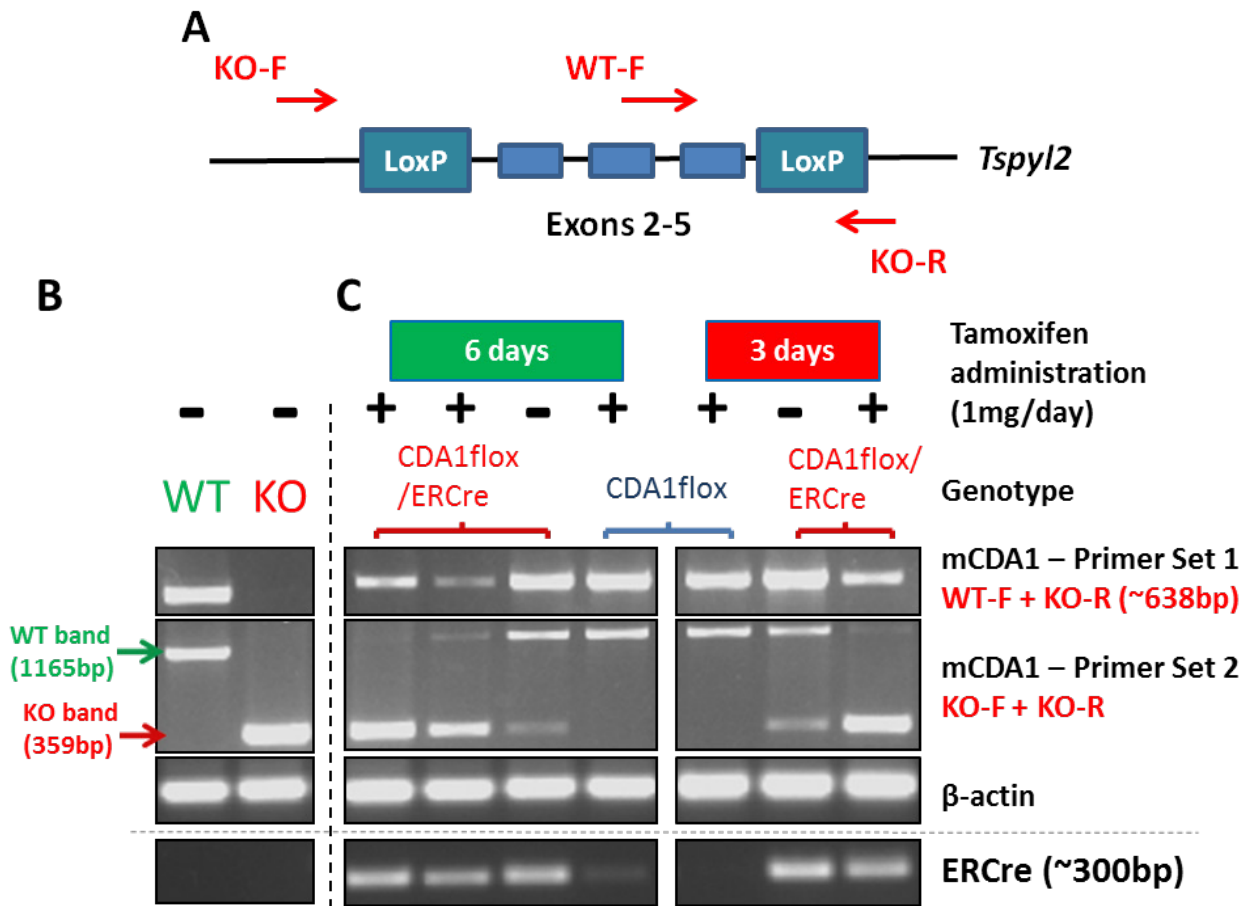


Figure 4.1. Detection of the genetic deletion of CDA1 in CDA1^{fllox}/ERCre mice treated with tamoxifen. A schematic diagram of the CDA1 gene with exons 2-5 flanked by LoxP sites and the location of primers used in genotyping, as indicated by red arrows (A). Representative images of the use of different primer sets to determine knockout of CDA1 in kidney tissues from CDA1^{fllox}/ERCre mice. (B) WT: CDA1 wild type mouse; KO: global CDA1 KO mouse. Kidney tissues from CDA1^{fllox}/ERCre mice treated with tamoxifen (+) (1 mg/mouse/day) or vehicle (-) for 6 and 3 consecutive days (C).

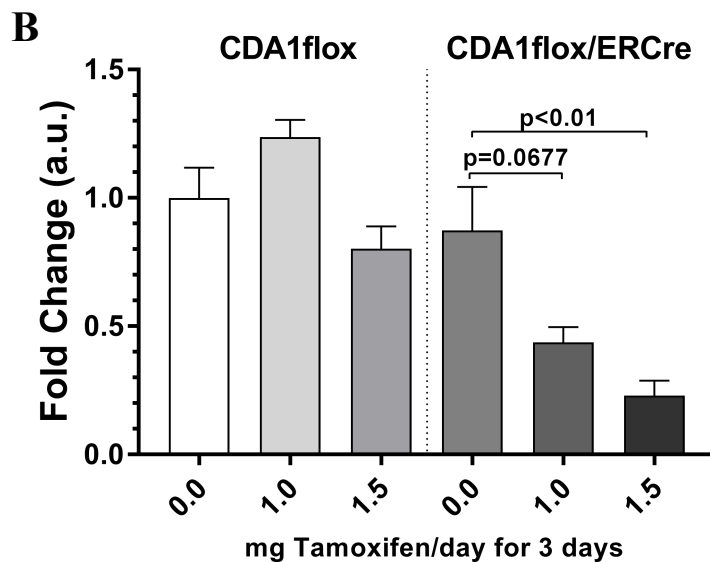
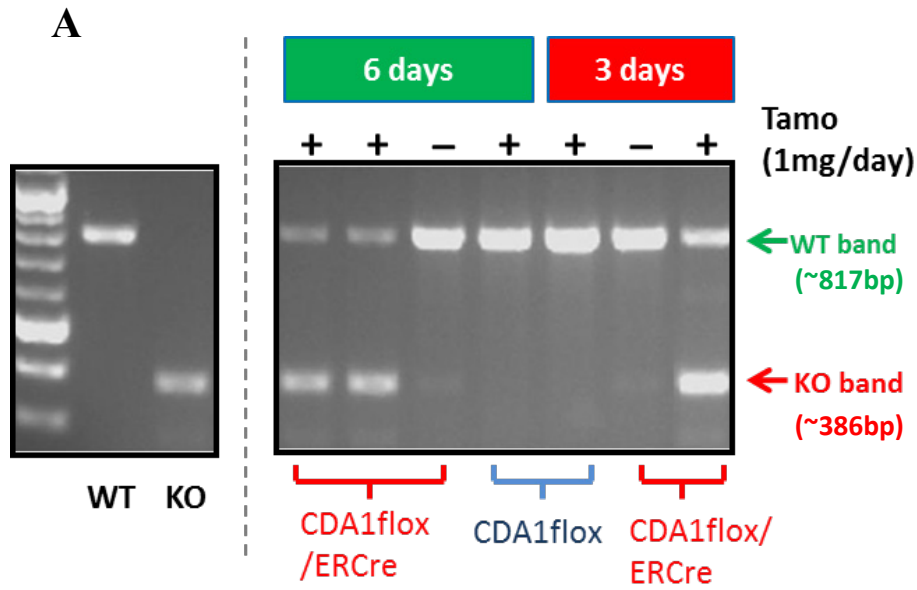


Figure 4.2. Detection of CDA1 deletion from CDA1flox/ERCre mice treated with tamoxifen. PCR analysis of cDNA synthesized from renal CDA1 mRNA from CDA1flox/ERCre mice treated with tamoxifen (+) (1 mg/mouse/day) or with vehicle (-) for 6 and 3 consecutive days. Full-length functional CDA1 is represented by the presence of a larger (WT) band (~817 bp), while a lower (KO) band (~386 bp) represents the excised CDA1 gene transcript (A). The relative expression levels of full-length/wild type CDA1 gene transcript in kidney tissues was quantified by qRT-PCR, suggesting a dose-dependent decrease of CDA1 mRNA with tamoxifen administration (B, n=4).

4.4. Discussion and Conclusion

The Cre/lox site-specific recombination system is frequently utilised to examine the physiological and pathological roles of a gene of interest. Insight gained from these studies generally involves the examination of effects associated with the absence or transgenic overexpression of the gene of interest at either a global level, or, when driven by a tissue-specific promoter, in the context of a particular cell type/tissue.²⁸⁶ The development of inducible Cre mouse strains, with tamoxifen-inducible ERCre mice being the most commonly used, has provided another level of control, enabling the possibility to manipulate gene expression at a certain timepoint during development or the lifespan of the animal. Among other applications, the inducible Cre system has been used previously to delete regions between loxP sites using various doses of tamoxifen.²⁸⁷

As mentioned previously, I planned to utilise the CDA1^{fl}/ERCre mice to examine the effects of induced genetic deletion of CDA1 during the progression of renal disease. Prior to those studies, optimisation of tamoxifen administration needed to be performed. Other researchers have previously reported that administration of 1-2 mg of tamoxifen/mouse/day for 3-6 consecutive days can be used to activate ERCre.^{288, 289} I initially administered 1.0 mg/mouse/day of tamoxifen to CDA1^{fl}/ERCre mice for 3 and 6 consecutive days, while littermate CDA1^{fl} mice were used as genotype controls. Administration of tamoxifen (1.0 mg/mouse/day) for either 3 or 6 consecutive days to CDA1^{fl}/ERCre mice resulted in deletion of the CDA1 gene, particularly in the kidney, as seen by the reduction in CDA1 WT band intensity and generation of a lower PCR product with the use of Primer Sets 1 and 2, respectively (**Figure 4.1C**). Further quantitative analysis revealed a dose-dependent reduction in intact CDA1 gene transcript expression in CDA1^{fl}/ERCre mice receiving tamoxifen for 3 consecutive days (**Figure 4.2B**).

Although the ERCre enzyme is theoretically retained in the cytoplasm in the absence of tamoxifen (more specifically 4-hydroxytamoxifen), there was a detectable amount of background activity. Genotyping analysis of genomic DNA from CDA1^{fl}/ERCre mice administered vehicle detected the presence of KO bands in these mice. Further analysis, however, demonstrated that the relative expression levels of intact CDA1 mRNA in CDA1^{fl}/ERCre mice receiving vehicle, as determined by qRT-PCR, was comparable to CDA1 WT mice (**Figure 4.2B**). This finding indicated that the majority of renal cells in vehicle-treated CDA1^{fl}/ERCre mice still retained the intact CDA1 gene and that basal ERCre activity did not significantly affect CDA1 gene expression in these mice.

Based on the results obtained from these pilot studies, 1.5 mg/mouse/day tamoxifen for 3 consecutive days was chosen to induce genetic deletion of CDA1 in subsequent animal studies. As described in this chapter, this dose, which amounted to ~50 mg Tamoxifen/ kg *body weight* (BW), resulted in a ~80% reduction of CDA1 gene expression in CDA1^{fl}/ERCre mice. The complete ablation of CDA1 expression through increased dosage of tamoxifen was not performed for several reasons. Firstly, it appeared unlikely that gene expression of CDA1 would be reduced significantly

with a higher dose. This was seen in preliminary studies where CDA1flox/ERCre mice treated with tamoxifen (1 mg/mouse/day) for three and six consecutive days led to a ~60% and ~70% reduction in CDA1 expression, respectively (**data not shown**), while tamoxifen administration for 3 consecutive days at 1.0 and 1.5 mg/mouse/day led to a ~50% and ~80%, respectively. Secondly, as these studies mimic a therapeutic intervention, it would be highly unlikely, even unrealistic, to achieve complete blockade of the target molecule using a pharmacological approach. Thirdly, tamoxifen, which is known to interact with the estrogen receptor, may have offsite effects on physiology, including anabolic trabecular bone formation,²⁹⁰ and estrogen receptor-mediated transcriptional regulation in the kidney.^{291, 292} Furthermore, tamoxifen has been reported to exhibit anti-fibrotic effects through an estrogen receptor- α -dependent mechanism in a number of rodent models of renal fibrosis.²⁹²⁻²⁹⁶ Thus, to avoid any potential side effects, as well as to mitigate any confounding factors, 1.5 mg/mouse/day of tamoxifen for 3 consecutive days was deemed suitable for subsequent studies.

In conclusion, this chapter describes the optimisation of tamoxifen doses required to achieve a significant reduction in renal CDA1 expression in CDA1flox/ERCre mice. Indeed, I have demonstrated that the administration of tamoxifen in CDA1flox/ERCre mice was able to cause the recombination of the CDA1 gene in a rapid, consistent and dose-dependent manner. This preliminary study is part of a larger proof-of-concept experiment to investigate the effect of induced CDA1 deficiency in a mouse model of diabetic nephropathy. Although I did not pursue a complete ablation of CDA1 expression, the tamoxifen regiment of 1.5 mg/day for 3 consecutive days has proven sufficient to induce a substantial reduction in CDA1 expression in CDA1flox/ERCre mice and was therefore utilised for the subsequent studies in diabetic mice.

Chapter 5. Induced genetic deletion of CDA1 in Diabetic

Nephropathy: Early Intervention Study

5.1. Background

Cell Division Autoantigen 1 (CDA1) is a nuclear phosphoprotein and a member of the SET/NAP/TSPY protein family.²⁴⁸⁻²⁵¹ With elevated expression observed in rodent models of diabetic nephropathy and diabetes-associated atherosclerosis, CDA1 has been implicated to play a role in the development of fibrosis.^{255, 256, 262} Indeed, renal biopsy samples from human patients with renal fibrosis were associated with elevated levels of CDA1 protein.²⁵⁶ The pathological role of CDA1 in renal fibrosis has been attributed to its ability to enhance the profibrotic actions of TGF β signalling, with *in vitro* studies revealing a synergistic relationship between TGF β and CDA1.^{250, 255, 261-263} The inhibition or absence of CDA1 has been demonstrated to attenuate the development of fibrosis *in vitro* and *in vivo*.²⁵⁶ These findings suggest that CDA1 is a potential molecular candidate to target against renal diseases associated with enhanced TGF β activity, such as diabetic nephropathy.

On the basis of these pioneering studies, I will further examine the role of CDA1 in renal fibrosis and investigate the therapeutic potential of CDA1 inhibition in a mouse model of diabetic nephropathy using the inducible CDA1 KO mouse strain, CDA1 flox /ERCre. As described in **Chapter 4**, the CDA1 flox /ERCre mouse strain was designed to delete exons 2-5 of the CDA1 gene upon the administration of tamoxifen. As such, this method can be used to mimic the therapeutic intervention against CDA1 in DN, whereby the disease develops in the presence of CDA1 which can be deleted at a later selected timepoint. I hypothesise that the deletion of CDA1 at early and later stages of induced diabetic renal disease will mimic the therapeutic inhibition of CDA1 and thus lead to an attenuation in renal fibrosis.

5.2. Methods

5.2.1. CDA1 flox /ERCre mice, induction of diabetes and induced genetic deletion of CDA1

CDA1 flox /ERCre male mice (6-8 weeks of age) were rendered diabetic by multiple injections of STZ (55 mg/kg per day for 5 consecutive days) with littermate CDA1 flox mice serving as genotype controls. Animals serving as non-diabetic controls were injected with citrate buffer alone. Tamoxifen (1.5 mg/mouse/day for 3 consecutive days) or vehicle was administered intraperitoneally at 5 weeks after STZ injections to represent an early intervention against CDA1 activity (**Figure 5.1**). Mice were culled at 10 weeks after diabetes induction to represent an early stage of diabetic nephropathy progression and tissues collected for analysis (**Refer to Chapter 3 for details**).

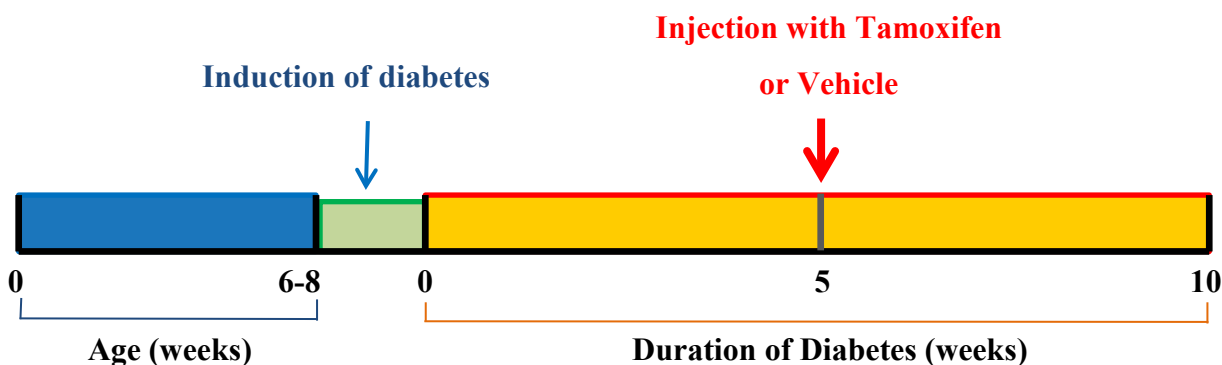


Figure 5.1. Timeline of the 10-week STZ-induced diabetic study. Male mice at 6-8 weeks of age were injected with STZ to induce diabetes or with citrate buffer to serve as non-diabetic controls. Mice were randomly allocated to receive injections of tamoxifen or vehicle at 5 weeks after diabetes induction. Mice were culled at 10 weeks after STZ injections and organs were harvested for analysis.

5.3. Results

5.3.1. Reduced renal CDA1 gene expression in tamoxifen-treated CDA1^{flx}/ERCre mice

One week prior to administration with either tamoxifen or vehicle, both CDA1^{flx} and CDA1^{flx}/ERCre mice injected with STZ exhibited typical diabetes-associated changes in metabolic parameters, including polydipsia, polyuria and albuminuria (**Table 5.1**, $p < 0.001$ vs non-diabetic mice). Interestingly, although there were no differences in body weight or food intake, diabetic CDA1^{flx}/ERCre mice appeared to have reduced water intake, urine output and urinary albumin levels than diabetic CDA1^{flx} mice at 4 weeks after induction of diabetes (**Table 5.1**). Nonetheless, all mice were randomly allocated to receive either tamoxifen or vehicle at 5 weeks after STZ injections. At the 10-week timepoint, CDA1^{flx} mice, that did not possess the ERCre transgene, had similar levels of renal CDA1 gene expression, regardless of whether they were administered with vehicle or tamoxifen (**Figure 5.2A**). There was a tendency towards diabetes-associated elevated CDA1 expression in these mice, albeit the difference was not statistically significant in this study. Daily injections of tamoxifen at 1.5 mg/day over 3 consecutive days of CDA1^{flx}/ERCre mice led to ~75-80% reduction in renal CDA1 gene expression compared to vehicle-treated animals, regardless of diabetic status (**Figure 5.2A**, $p < 0.001$ compared to vehicle-treated mice). Genetic deletion of CDA1 was also confirmed using PCR analysis with renal cDNA as templates, where the presence and band intensity of a smaller PCR product, signifying the deletion of exons 2-5 of the CDA1 transcript, was significantly greater in CDA1^{flx}/ERCre mice receiving tamoxifen (**Figure 5.2B**). Thus, these results confirm that tamoxifen administration in CDA1^{flx}/ERCre mice led to CDA1 deficiency in these mice.

Table 5.1. Metabolic parameters of mice at 4 weeks after STZ-induced diabetes induction

Treatment	CDA1flox			CDA1flox/ERCre		
	Control	Diabetic		Control	Diabetic	
<i>Body weight (g)</i>	30 ±0.7	25 ±0.4	***	30 ±0.9	26 ±2.2	***
<i>Water intake (mL/day)</i>	1.5 ±0.2	18.4 ±0.8	***	2.2 ±0.2	16.0 ±1.3	***, □
<i>Food intake (g/day)</i>	2.3 ±0.1	4.8 ±0.1	***	1.9 ±0.2	4.5 ±0.2	***
<i>Urine Output(mL/day)</i>	0.7 ±0.1	15.5 ±0.9	***	0.8 ±0.1	11.4 ±1.3	***, ††
<i>Albuminuria (µg/day)</i>	17.5 ±2.5	106.9 ±20.6	***	11.7 ±1.5	44.5 ±4.2	††

***p<0.001 vs corresponding non-diabetic control, □p=0.0788, ††p<0.01 vs diabetic CDA1flox

Samples sizes were >16 for control mice, 22 for diabetic mice

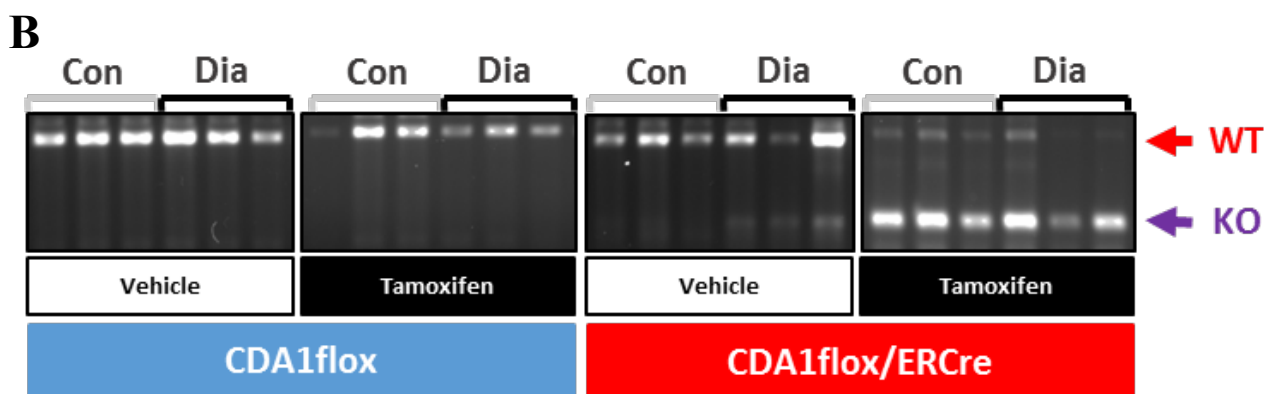
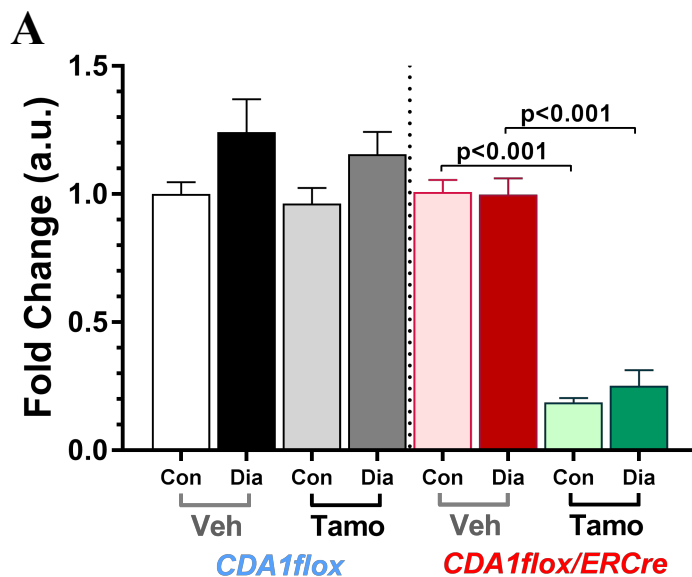


Figure 5.2. Induced genetic deletion of CDA1 in renal cortex of 10-week diabetic CDA1flox/ERCre mice. Male CDA1flox and CDA1flox/ERCre mice were rendered diabetic (Dia) with STZ injections, (or buffer alone to serve as non-diabetic controls (Con)) at 6-8 weeks of age and were injected with tamoxifen (Tamo) or vehicle to delete the CDA1 gene in CDA1flox/ERCre mice at 5 weeks of diabetes. Kidneys were collected at 10 weeks of diabetes. Renal CDA1 mRNA levels are expressed as mean±SE (A, n=6-9 for nondiabetic controls, >11 for diabetic animals). Representative images of reverse transcriptional PCR analysis of kidneys from CDA1flox and CDA1flox/ERCre mice (B), which validates recombination as a result of tamoxifen administration in CDA1flox/ERCre mice with the presence of the lower KO band (purple arrow).

5.3.2. CDA1 deficiency does not affect diabetes-associated metabolic parameters

Ten weeks after STZ-induced diabetes, metabolic parameters of diabetic mice exhibited expected changes associated with insulin-deficient diabetes, such as hyperglycaemia, elevated levels of glycated haemoglobin, polydipsia, polyuria, renal hypertrophy and increased urinary albumin excretion (**Table 5.2 and Figure 5.3A and B**, $p < 0.01$ vs corresponding non-diabetic control groups). Furthermore, there was a ~36.9-fold increase in urinary *kidney injury molecule 1* (KIM1) excretion in diabetic CDA1flox/ERCre mice (**Figure 5.3C**, $p < 0.001$ vs. non-diabetic controls).

Many of the diabetes-associated changes to metabolic parameters were unchanged with tamoxifen administration in both CDA1flox and CDA1flox/ERCre mice. This included a lack of changes in diabetes-associated albuminuria in CDA1flox/ERCre mice administered with tamoxifen, a finding confirmed even after corrections for urinary creatinine (**Figure 5.3A and B**). There was a trend towards an attenuation of diabetes-associated urinary KIM1 levels in tamoxifen-treated CDA1flox/ERCre mice (**Figure 5.3C** $p = 0.09$ vs. diabetic vehicle-treated mice), suggesting a reduction in tubular injury in these mice.

5.3.3. CDA1 deficiency attenuates diabetes-associated renal injury and fibrosis

At ten weeks of diabetes, there was a ~1.5-fold increase in TGF β 1 gene expression levels in STZ-injected mice, specifically CDA1flox and CDA1flox/ERCre mice receiving vehicle ($p < 0.05$ vs. non-diabetic controls), with concomitant upregulation of profibrotic genes, such as fibronectin, collagens I and III, as well as other genes known to be elevated by renal injury, including *matrix metalloproteinase-2* (MMP2) and *plasminogen activator inhibitor-1* (PAI1) (**Figure 5.4**, $p < 0.05$ vs non-diabetic controls). In addition to these transcriptional changes, while ECM accumulation as assessed by Masson's Trichrome staining was not statistically significant between non-diabetic and diabetic control mice (**Supplementary Figure 2**), there was a ~2.9-fold increase in collagen IV accumulation in renal cortex of diabetic CDA1flox/ERCre treated with vehicle (**Figure 5.5**, $p < 0.05$ vs. non-diabetic controls).

Induced genetic deletion of CDA1 during the progression of disease led to the attenuated expression of many of the profibrotic genes examined (ranging from 15-30% reduction), such as collagen III and MMP2 (**Figure 5.4**, $p < 0.05$ vs diabetic CDA1flox/ERCre vehicle-treated mice). CDA1 deficiency also led a reduction in renal ECM deposition (**Supplementary Figure 2**, $p < 0.05$ vs CDA1flox/ERCre vehicle-treated mice) with an associated decrease in diabetes-associated collagen IV immunostaining in these mice (**Figure 5.5**, $p < 0.05$ vs. diabetic vehicle-treated mice).

Table 5.2. Metabolic parameters of mice from the 10-week diabetic study

Treatment	CDA1flox					
	Vehicle			Tamoxifen		
	Control	Diabetic		Control	Diabetic	
<i>Blood Glucose (mmol/L)</i>	14.7 ±0.9	23.5 ±2.3	*	15.6 ±0.5	24.0 ±2.2	**
<i>Glycated Haemoglobin (%)</i>	4.7 ±0.1	11.8 ±0.7	**	5.2 ±0.3	10.5 ±0.9	**
<i>Body weight (g)</i>	32 ±1	24 ±1	***	33 ±1	24 ±1	***
<i>Total Kidney Weight/BW (%)</i>	1.12 ±0.03	1.80 ±0.06	***	1.09 ±0.03	2.20 ±0.57	***
<i>Water intake (mL/day)</i>	5.2 ±1.6	26.5 ±1.7	***	1.8 ±1.3	21.3 ±2.7	***
<i>Food intake (g/day)</i>	2.1 ±0.4	5.81 ±0.2	***	2.94 ±0.1	5.19 ±0.3	*
<i>Urine Output(mL/day)</i>	1.0 ±0.2	23.3 ±1.7	***	1.4 ±0.7	17.0 ±2.5	**

Treatment	CDA1flox/ERCre					
	Vehicle			Tamoxifen		
	Control	Diabetic		Control	Diabetic	
<i>Blood Glucose (mmol/L)</i>	14.7 ±1.2	29.5 ±1.5	***	16.5 ±1.9	23.2 ±2.5	
<i>Glycated Haemoglobin (%)</i>	4.8 ±0.2	12.3 ±0.6	***	4.9 ±0.2	9.9 ±0.8	***
<i>Body weight (g)</i>	33 ±1	24 ±1	***	34 ±2	26 ±1	***
<i>Total Kidney Weight/BW (%)</i>	1.08 ±0.10	1.78 ±0.04	***	1.13 ±0.04	1.54 ±0.07	
<i>Water intake (mL/day)</i>	3.9 ±1.0	23.7 ±1.2	***	1.1 ±0.3	18.7 ±2.0	***
<i>Food intake (g/day)</i>	1.6 ±0.3	5.31 ±0.2	***	2.14 ±0.2	4.87 ±0.4	***
<i>Urine Output(mL/day)</i>	1.1 ±0.2	20.1 ±1.4	***	1.3 ±0.2	14.4 ±2.8	***

*p<0.05, **p<0.01, ***p<0.001 vs corresponding non-diabetic control

n= 6-12 for non-diabetic control mice, 10-13 for diabetic mice

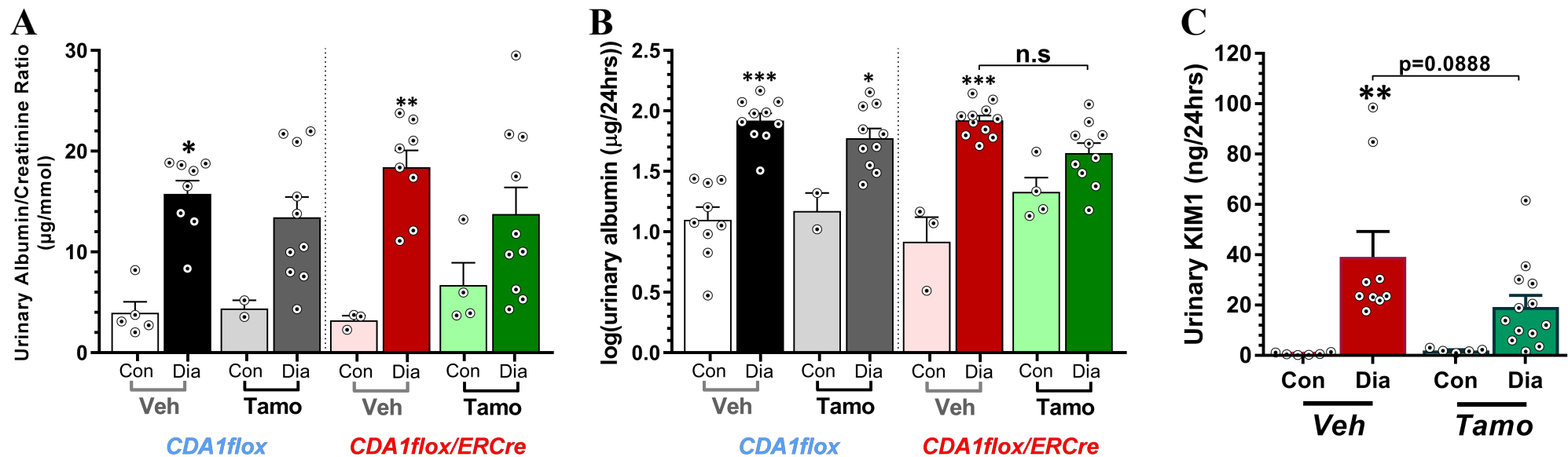


Figure 5.3. Induced CDA1 deficiency does not affect diabetes-associated albuminuria but may reduce urinary KIM-1 excretion. Analysis of urinary albumin levels (A), with correction with urinary creatinine levels (B), was performed in male CDA1 flox and CDA1 flox/ERCre mice which were either rendered diabetic with STZ for a period of 10 weeks (Dia) or received buffer to serve as non-diabetic controls (Con). At the midpoint of the study, 5 weeks after disease induction, mice were either administered tamoxifen (Tamo) or vehicle (Veh). Urinary KIM1 excretion was also analysed in CDA1 flox/ERCre mice only (C). Data shown as mean±SE (n= 3-6 for Con, n>9 for Dia). *p<0.05, **p<0.01, ***p<0.001 vs corresponding non-diabetic control

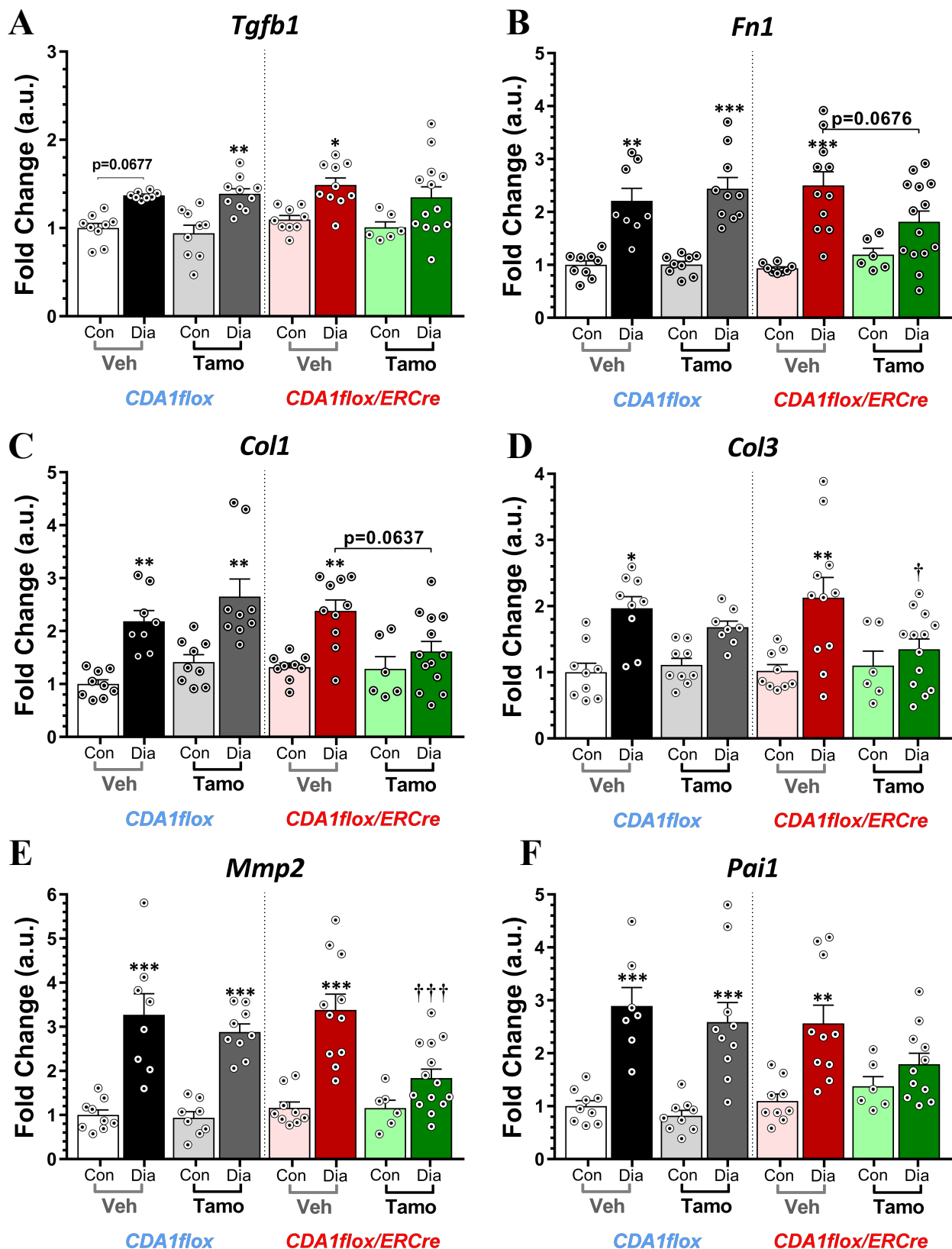


Figure 5.4. Induced genetic deletion of CDA1 attenuates diabetes-associated profibrotic gene expression in mice. qRT-PCR analysis for the relative TGF β 1 (A), fibronectin (B), collagens I (C) and III (D), MMP2 (E) and PAI1 (F) mRNA levels. Fold changes are shown as mean \pm SE (n>6 for Con, n>10 for Dia). *p<0.05, **p<0.01, ***p<0.001 vs corresponding non-diabetic control, #p<0.05 vs vehicle-treated non-diabetic mice, †p<0.05, †††p<0.001 vs vehicle-treated diabetic mice.

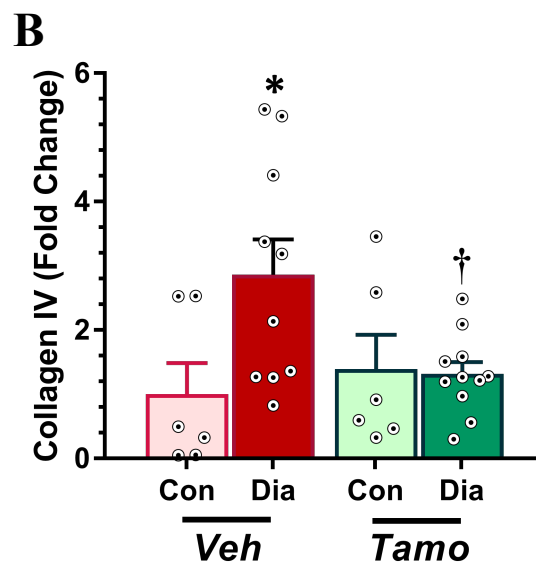
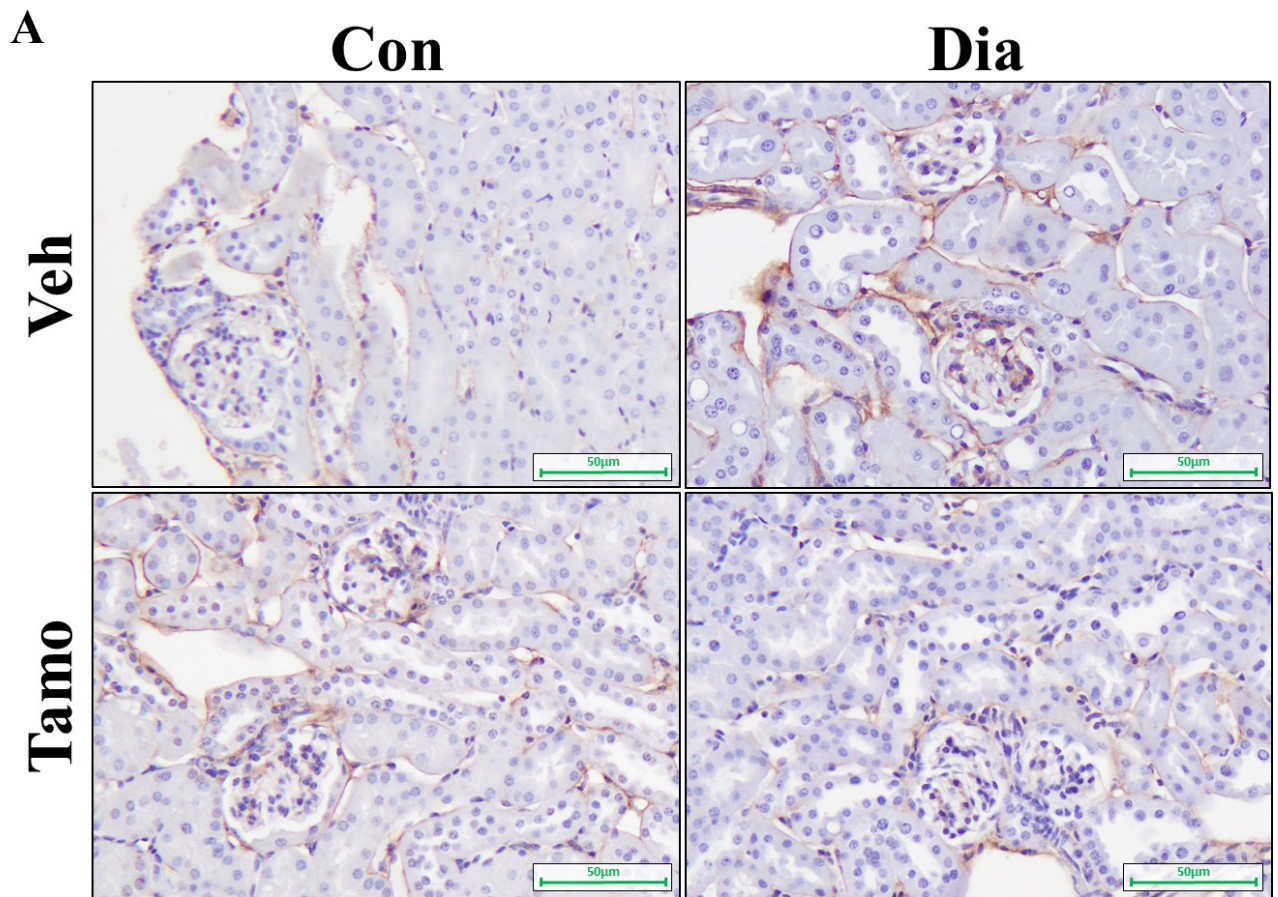


Figure 5.5. Induced genetic deletion of CDA1 attenuates diabetes-associated Collagen IV deposition in mice. (A) Representative images of immunohistochemical staining for renal collagen IV accumulation in 10-week non-diabetic (Con) and diabetic (Dia) CDA1^{flox}/ERCre mice treated with tamoxifen (Tamo) or vehicle (Veh) is shown in brown (magnification x200). (B) Quantification of the staining is represented as a bar graph, with fold changes are shown as mean±SE and individual samples (circles with dots) plotted within each group (n=6-7 for Con, >7 for Dia). *p<0.05 vs Veh Con, †p<0.05 vs Veh Dia.

5.3.4. Renoprotective effect of CDA1 deficiency is myofibroblast independent.

Renal cortical α -smooth muscle actin (α SMA) expression was also examined as a marker of myofibroblasts activation and infiltration. α SMA protein levels were increased in diabetic CDA1^{flox}/ERCre mice (**Figure 5.6**, $p < 0.05$ vs. nondiabetic vehicle-treated mice), which were unchanged with tamoxifen-administration. Thus, this finding suggests that CDA1 deficiency does not affect myofibroblast activation in this model.

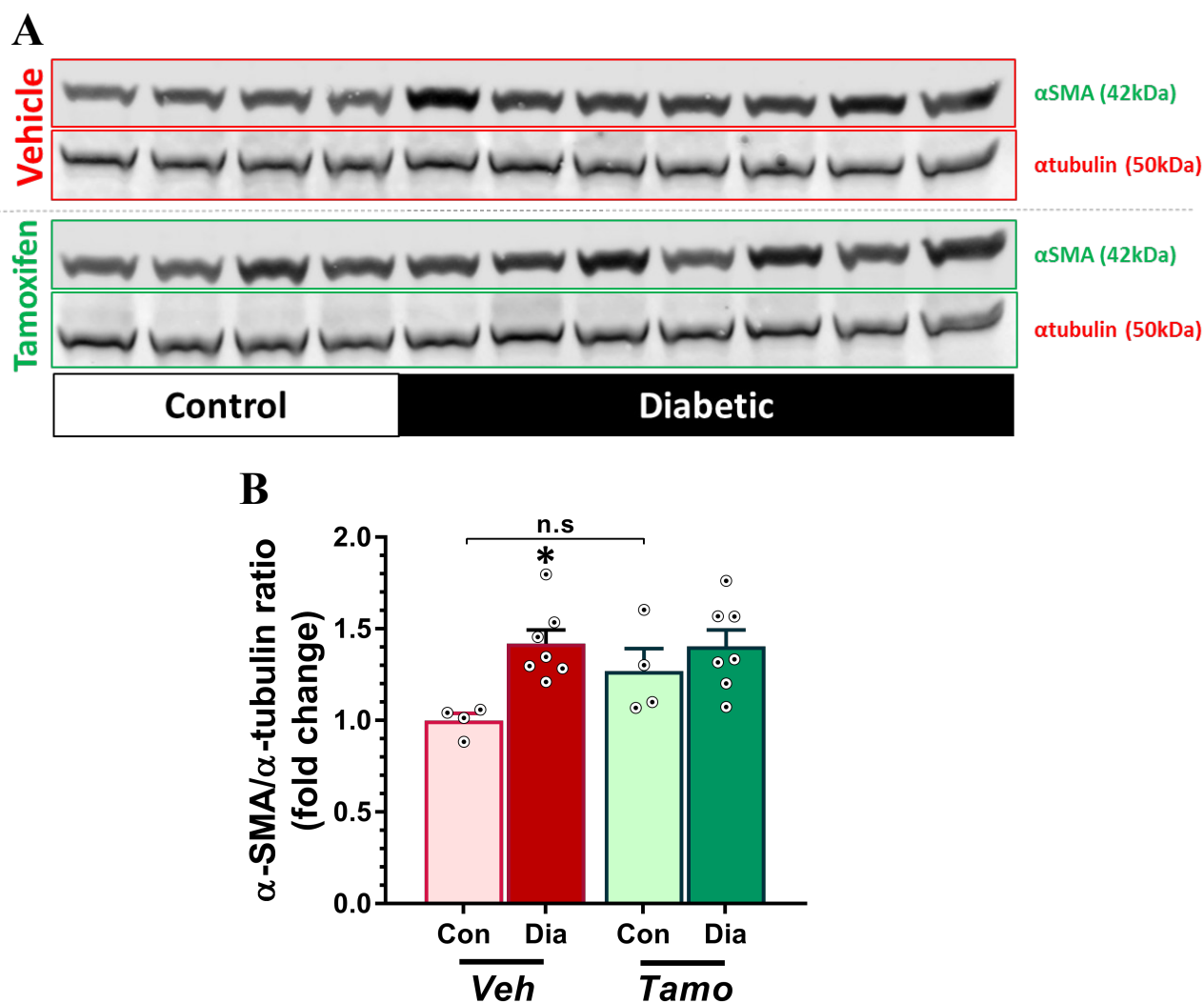


Figure 5.6. Induced genetic deletion of CDA1 does not affect diabetes-associated α SMA upregulation in mice. (A) Immunoblotting for renal α SMA expression in 10-week Con and Dia CDA1^{flox}/ERCre mice treated with tamoxifen (Tamo) or vehicle (Veh), and (B) quantification of band intensity. Fold changes are shown as mean \pm SE (n=4 for Con, 7 for Dia). * $p < 0.05$ vs Veh Con.

5.4. Discussion

In this chapter, I utilised the inducible ERCre strain of mice to induce the knockout of a gene through a site-specific recombination after induction of diabetes by serial STZ injections. In contrast to the scenario observed in conventional/global CDA1 KO mice, the use of CDA1^{flox}/ERCre mice allows for the development of diabetic kidney disease in the presence of CDA1. The administration of tamoxifen in these mice induces the deletion of exons 2-5 of the CDA1 gene, leading to the resultant protein product being non-functional. The reduction in available intact CDA1 gene upon tamoxifen administration, as well as the short half-life of the CDA1 protein,^{251, 272} effectively replicates the therapeutic intervention of CDA1 activity by, ultimately, reducing functional CDA1 protein levels. This strategy has been utilised previously, in inducible *nicotinamide adenine dinucleotide phosphate-oxidase-4* (NOX4) KO mice where the intervention occurred during the progression of diabetic kidney disease, specifically 10 days after the induction of diabetes.²⁹⁷ By contrast, this study intervened at a timepoint when signs of diabetic kidney disease were already evident, particularly after the development of diabetes-associated albuminuria (**Table 5.1**). Histological analysis of mice undergoing STZ-induced diabetic nephropathy at this timepoint has previously revealed that glomerular hypertrophy is present in diabetic mice at this timepoint.²⁹⁸ Analysis of renal tissue at the 10 week timepoint revealed that tamoxifen administration to CDA1^{flox}/ERCre mice 5 weeks earlier, at a dose of 1.5 mg/mouse/day for 3 consecutive days, led to a reduction of renal CDA1 gene expression levels to ~20-40% of vehicle-treated mice, regardless of diabetic status (**Figure 5.2**). Further analysis revealed that in this 10-week diabetic study only in CDA1^{flox}/ERCre mice receiving tamoxifen was there an attenuation of diabetes-associated renal injury. In contrast, tamoxifen administration to the genotype control CDA1^{flox} mice had no effect on any of the diabetes-associated metabolic parameters and/or upregulation of profibrotic genes examined. Thus, only induced CDA1 deficient mice exhibited a reduction in diabetes-associated profibrotic gene expression, which likely led to a subsequent reduction in cortical ECM deposition in this study.

Due to the ability of CDA1 to augment the TGF β signalling pathway, the inhibition and/or absence of CDA1 was expected to reduce disease burden through the attenuation of TGF β activity. Indeed, we have previously reported that primary renal cells from CDA1 KO mice exhibited an attenuated response to exogenous TGF β 1 stimulation.²⁵⁶ In agreement with previous reports, induced CDA1 deficiency was associated with an attenuation of profibrotic gene expression in diabetic CDA1^{flox}/ERCre mice receiving tamoxifen (**Figure 5.4**). Interestingly, the renoprotective effect associated with induced CDA1 deficiency occurred despite no effect on diabetes-associated upregulation of TGF β 1 gene expression, nor α SMA protein expression, in this study (**Figure 5.6**). These collective findings suggest that the actions of CDA1 in the development of fibrosis are downstream of the actions of the cytokine TGF β 1 and are independent of myofibroblast activation.

Furthermore, as α SMA expression is induced by TGF β in a Smad3-dependent manner,¹⁷² the mechanisms behind the promoting effects of CDA1 towards TGF β -induced profibrotic gene expression may be different from those which mediate the transcription of α SMA. However, further analysis will be required to better elucidate the molecular actions of CDA1.

In summary, this study examined the effect of induced genetic deletion of CDA1 on the progression of renal fibrosis in a mouse model of diabetic nephropathy. By utilising the inducible loxP/Cre system, the development of diabetes occurs in the presence of CDA1 in these mice until the administration of tamoxifen at 5 weeks after STZ-induced diabetes. Analysis of renal tissues after an additional 5 weeks of diabetes revealed an attenuation of diabetes-associated profibrotic gene expression and subsequent reduction in renal collagen deposition in induced CDA1 deficient mice. Thus, this finding further supports the concept that targeting CDA1 is a potential approach to combat CKD where fibrosis is a common pathological feature, such as diabetic nephropathy.

Chapter 6. Induced genetic deletion of CDA1 in Diabetic

Nephropathy: Delayed Intervention Study

6.1. Background

Targeting CDA1 activity at an early stage during the progression of disease, using an inducible genetic knockout mouse strain, has been shown to provide renoprotective effects in a mouse model of diabetic nephropathy (See **Chapter 5**). Ten weeks after STZ injections (~16-18 weeks of age), CDA1 wildtype mice presented with diabetes-associated metabolic changes, such as hyperglycaemia, albuminuria and renal hypertrophy. These were accompanied with upregulation of proinflammatory and profibrotic markers, as well as increases in ECM deposition in the renal cortex. Thus, in this study, I have chosen to induce the genetic deletion of CDA1 at this timepoint when renal injury is already established in order to investigate whether targeting CDA1 activity at this timepoint would result in the attenuation and/or reversal of the long-term development of diabetes-associated renal fibrosis.

6.2. Methods

6.2.1. CDA1^{flx}/ERCre mice, induction of diabetes and induced genetic deletion of CDA1

CDA1^{flx}/ERCre male mice (6-8 weeks of age) were rendered diabetic by multiple injections of STZ (55 mg/kg per day for 5 consecutive days) with littermate CDA1^{flx} mice serving as genotype controls. Animals serving as non-diabetic controls were injected with citrate buffer alone. Tamoxifen was administered at 10 weeks after STZ injections to induce the genetic deletion of CDA1 at this timepoint, representing delayed intervention against CDA1 activity. As controls, both CDA1^{flx} and CDA1^{flx}/ERCre mice were injected with vehicle, which would have no effect on the CDA1 gene and thus serve as CDA1 “wildtype” controls (**Figure 6.1**). Mice were culled at 20 weeks after diabetes induction to represent a later stage of diabetic nephropathy progression and tissues collected for analysis (**Refer to Chapter 3 for details**).

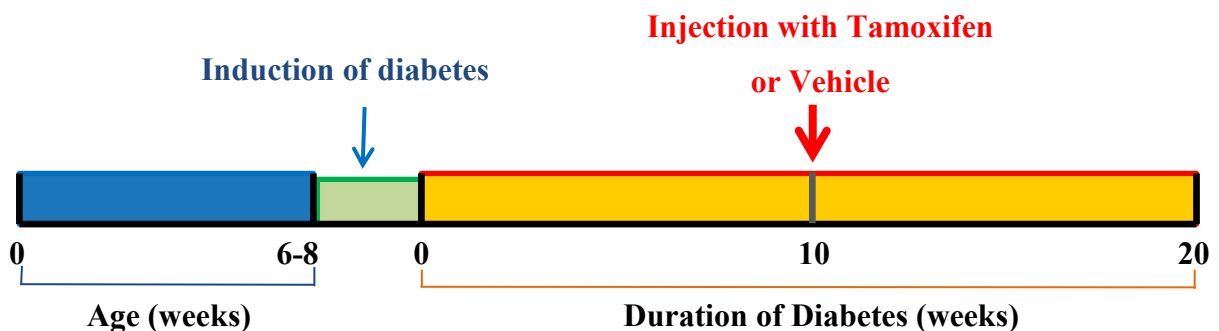


Figure 6.1. Timeline of the 20-week STZ-induced diabetes study. Male mice at 6-8 weeks of age were injected with STZ to induce diabetes or with citrate buffer to serve as non-diabetic controls. Mice were randomly allocated to receive injections of tamoxifen or vehicle at 10 weeks after diabetes induction. Mice were culled at 20 weeks after STZ injections and organs were harvested for analysis.

6.3. Results

6.3.1. CDA1 deficiency does not affect diabetes-associated metabolic parameters

At ten weeks after the induction of diabetes, non-diabetic and diabetic CDA1flox and CDA1flox/ERCre mice were randomly allocated to receive vehicle to serve as “wildtype” controls or administered tamoxifen which would induce CDA1 gene deletion only in CDA1flox/ERCre mice. One week prior to this timepoint, metabolic parameters were measured to confirm the diabetic status of mice injected with STZ. There was no statistically significant difference between non-diabetic CDA1flox and CDA1flox/ERCre mice with respect to any of the metabolic parameters examined. Both CDA1flox and CDA1flox/ERCre mice injected with STZ exhibited typical diabetes-associated changes in metabolic parameters, including polydipsia and polyuria (**Table 6.1**, $p < 0.001$ vs non-diabetic mice). Although there was an increase in urinary albumin excretion in diabetic CDA1flox/ERCre mice, this was not statistically significant ($p = 0.14$ vs non-diabetic CDA1flox/ERCre mice), possibly due to the high variability of this parameter between individual mice in that group. Interestingly, water intake and urine output were lower in diabetic CDA1flox/ERCre mice than diabetic CDA1flox mice (**Table 6.1**, $p < 0.05$ vs diabetic CDA1flox mice), similar to observations seen in the early intervention study (**Section 5.3.1**), despite no differences between the two groups in food intake and urinary albumin excretion.

Table 6.1. Metabolic parameters of mice at 10 weeks after STZ-induced diabetes induction

Treatment	CDA1flox			CDA1flox/ERCre		
	Control	Diabetic		Control	Diabetic	
<i>Body weight (g)</i>	33 ±1	27 ±1	***	32 ±1	26 ±0	***
<i>Water intake (mL/day)</i>	4.6 ±0.6	18.6 ±1.3	***	3.8 ±0.7	13.8 ±1.5	***, ††
<i>Food intake (g/day)</i>	2.3 ±0.2	4.3 ±0.2	***	1.8 ±0.2	3.8 ±0.3	***
<i>Urine Output (mL/day)</i>	1.0 ±0.1	14.6 ±1.2	***	0.9 ±0.1	11.1 ±1.3	***, †
<i>Albuminuria (µg/day)</i>	17.5 ±2.3	86.6 ±13.7	***	29.7 ±6.3	63.1 ±9.4	

*** $p < 0.001$ vs corresponding non-diabetic control, † $p < 0.05$, †† $p < 0.01$ vs diabetic CDA1flox mice

n=16-19 for non-diabetic control mice, 26-31 for diabetic mice

Metabolic parameters were once again analysed after an additional ten weeks. After a total of twenty weeks, STZ-induced diabetic mice exhibited expected changes in metabolic parameters as a result of insulin deficiency (**Table 6.2**), including increases in urinary albumin and KIM1 levels (**Figure 6.2**, $p < 0.01$ vs non-diabetic mice). Tamoxifen administration to CDA1flox and CDA1flox/ERCre mice had no effect on any of the metabolic parameters examined in this delayed intervention study. Thus, similar to findings seen in the early intervention study (**Chapter 5**), induced genetic deletion of CDA1 in this study had no effect on diabetes-associated metabolic parameters.

Table 6.2. Metabolic parameters of mice from the 20-week diabetic study

Treatment	CDA1flox									
	Vehicle				Tamoxifen					
	Control		Diabetic		Control		Diabetic			
<i>Blood Glucose (mmol/L)</i>	11.0	±1.5	28.1	±1.7	***	10.3	±0.5	30.7	±1.7	***
<i>Glycated Haemoglobin (%)</i>	4.6	±0.2	10.5	±0.7	***	4.7	±0.1	11.7	±0.7	**
<i>Body weight (g)</i>	37	±2	26	±1	***	38	±1	26	±1	***
<i>Total Kidney Weight/BW (%)</i>	1.15	±0.05	1.81	±0.06	***	1.06	±0.05	1.86	±0.08	***
<i>Water intake (mL/day)</i>	2.4	±0.7	21.8	±2.5	***	4.0	±0.4	27.4	±2.1	***
<i>Food intake (g/day)</i>	2.14	±0.39	3.99	±0.37	***	2.43	±0.20	4.74	±0.22	***
<i>Urine Output(mL/day)</i>	1.1	±0.2	20.8	±2.3	***	0.9	±0.2	25.1	±1.7	***

Treatment	CDA1flox/ERCre									
	Vehicle				Tamoxifen					
	Control		Diabetic		Control		Diabetic			
<i>Blood Glucose (mmol/L)</i>	11.2	±1.2	29.9	±2.5	***	12.1	±0.9	32.1	±1.2	***
<i>Glycated Haemoglobin (%)</i>	4.6	±0.1	12.6	±0.6	***	4.7	±0.0	11.6	±0.8	***
<i>Body weight (g)</i>	37	±1	26	±1	***	36	±1	26	±1	***
<i>Total Kidney Weight/BW (%)</i>	1.18	±0.03	1.83	±0.06	***	1.11	±0.03	1.86	±0.08	***
<i>Water intake (mL/day)</i>	3.6	±0.7	23.7	±2.5	***	4.7	±0.8	23.2	±2.3	***
<i>Food intake (g/day)</i>	1.39	±0.33	3.82	±0.41	***	2.11	±0.11	3.71	±0.37	***
<i>Urine Output(mL/day)</i>	1.0	±0.1	21.9	±2.5	***	0.8	±0.1	20.8	±2.7	***

***p<0.001 vs corresponding non-diabetic control, n= 7-12 for non-diabetic control mice, 12-17 for diabetic mice

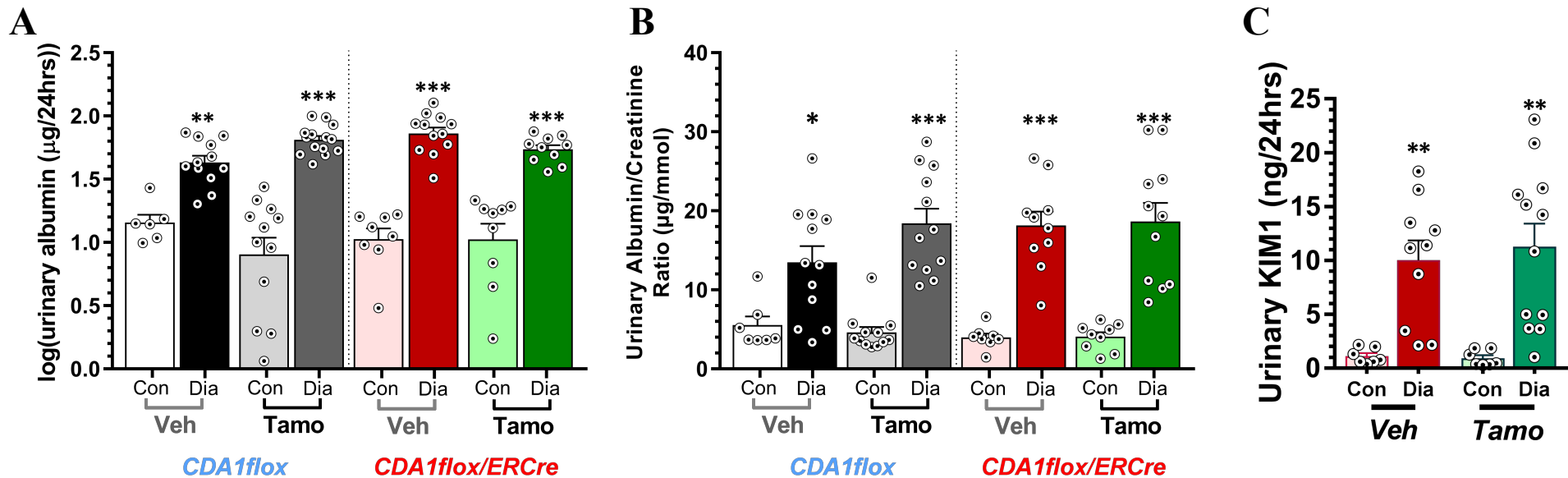


Figure 6.2. Delayed induced CDA1 deficiency does not affect diabetes-associated albuminuria, nor urinary KIM1 excretion. Analysis of urinary albumin levels (A), with correction with urinary creatinine levels (B), was performed in male CDA1flox and CDA1flox/ERCre mice which were either rendered diabetic with STZ for a period of 20 weeks (Dia) or received buffer to serve as non-diabetic controls (Con). At the midpoint of the study, 10 weeks after disease induction, mice were either administered tamoxifen (Tamo) or vehicle (Veh). Urinary KIM1 excretion was also analysed in CDA1flox/ERCre mice only (C). Data shown as mean±SE (n>7 for Con, n>11 for Dia). *p<0.05, **p<0.01, ***p<0.001 vs corresponding non-diabetic control, †p<0.05 vs vehicle-treated diabetic mice.

6.3.2. Reduced renal CDA1 mRNA levels in tamoxifen-treated CDA1flox/ERCre mice

Similar to the early intervention study (**Chapter 5**), administration of tamoxifen did not affect CDA1 gene expression levels in CDA1flox mice and levels of the CDA1 gene in CDA1flox/ERCre mice receiving vehicle were comparable to those observed in CDA1flox mice (**Figure 6.3A**). There was a diabetes-associated increase in CDA1 gene expression in mice which were expected not to have the CDA1 gene deleted; the tamoxifen-treated CDA1flox and vehicle-treated CDA1flox/ERCre mice (**Figure 6.3A**, $p < 0.001$ vs non-diabetic mice). Although there appears to be a diabetes-associated-increase in CDA1 mRNA in vehicle-treated CDA1flox mice, this did not reach statistical significance ($p = 0.14$ vs non-diabetic vehicle-treated CDA1flox mice). Administration of tamoxifen to CDA1flox/ERCre mice during disease progression led to a reduction in renal CDA1 gene expression by ~75-82% compared to vehicle-treated CDA1flox/ERCre mice as determined by qRT-PCR (**Figure 6.3A**, $p < 0.001$ vs vehicle treated mice). These results were confirmed by agarose gel electrophoresis analysis of PCR products from renal cDNA as templates (**Figure 6.3B**). Furthermore, this effect was not restricted to kidneys alone, as preliminary studies demonstrated a reduction in CDA1 gene expression in aortas collected from these mice (**Supplementary Figure 3**), regardless of diabetic status. Thus, the induced genetic deletion of CDA1 only occurs in CDA1flox/ERCre mice, with a significant reduction in CDA1 mRNA levels upon tamoxifen administration, regardless of their diabetic status.

6.3.3. Delayed intervention against CDA1 activity does not affect development of diabetes-associated renal fibrosis

Quantitative analysis of renal mRNA extracted from mice 20 weeks after STZ injections revealed that the expression levels of TGF β -related genes, such as fibronectin, MMP2 and p21 were significantly upregulated in diabetic mice when compared to their non-diabetic counterparts (**Figure 6.4D-F**, $p < 0.05$ vs non-diabetic controls). Induced deletion of CDA1, however, failed to attenuate the diabetes-associated upregulation of these genes, as reflected by the comparable mRNA levels of these genes between tamoxifen-treated diabetic CDA1flox/ERCre mice with the other diabetic CDA1 “wildtype” groups (**Figure 6.4**). Surprisingly, the expression levels of other profibrotic genes, particularly TGF β 1, collagens I and III were unchanged by diabetes in both CDA1flox and CDA1flox/ERCre mice, regardless of whether mice received tamoxifen or vehicle (**Figure 6.4A-C**). These results were confirmed with repeated extractions of RNA from renal cortical samples in at least three independent rounds of experiments, all showing the same results.

Transcription of ECM components are an early event in their biogenesis, with increased gene expression typically leading to increased ECM protein production and accumulation. Although the typical diabetes-associated upregulation of ECM components, such as collagens I and III, was not observed in this study, it is nonetheless important to assess the renal ECM accumulation in this long-term diabetes study, especially in the event that the early transcriptional changes in gene expression

may have already diminished, by the time of sacrifice of these animals. Immunohistochemical staining showed that there was a diabetes-associated increase in cortical collagen III accumulation by ~31-fold in vehicle-treated CDA1flox/ERCre (Figure 6.5, $p < 0.01$ vs vehicle-treated CDA1flox/ERCre mice). Interestingly, in CDA1flox/ERCre mice receiving tamoxifen to delete CDA1, diabetes failed to stimulate the accumulation of renal collagen III, with comparable levels observed between non-diabetic and diabetic CDA1flox/ERCre mice. However, there were lower levels of renal collagen accumulation in tamoxifen-treated diabetic CDA1flox/ERCre mice when compared to vehicle-treated diabetic CDA1flox/ERCre mice (Figure 6.5B, 16.8 ± 3.7 vs. 30.8 ± 3.6 , respectively, $p < 0.05$ vs diabetic vehicle-treated CDA1flox/ERCre mice). On the other hand, there were increases in collagen IV deposition by ~5.2 and ~3.8-fold in the cortex and glomeruli, respectively, in diabetic vehicle-treated CDA1flox/ERCre mice (Figure 6.6, $p < 0.05$ vs vehicle-treated CDA1flox/ERCre mice). Surprisingly, there was increased accumulation of collagen IV in non-diabetic CDA1flox/ERCre receiving tamoxifen to delete CDA1, which was greater than 4-fold when compared to vehicle-treated non-diabetic CDA1flox/ERCre mice (Figure 6.6, $p < 0.05$ vs vehicle-treated CDA1flox/ERCre mice). Diabetes did not further increase collagen IV accumulation in these mice. These findings suggest that delayed intervention against CDA1 activity may provide a moderate degree of renoprotection in STZ-induced diabetic nephropathy, but the exact effect needs to be explored in more detail.

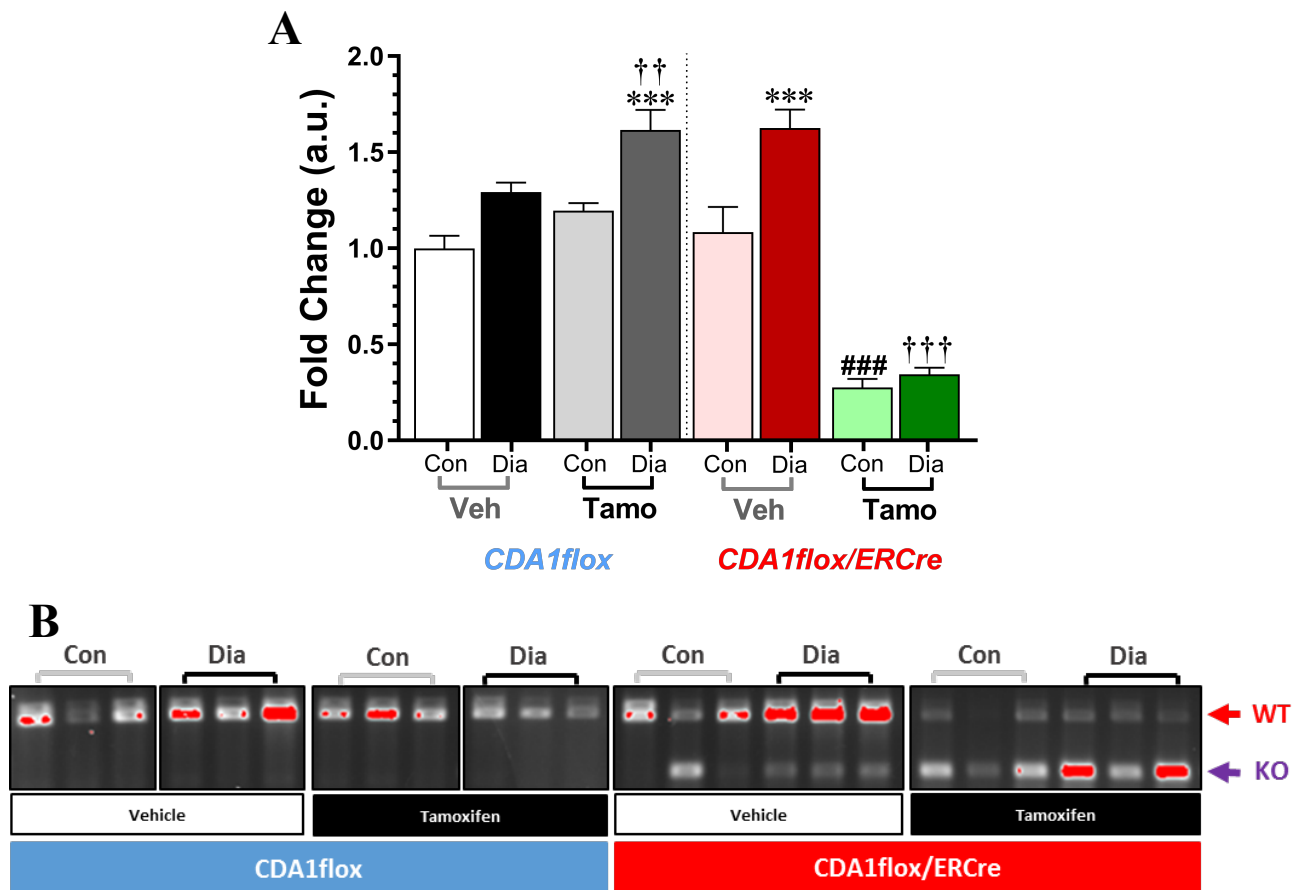


Figure 6.3. Induced genetic deletion of CDA1 in renal cortex of 20-week diabetic *CDA1lox/ERCre* mice. Renal CDA1 mRNA level, as determined by qRT-PCR analysis, are expressed as mean±SE (A, n=6-9 for nondiabetic controls, >11 for diabetic animals). ***p<0.001 vs corresponding non-diabetic control, ###p<0.001 vs corresponding non-diabetic control mice, †p<0.01, ††p<0.001 vs corresponding vehicle-treated diabetic mice. Representative images of reverse transcriptional PCR analysis of kidneys from *CDA1lox/ERCre* mice (B), with the presence of the top band indicating the intact CDA1 gene (WT, red arrow), while the presence of the lower band confirming the genetic deletion of the CDA1 gene as a result of tamoxifen administration in *CDA1lox/ERCre* mice (KO, purple arrow).

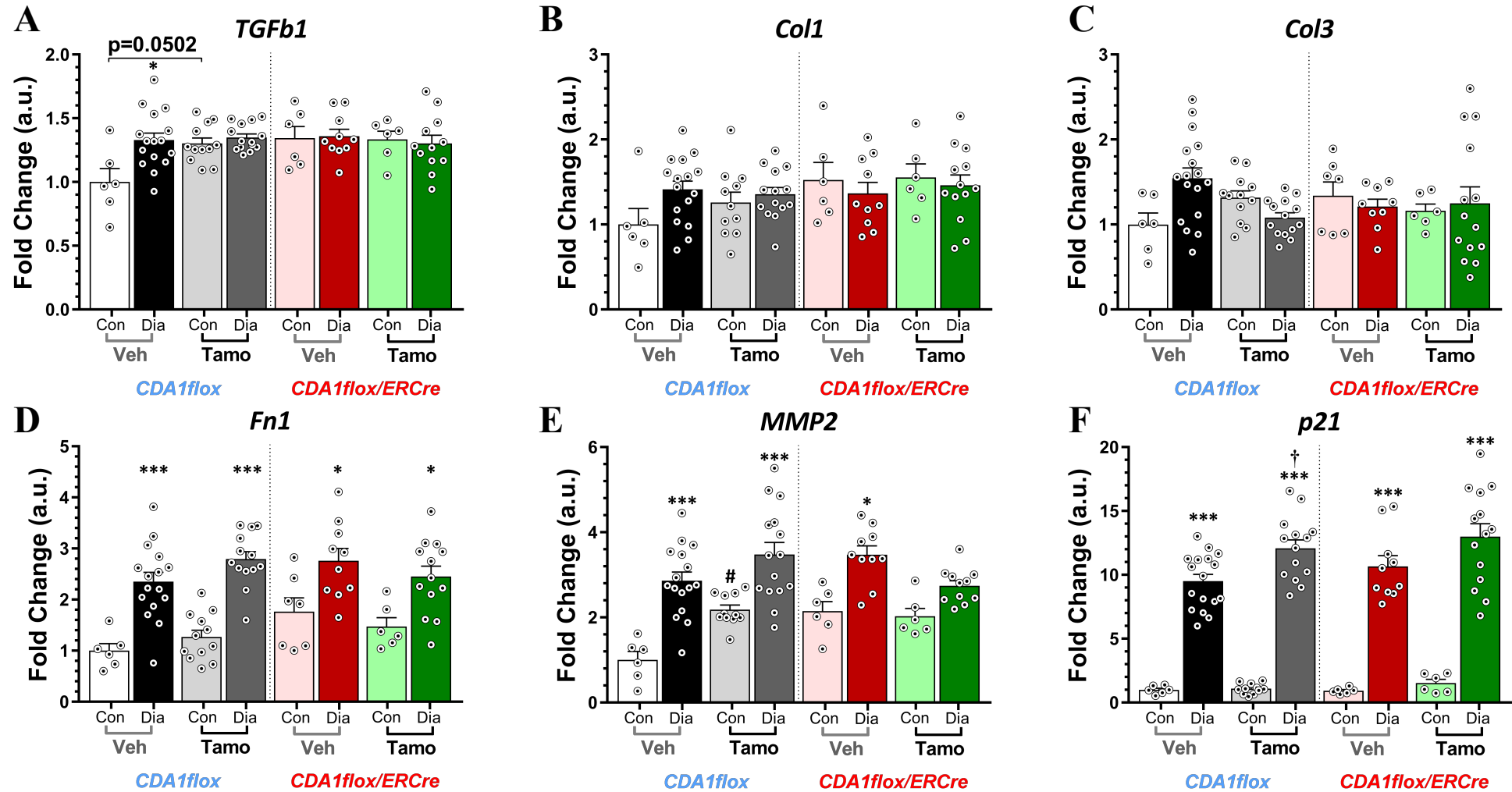


Figure 6.4. Induced genetic deletion of CDA1 does not affect diabetes-associated profibrotic gene expression in mice. qRT-PCR analysis for the relative TGFβ1 (A), collagens I (B) and III (C), fibronectin (D), MMP2 (E) and p21 (F) mRNA levels. Fold changes are shown as mean±SE (n>6 for Con, n>8 for Dia). *p<0.05, **p<0.01, ***p<0.001 vs corresponding non-diabetic control, #p<0.05 vs vehicle-treated non-diabetic mice, †p<0.05, †††p<0.001 vs vehicle-treated diabetic mice.

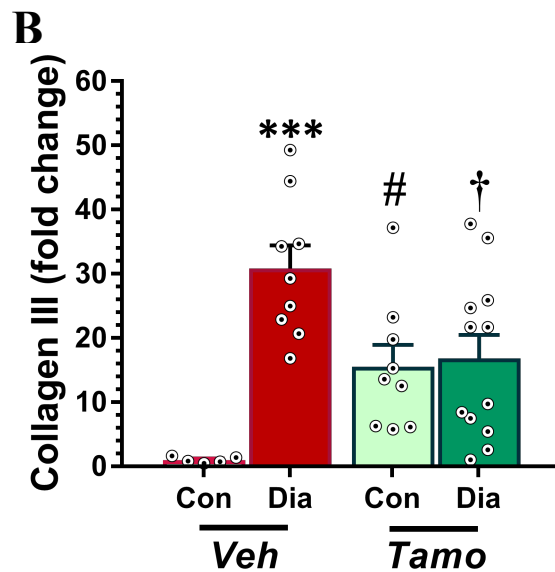
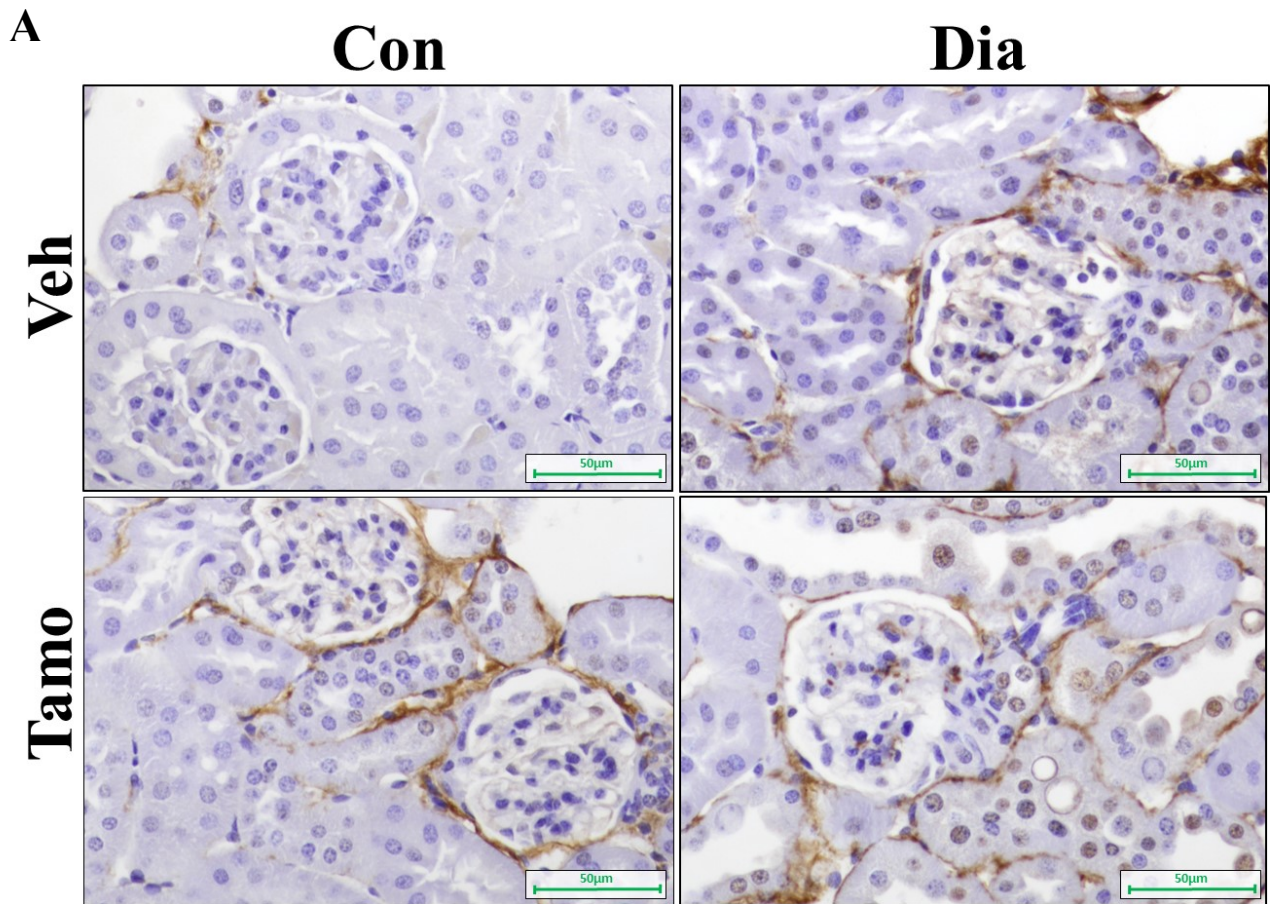


Figure 6.5. Delayed induction of CDA1 genetic deletion attenuates diabetes-associated collagen III deposition. Immunohistochemical staining for renal collagen III (A) accumulation in 20-week Con and Dia CDA1^{flox}/ERCre mice treated with Tamo or Veh is shown in brown, and (B) quantification of Collagen III staining (magnification 200x). Fold changes are shown as mean±SE (n=5-9 for Con, >11 for Dia). ***p<0.01, #p<0.05 vs Veh Con, †p<0.05 vs Veh Dia.

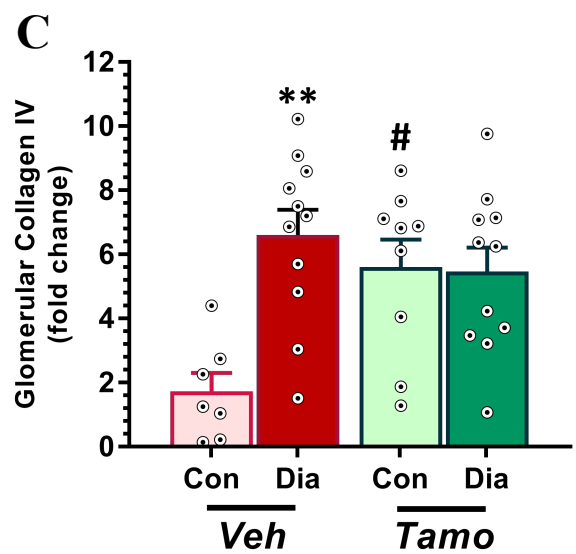
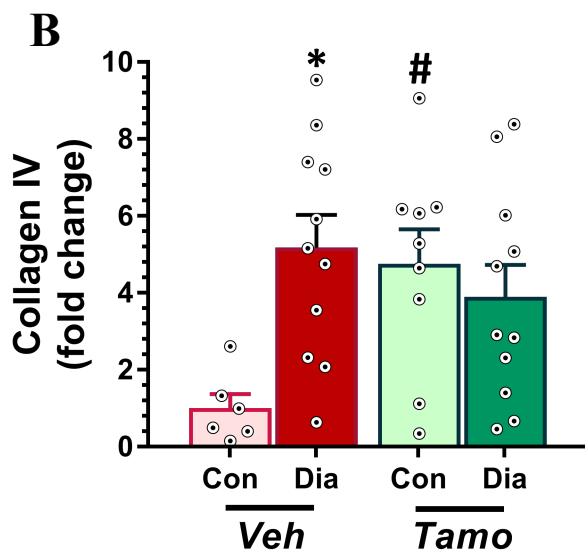
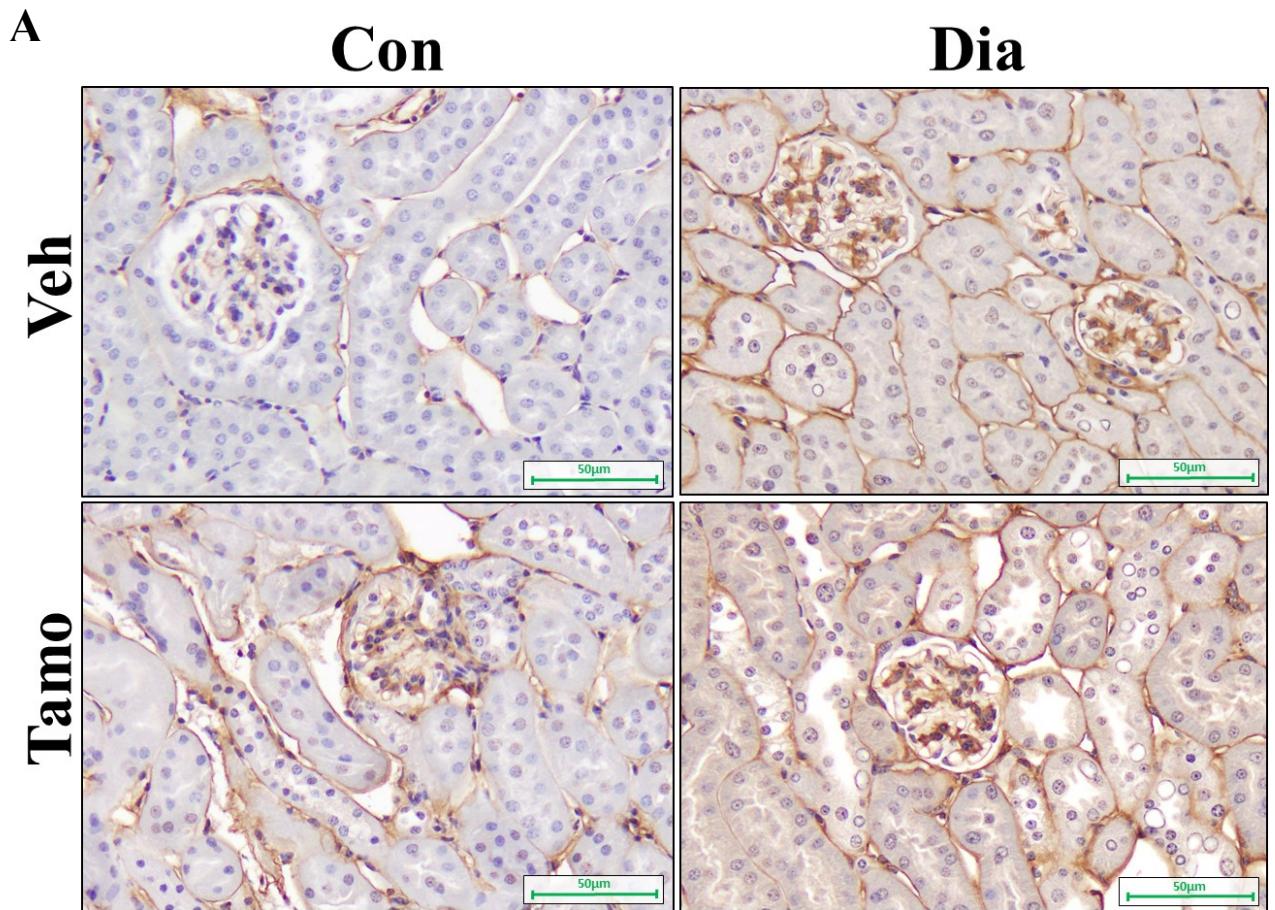


Figure 6.6. Delayed induction of CDA1 genetic deletion does not affect diabetes-associated collagen IV deposition. Immunohistochemical staining for renal collagen IV (A) accumulation in 20-week Con and Dia CDA1^{flox}/ERCre mice treated with Tamo or Veh is shown in brown, and (B and C) quantification of Collagen IV in the cortex and glomeruli, respectively (magnification 200x). Fold changes are shown as mean±SE (n=5-9 for Con, >11 for Dia). *p<0.05, **p<0.01, #p<0.05 vs Veh Con, †p<0.05 vs Veh Dia.

6.4. Discussion

In the previous chapter, I demonstrated that early intervention against CDA1 activity, through induced CDA1 genetic deletion, was protective against the development of renal fibrosis in diabetic nephropathy (See **Chapter 5**). CDA1 deficiency induced 5 weeks after diabetes induction was associated with an attenuation of diabetes-associated expression of profibrotic genes and subsequent collagen deposition. In this chapter, I examined the effect of genetic deletion of CDA1 at a more delayed timepoint on the long-term development of renal fibrosis in a mouse model of DN, where CDA1 deletion was induced 10 weeks after diabetes induction. At this delayed intervention timepoint, diabetic mice with functional CDA1 exhibited typical diabetes-associated changes in metabolic parameters, such as hyperglycaemia, albuminuria and renal hypertrophy, as well as robust upregulation of proinflammatory and profibrotic markers with associated increases in ECM deposition (**Chapter 5**). Thus, this represents a timepoint with readily detectable renal structural injury. Tamoxifen administration to CDA1 flox/ERCre mice at this timepoint resulted in the reduction in CDA1 mRNA expression by ~70% as determined 10 weeks later at the endpoint of this study, regardless of diabetic status (**Figure 6.2**). Despite this significant reduction in functional CDA1 expression in tamoxifen-treated CDA1 flox/ERCre mice, there was no effect observed in many of the diabetes-associated parameters examined in this study, including urinary albumin and KIM1 levels. In addition, induced CDA1 deficiency did not affect diabetes-associated upregulation of profibrotic genes, such as fibronectin and MMP2 (**Figure 6.4**), as well as diabetes-associated collagen IV deposition in this study (**Figure 6.6**). Interestingly, there was a reduction in diabetes-associated collagen III deposition in tamoxifen-treated CDA1 flox/ERCre mice, suggesting a certain degree of renoprotection with induced CDA1 deletion. Overall, it appears that this more delayed intervention against CDA1 expression was unable to prevent diabetes-associated renal fibrosis in this model.

The hypothesis which I planned to examine in these studies relies on at least two core principles. Firstly, the assumption that the TGF β signalling pathway is critical in the fibrotic process, especially in the kidney. Indeed, a recent study demonstrates that increasing levels of transgenic TGF β expression correlates with severity of renal injury in a genetic mouse model of diabetic nephropathy.¹³⁹ Secondly, inhibition of CDA1 activity is expected to attenuate TGF β signalling. Although the degree of the reduction in renal CDA1 gene expression in this study is comparable to the reduction observed in the early intervention study (**Chapter 5**), delayed intervention against CDA1 activity had no effect on most of the diabetes-associated fibrotic markers. This suggests that, by extension, delayed intervention against TGF β signalling may have a diminishing effect in attenuating diabetes-associated renal fibrosis. While a wealth of experimental data on the renoprotective effects of inhibiting the TGF β signalling pathway exists (**Table 2.1**), many, if not all, of these studies use preventative approaches. The literature detailing the therapeutic intervention against the TGF β signalling pathway at established stages of renal disease and their effects on

established fibrotic process are limited. Although the administration of TGF β neutralising antibodies after the onset of disease has shown promising results in rodent models of Type 1 and 2 diabetic nephropathy,^{219, 220} as well as in adriamycin-induced nephropathy,¹⁸³ the therapeutic efficacy of direct TGF β antagonism in established stages of disease have been questioned due to the alleged ineffectiveness observed in a phase II clinical trial in diabetic nephropathy.²⁰⁴ Nonetheless, the TGF β signalling pathway remains an attractive target to combat fibrosis progression in diabetic nephropathy, with the renoprotective efficacy of indirect therapies, such as RAAS blockade, historically being associated with reduced TGF β levels and/or signalling activity.²⁰⁵⁻²⁰⁸ Furthermore, targeted inhibition of particular components, or downstream effectors, of the TGF β signalling pathway have been proposed as a means to safely combat TGF β -associated fibrosis development. In particular, therapeutic interventions against miRNA-21, which is induced by TGF β signalling, have been shown to attenuate renal fibrosis in mouse models of Type 1,²³⁸ and Type 2 diabetes.²³⁹ As I have observed an attenuation of diabetes-associated renal fibrosis with the earlier intervention against CDA1 (**Chapter 5**), close examination of the intervention against CDA1 at different timepoints of disease progression is required to obtain a more thorough understanding of the pathological role of CDA1 in renal disease development.

The findings presented in this chapter once again support the view that while CDA1 may modulate TGF β activity, it is not an integral component of the TGF β signalling pathway. Although there were higher levels of collagen III and IV accumulation in non-diabetic CDA1 $^{flx}/ERCre$ mice receiving tamoxifen when compared to those receiving vehicle (**Figure 6.5 and 6.6**), it is anticipated that CDA1 deficiency did not lead to renal injury in non-diabetic mice as seen by the lack of changes to other parameters associated with renal injury, particularly urinary excretion of albumin and KIM1, as observed when comparing non-diabetic CDA1 $^{flx}/ERCre$ mice receiving either tamoxifen or vehicle. Furthermore, there were no statistically significant differences observed in ECM accumulation between diabetic CDA1 $^{flx}/ERCre$ mice receiving either vehicle or tamoxifen, as assessed by Masson's trichrome (**Supplementary Figure 4**) and collagen IV staining (**Figure 6.5**). These findings support the notion that induced CDA1 deficiency was not associated with exacerbation of diabetes-associated renal injury.

Unexpectedly, there appeared to be statistically significant differences in the expression of a number of genes between mice administered tamoxifen or vehicle. In particular, there were increases in MMP2 and TGF β 1 in non-diabetic tamoxifen-treated CDA1 flx mice (**Figure 6.4A and E**, $p \leq 0.05$ vs vehicle-treated CDA1 flx mice), while there was a further increase in diabetes-associated p21 gene expression in tamoxifen-treated CDA1 flx mice (**Figure 6.4 F**, $p < 0.05$ vs vehicle-treated CDA1 flx mice). As these results have consistently been observed after repeated rounds of RNA extraction and subsequent analysis, it is unclear what the underlying reason for this phenomenon.

Ultimately, these tamoxifen-associated effects on transcriptional changes were not observed in the CDA1^{flox}/ERCre strain, nor affected metabolic or functional parameters of these mice in this study. In fact, this phenomenon is observed in many of the genes examined at this timepoint, particularly collagens I and III, albeit not reaching statistical significance (**Figure 6.4**).

Interestingly, induced CDA1 deficiency at a delayed timepoint was associated with an attenuation of diabetes-associated collagen III deposition, with a >50% reduction observed in diabetic tamoxifen-treated CDA1^{flox}/ERCre mice when compared to diabetic vehicle-treated CDA1^{flox}/ERCre mice (**Figure 6.6**). There was, however, no change in gene expression levels of collagen III observed between non-diabetic and diabetic mice, regardless of treatment with tamoxifen or vehicle. Although there were diabetes-associated increases in gene expression levels of fibronectin, MMP2 and p21, an overall lack of transcriptional changes with diabetes at this later timepoint in disease development, particularly TGF β 1 and collagen I, was observed (**Figure 6.4**). This is not entirely unexpected, as other researchers in our department have previously observed the same lack of transcriptional changes in an advanced stage of diabetic nephropathy [Tikellis, C., unpublished data]. This is likely due to the disease progressing to a more chronic state, where changes in protein expression and subsequent alterations in renal architecture have already occurred, with transcriptional changes more readily detectable at earlier stages of disease development. Thus, any effects of the induced genetic deletion of CDA1 on transcriptional changes are likely to have occurred prior to this timepoint, as was clearly observed in the early intervention study (**Chapter 5**). Conversely, the general lack of transcriptional changes at this timepoint can also be due to the strain of the mice, as well as being an inherent feature of this disease model. Firstly, the background strain of mice used in this study is the C57BL6 mouse strain, which is known to be relatively resistant to glomerulosclerosis,^{273, 299} as seen by the lack of mesangial expansion in response to diabetes in these mice (**Supplementary Figure 5**). Secondly, mouse models of STZ-induced diabetic nephropathy do not progress towards ESRD and, thus, only exhibit early pathological features of diabetic nephropathy.³⁰⁰ Therefore, diabetes-associated renal injury in these mice may not be severe enough to sustain continuous and prolonged transcriptional changes. Indeed, although immunohistochemical staining for specific collagens was sensitive enough to detect significant differences between non-diabetic and diabetic mice, the diabetes-associated increase in total ECM accumulation as assessed by Masson's trichrome staining was not statistically significant (**Supplementary Figure 4**). Nevertheless, the diabetic studies presented in this thesis represent a proof-of-principle concept that the genetic deletion of CDA1 can be induced after the onset of disease and have renoprotective effects in a mouse model of diabetic nephropathy. Thus, to further validate the findings obtained from these studies, a more susceptible or severe mouse model of diabetic nephropathy should be considered. Indeed, as seen previously with the use of the more glomerulosclerotic-prone ApoE KO mouse

strain,²⁵⁶ it might be possible that the renoprotective effect of CDA1 deletion is more readily detectable in a more advanced model of nephropathy.

In summary, although early intervention against CDA1 activity using CDA1^{flox}/ERCre mice attenuated diabetes-associated ECM accumulation, a more delayed intervention against CDA1 activity had minimal effect on long-term diabetes-associated renal fibrosis development. Indeed, while delayed induced CDA1 deficiency led to an attenuation of diabetes-associated collagen III accumulation, it was not consistently shown to retard diabetes-associated renal fibrosis, as seen by the lack of an effect on a broad range of renal structural parameters. These combined findings suggest that targeting CDA1 appears to have only a partial effect towards the attenuation of renal fibrosis in this model and could be time-dependent. Indeed, the best effect could potentially be observed if CDA1 activity is inhibited at an earlier stage of disease development and for a more prolonged period of time. These observations are consistent with the view that targeting CDA1 attenuates but does not completely block TGF β signalling activity. Therefore, while further study is required to further validate the therapeutic potential of CDA1 inhibition, targeting CDA1 is likely to be a safe option towards new approaches to inhibit TGF β -stimulated profibrotic processes in renal diseases, including diabetic nephropathy.

Chapter 7. Genetic deletion of CDA1 in non-diabetic renal fibrosis

7.1. Background

Regardless of aetiology, fibrosis is the common final pathological feature in most chronic organ diseases and considered to be a significant process driving the progressive loss of nephrons in CKD. In fact, the severity of fibrotic lesions in the kidney, especially within the tubulointerstitial area, generally correlates with decline in renal function, as well as progression towards kidney failure.^{1, 61, 62} This is not surprising since tubules, which encompass ~90% of the renal cortex, are susceptible to ischemic and/or toxic injury due to their high metabolic demands and their position downstream of the glomerulus in the nephron. Indeed, many of the initial pathological changes observed in CKD, such as glomerulosclerosis, mesangial expansion and capillary constriction, lead to ischaemic conditions. Although initial pathological insults may be halted and even reversed, restoration of blood flow to the affected tissue ultimately results in the activation and infiltration of inflammatory cells into the site of injury.^{11, 301} The production of reactive oxygen species and proinflammatory cytokines, as well as the persistent activation of inflammatory pathways, leads to subsequent tubular injury and renal fibrosis. Thus, it is imperative to study the effects of targeting profibrotic pathways in disease states with characteristic tubular injury.

The pathological actions of TGF β have been revealed to be, at least in part, modulated by CDA1.^{255, 256} This pathological role of CDA1 in renal fibrosis is supported by observations of elevated CDA1 protein levels in human renal biopsies from patients with both diabetic and non-diabetic sclerotic renal diseases, as well as findings from our *in vivo* studies using murine models of diabetic nephropathy.²⁵⁶ It has been previously demonstrated that targeting CDA1 led to an attenuation in diabetes-associated renal fibrosis through reduced TGF β activity. The pathological role of CDA1 in the development of non-diabetic renal fibrosis has yet to be examined experimentally. Thus, in order to investigate the antifibrotic potential of targeting CDA1 in non-diabetic kidney disease, this chapter will examine the effect of the genetic deletion of CDA1, using our previously described global CDA1 *knockout* (KO) mouse,²⁵⁶ in two mouse models of non-diabetic renal diseases; *unilateral ureteral obstruction* (Uuo) and renal *ischaemic/reperfusion* (IR) injury.

There are a couple of similarities shared between the two *acute kidney injury* (AKI) models utilised in this chapter. Firstly, renal injury is induced by a simple surgical operation to obstruct the ureter or the renal pedicle/artery for Uuo and IR injury, respectively. Thus, these models require no immune or toxic insult, nor does it involve any confounding factors such as hypertension, proteinuria or hyperlipidaemia.^{60, 302, 303} Secondly, although the contralateral kidney may undergo compensatory changes,³⁰⁴ it is left intact and thus the animal's lifespan is not compromised. However, due to the difference in aetiology, the progression of disease differs between the two. The Uuo model presents with all of the key features of the typical fibrogenic process, with ECM deposition being observed

within 3 days after obstruction and progresses rapidly over a short timeframe.¹⁵⁵ The IR injury model used in this chapter is a unilateral IR injury model without contralateral nephrectomy, with a period of ischaemic injury set to induce the most injury without significant mortality. Generally, renal IR injury in mice and humans is associated with loss of proximal tubular brush borders, formation of tubular protein casts and renal inflammation.^{7, 305, 306} Proliferation of tubular cells is evident within 24–48 hours of injury, and the epithelial morphology is apparently restored after 5–7 days.³⁰⁷ While the IR model typically develops extensive fibrosis at later timepoints,^{308, 309} the relatively early timepoints used in this IR study were expected to exhibit molecular and cellular changes which reflect early stages of renal injury development.

7.2. Methods

7.2.1. Unilateral Ureteral Obstruction (UO)

Unilateral ureteral obstruction (UO) was performed as previously described,^{310, 311} with minor modifications. In brief, 10-12 week old CDA1 *wild-type* (WT) and CDA1 KO male mice were anaesthetized with ketamine:xylazine:atropine solution (100:20:1.2 mg/kg) and an incision was made in the abdomen. The left ureter was exposed and ligated with a 4.0 surgical silk suture, while the contralateral kidney was left intact. Sham surgery was performed on mice used as unobstructed controls. The incision was closed and mice were allowed to recover after carprofen/antisedan administration. Animals were euthanised at 5, 10 or 14 days after the UO procedure and kidneys were collected for analysis (**Figure 7.1**).

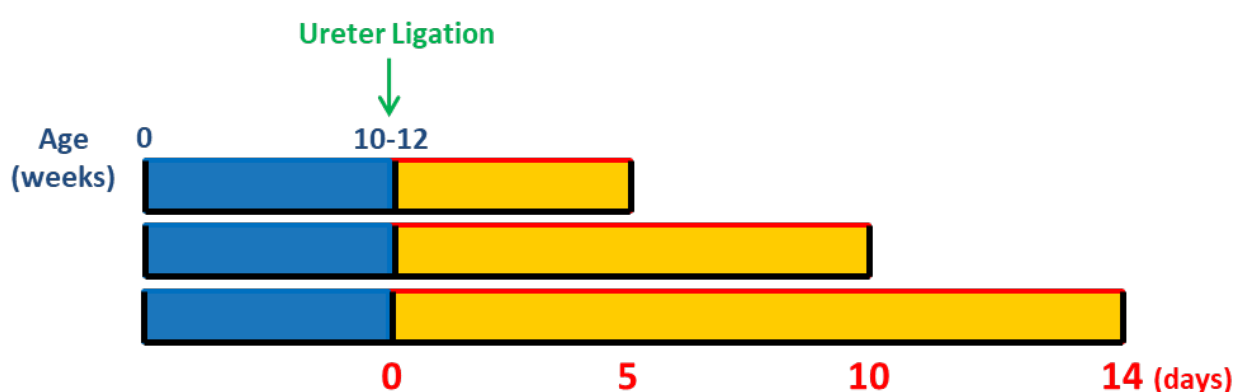


Figure 7.1. Timeline of UO model. Male CDA1 WT and KO mice at 10-12 weeks of age had their left ureter ligated to induce renal injury or underwent sham surgery to serve as sham controls. Mice were culled 5, 10 and 14 days after surgery and kidneys were harvested for analysis.

7.2.2. Ischemia/Reperfusion (IR) Injury

Unilateral renal *Ischemia/Reperfusion* (IR) injury was performed as previously described,³¹² with minor modifications. Renal IR was performed on 10-12 week old CDA1 WT and KO male mice after being anaesthetized with isoflurane and kept on a 37°C heat pad. The left renal pedicle was exposed with a flank incision and ligated with a 4.0 surgical silk suture to prevent blood flow and induce ischaemia for 45 mins, or a sham surgery was performed on unobstructed control mice. The contralateral kidney was left intact. The ligation was reversed to restore blood flow to the affected kidney before the incision was closed. Animals were euthanised at 4 and 8 days after the surgery and kidneys were collected for further analysis (**Figure 7.2**).

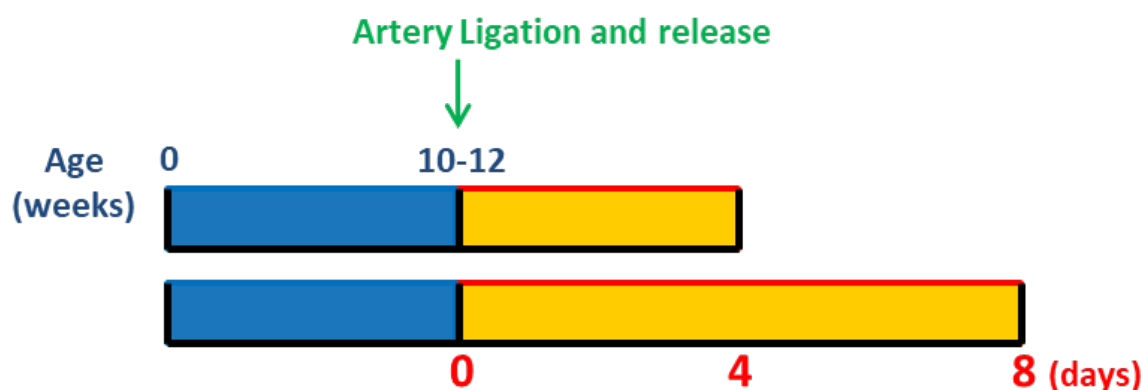


Figure 7.2. Timeline of IR injury model. Male CDA1 WT and KO mice at 10-12 weeks of age had their left renal pedicle obstructed for 45 mins before release to induce IR injury or underwent sham surgery to serve as sham controls. Mice were culled 4 and 8 days after surgery and kidneys were harvested for analysis.

7.3. Results

7.3.1. CDA1 and Unilateral Ureteral Obstruction

7.3.1.1. Morphological changes in obstructed kidneys of CDA1 WT and KO mice

To investigate the effect of CDA1 deficiency on the development of non-diabetic renal fibrosis, the severity of renal fibrosis and inflammation caused by UUO was compared between CDA1 WT and KO mice at 5, 10 and 14 days after surgery. Increases in *kidney-to-body weight ratio* (K:BW) of obstructed kidneys (Left K) were observed in CDA1 WT and KO mice 5 days after ligation (**Table 7.1**, $p < 0.05$ vs Sham animals), while the contralateral kidney (Right K) showed no changes in kidney-to-body weight ratio. There was no difference in kidney-to-body weight ratio seen between CDA1 WT and KO mice.

Obstruction of the ureter led to severe hydronephrosis occurring in 71% (10/14) of CDA1 WT mice and 58% (7/12) of CDA1 KO mice at 10 days after surgery, while 86% (12/14) of CDA1 WT and 93% (13/14) of CDA1 KO mice were affected at 14 days after surgery. There does not appear to

be a difference in the incidence rate of hydronephrosis between WT and KO groups. These kidneys were punctured to release the accumulated fluid, which allowed for accurate weight measurements of the kidney tissue. Unlike observations seen in the 5d UUO mice, there was no change in left kidney-to-body weight ratio between Sham and UUO mice at 10 days, nor at 14 days after surgery (**Table 7.1**). Interestingly, while there was a lower mean ratio of left kidney-to-body weight in CDA1 KO UUO mice when compared to CDA1 WT UUO mice at 14 days after surgery, this was not statistically significant (0.539 ± 0.047 vs 0.822 ± 0.128 , $p=0.1322$). In addition, hypertrophy of the contralateral kidney was generally observed at 10 and 14 days after surgery in UUO mice ($p < 0.05$ vs Sham), probably reflecting compensation for the failing kidney. The right kidney-to-body weight ratio of CDA1 WT mice was not significantly different between Sham and UUO mice at 14 days after UUO which was possibly due to the low sample size in the CDA1 WT Sham group ($n=3$).

Table 7.1. Kidney-to-Body Weight ratio of CDA1 WT and KO mice undergoing UUO

		CDA1 WT				CDA1 KO					
		Sham		UUO		Sham		UUO			
5 days	Left K:BW	0.587	± 0.020	0.719	± 0.023	**	0.614	± 0.023	0.703	± 0.026	*
	Right K:BW	0.656	± 0.018	0.697	± 0.015		0.653	± 0.021	0.679	± 0.016	
10 days	Left K:BW	0.600	± 0.019	0.666	± 0.059		0.593	± 0.018	0.605	± 0.036	
	Right K:BW	0.660	± 0.021	0.737	± 0.017	*	0.622	± 0.015	0.701	± 0.021	*
14 days	Left K:BW	0.625	± 0.012	0.822	± 0.128		0.553	± 0.020	0.539	± 0.047	
	Right K:BW	0.672	± 0.038	(n=3)	0.791	± 0.031		0.635	± 0.021	0.785	± 0.037

Left K: left kidney, Right K: right kidney which served as a contralateral unobstructed control

* $p < 0.05$, ** $p < 0.01$ vs corresponding Sham control

7.3.1.2. UUO-induced upregulation of profibrotic markers in CDA1 WT mice

Obstruction of the left ureter was associated with increased expression of profibrotic genes in CDA1 WT mice. qRT-PCR analysis revealed that CDA1 mRNA levels were elevated by ~ 3.0 fold in 5d UUO CDA1 WT animals (**Figure 7.3**, $p < 0.001$ vs Sham), while mRNA levels of TGF β 1 and T β R2 were elevated ~ 4.7 and ~ 4.4 fold, respectively (**Figure 7.4**, $p < 0.01$ vs Sham) and these mRNA levels were sustained even after 14 days of UUO. This was accompanied by upregulated expression of genes related to fibrosis, such as collagens I and III by ~ 19.5 and ~ 6.0 fold, respectively (**Figure 7.5**, $p < 0.05$ vs Sham), inflammation and the complement system, including IL6 and *vascular cell adhesion molecule 1* (VCAM1) by ~ 40.2 and ~ 15.5 fold, respectively (**Figure 7.6**, $p < 0.05$ vs Sham). These transcriptional changes were consistent with elevated levels of ECM accumulation and total collagen content in these mice, as assessed by Masson's trichrome staining and hydroxyproline analysis, respectively (**Figure 7.7**). ECM deposition was increased by ~ 19.0 fold 5 days after surgery (**Figure 7.7B**, $p < 0.001$ vs. Sham), which was further increased to ~ 42.8 fold at 10 days (**Figure 7.7E**, $p < 0.01$ vs Sham). Consistent with the histological findings, total collagen content was increased by ~ 1.5 fold in 5 and 10-day UUO mice (**Figure 7.7C and F**, $p < 0.05$ vs Sham). Likewise, deposition of collagens III and IV, as determined by IHC staining, was elevated in obstructed CDA1 WT kidneys by ~ 5.2 and ~ 2.6 fold respectively after 5 days of UUO (**Figure 7.7**, $p < 0.001$ vs Sham), increasing

further to ~6.5 and ~8.2 fold for each collagen isotype, respectively, by 10 days of UUO (**Figure 7.8**, $p < 0.001$ vs Sham).

7.3.1.3. Genetic deletion of CDA1 does not affect UUO-induced renal fibrosis

As CDA1 WT mice showed typical sclerotic injury in UUO kidneys, I then examined the effect of the absence of functional CDA1 on renal disease development, in order to elucidate the role that CDA1 played in this model. As CDA1 was observed to be upregulated by UUO injury, I first examined the expression of CDA1 transcript levels in CDA1 KO mice. Since knockout of CDA1 was achieved through the deletion of exons 2-5, primers/probes were used to recognise sequences which are common in both CDA1 WT and CDA1 KO mice, thereby enabling the detection of remnant CDA1 transcript in CDA1 KO mice. Indeed, qRT-PCR analysis revealed that remnant CDA1 mRNA was transcribed in CDA1 KO mice (**Figure 7.3**), indicating that the promoter of the CDA1 gene was active despite the loss of functional CDA1 in these mice. While CDA1 mRNA levels in CDA1 WT mice were elevated by ~3.0 fold after UUO injury, UUO-associated upregulation of remnant CDA1 mRNA levels were, interestingly, attenuated by ~50% in CDA1 KO mice (**Figure 7.3**, $p < 0.05$ vs CDA1 WT UUO mice). In addition, the basal mean levels of the remnant CDA1 mRNA in Sham CDA1 KO mice were ~50% lower than those observed in CDA1 WT Sham mice, although this difference was not statistically significant. The genetic deletion of CDA1 in these mice was confirmed by genotyping analysis using genomic DNA (data not shown), as well as qRT-PCR analysis using a specific set of primers used for the detection of exons 2-5 of the CDA1 gene (**Supplementary Figure 7**). These collective findings confirmed that the CDA1 gene was deleted in CDA1 KO mice and, subsequently, may affect relevant pathways, such as the TGF β signalling pathway, in order to reduce the transcriptional upregulation of CDA1 in response to renal injury.

Next, I then examined whether CDA1 deficiency had any effect on UUO-associated renal injury in these mice. Contrary to expectations, genetic deletion of CDA1 did not appear to affect UUO-associated renal fibrosis development. This was evident by the lack of effects on UUO-associated upregulation of profibrotic genes, such as TGF β 1, T β RII, collagen I and III and MMP2, at many of the timepoints examined (**Figure 7.4 and 7.5**). Interestingly, there were increases in UUO-associated gene expression of T β RII and collagen I in CDA1 KO mice (by 127% and 176% compared to CDA1 WT mice, respectively) at 10 days after surgery (**Figure 7.4B and 7.5C**, $p < 0.05$ vs 10d CDA1 WT UUO), despite an apparent attenuation of fibronectin gene expression by ~37% in these mice (**Figure 7.5A**, $p < 0.05$ vs 10d CDA1 WT UUO). While the expression levels of these genes were not different between CDA1 WT and KO mice at 14 days after surgery, expression levels of MMP2, collagen III and osteopontin were higher in CDA1 KO UUO mice than in CDA1 WT UUO mice by 187%, ~211% and ~135%, respectively, at 14 days after surgery mice (**Figure 7.5**, $p < 0.05$ vs 14d CDA1 WT UUO).

Although there was a trend towards an attenuation of ECM deposition, as assessed by Masson's trichrome staining, in CDA1 KO mice at 5 days after surgery (**Figure 7.7B**, $p=0.0974$ vs CDA1 WT UUO 5d UUO), genetic deletion of CDA1, overall, had no effect on UUO-associated collagen accumulation. Indeed, as assessed by hydroxyproline analysis and immunohistochemical staining for collagens III and IV, there was no difference in collagen accumulation between CDA1 WT and KO mice at 5 days after surgery (**Figures 7.7C and 7.8**). These findings were consistent with a lack of an effect of CDA1 deletion on UUO-associated ECM accumulation at 10 days after surgery (**Figure 7.7D-F**). Furthermore, preliminary studies suggest that these findings were similarly found at later timepoints in this model, with no difference in UUO-associated increases in total collagen content between CDA1 WT and KO mice at 14 days after UUO (**Supplementary Figure 7**). There was, surprisingly, a trend towards an increase in cortical collagen III deposition (**Figure 7.9B**, by $\sim 28.0\%$, $p=0.0554$) while a decrease in collagen IV deposition was observed in CDA1 KO mice 10 days after surgery (**Figure 7.9D**, by $\sim 26.8\%$ $p<0.05$ vs CDA1 WT UUO). The combined findings from analysis of gene and proteins levels of profibrotic markers suggests that the absence of CDA1 appears to affect the expression of profibrotic markers, with a tendency towards exacerbation of profibrotic processes in this model. Whether CDA1 plays a protective role in fibrosis at later stages of UUO development is unclear and will need additional timepoints to determine its overall long-term effect in this disease model.

7.3.1.4. The effect of CDA1 deficiency on complement and inflammatory markers

Genetic deletion of CDA1 had no effect on the UUO-associated upregulation of genes related to inflammation and the complement system, including IL6, *intracellular adhesion molecule 1* (ICAM1) and *complement component 3* (C3) (**Figure 7.6**). There was, however, a trend towards an attenuation of UUO-associated VCAM1 upregulation in CDA1 KO mice at 5 days post-injury (**Figure 7.6F**, $p=0.0597$ vs CDA1 WT 5d UUO). Interestingly, there was also an attenuation of UUO-associated gene expression of *inducible nitric oxide synthase* (iNOS) and *macrophage scavenger receptor 1* (MSR1) at later stages of UUO development (**Figure 7.6B and C**, $p<0.05$ vs CDA1 WT UUO mice). Why the absence of CDA1 would lead attenuation of proinflammatory gene expression at later stages of UUO disease development and what effect that would have on fibrosis development is unclear and will require further investigation.

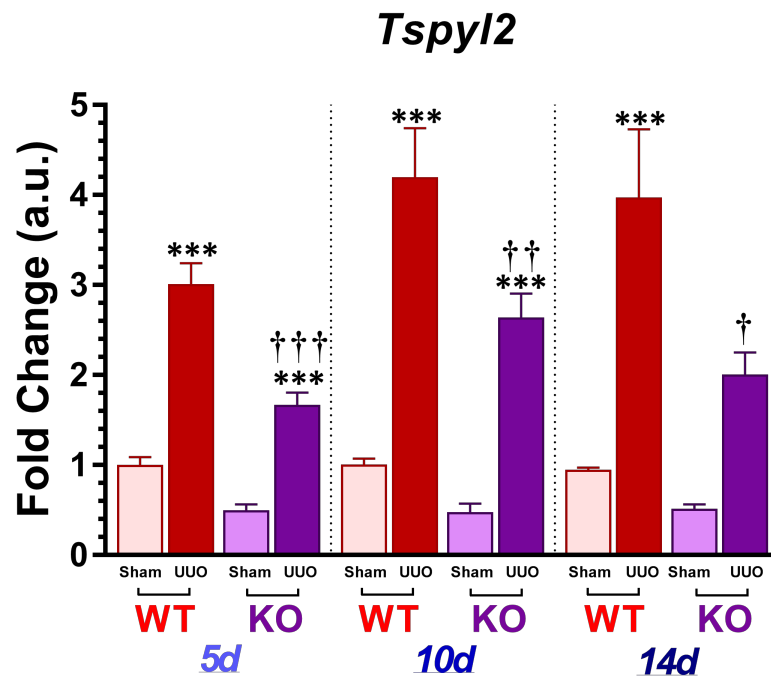


Figure 7.3. Upregulation of CDA1 gene expression in UUO. Male CDA1 WT and KO mice had their left ureter obstructed (UUO; darker columns) or underwent sham operation (Sham; lighter columns) and kidneys were collected 5, 10 and 14 days after obstruction. Kidney CDA1 mRNA levels were determined by qRT-PCR using primers detecting CDA1 transcripts from both WT CDA1 gene (A) and the remnant CDA1 gene from the knockout allele. Data shown as mean±SE (n>5 for sham, n>6 for UUO). ***p<0.001 vs corresponding Sham control, †p<0.05, ††p<0.01, †††p<0.001 vs CDA1 WT UUO mice.

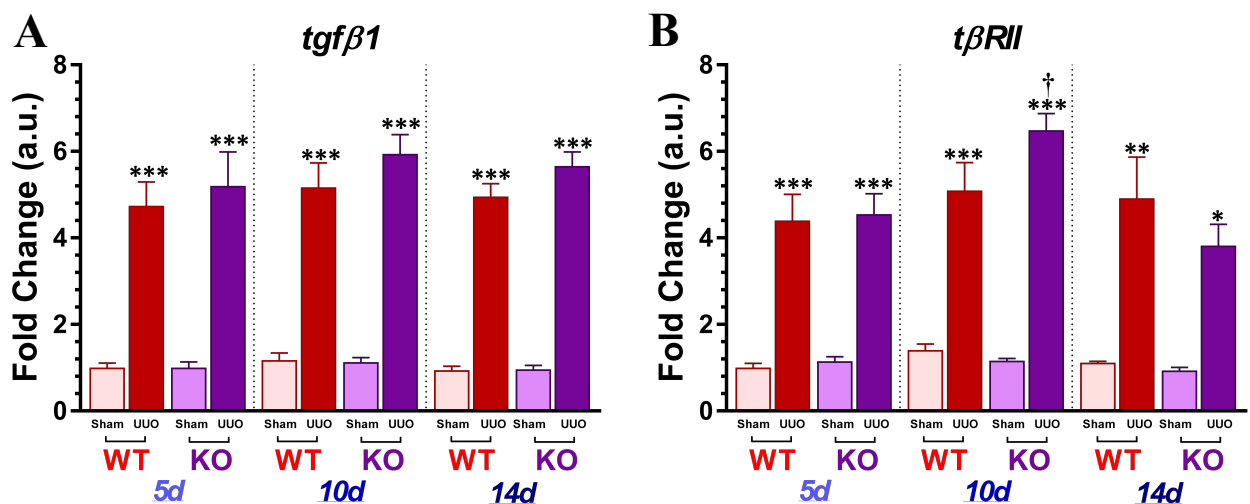


Figure 7.4. Genetic deletion of CDA1 does not affect UUO-associated upregulation in TGFβ gene expression, nor its receptor. qRT-PCR analysis for the relative TGFβ1 (A) and TβRII (B) mRNA levels in CDA1 WT and KO mice which underwent UUO or sham surgery for 5, 10 and 14 days. Data shown as mean±SE (n>5 for sham, n>6 for UUO). *p<0.05, **p<0.01, ***p<0.001 vs corresponding Sham control, †p<0.05 vs CDA1 WT UUO mice.

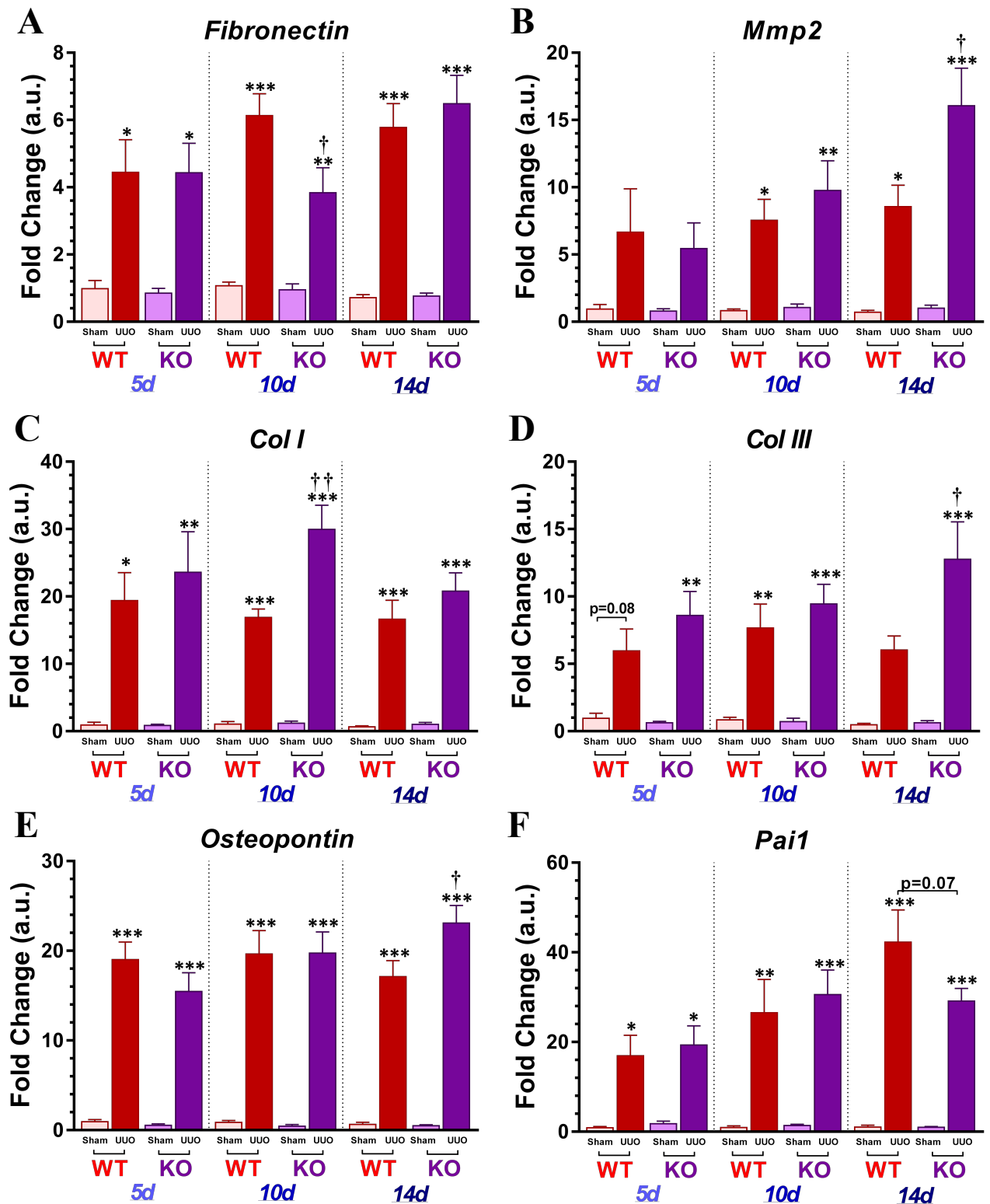


Figure 7.5. Genetic deletion of CDA1 does not affect UUO-associated changes in profibrotic gene expression. qRT-PCR analysis for the relative fibronectin (A), MMP2 (B), collagens I (C) and III (D), osteopontin (E) and PAI1 (F) mRNA levels in CDA1 WT and KO mice which underwent UUO or sham surgery for 5, 10 and 14 days. Data shown as mean±SE (n>5 for sham, n>6 for UUO). *p<0.05, **p<0.01, ***p<0.001 vs corresponding Sham control, †p<0.05, ††p<0.01 vs CDA1 WT UUO mice.

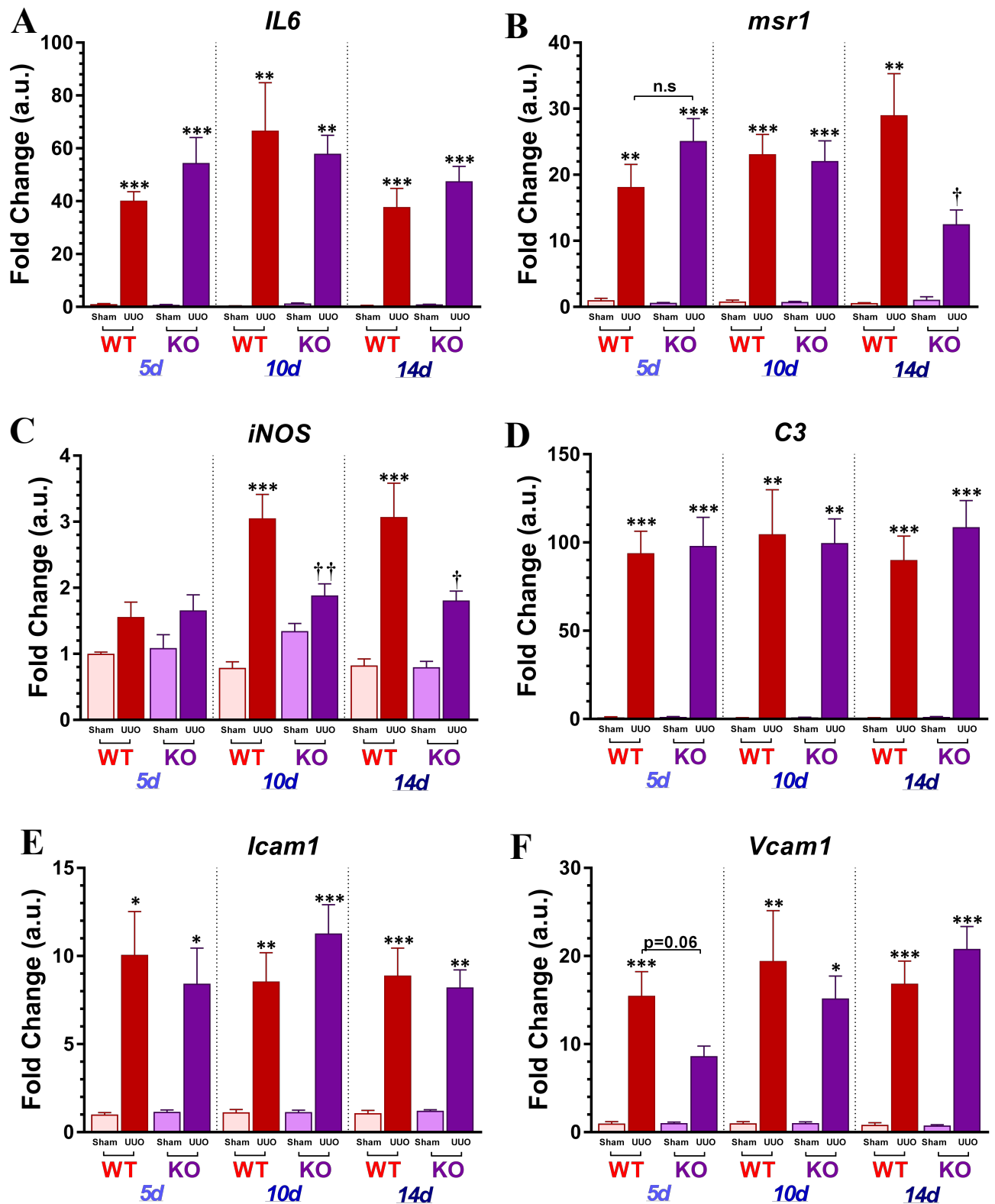


Figure 7.6. The effect of CDA1 deficiency on UUO-associated activation of inflammatory and complement pathways. qRT-PCR analysis for the relative *IL6* (A), *MSR1* (B), *iNOS* (C), *C3* (D), *ICAM1* (E) and *VCAM1* (F) mRNA levels in CDA1 WT and KO mice which underwent UUO or sham surgery for 5, 10 and 14 days. Data shown as mean±SE (n>5 for sham, n>6 for UUO). *p<0.05, **p<0.01, ***p<0.001 vs corresponding Sham control, †p<0.05, ††p<0.01 vs CDA1 WT UUO.

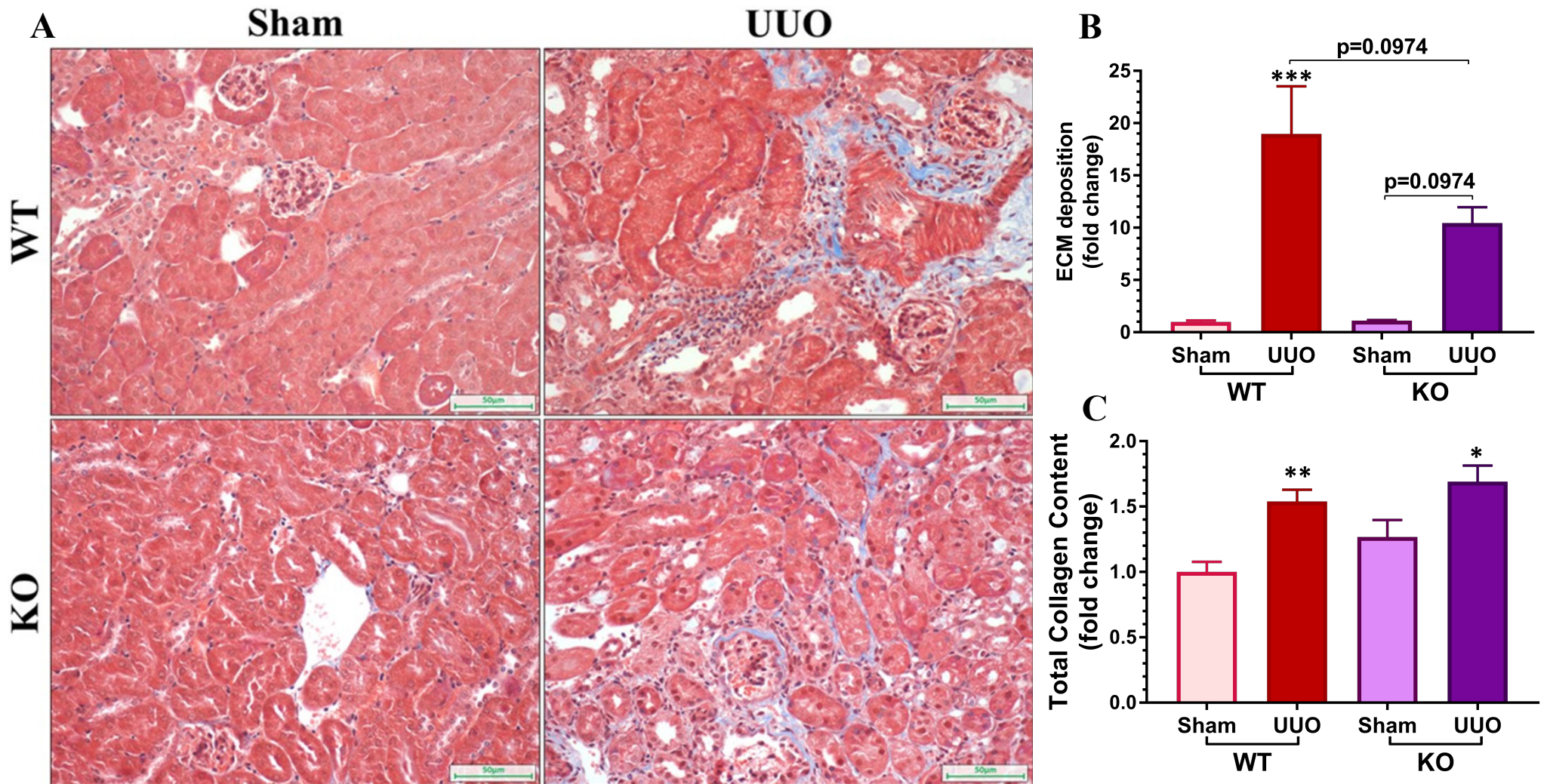


Figure 7.7.a. UUO-associated ECM deposition in mice is not affected by CDA1 deficiency. Representative images of Masson's Trichrome staining of renal cortex from CDA1 WT and KO mice 5 (A) and 10 days (D) after surgery are shown (magnification 200x). Quantitation of Masson's trichrome staining are shown as mean±SE for their respective timepoint (B and E). Total collagen content as measured by hydroxyproline assay of renal cortex from these mice, 5 days (C) and 10 days (F) post UUO. * $p < 0.05$, ** $p < 0.01$, *** $p < 0.001$ vs corresponding Sham control ($n > 7$).

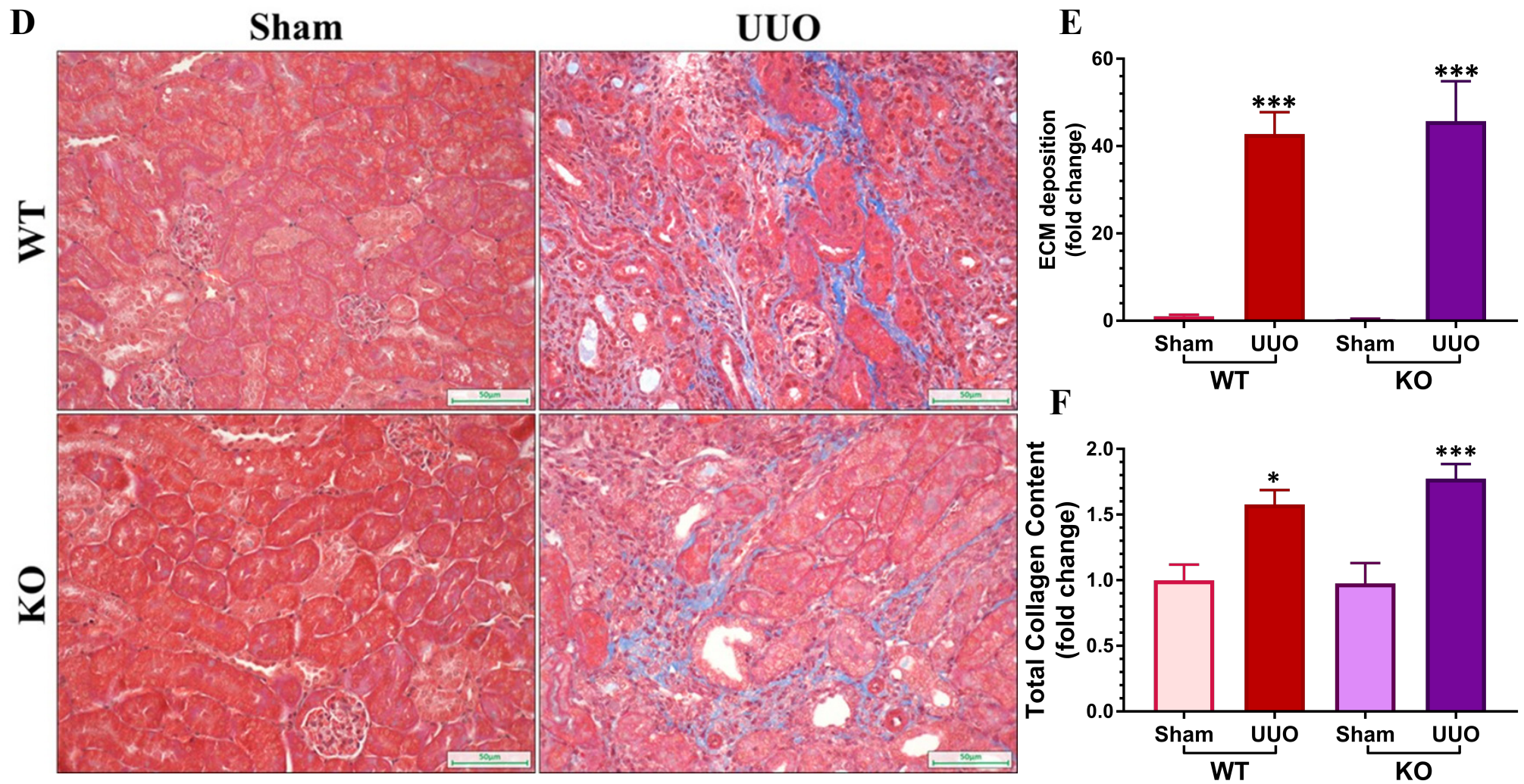


Figure 7.7.b. UUO-associated ECM deposition in mice is not affected by CDA1 deficiency. Continued from previous page.

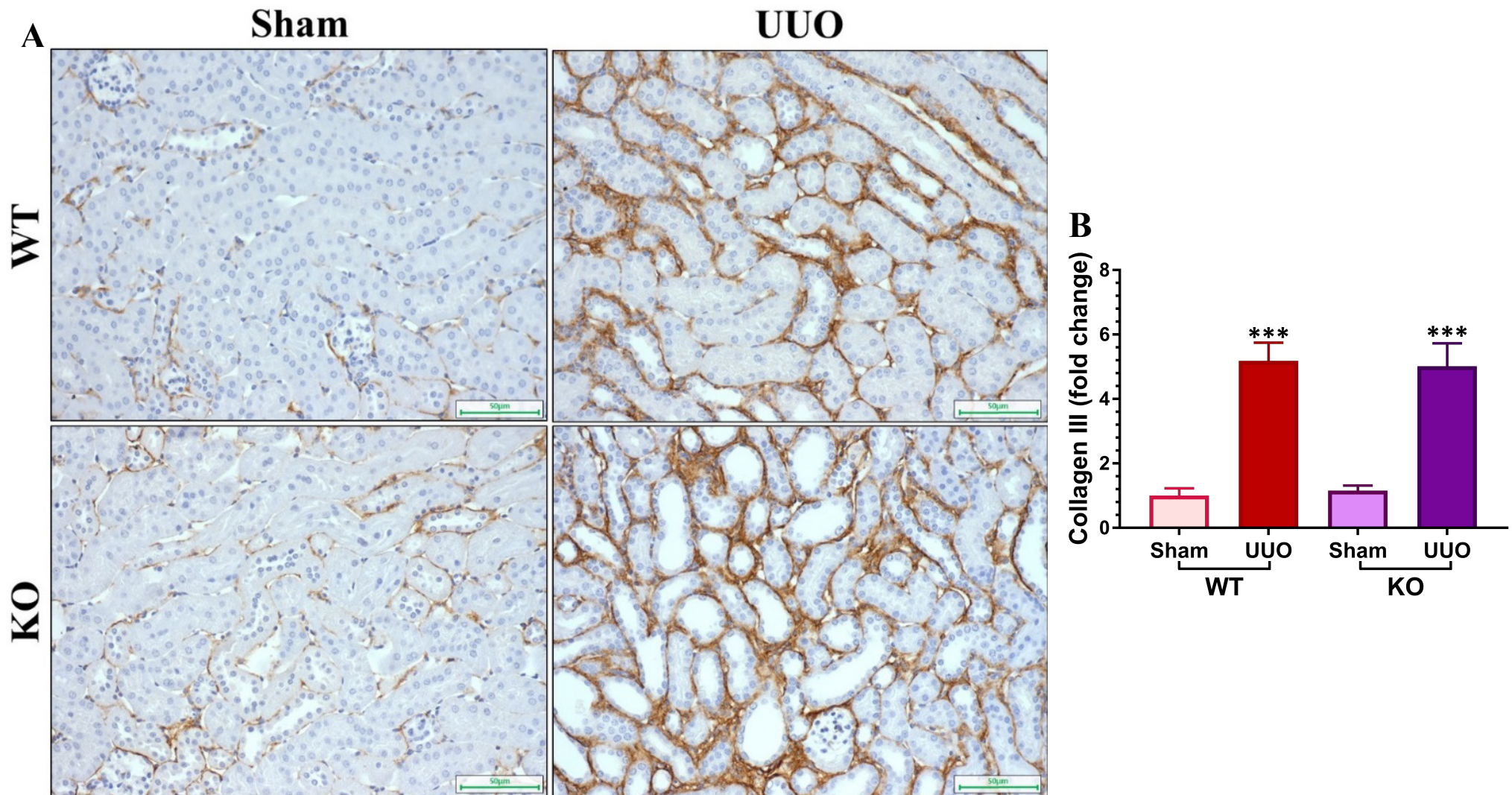


Figure 7.8.a. UUU-associated collagen deposition is unchanged in CDA1 KO mice after 5 days of obstruction. Representative images of immunohistochemical staining for cortical collagens III (A) and IV (C) in mice after 5 days of UUU (magnification 200x), with quantitation of each collagen (B and D). Fold changes are shown as mean \pm SE (n=9 for sham, n>11 for UUU). ***p<0.001 vs corresponding Sham control.

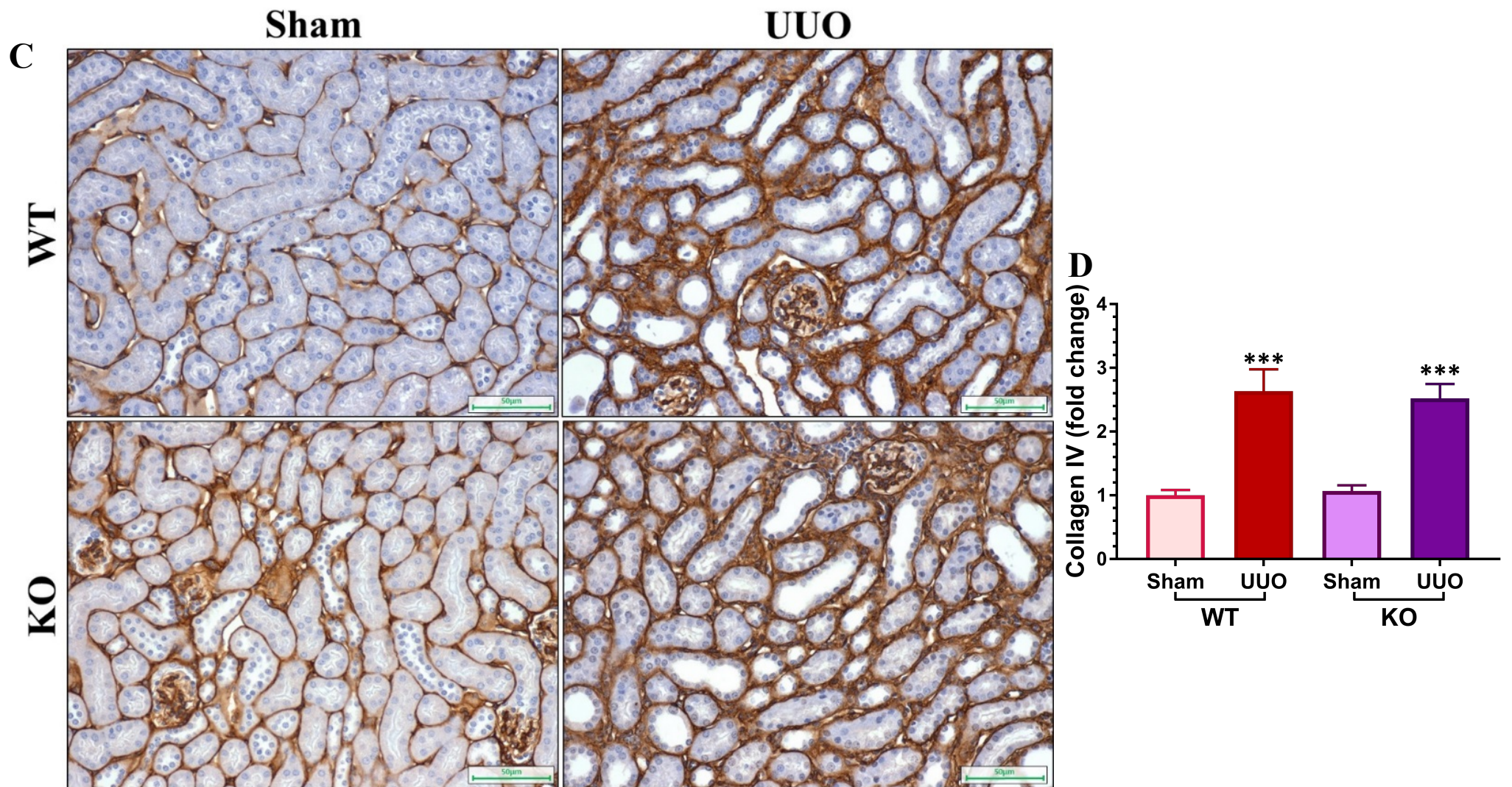


Figure 7.8.b. UUO-associated collagen deposition is unchanged in CDA1 KO mice after 5 days of obstruction. Continued from previous page.

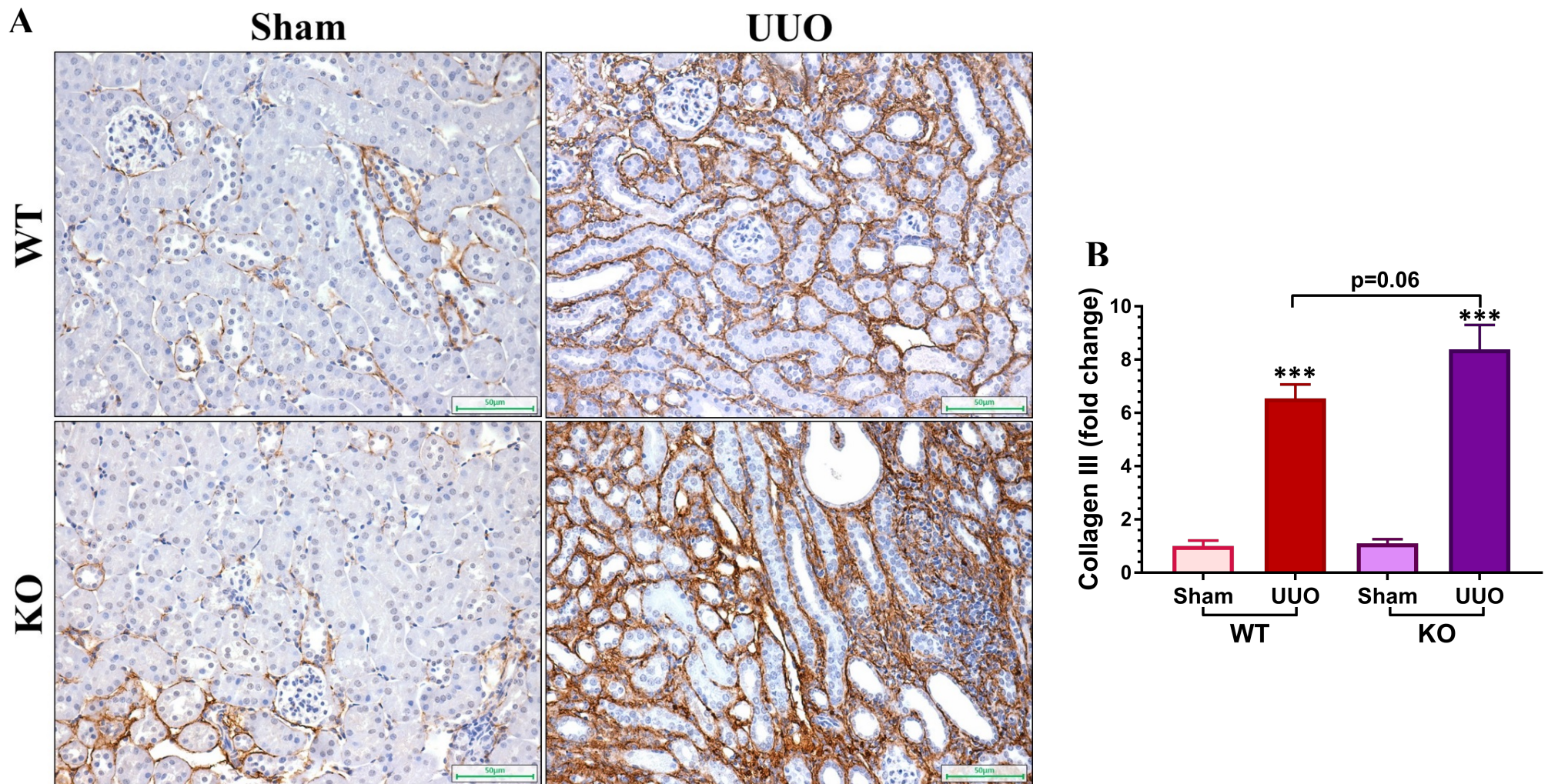


Figure 7.9.a. UUO-associated collagen deposition is affected by CDA1 deficiency after 10 days of obstruction. Representative images of immunohistochemical staining for cortical collagens III (A) and IV (C), in mice after 10 days of UUO (magnification 200x), with quantitation of each collagen (B and D). Fold changes are shown as mean±SE (n=6-9 for sham, n=12-14 for UUO). *p<0.05, ***p<0.001 vs corresponding Sham control, †p<0.05 vs CDA1 WT UUO mice.

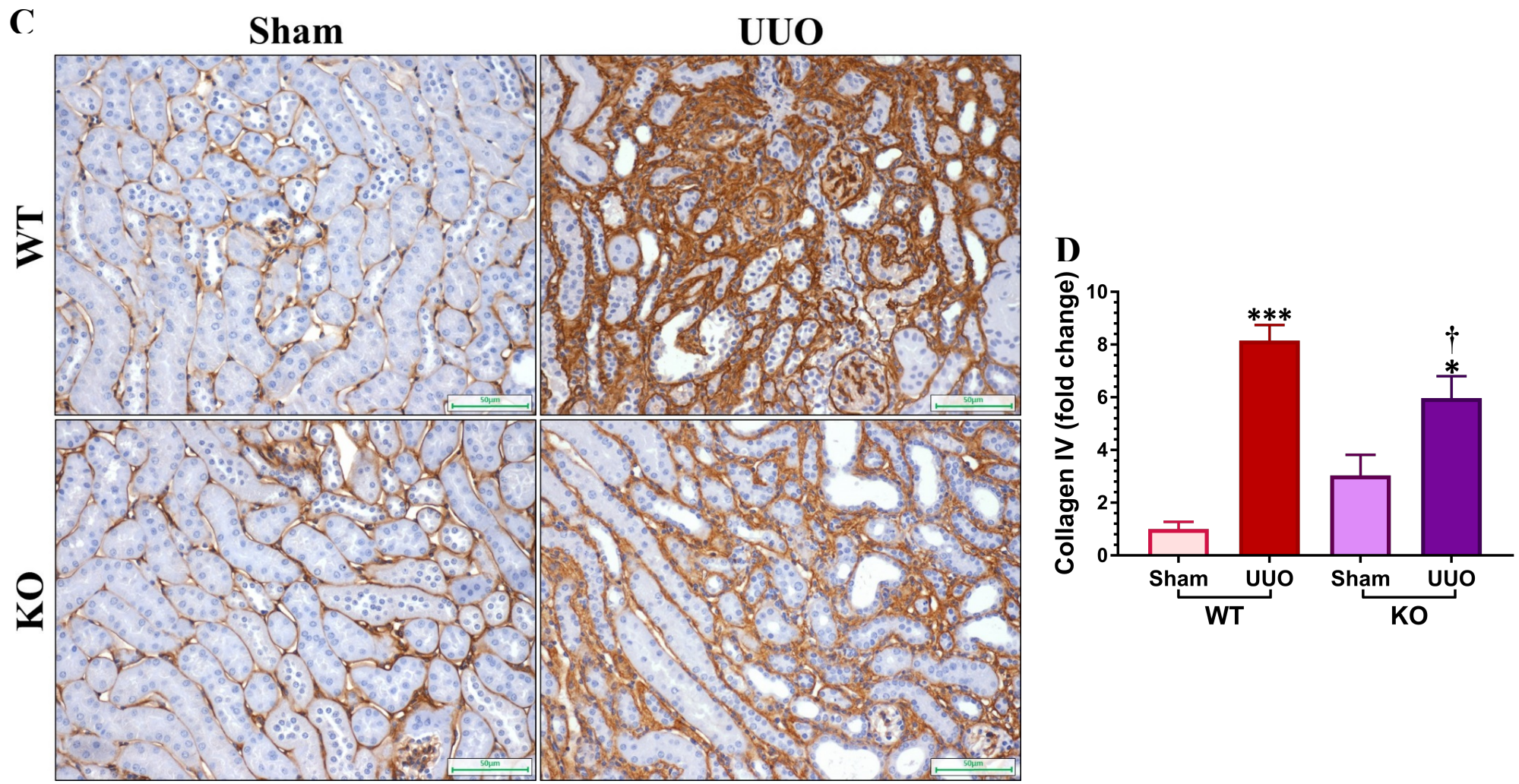


Figure 7.9.b. UUO-associated collagen deposition is affected by CDA1 deficiency after 10 days of obstruction. Continued from previous page.

7.3.2. CDA1 and Ischaemia/Reperfusion Injury

7.3.2.1. IR-associated activation of TGF β signalling and changes in profibrotic and proinflammatory gene expression

The left renal pedicle of CDA1 WT and KO mice was ligated for 45 minutes and then released to induce ischaemic conditions and subsequent reperfusion injury, respectively. Mice were followed for 4 and 8 days post-injury before kidneys were collected and analysed. CDA1 gene expression in the left kidney was increased ~2.0 fold in CDA1 WT IR mice 4 days post-injury (**Figure 7.10A**, $p=0.059$ vs CDA1 WT Sham), accompanied by a ~4.6 and ~2.2 increase in TGF β 1 and T β RII gene expression, respectively (**Figure 7.11**, $p<0.05$ vs Sham). In addition, there was enhanced activation of the TGF β signalling in IR-injured kidneys, as seen by the presence and increased intensity of bands corresponding to *phosphorylated Smad3* (pSmad3) in CDA1 WT mice 4 and 8 days post-injury (**Figure 7.12**). $p<0.01$ vs CDA1 WT Sham mice). Quantification of the pSmad3/ β -actin ratio revealed that there was a ~3.1-fold increase in renal pSmad3 expression in CDA1 WT mice 4 days (**Figure 7.12B**, $p<0.01$ vs CDA1 WT Sham mice). In contrast, pSmad3 expression in CDA1 WT kidneys appeared to be higher at 8 days after IR injury when compared to CDA1 WT Sham mice but formal quantification analysis failed to show a statistically significant difference (**Figure 7.12C and D**). Accurate quantification of the samples may have been hindered by the presence of non-specific bands on the immunoblot samples from Sham mice, as well the relatively low sample sizes used (9 mice for 4d IR vs 7 mice for 8d IR).

Coinciding with the transcriptional upregulation and activation of the TGF β signalling pathway in IR injured kidneys, the expression of profibrotic genes was upregulated by 4 days post-IR injury, with collagen III and fibronectin increasing by ~35.3 and ~16.2-fold, respectively (**Figure 7.13**, $p<0.01$ vs Sham CDA1 WT 4 IR mice). Additionally, it appears that the expression of these genes increased further 8 days after reperfusion ($p<0.05$ vs CDA1 WT 4d IR mice). Proinflammatory genes, such as MCP1, MSR1, and ICAM1, were also upregulated by IR injury, with a ~37.2, ~94.7 and ~4.7-fold increase in gene expression in 4d CDA1 WT IR mice, respectively (**Figure 7.14**, $p<0.05$ vs Sham). In addition, activation of the complement system was also observed with IR injury, as seen by the IR-associated upregulation of *complement component 5* (C5) in IR kidneys by ~9.9-fold (**Figure 7.14 H**, $p<0.05$ vs Sham CDA1 WT 4d mice). Although not statistically significant, there were tendencies towards IR-associated increases in many genes related to fibrosis and inflammation at 4 days after surgery, including but not limited to *tissue inhibitors of metalloproteinases 1* (TIMP1), VCAM1, and iNOS (**Figures 7.13 and 7.14**).

7.3.2.2. Effect of CDA1 deficiency on the gene expression of TGF β signalling components in renal IR injury

There was an attenuation of IR-induced expression of the remnant CDA1 gene transcript in CDA1 KO mice 4 and 8 days after surgery (**Figure 7.10A**, $p<0.05$ vs CDA1 WT IR mice). As the

genetic deletion of CDA1 was confirmed using a different set of primers (**Figure 7.10B**), as well as genotyping (**data not shown**), these findings suggest that stimulation of the CDA1 promoter may be affected by the absence of functional CDA1 in these mice. While CDA1 deficiency had no effect on IR-associated TGF β expression (**Figure 7.11A**), there were trends towards a reduction in T β RI gene expression (**Figure 7.11B**, $p=0.08$ vs CDA1 WT 4d IR) and an attenuation of IR-induced T β RII gene expression in CDA1 KO mice 4 days post-injury (**Figure 7.11C**, $p<0.05$ vs CDA1 WT 4d IR). Interestingly, there was no difference between CDA1 WT and KO mice in the gene expression levels of either TGF β receptor by 8 days after surgery (**Figure 7.11B and C**), as well as IR-associated pSmad3 expression (**Figure 7.12D**), suggesting that CDA1 may transcriptionally modulate components of the TGF β signalling pathway at early stages of AKI development, and that its actions may be dynamic.

7.3.2.3. *Effect of CDA1 deficiency on IR-associated profibrotic and proinflammatory gene changes*

While IR-associated gene expression of collagen III was not affected by CDA1 deficiency, surprisingly, IR-associated gene expression of fibronectin and PAI1 was exacerbated in CDA1 KO mice at 4 days after surgery (**Figure 7.13B and C**, $p<0.05$ vs CDA1 WT IR mice). Interestingly, there were lower levels of MMP2 gene expression, albeit not statistically significant (**Figure 7.13D**), with a concomitant increase in TIMP1 gene expression, at 4 days after IR-induced injury in CDA1 KO mice (**Figure 7.13E**, $p<0.001$ vs CDA1 WT 4d IR). In addition, it appears that CDA1 deficiency exacerbated the expression of certain proinflammatory genes, with TNF α , iNOS, and IL6 being ~ 2.4 , ~ 4.0 , and ~ 7.5 times higher in CDA1 KO mice, respectively, at four days post-IR injury (**Figure 7.14**, $p<0.01$ and $p=0.07$, respectively vs CDA1 WT 4d IR mice). Conversely, the transcriptional upregulation of adhesion molecules 4 days after obstruction in association with IR injury appears to be attenuated in CDA1 deficient mice, with trends towards decreased VCAM1 and ICAM1 gene expression levels in CDA1 KO mice (**Figure 7.14C and D**, $p=0.11$ and $p=0.07$ respectively vs CDA1 WT 4d IR mice).

Interestingly, many of the transcriptional changes which were exacerbated by CDA1 deficiency at 4 days after IR-induced injury were not different between CDA1 WT and KO mice at 8 days after surgery. There was, however, an exacerbation of IR-associated MMP2 and MSR1 expression in CDA1 KO mice at 8 days post-injury, being ~ 1.4 and ~ 1.7 times higher than seen in CDA1 WT mice (**Figure 7.13 and Figure 7.14**, $p<0.01$ vs CDA1 WT 8d IR).

7.3.2.4. *The effects of CDA1 deficiency in IR-associated ECM accumulation*

Renal IR injury was associated with changes in renal histological morphology, with abnormal tubular morphology and the appearance of infiltrating inflammatory cells being evident by 4 days after IR-induced injury (**Figure 7.15**). Despite the robust transcriptional changes (described in **Section 7.3.2.3**) and severe tubular damage associated with renal IR injury, increased ECM deposition was not observed in these mice until at least 8 days after IR-induced injury, as observed

by hydroxyproline analysis (**Figure 7.16**) and immunohistochemical staining for specific collagens (**Figure 7.17**). Indeed, while the total collagen content was not statistically different after IR injury in CDA1 WT mice when compared to Sham mice (**Figure 7.16**), there was a ~6.1-fold increase in collagen III accumulation in CDA1 WT mice 8 days after IR-induced injury (**Figure 7.17B**, $p < 0.05$ vs CDA1 WT Sham). Genetic deletion of CDA1 had no effect on IR-associated renal ECM deposition, as seen by the lack of differences between CDA1 WT and KO mice in total collagen content and IR-associated collagen deposition (**Figure 7.17**).

7.3.2.5. The effects of CDA1 deficiency on transcriptional changes concerning cell cycle regulation and apoptosis

As significant tubular atrophy and increased infiltration and/or proliferation of cells was observed in this model (**Figure 7.15**), I examined the effects of CDA1 deficiency on certain genes related to cell cycle regulation and apoptosis. Surprisingly, IR-induced upregulation of p21 expression was exacerbated in CDA1 KO mice (**Figure 7.18A**, $p < 0.05$ vs CDA1 WT 4d IR mice) 4 days after surgery. Conversely, IR-associated upregulation of p53 and BAK1 were attenuated in CDA1 KO mice 4 days post-injury (**Figure 7.18B and D**, $p < 0.001$ vs CDA1 WT 4d IR mice). In addition, gene expression of Bcl2 and caspase 8 were reduced in CDA1 KO mice 4 days post-injury (**Figure 7.18**, $p < 0.001$ vs CDA1 WT 4d IR mice). There was an IR-associated increase in ki67 gene expression in both CDA1 WT and KO mice at 4 days after IR injury (**Figure 7.18F**, $p < 0.05$ vs Sham mice), which is indicative of cellular proliferation. Interestingly, while there was no difference in IR-associated ki67 gene expression between CDA1 WT and KO mice at 4 days after IR injury, CDA1 deficiency was associated with a tendency towards an IR injury-associated increase, albeit not statistically significant, in ki67 gene expression (**Figure 7.18F**, $p = 0.12$ vs CDA1 WT 8d IR).

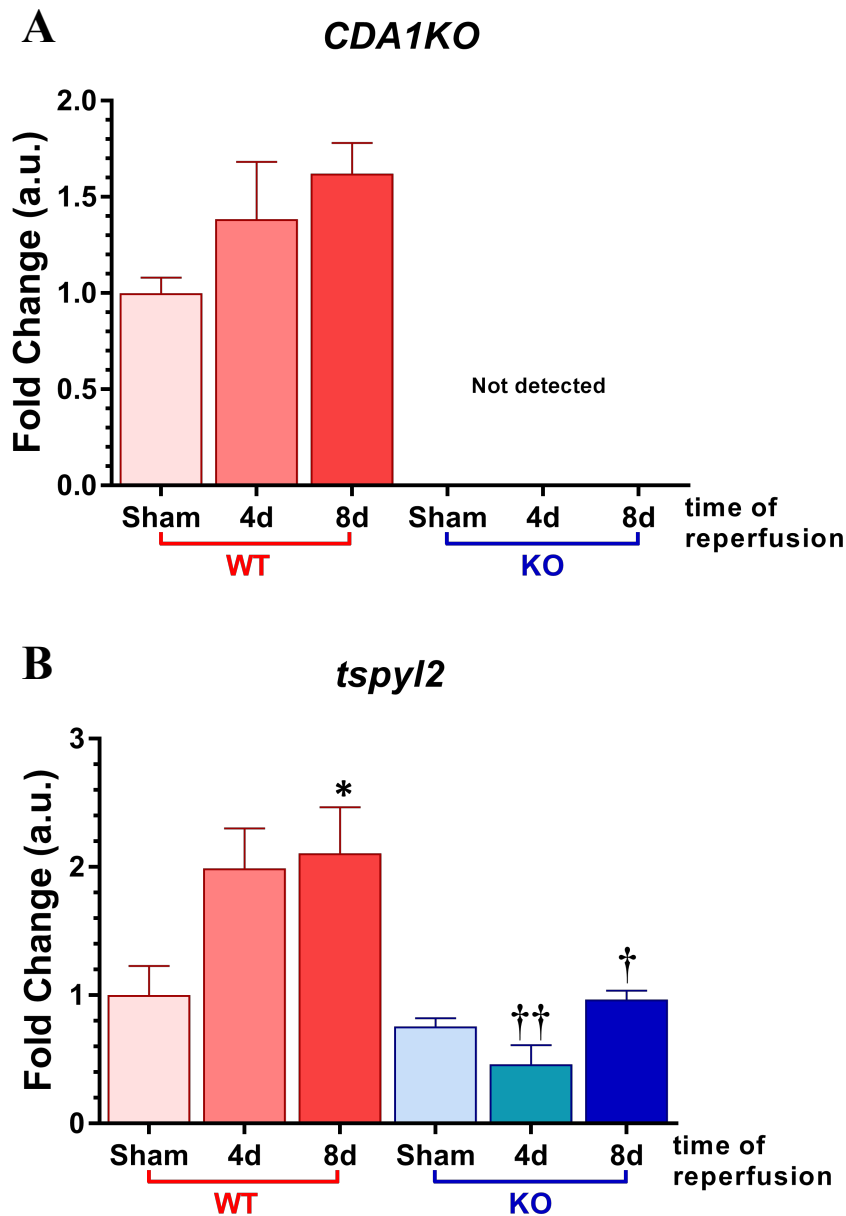


Figure 7.10. Gene expression of CDA1 in IR injury. Male CDA1 WT and KO mice had their left renal artery obstructed for 45 mins or underwent sham operation (Sham; lighter columns) before being released and kidneys were collected 4 and 8 days after obstruction. Kidney CDA1 mRNA levels were determined by qRT-PCR using primers detecting CDA1 transcripts from both WT CDA1 gene (A) and the remnant CDA1 gene from the knockout allele. Genetic deletion of CDA1 in KO mice was confirmed by genotyping as well as qRT-PCR using primers specific for the region of CDA1 gene which was deleted in KO mice (B). Fold changes are shown as mean±SE (n=6 for sham, n=8-10 for IR). *p<0.05 vs corresponding Sham control and †p<0.05, ††p<0.01 vs time-matched CDA1 WT IR mice.

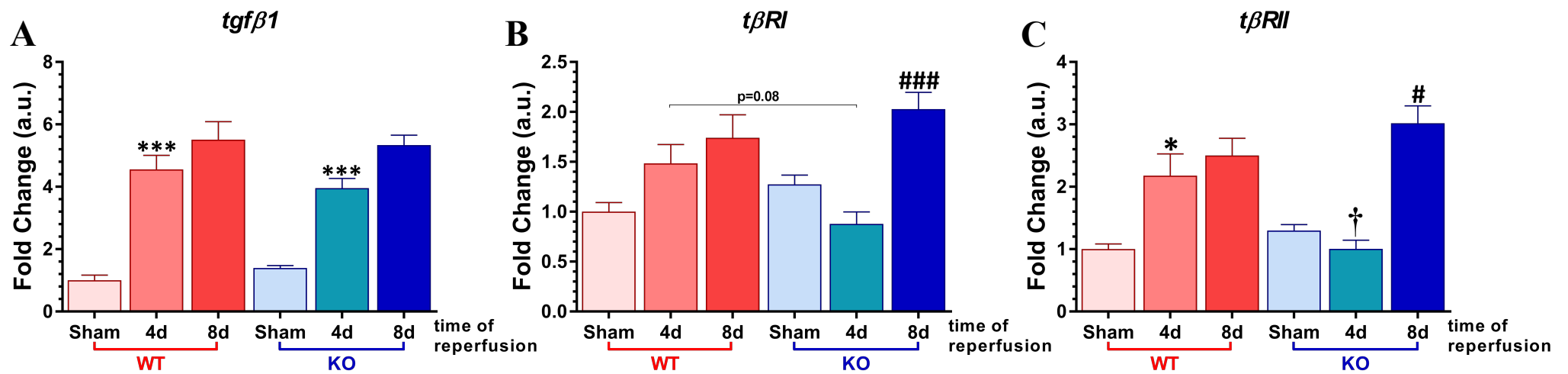


Figure 7.11. Activation of TGFβ signalling in IR injury. qRT-PCR analysis for the relative TGFβ1 (A), TβRI (B) and TβRII (C) mRNA levels in CDA1 WT and KO mice which underwent IR injury or sham surgery for 4 and 8 days. Fold changes are shown as mean±SE (n=6 for sham, n=8-10 for IR). *p<0.05, ***p<0.001 vs corresponding Sham control, #p<0.05, ###p<0.001 vs corresponding 4d IR mice and †p<0.05 vs time-matched CDA1 WT IR mice.

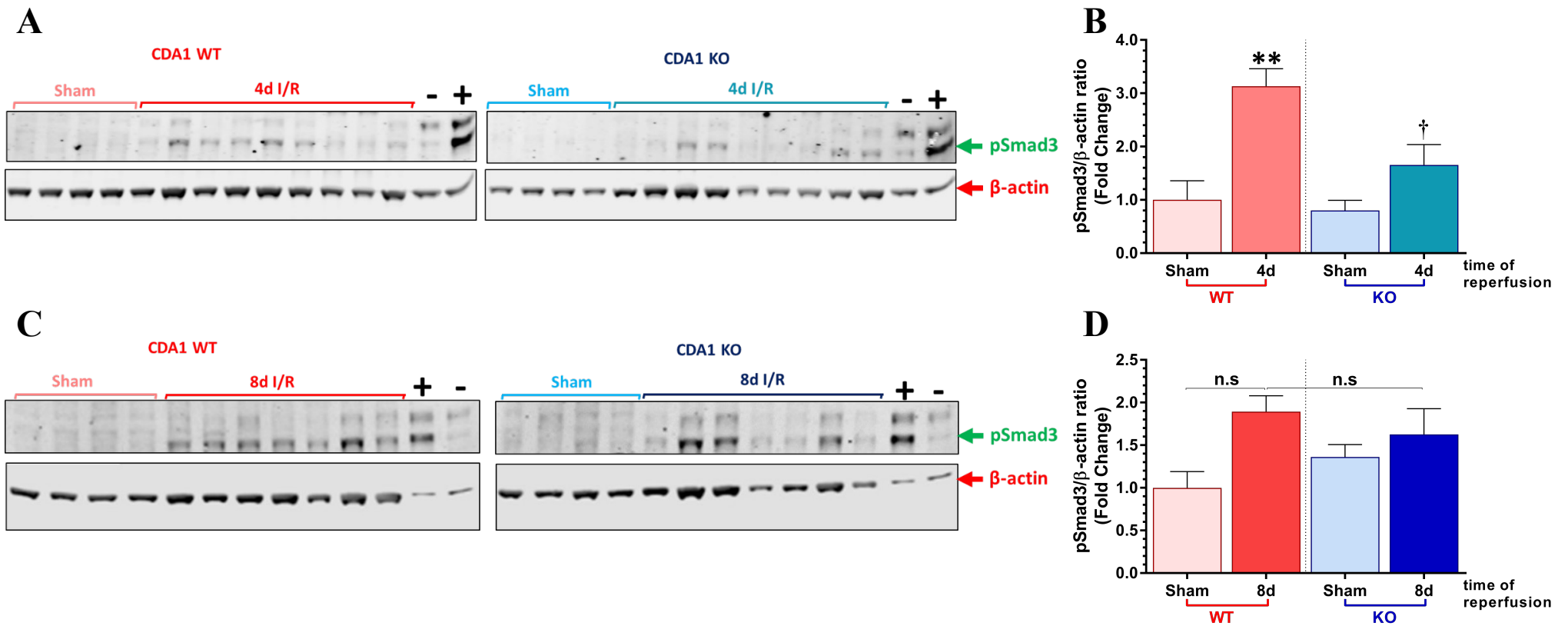


Figure 7.12. IR-associated activation of the TGF β signalling pathway is attenuated by CDA1 deficiency early in disease development. Western blot analysis for the relative expression of pSmad3 expression in renal protein lysates from CDA1 WT and KO mice 4 days (A) and 8 days (C) after renal IR injury, with quantification performed by normalising the band intensity of pSmad3 with β -actin (B and D for 4 and 8 days after IR injury, respectively). lysates of mouse aortic endothelial cells which were either treated with 1ng/mL recombinant TGF β 1 for 30 mins or left untreated were used as positive (+) and negative (-) controls, respectively. Fold changes are shown as mean \pm SE (n=4 for sham, n=7-9 for IR). **p<0.01 vs corresponding Sham control, †p<0.05 vs time-matched CDA1 WT IR mice.

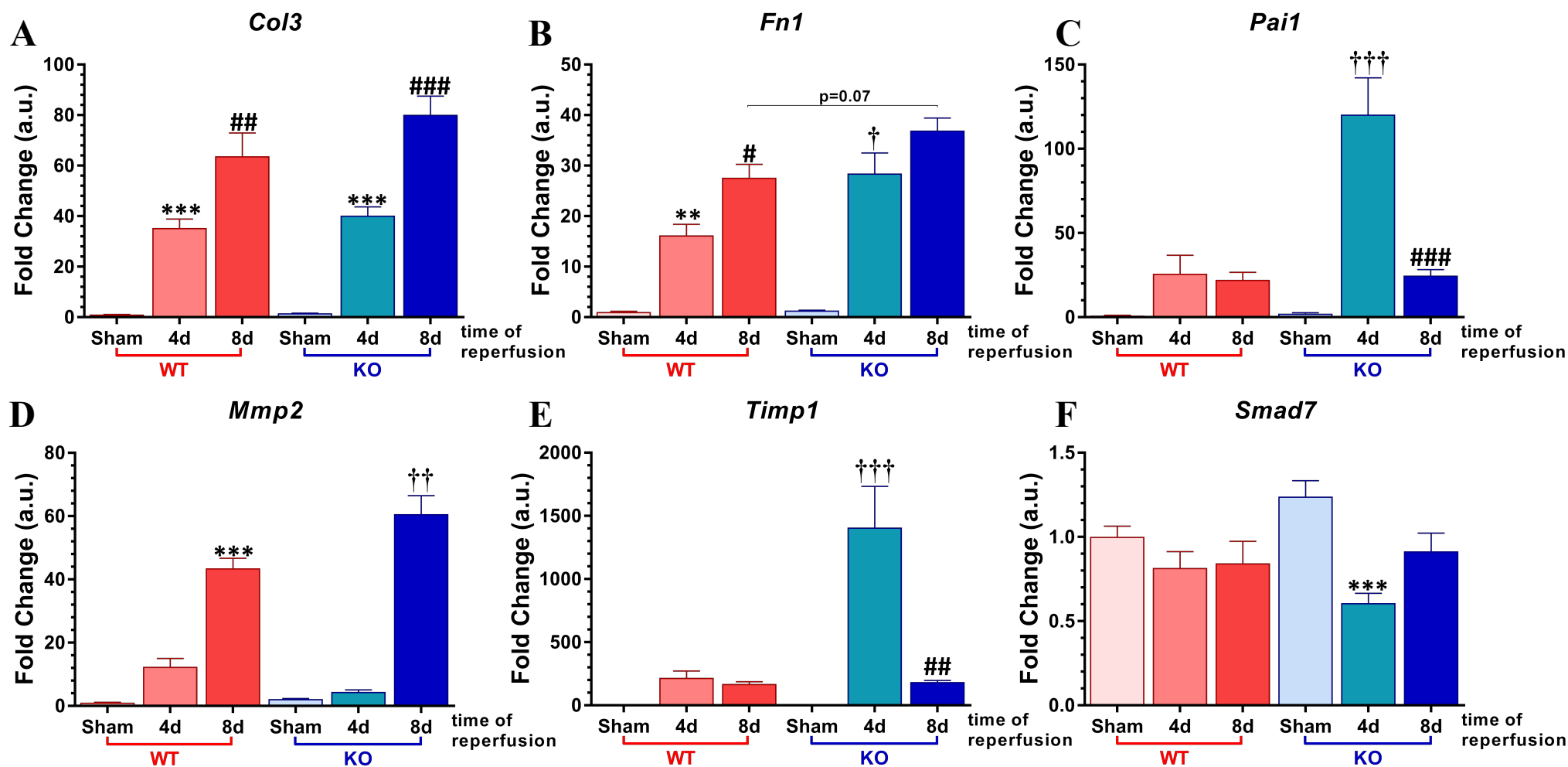


Figure 7.13. Effects of CDA1 deficiency on profibrotic gene expression in response to renal ischaemic/reperfusion injury in mice. qRT-PCR analysis for the relative collagen III (A), fibronectin (B), MMP2 (C), TIMP1 (D), TβRI (E) and TβRII (F) mRNA levels in CDA1 WT and KO mice which underwent IR injury or sham surgery for 4 and 8 days. Fold changes are shown as mean±SE (n=6 for sham, n=8-10 for IR). *p<0.05, **p<0.01, ***p<0.001 vs corresponding Sham control, ###p<0.001 vs corresponding 4d IR mice and †p<0.05, ††p<0.01, †††p<0.001 vs time-matched CDA1 WT IR mice.

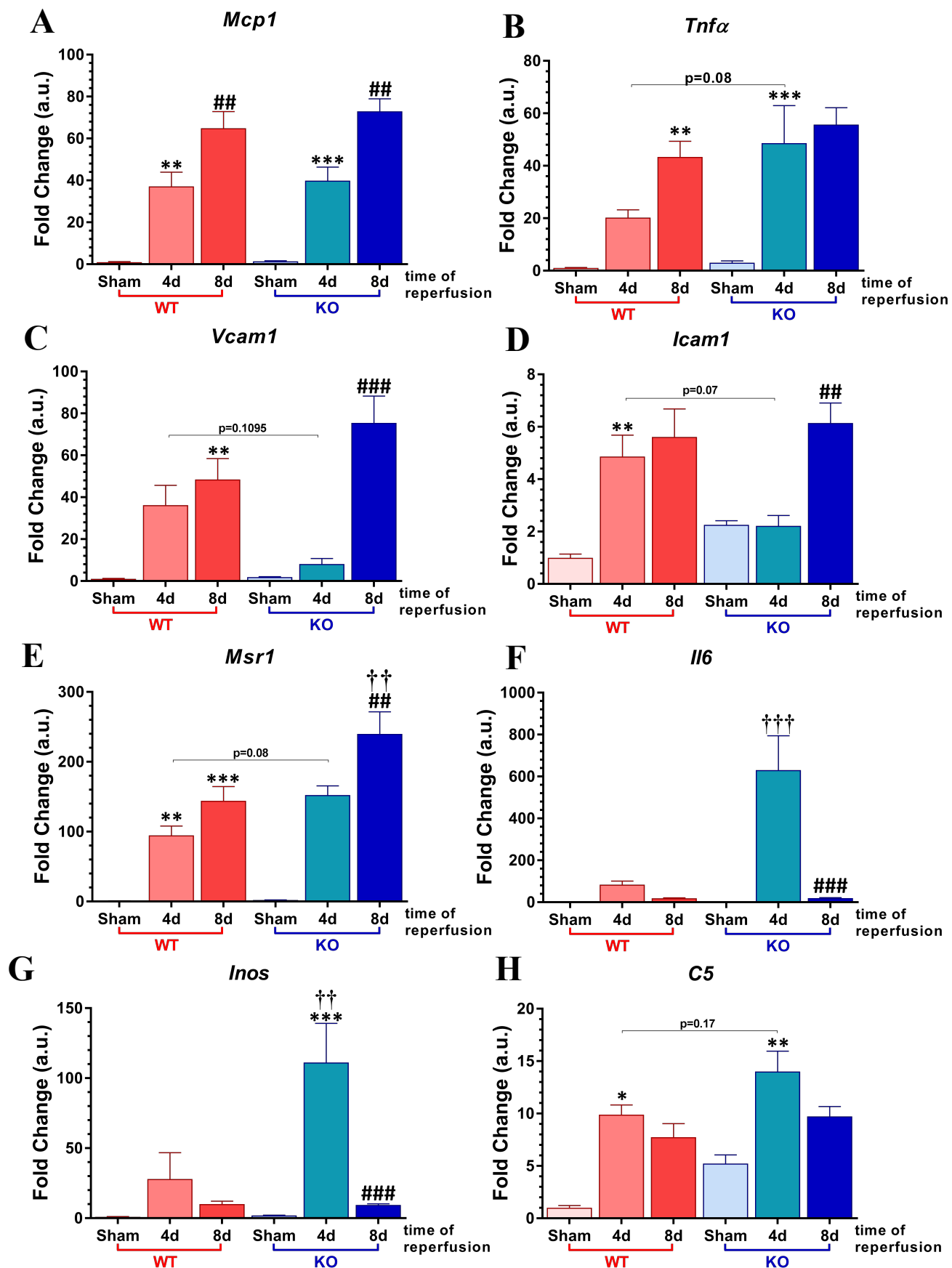


Figure 7.14. Effects of CDA1 deficiency on proinflammatory gene expression in response to renal ischaemic/reperfusion injury in mice. qRT-PCR analysis for the relative MCP1 (A), TNF α (B), VCAM1 (C), ICAM1 (D), MSR1 (E), IL6 (F), iNOS (G) and C5 (H) mRNA levels in CDA1

WT and KO mice which underwent IR injury or sham surgery for 4 and 8 days. Fold changes are shown as mean±SE (n>3 for sham, n>8 for IR). *p<0.05, **p<0.01, ***p<0.001 vs corresponding Sham control, ##p<0.01, ###p<0.001 vs corresponding 4d IR mice and ††p<0.01, †††p<0.001 vs time-matched CDA1 WT IR mice.

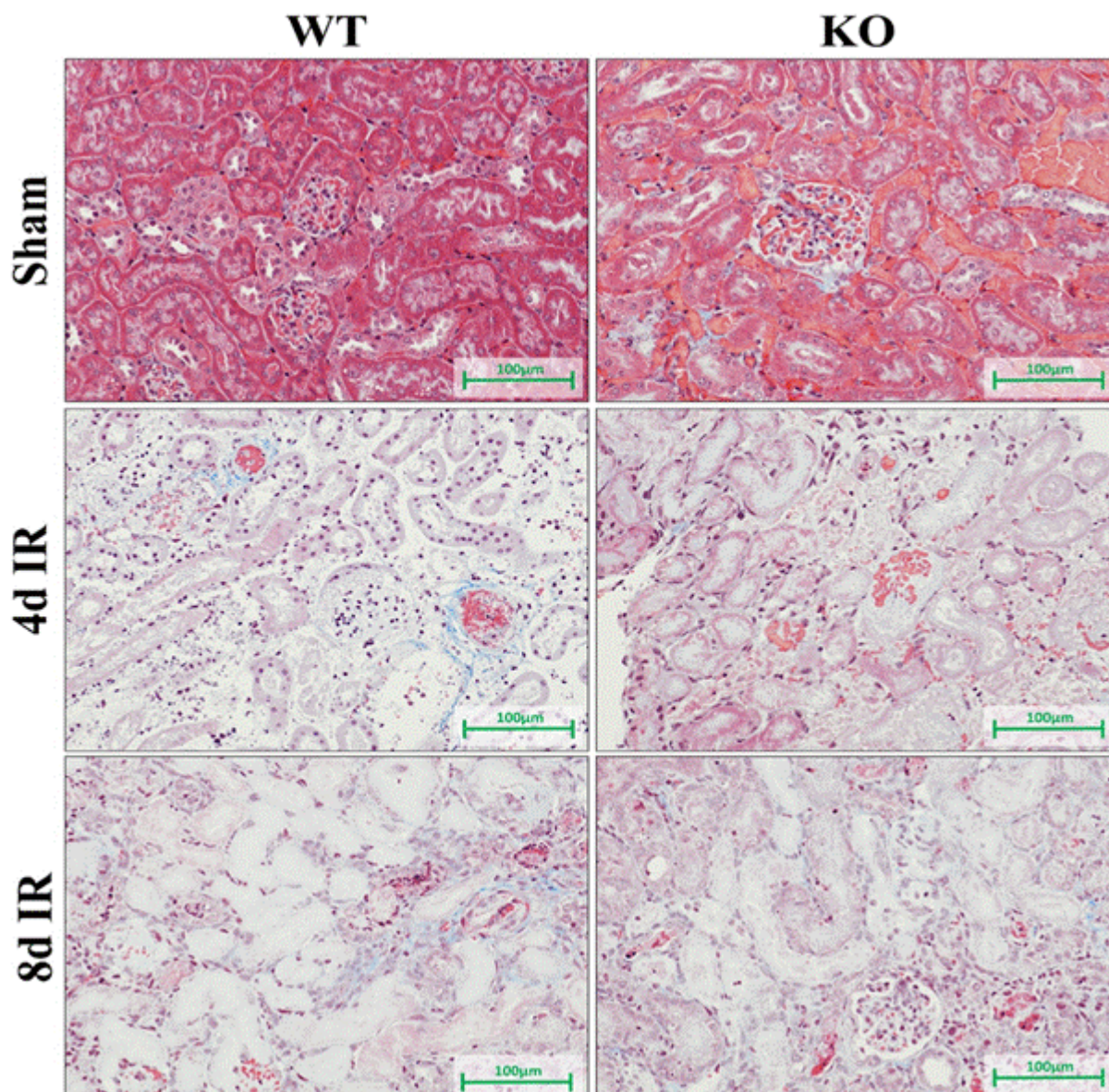


Figure 7.15. ECM deposition and renal morphology in a mouse model of renal IR injury. Representative images of Masson's trichrome staining of kidneys from CDA1 WT and KO mice at 4 and 8 days after IR injury, with sham mice used as uninjured controls (magnification 200x). Notice the general lack of ECM accumulation (blue staining) despite abnormal renal morphology.

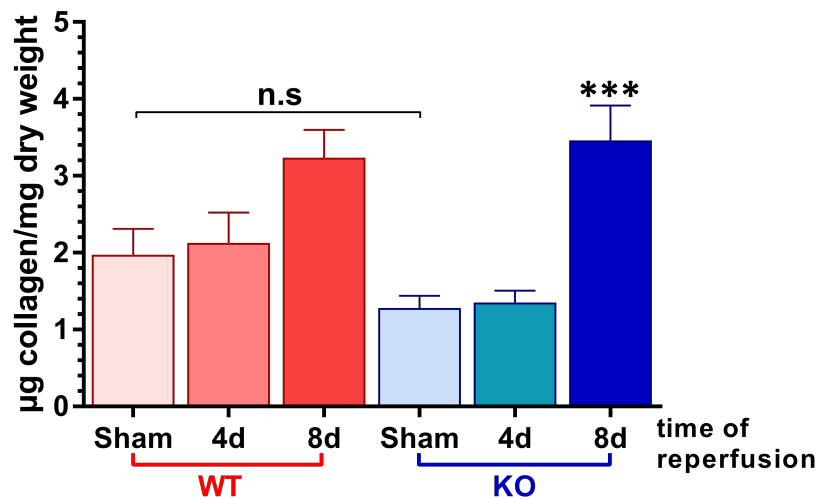


Figure 7.16. CDA1 deficiency does not affect total collagen content in response to renal ischaemic/reperfusion injury in mice. Hydroxyproline analysis of kidneys extracted from CDA1 WT and KO mice which underwent IR injury or sham surgery for 4 and 8 days. Data are shown as mean±SE (n=6 for sham, n=8-10 for IR). ***p<0.001 vs corresponding Sham control.

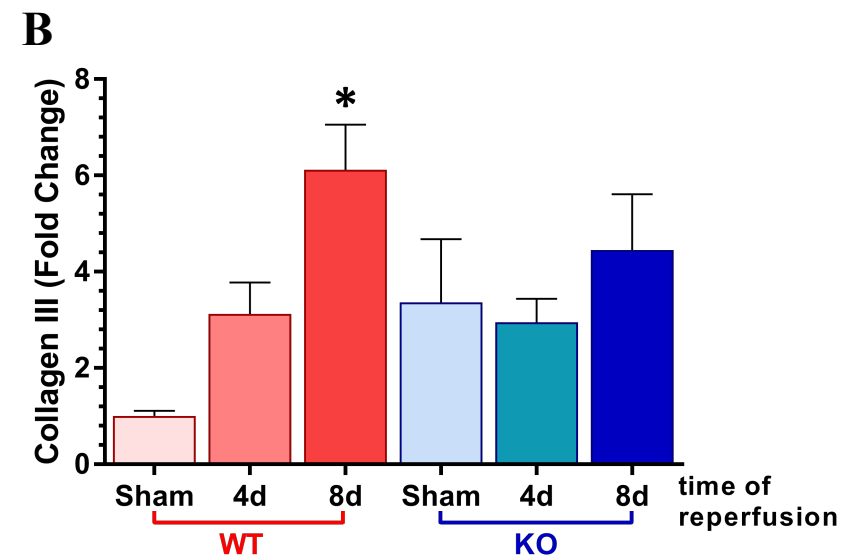
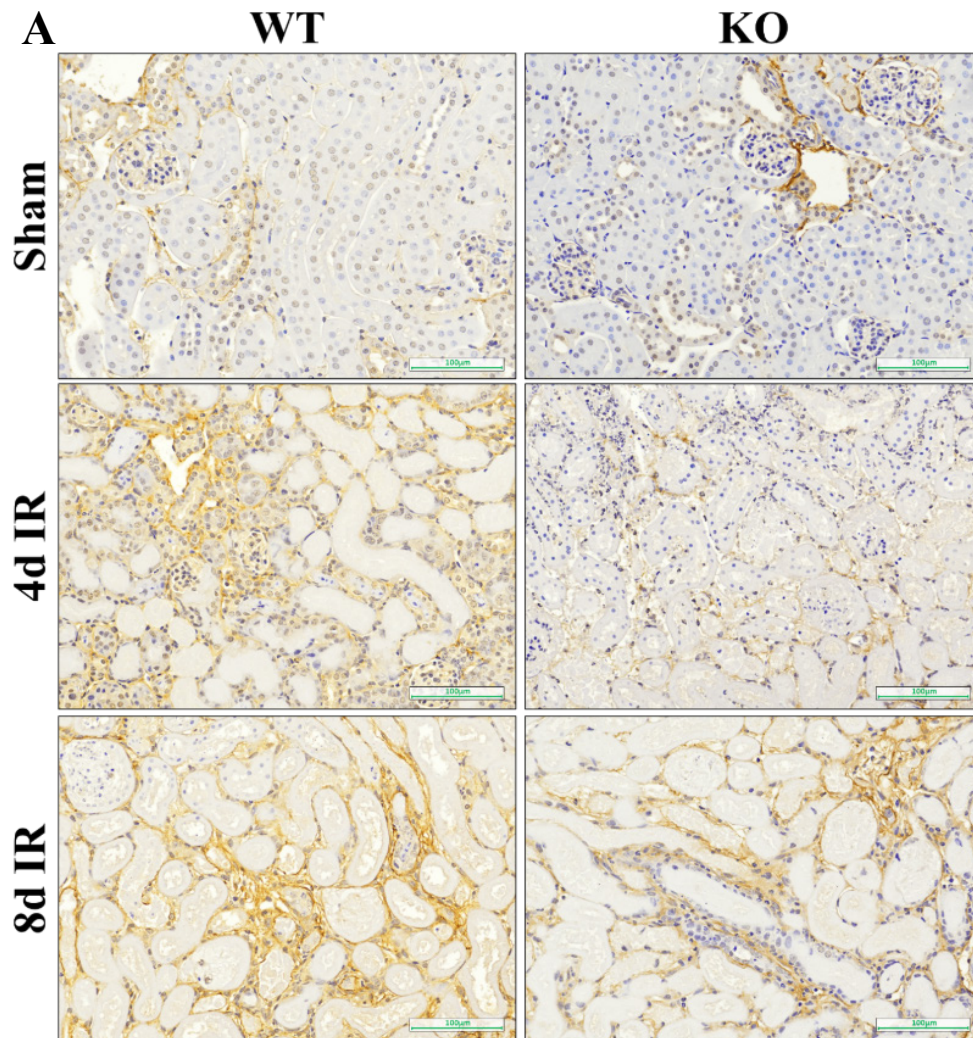


Figure 7.17.a. CDA1 deficiency does not affect collagen deposition in response to renal ischaemic/reperfusion injury in mice. Representative images of immunohistochemical staining of cortical collagens III (A) and IV (C) in kidneys extracted from CDA1 WT and KO mice which underwent IR injury or sham surgery for 4 and 8 days (magnification 200x), with quantitation of each collagen (B and D). Data are shown as mean±SE (n=4 for sham, n>6 for IR). *p<0.05 vs corresponding Sham control.

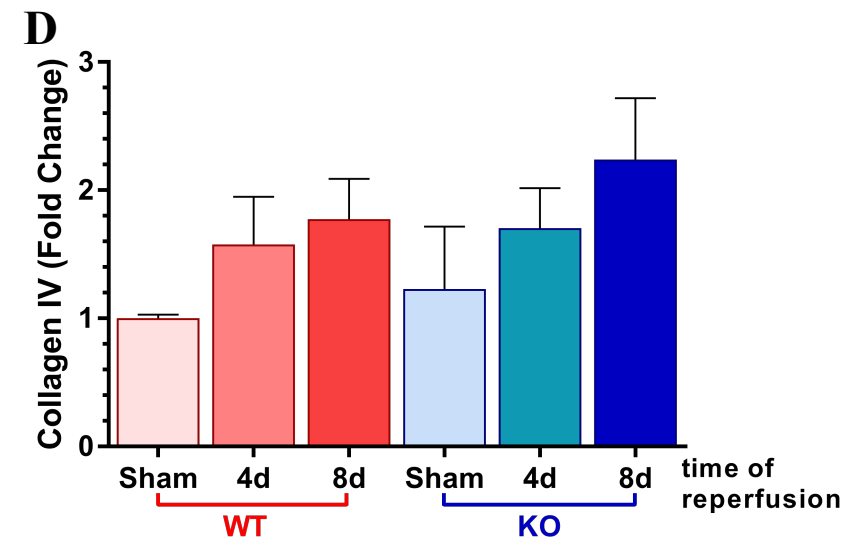
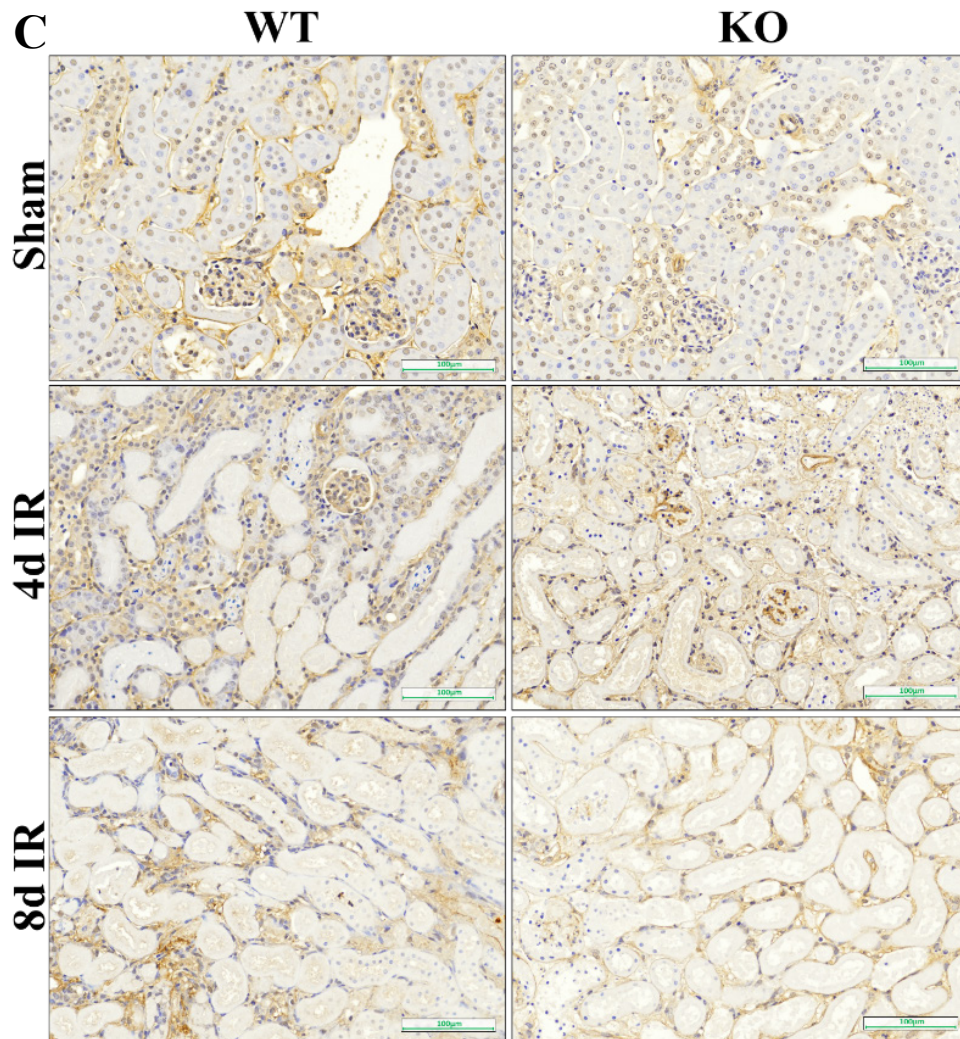


Figure 7.17.b. CDA1 deficiency does not affect collagen deposition in response to renal ischaemic/reperfusion injury in mice. Continued from previous page.

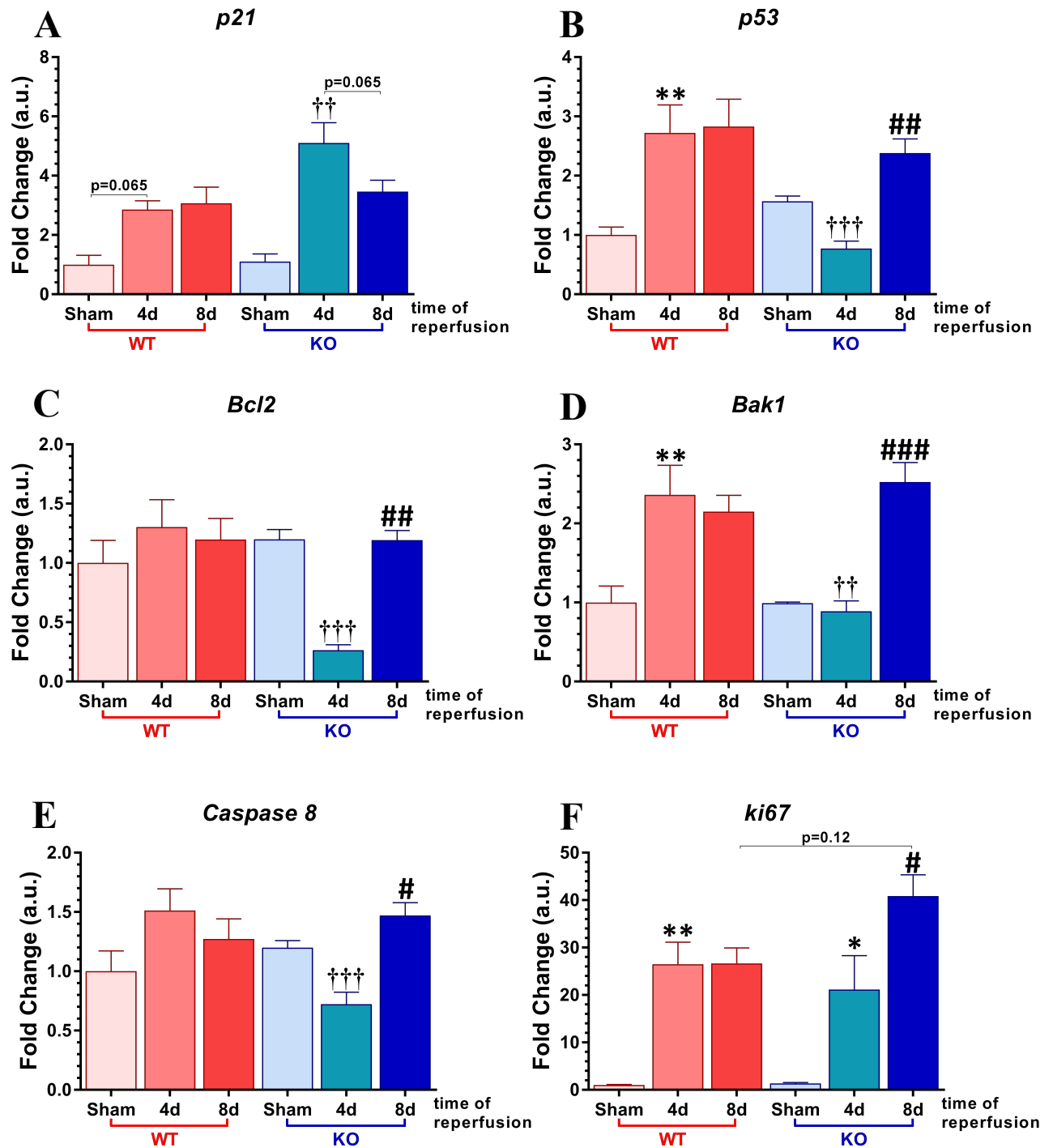


Figure 7.18. Effects of CDA1 deficiency on gene expression related to apoptosis, cell cycle regulation and proliferation in response to renal ischaemic/reperfusion injury in mice. qRT-PCR analysis for the relative p21 (A), p53 (B), Bcl2 (C), BAK1 (D), Caspase 8 (E) and ki67 (F) mRNA levels in CDA1 WT and KO mice which underwent IR injury or sham surgery for 4 and 8 days. Fold changes are shown as mean±SE (n=6 for sham, n=8-10 for IR). **p<0.01, vs corresponding Sham control, #p<0.05, ##p<0.01, ###p<0.001 vs corresponding 4d IR mice and ††p<0.01, †††p<0.001 vs time-matched CDA1 WT IR mice.

7.4. Discussion

The TGF β signalling pathway is critical in the pathogenesis of most CKD. Inhibition and genetic deletion of TGF β signalling components has previously been demonstrated to attenuate renal fibrosis in animal models of *acute kidney injury* (AKI) (see **Table 2.1**), including genetic deletion of Smad3,^{212, 216, 218} and miRNA-21,²⁴⁰ as well as the use of TGF β neutralising antibodies,^{184, 222} in rodent models of UUO and renal IR injury. Direct inhibition of TGF β activity, while appealing, is unviable due to the pleiotropic nature of TGF β activity, as well as the adverse side effects associated with its complete inhibition. In addition, attempts to elucidate specific roles of TGF β in renal disease, through the use of cell-specific knockout mouse strains, have demonstrated the complex nature of TGF β signalling. For example, although tubule-specific Smad4 mutant mice exhibited an attenuation in UUO-associated renal fibrosis, these mice also exhibited an exacerbation of proinflammatory signalling and leukocyte infiltration.²⁰¹ In other cases, renal fibrosis was not affected by the knockout of T β RII in ECM depositing cells,²³¹ nor TGF β -knockout in macrophages.²²³ Thus, we hypothesised that targeting CDA1, which has been previously shown to significantly attenuate but not completely block TGF β signalling, would have antifibrotic potential in renal disease. In this study, I used the global CDA1 KO mouse strain, which had previously exhibited an attenuation in diabetes-associated renal fibrosis.²⁵⁶ As CDA1 deficiency was not associated with the development of any obvious deleterious phenotype, it was expected that targeting CDA1 would be a safe option in modulating the TGF β signalling pathway and attenuating the development of renal fibrosis in CKD. Surprisingly, however, CDA1 deficiency was found to have no obvious impact on the development of renal fibrosis in the two models of AKI examined in this study.

In this chapter, I examined the effect of CDA1 deficiency *in vivo* on the progression of renal fibrosis in two models of acute renal injury. Although both models had a similar experimental duration of time, the degree and development of fibrosis observed differed due to the specific nature of injury in each model. In the UUO model, the obstructed kidney is permanently ligated, leading to continuous injury and eventual hydronephrosis, with ECM deposition evident by 5 days post-injury. On the other hand, development of fibrotic lesions in the IR model, which was the result of an initial injurious event (ischaemia) followed by secondary tissue injury (reperfusion), occurred by 8 days post-injury. Despite abnormal renal morphology being observed at this timepoint, renal fibrosis in the IR study was noticeably less severe than lesions observed in the UUO study. Fibrotic lesions in the IR model are reported to be seen by 9 days,²⁴³ with severe lesions observed by 12 weeks, after IR injury,^{305, 308, 313} with the progressive development of renal fibrosis being attributed to the eventual downregulation of IR-induced MMP2 expression with a concomitant increase in TIMP1 expression over time.³¹⁴ Indeed, regulatory pathways, such as the TGF β signalling pathway, are presumed to play key roles in modulating processes which lead to renal fibrosis. Thus, with the timepoints utilised in this study, the UUO model represents severe renal injury and an established fibrotic state, while

the IR injury model represents moderate renal injury, with pathological processes recapitulating early stages of renal disease development.

Acute renal injury was associated with an upregulation of CDA1 gene expression in CDA1 WT mice in both models (**Figure 7.3 and 7.10**). This was accompanied by concomitant increases in expression of TGF β and other profibrotic genes. These findings further validate previous observations whereby CDA1 expression is upregulated in diabetic and non-diabetic renal fibrosis, as well as supporting the notion that there is a synergistic relationship between the expression of CDA1 and TGF β . However, surprisingly, there was no difference between CDA1 WT and KO mice in UUO-associated, nor IR-associated, upregulation of profibrotic gene expression, as well as a lack of changes in ECM accumulation, particularly collagen, at any of the timepoints examined in this study. While this is the common outcome for both of the acute renal injury models utilised in this chapter, the differences in disease progression between the two models, as well as the different timepoints for each model, may provide some insight to the underlying mechanism to explain this phenomenon.

Silencing or genetic deletion of CDA1 has previously been demonstrated to ameliorate TGF β signalling *in vitro* and *in vivo*. In particular, primary renal cells extracted from CDA1 KO mice exhibited an attenuated response towards TGF β 1 treatment.²⁵⁶ This suggests that the absence of functional CDA1 in CDA1 KO mice contributed towards the attenuation of diabetes-associated TGF β signalling and subsequent reduction of renal fibrosis in a mouse model of diabetic nephropathy. While the same CDA1 KO mouse strain was used in this study, CDA1 deficiency was unable to attenuate renal fibrosis in these acute renal injury models. Enhanced activation of the TGF β signalling pathway was observed in both models, as reflected by the upregulated expression of TGF β -related genes, particularly TGF β receptors, as well as elevated expression of pSmad3 in injured kidneys (**Figure 7.12**). Interestingly, the absence of CDA1 appeared to affect TGF β signalling activation differently between the two models of AKI. In the IR model, there was a reduction in gene expression of TGF β receptors, T β RI and T β RII, in CDA1 deficient mice 4 days after IR injury (**Figure 7.11**). This was associated with an apparent reduction in IR-associated pSmad3 expression in these mice (**Figure 7.12B**). Surprisingly, this reduction of pSmad3 in CDA1 deficient mice was not observed at 8 days post-IR-injury (**Figure 7.12D**), which coincided with the expression of many genes associated with IR injury, in particular TGF β receptor genes. Indeed, expression of the TGF β receptor genes were not different to those observed in CDA1 WT mice at this timepoint. In contrast, there was no indication that TGF β signalling was affected by CDA1 deletion in the UUO model. These results collectively suggest that the increasing severity of renal disease may surpass any potential effect of CDA1 deficiency had on the enhanced TGF β signalling observed in these disease models. Indeed, CDA1 deficiency, ultimately, was not associated with an attenuation of profibrotic gene expression, and subsequent ECM deposition at any timepoint examined in this study. In fact, it appears that CDA1 deficiency may have been associated with the exacerbation of profibrotic gene expression in the UUO

model, albeit at different times of UUO development. Whether or not the absence of CDA1 causes further renal injury in this model appears to be inconclusive, as seen by the contradictory nature of collagen deposition in CDA1 KO mice, as well as the attenuation of proinflammatory genes at later timepoints in the UUO model. As there is considerable cross-talk between TGF β and other signalling pathways, it is possible that absence of CDA1 and/or the attenuation of TGF β signalling in these AKI models might be compensated by the upregulation of other profibrotic factors. Nonetheless, although these two AKI models represent different severities of renal fibrosis, CDA1 deletion was unable to attenuate fibrosis progression in either of the models examined.

Although CDA1 deficiency appeared to have no effect on the progression of fibrosis in these AKI models, the most profound effect of CDA1 deficiency was observed on markers involved with inflammation, particularly in the early stages of the IR injury model. As seen from qRT-PCR analysis of kidneys after 4 days of reperfusion, CDA1 deficiency was associated with an exacerbation of IR-induced proinflammatory gene expression, notably TNF α , IL6 and iNOS (**Figure 7.13**). This phenomenon may be due to the amelioration of IR-induced TGF β signalling in CDA1 KO mice, as TGF β has been known to confer anti-inflammatory properties.⁷⁰ Indeed, TGF β 1-deficient mice have been previously shown to exhibit an exacerbation of IR-associated renal cortical injury, with those authors suggesting that TGF β deficiency increased the sensitivity of tubular cells to TNF α -mediated apoptosis.²²⁴

Despite the aforementioned IR-associated proinflammatory gene changes in CDA1 KO mice, CDA1 deficiency has various effects on markers associated with macrophages and/or inflammatory cell infiltration in both UUO and IR models. Adhesion molecules, particular ICAM1 and VCAM1, play important roles in inflammation such as leukocyte adhesion and transendothelial migration into inflammatory sites.^{315,316} Interestingly, there were trends towards decreases in the gene expression of these adhesion molecules, especially VCAM1, in CDA1 KO mice at early timepoints in both the UUO and IR studies (**Figures 7.6 and 7.13**). Previous studies have demonstrated that inhibition and/or absence of ICAM attenuates renal injury in mouse models of IR and UUO,³¹⁷⁻³²⁰ while inhibition of VCAM1 has been proposed as a viable therapeutic strategy against the development of atherosclerosis.³²¹ Paradoxically, however, there appears to be an exacerbation of IR-associated gene expression of various macrophage markers, such as iNOS and MSR1 in IR-injured kidneys of CDA1 KO mice 4 days of reperfusion (**Figure 7.13**). The increased levels of iNOS and MSR1, which are markers of pro-inflammatory M1³²² and anti-inflammatory M2 macrophages,³²³ respectively, suggest that CDA1 deficiency is associated with increased macrophage infiltration, of both subtypes, in this model. Furthermore, as the effects of CDA1 deficiency on MSR1 expression are sustained at 8 days after IR injury while levels of iNOS gene expression in CDA1 KO mice became comparable to those in CDA1 WT, it is possible that CDA1 deficiency facilitates a switch of macrophage subtypes, which may result in anti-inflammatory effects. Whether CDA1 deficiency was associated with elevated

macrophage infiltration and changes in specific macrophage populations in these models requires further investigation.

In addition to being a marker of M1 macrophages, iNOS is a major source of *nitric oxide* (NO) in renal diseases.³²⁴ Interestingly, gene expression of iNOS, which was elevated in UUO and IR mice (**Figure 7.6 and 7.13**), was exacerbated by CDA1 deficiency at an early stage of IR injury. As both CDA1 and TGF β have been reported to suppress iNOS expression,^{271, 325} it is possible that this phenomenon is due to either the direct effect of the absence of CDA1 and/or amelioration of TGF β signalling. Indeed, iNOS expression, which is modulated via Smad2 and/or Smad3-dependent pathways,^{198, 326} has been reported to be elevated in TGF β 1 null mice, as well as in Smad3 KO mice, with concomitant inflammation, in a model of abdominal aortic aneurysm.³²⁷ However, as iNOS KO mice have been associated with an increase in TGF β expression and signalling in a model of cardiac IR injury,³²⁸ and NO production inhibits Smad2/3 activity,³²⁹ iNOS and TGF β may mutually modulate each other. Further complicating this issue, iNOS expression was attenuated at later stages of UUO in CDA1 KO mice (**Figure 7.6**). Although it is possible that these findings may reflect a dynamic role of CDA1 in the modulation of iNOS expression at different stages of renal disease development, it is also possible that this may reflect a difference between the UUO and IR model. Indeed, deficiency of iNOS has been associated with an exacerbation of renal fibrosis, inflammation and tubular apoptosis in the UUO model,^{330, 331} while the inhibition of iNOS attenuates renal IR injury.³³² Whether the deficiency of CDA1 in these models leads to worsening of disease progression through its effects on iNOS expression requires further investigation.

Overall, CDA1 deficiency and its exacerbation of proinflammatory gene expression in the early stages of IR injury appear to have no effect on disease outcome. Indeed, I observed no greater susceptibility towards renal fibrosis, the final pathological feature in many chronic diseases and a contributing factor towards organ failure, in either the CDA1 KO mice in the IR study, nor in the severe renal fibrosis model of UUO. In fact, many of the proinflammatory genes which were exacerbated by CDA1 deficiency 4 days after IR injury were not different to that seen in CDA1 WT mice at 8 days post-injury. In addition to the lack of overall transcriptional changes in the UUO model, these findings suggest that CDA1 may have a role in suppressing renal inflammation at early stages of disease progression. As inhibition of TGF β signalling has previously been shown to potentially exacerbate inflammation while also attenuating renal fibrosis in both IR injury,²²² and UUO,²³⁰ it will be necessary to examine the long-term effects of CDA1 deficiency in IR injury by including later timepoints.

As a result of severe renal injury, the inhibition of cell cycle progression, as well as activation of apoptotic pathways, is seen in AKI and is considered to play a role in removing any damaged and unviable cells. Furthermore, tubular cell cycle arrest has been suggested to promote profibrotic responses in kidney disease.³³³ There is an increasing body of evidence that CKD is associated with

cell cycle arrest of the tubular epithelial cells,³³⁴ which may contribute to enhanced profibrotic cytokine activity.³³³ It was expected that targeting CDA1, which has been shown to exert antiproliferative properties in a p21 and cyclin B/CDK1-dependent manner,^{266, 272} would have had an effect on cell cycle markers in AKI. However, surprisingly, CDA1 deficiency was associated with an exacerbation of IR-induced p21 expression at 4 days post-injury. Furthermore, expression of many genes involved in cell cycle regulation, such as p53, and apoptosis, such as Bcl2, Bax1 and caspase-8, were reduced in CDA1 KO mice 4 days after IR injury. This is in contrast to previous reports whereby CDA1 deficiency had no effect on apoptosis,²⁶⁴ nor did CDA1 overexpression lead to an increase in cell death.²⁴⁸ As Bcl2 is a known anti-apoptotic protein, while Bak1 is generally apoptotic, it is not clear what would be the result of a reduction in both proteins. In addition, the expression of these genes was not different between CDA1 WT and CDA1 KO at 8 days post-injury, nor at later timepoints in the UUO study. This suggests, similar to that seen in respect to renal inflammation, CDA1 may modulate cell cycle responses as well as apoptotic processes in early AKI development. Thus, further examination, particularly at the protein level, is warranted to determine the role of CDA1 on cell cycle control and apoptosis in renal disease.

Interestingly, I also observed a tendency towards an increase in ki67 expression at later stages of IR injury in CDA1 KO mice when compared to WT mice. This finding suggests that CDA1 deficiency might be associated with increased proliferation of cells at later stages of AKI development. As renal IR injury has been reported to resolve if given sufficient time in this model,³³⁵ whether the absence of CDA1 has any effect on proliferation of tubular cells after IR injury remains to be investigated.

Overall, CDA1 deficiency was not associated with the attenuation of renal fibrosis in two models of acute renal injury. Surprisingly, however, there was an exacerbation of IR-associated proinflammatory gene expression, suggesting that CDA1 may play a role in the transcriptional modulation of inflammation in early disease development, potentially through the TGF β signalling pathway. Although CDA1 deficiency was associated with an exacerbation of proinflammatory gene expression, and paradoxically a minor reduction in adhesion molecule expression, the absence of CDA1 ultimately had no effect on renal injury or fibrosis in the two AKI models examined. As these proinflammatory effects of CDA1 deficiency are associated with a reduction in TGF β signalling, caution is advised when pursuing the pharmacological inhibition of CDA1 in certain fibrotic diseases.

Chapter 8. Discussion & Conclusion

8.1. Summary of major findings

8.1.1. Overview

CDA1 has been implicated to play a role in the development of fibrosis in vascular and renal diseases.^{255, 256, 262, 270} Pioneering studies suggest that CDA1 drives profibrotic processes in these diseases through its augmentation of the TGF β signalling pathway. In addition, the inhibition and absence of CDA1 has been demonstrated to attenuate TGF β -induced upregulation of profibrotic markers *in vitro* and *in vivo*, leading to the subsequent attenuation of renal fibrosis development.^{255, 256} The studies presented in this thesis aimed to further examine the pathological role of CDA1 in renal fibrosis through the use of conventional and inducible genetic knockout mouse strains in experimental models of non-diabetic and diabetic kidney disease, respectively. Overall, the findings described in this thesis show that the potential renoprotective effect of targeting CDA1 in renal disease appears to be context-dependent. In the diabetic nephropathy studies, early intervention against CDA1 activity through induced genetic deletion of CDA1 at an early stage of diabetic kidney disease attenuated renal fibrosis, while delayed intervention was found to be less effective on long-term disease development. In the non-diabetic renal fibrosis studies, the absence of functional CDA1, as seen in CDA1 KO mice, failed to attenuate renal fibrosis in two models of AKI, UO and IR injury. However, CDA1 deficiency at early stages of AKI development was associated with profound effects on pathological processes which are known to be modulated and may influence the response of the TGF β signalling pathway, such as inflammation and apoptosis. Collectively, these findings further suggest that the involvement of CDA1 on the pathogenesis of renal disease extends beyond its role in promoting the fibrotic process. Indeed, the effects associated with the absence of CDA1 appear to be overwhelmed by the robust stimuli used in these non-diabetic models. Thus, targeting CDA1 in renal disease appears to be more effective at early stages of disease development. Furthermore, these findings are consistent with the concept that while CDA1 is able to modulate TGF β signalling, it is not an intrinsic component of the TGF β pathway, and that the absence of CDA1 may attenuate TGF β signalling but cannot totally block this physiologically important pathway.

8.1.2. Induced genetic deletion of CDA1 and its effects on the progression of diabetic nephropathy

8.1.2.1. Inducible CDA1 KO mice

Although the effects of CDA1 deficiency in an experimental model of diabetic nephropathy had been previously investigated,²⁵⁶ direct inhibition of CDA1 and its effect on the progression of established diabetic kidney disease had not been investigated previously. As the development and characterisation of a pharmacological inhibitor of CDA1 is still at an early stage [Wu, T., submitted manuscript], I utilised an inducible genetic knockout mouse strain, CDA1^{flox}/ERCre strain, to

“imitate” certain aspects of the pharmacological inhibition of CDA1 activity in a mouse model of diabetic nephropathy. As seen in **Chapter 4**, the administration of tamoxifen to CDA1^{flox}/ERCre mice was able to induce the genetic deletion of CDA1 in a rapid and consistent manner. Although deletion of the CDA1 gene upon tamoxifen administration occurred in a dose-dependent manner in these mice, I chose not to increase the dose beyond 1.5 mg/mouse for 3 consecutive days used, nor did I attempt to achieve a complete ablation of CDA1 expression, in order to avoid potential side effects associated with high doses of tamoxifen administration (As described in **Section 4.4**). Fortunately, with the dose utilised in this thesis, I observed no tamoxifen-associated effect on metabolic and biochemical parameters in both non-diabetic control and diabetic CDA1^{flox} mice. Thus, any effect of tamoxifen-administration to the CDA1^{flox}/ERCre mice was largely, if not solely, due to the substantial reduction of CDA1 expression and resultant activity in these mice.

8.1.2.2. The effect of early versus delayed intervention against CDA1 in diabetic nephropathy

As seen in **Chapter 5**, early intervention against CDA1 activity via induced genetic deletion of CDA1 attenuates the development of diabetes-associated renal fibrosis. Induced genetic deletion of CDA1 five weeks after the induction of diabetes was associated with an attenuation of diabetes-associated profibrotic gene expression, with a consequent reduction in renal collagen accumulation. This is consistent with the findings from previous studies, where the renoprotective effects observed in CDA1 deficient mice were shown to be due to an attenuation of diabetes-associated TGF β signalling.²⁵⁶ By contrast, delayed intervention against CDA1 at a more established stage of renal disease appeared to have had minimal effect on the long-term development of renal fibrosis in this disease model (**Chapter 6**). While diabetes-associated collagen III deposition at 20 weeks after diabetes induction was attenuated in mice with induced CDA1 deficiency at 10 weeks after diabetes induction, there was no effect on any other parameter associated with renal fibrosis that was examined, including diabetes-associated profibrotic gene expression, nor collagen IV accumulation. The lack of renoprotective effects in the delayed intervention study is consistent to the lack of efficacy associated with TGF β inhibition in established stages of diabetic kidney disease, as seen in a recent clinical study using TGF β neutralising antibodies.²⁰⁴ Whether the minimal effect of CDA1 intervention at later stages of diabetic kidney disease development is due to the ineffectiveness of targeting either CDA1 or the TGF β signalling pathway in established renal disease requires further examination.

8.1.3. Global CDA1 KO and its effect on renal fibrosis in mouse models of AKI

Although knockout of CDA1 has been previously demonstrated to attenuate fibrosis in a mouse model of DN, the development of renal fibrosis was not affected by the absence of CDA1 in two models of AKI presented in this thesis (**Chapter 7**). Based on previous observations, knockout of CDA1 was considered to be associated with an attenuation of TGF β activity in these disease models. Indeed, CDA1 KO mice exhibited an attenuation of IR-associated upregulation of TGF β

receptors at an early timepoint, with western blot analysis also demonstrating reduced IR-associated expression of pSmad3 in these mice. Despite this, the absence of CDA1 did not affect the upregulation of profibrotic genes, nor the overall ECM accumulation, in both AKI models. CDA1 deficiency, however, was associated with profound effects on transcriptional changes related to inflammation, cell cycle regulation and apoptosis in early stages of AKI (**See Section 7.3**). Indeed, there appeared to be an exacerbation of IR-associated proinflammatory genes, particularly IL6, iNOS and MSR1, in IR-injured CDA1 KO mice at an early stage of disease development. These mice were also associated with reduced expression of genes such as adhesion molecules involved in recruitment of inflammatory cells, such as VCAM1 and ICAM1, and apoptotic modulators, such as Bcl2, Bak1 and Caspase 8, at this timepoint. As many of these transcriptional changes can be attributed to a reduction in TGF β signalling activity, it was surprising to observe that the expression of many of these genes was not different between CDA1 WT and KO mice at later stages of renal IR injury development, as well as in the more severe renal injury model, UUO. Nonetheless, both AKI models were associated with profound renal injury with robust upregulation of profibrotic and proinflammatory genes. The overwhelming response observed in these AKI models may involve the activation of a multitude of different pathological pathways. Thus, while targeting CDA1 may attenuate TGF β signalling activity in these models, particularly at early stages of disease development, it does not completely block the TGF β signalling pathway. Furthermore, it is possible that other profibrotic pathways are either not affected and/or enhanced to compensate for the absence of CDA1 in these non-diabetic renal disease models.

8.2. The pathological role of CDA1 in renal disease

8.2.1. Renal disease is associated with an elevation in CDA1 expression

From the findings presented in this study, it is abundantly clear that the role of CDA1 in renal disease is more complicated than originally thought. As previously reported, the physiological levels of CDA1 in the adult kidney are low.^{252-254, 268} In agreement with previous studies,^{255, 256, 262} I have observed elevations in CDA1 gene expression with injury, in a number of diabetic and non-diabetic models of renal injury. In fact, based on the qRT-PCR analysis presented in this thesis, levels of CDA1 appears to increase with severity of disease, with the gene expression of CDA1 increasing to ~1.5-fold in diabetic nephropathy, ~2.0-fold in renal IR injury and more than 3.0-fold in UUO, when compared to control mice. While upregulation of CDA1 has been considered to occur as a result of enhanced TGF β signalling in vascular and renal disease,^{255, 262} CDA1 may also be transcriptionally induced by various factors associated with the development of CKD,^{336, 337} such as X-box binding protein-1,³³⁸ and the arylhydrocarbon receptor,³³⁹ as well as in response to DNA damage,²⁷² and hypoxia [Li, J., unpublished work]. Coinciding with the concomitant increases in expression of TGF β and TGF β -related molecules, it is clear that CDA1 is involved in the development of renal fibrosis. While the pathological role of CDA1 in renal disease has been found to be associated with its ability

to enhance the TGF β signalling pathway through a T β RI-dependant manner (**described in Section 2.4**), the direct mechanism responsible for its activity remain unclear. However, based on findings from domain-swapping and gene deletion studies, CDA1 may be involved in the transcriptional and post-translational regulation of a variety of targets, which, in turn, may modulate the pathological actions of TGF β .

8.2.2. Speculated mechanisms behind CDA1 ability to enhance TGF β signalling

Among the many studies which have investigated the role of CDA1 in a variety of diseases, the most common observable characteristic of CDA1 is its antiproliferative ability. This property may be relevant to its activity in renal fibrosis, given that there is increasing evidence demonstrating that cell cycle arrest in renal tubular cells may contribute towards enhanced profibrotic cytokine activity in renal disease.³³³ Interestingly, findings from several independent studies strongly suggest that the antiproliferative ability of CDA1 might be related to its TGF β -enhancing properties. Firstly, like CDA1,²⁷² TGF β is able to transcriptionally upregulate p21 expression through a MAPK-dependent pathway.^{340, 341} Indeed, a preliminary study demonstrated that CDA1-mediated activation of p21 promoter and its subsequent transcription *in vitro* was also T β RI-dependent [Tu, Y., unpublished work]. Furthermore, CDA1 has been shown to induce cell cycle arrest at the G2/M phase in a cyclin B/CDK1-dependent manner,²⁶⁶ while there have been reports of strong associations between cell cycle arrest and TGF β levels.^{221, 333} Secondly, chromatin immunoprecipitation assays demonstrate that CDA1 does not bind to the p21 promoter,²⁵⁹ suggesting that CDA1 indirectly promotes the transcriptional upregulation of p21. Collectively, these findings suggest that CDA1 may confer its antiproliferative properties through the TGF β signalling pathway.

As described in **Section 2.3.1**, both the NAP domain and the acidic carboxyl tail have been extensively investigated for their role in the antiproliferative properties of CDA1. The importance of these structural features is emphasised by findings obtained from our CDA1 KO mice. The deletion of exons 2-5 of the mouse CDA1 gene, which encodes a portion of the NAP domain (residues 238-381), results in an open-reading frame shift, leading to the introduction of a stop codon within 6 residues downstream of the deleted region (**Figure 8.1**). Thus, the resultant protein translated from the truncated gene of CDA1 KO mice contains the amino-terminal portion of CDA1, while lacking both a functional NAP domain and the acidic carboxyl-terminal tail. Although it has been proposed by an independent group that the amino-terminal portion of CDA1 may be involved in the interaction with certain transcription factor complexes, such as *repressor element 1-silencing transcription factor/neuron-restrictive silencer factor* (REST/NRSF), it is likely that the remnant CDA1 protein in our CDA1 KO mice is non-functional.²⁶³ Indeed, in the same study, these authors demonstrated that a mutant variant of the human CDA1 protein encoding residues 1-216 alone was unable to suppress proliferation nor enhance TGF β signalling *in vitro* and required the presence of other structural domains to exert these effects. Furthermore, consistent with this finding, primary cells from CDA1

mutant mice, despite the presence of the amino-terminal end of CDA1 in these mice with deletion of exons 2-5 of the CDA1 gene, have not only exhibited stunted profibrotic responses towards TGF β 1,²⁵⁶ but also had impaired ability to undergo cell cycle arrest.²⁶⁴

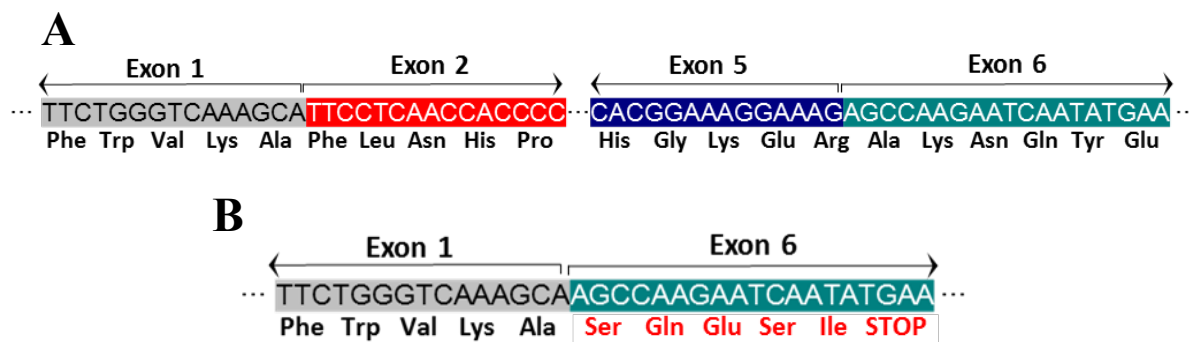


Figure 8.1. Deletion of exons 2-5 of the mouse CDA1 gene leads to a non-functional gene product. A schematic diagram of the mouse CDA1 gene, with the resultant translated amino acid sequence listed below, in CDA1 wildtype mice (A). In CDA1 KO mice, an open-reading frame shift occurs after the excision of exons 2-5 of the CDA1 gene, resulting in the introduction of a STOP codon within 6 residues after exon 1 of the truncated gene (B). Thus, the resultant protein from the CDA1 KO allele will contain the amino-terminal portion of CDA1, while lacking both a functional NAP domain and the acidic carboxyl-terminal tail.

8.2.3. The inhibition or absence of CDA1 activity affects TGF β signalling and subsequent renal fibrosis development in a time and context-dependent manner

In agreement with previous studies using global CDA1 KO mice,^{256, 270} early intervention against CDA1 activity was demonstrated to attenuate the development of diabetes-associated renal fibrosis (Chapter 5). Based on *in vitro* and *in vivo* data from previously reported studies,^{255, 256} it is assumed that the renoprotective effect associated with the absence or inhibition of CDA1 activity in the development of diabetic nephropathy is due to reduced TGF β signalling activity. The reduction in TGF β signalling activity may also be associated with profound transcriptional effects as was observed in CDA1 KO mice at early stages of renal IR injury development. Indeed, CDA1 deficiency was associated with transcriptional changes in IR-associated expression of genes related to inflammation, cell cycle control and apoptosis at 4 days after renal IR injury, which coincided with an attenuation in IR-associated pSmad3 expression in these mice (Chapter 7).

However, the effects of CDA1 deficiency on TGF β signalling and subsequent renal disease development appear to be temporal in nature, particularly at advanced stages of renal disease. Indeed, delayed intervention against CDA1 through the induced genetic deletion of CDA1 had minimal, if any, effect on long-term renal fibrosis development in a mouse model of diabetic nephropathy

(**Chapter 6**). Similarly, despite the profound transcriptional changes associated with reduced TGF β signalling observed at early stages of IR-injury disease development in CDA1 deficient mice, the absence of functional CDA1 had little, if any, effect on profibrotic gene expression nor on subsequent ECM deposition in two disparate mouse models of AKI (**Chapter 7**). Interestingly, the differences in transcriptional changes, particularly of genes related to inflammation such as IL6 and iNOS, and IR-associated pSmad3 expression between CDA1 WT and KO mice at early stages of IR-associated disease development were not observed at a later timepoint. In addition, I observed no difference between CDA1 WT and CDA1 KO mice in expression levels of genes related to inflammation, cell cycle control and apoptosis in the more severe AKI model, UUO. As primary renal cells extracted from CDA1 KO mice have previously been demonstrated to have a stunted response to exogenous TGF β 1 stimulation,²⁵⁶ it is possible that other signalling pathways are activated to sustain profibrotic processes in the absence of CDA1 activity in these models, particularly at later stages of renal disease development. Collectively, these findings suggest that CDA1, through the modulation of the TGF β signalling pathway, plays multiple roles in early renal disease development and, therefore, inhibition of CDA1 activity is more effective at early stages of renal disease. However, as renal disease develops, the activation of other pathological pathways may occur in order to compensate for the absence of CDA1 activity, potentially rendering CDA1 activity in some of these disease models redundant. These findings further support the concept that while CDA1 may modulate the TGF β signalling pathway in disease, the absence or inhibition of CDA1 activity does not completely block this physiologically important pathway. This could be an advantage since this would otherwise lead to undesirable side-effects. Thus, targeting CDA1 represent a non-aggressive approach towards the inhibition of TGF β -mediated profibrotic processes and could be used in combination with other potential therapeutic strategies to combat the development of fibrosis in CKD.

8.3. Questions left unanswered, study limitations and future directions

From the findings presented in this thesis, it is clear that the role of CDA1 in disease development is far more complex than originally predicted. Although CDA1 deficiency was associated with profound transcriptional changes in genes related to inflammation, cell cycle control and apoptosis at early stages of renal IR-injury development, these disease processes lie beyond the research focus of this thesis and, therefore, were not extensively examined. Furthermore, despite what appears to be an exacerbation of IR-associated proinflammatory expression at early stages of IR disease development in CDA1 deficient mice, ultimately, this did not appear to affect the development of renal fibrosis, as reflected by the lack of changes in profibrotic gene expression, nor subsequent ECM accumulation. Nonetheless, as these disease processes have been implicated in the development of renal fibrosis, it will be necessary to examine the role that CDA1 plays in modulating these processes in the future.

Although pioneering studies in our laboratory have demonstrated the ability of CDA1 to enhance TGF β signalling and independent mechanistic studies have unveiled potential mechanisms of CDA1 action, it is imperative towards our further understanding of CDA1 to examine the mechanisms which govern the direct actions of this protein in the context of fibrosis. Indeed, a more thorough understanding of the molecular and protein structure of CDA1 will not only assist in the identification of potential binding partners but will also assist in the development of pharmacological inhibitors towards CDA1. Furthermore, while I was able to demonstrate that CDA1 gene expression was upregulated in renal disease, I was unable to validate this expression at the protein level due to the lack of a suitable antibody. To address this issue, attempts have been made in our laboratory to generate specific antibodies suitable for the immunohistochemical staining of CDA1 protein in mouse kidney. Of particular interest, as CDA1 has been suggested to be post-translationally regulated by phosphorylation, the production of antibodies which can identify phosphorylated and non-phosphorylated forms of CDA1 may help to improve our understanding of CDA1 regulation and actions in disease.

One of the core hypotheses of my studies was that the absence of CDA1 activity attenuates TGF β signalling. While our initial investigations *in vitro* have demonstrated that silencing the expression or the complete absence of functional CDA1 is associated with reduced TGF β signalling activity, the absence or delayed inhibition of CDA1 activity was unable to attenuate renal fibrosis development in the non-diabetic renal fibrosis or experimental diabetic nephropathy models, respectively. However, more thorough analysis of TGF β signalling activation, such as immunohistochemical staining for pSmad3 expression, is required to further confirm our findings obtained from western blot analysis. Furthermore, to determine whether the effects associated with CDA1 deficient mice in these disease models were a direct consequence of reduced TGF β signalling, it will be necessary to perform further experiments using animal models utilising TGF β signalling inhibitors, alongside parallel studies in CDA1 KO mice. Not only will this help validate the relationship of CDA1 and TGF β in disease development but will determine whether the inability to affect renal fibrosis in these studies can be pinpointed to the lack of efficacy of CDA1 or TGF β inhibition.

I utilised a number of mouse models of diabetic and non-diabetic forms of renal disease to examine the pathological role of CDA1 in this thesis. While a number of interesting findings have been gathered from these studies, there are still questions left to be answered. Indeed, the mouse strain used in the diabetic nephropathy studies was on the C57BL6 background, which are known to be relatively resistant to glomerulosclerosis. Therefore, it would be interesting to examine our findings in a more clinically relevant model, such as the more glomerulosclerotic-prone ApoE KO strain or a genetic model of diabetes with nephropathy, such as the Akita mouse. In addition, while the two models of AKI used in this thesis, UUO and renal IR injury, may share certain pathological features

at certain timepoints in disease development, they are, nonetheless, disparate models of disease with important differences in disease progression and outcome. Thus, it would be important to examine additional timepoints in these models in order to investigate the role of CDA1 in pathological processes contributing to the progression of CKD, such as inflammation, cell cycle control and apoptosis.

8.4. Conclusions

In summary, the work presented in this thesis examined the effect of CDA1 deficiency on the development of renal fibrosis in mouse models of diabetic and non-diabetic renal diseases. Elevated CDA1 expression was observed with renal injury, which appears to increase with disease severity, suggesting a role for CDA1 in the initiation of renal disease in these models. Induced genetic deletion of CDA1 at early stages of disease development appears to afford renoprotection in a mouse model of diabetic nephropathy. In contrast, induced genetic deletion of CDA1 at a later timepoint had minimal effect on long-term diabetes-associated renal fibrosis. The latter finding is consistent with observations obtained from the more acute and severe non-diabetic mouse models of renal fibrosis. Indeed, although CDA1 deficient mice exhibited profound transcriptional changes associated with reduced TGF β signalling activity at early stages of IR injury development, the absence of CDA1 did not appear to affect profibrotic gene expression nor subsequent ECM accumulation in either AKI models examined in this study. Collectively, these findings suggest that CDA1 is involved in early stages of disease development, with inhibition of its activity at these early stages having profound effects on TGF β -mediated pathological processes. However, the effect of CDA1 deficiency on the TGF β signalling pathway and subsequent renal fibrosis development appears to be time and context-dependent. Overall, targeting CDA1 represents a relatively non-aggressive approach towards the attenuation of the TGF β signalling pathway. It is likely that these studies will aid in the development of future therapies, including the targeting of CDA1, against the development and progression of various fibrotic renal diseases including the most common cause of ESRD worldwide, diabetic nephropathy.

References

1. Zeisberg M, Neilson EG. Mechanisms of tubulointerstitial fibrosis. *Journal of the American Society of Nephrology : JASN*. 2010;21(11):1819-34.
2. Cooper ME. Pathogenesis, prevention, and treatment of diabetic nephropathy. *Lancet*. 1998;352(9123):213-9.
3. Guo JK, Cantley LG. Cellular maintenance and repair of the kidney. *Annual review of physiology*. 2010;72:357-76.
4. Droz ST, McLaughlin KA. Use of *Xenopus* Frogs to Study Renal Development/Repair. Results and problems in cell differentiation. 2017;60:77-107.
5. Berger K, Moeller MJ. Mechanisms of Epithelial Repair and Regeneration After Acute Kidney Injury. *Seminars in Nephrology*. 2014;34(4):394-403.
6. Bonventre JV. Dedifferentiation and proliferation of surviving epithelial cells in acute renal failure. *Journal of the American Society of Nephrology : JASN*. 2003;14 Suppl 1:S55-61.
7. Bonventre JV, Yang L. Cellular pathophysiology of ischemic acute kidney injury. *J Clin Invest*. 2011;121(11):4210-21.
8. Carlson BM. Some principles of regeneration in mammalian systems. *Anatomical record Part B, New anatomist*. 2005;287(1):4-13.
9. Kusaba T, Humphreys BD. Controversies on the origin of proliferating epithelial cells after kidney injury. *Pediatric nephrology (Berlin, Germany)*. 2014;29(4):673-9.
10. Noris M, Remuzzi G. Overview of complement activation and regulation. *Semin Nephrol*. 2013;33(6):479-92.
11. Jang HR, Rabb H. Immune cells in experimental acute kidney injury. *Nat Rev Nephrol*. 2015;11(2):88-101.
12. Wynn TA. Cellular and molecular mechanisms of fibrosis. *The Journal of pathology*. 2008;214(2):199-210.
13. Bhogal R, Stoica C, McGaha T, Bona C. Molecular aspects of regulation of collagen gene expression in fibrosis. *Journal of clinical immunology*. 2005;25(6):592-603.
14. Saran R, Robinson B, Abbott KC, Agodoa LY, Albertus P, Ayanian J, et al. US Renal Data System 2016 Annual Data Report: Epidemiology of Kidney Disease in the United States. *American journal of kidney diseases : the official journal of the National Kidney Foundation*. 2017;69(3 Suppl 1):A7-a8.
15. Tuttle KR, Bakris GL, Bilous RW, Chiang JL, de Boer IH, Goldstein-Fuchs J, et al. Diabetic kidney disease: a report from an ADA Consensus Conference. *Diabetes care*. 2014;37(10):2864-83.

16. Jha V, Garcia-Garcia G, Iseki K, Li Z, Naicker S, Plattner B, et al. Chronic kidney disease: global dimension and perspectives. *Lancet*. 2013;382(9888):260-72.
17. Reutens AT, Atkins RC. Epidemiology of diabetic nephropathy. *Contributions to nephrology*. 2011;170:1-7.
18. Thomas MC, Cooper ME, Zimmet P. Changing epidemiology of type 2 diabetes mellitus and associated chronic kidney disease. *Nat Rev Nephrol*. 2016;12(2):73-81.
19. Groop P-H, Thomas MC, Moran JL, Wadèn J, Thorn LM, Mäkinen V-P, et al. The Presence and Severity of Chronic Kidney Disease Predicts All-Cause Mortality in Type 1 Diabetes. *Diabetes*. 2009;58(7):1651-8.
20. Orchard TJ, Secrest AM, Miller RG, Costacou T. In the absence of renal disease, 20 year mortality risk in type 1 diabetes is comparable to that of the general population: a report from the Pittsburgh Epidemiology of Diabetes Complications Study. *Diabetologia*. 2010;53(11):2312-9.
21. Afkarian M, Sachs MC, Kestenbaum B, Hirsch IB, Tuttle KR, Himmelfarb J, et al. Kidney Disease and Increased Mortality Risk in Type 2 Diabetes. *Journal of the American Society of Nephrology*. 2013;24(2):302-8.
22. Russell ND, Cooper ME. 50 years forward: mechanisms of hyperglycaemia-driven diabetic complications. *Diabetologia*. 2015;58(8):1708-14.
23. Alicic RZ, Rooney MT, Tuttle KR. Diabetic Kidney Disease: Challenges, Progress, and Possibilities. *Clinical journal of the American Society of Nephrology : CJASN*. 2017.
24. Gregg EW, Li Y, Wang J, Burrows NR, Ali MK, Rolka D, et al. Changes in diabetes-related complications in the United States, 1990-2010. *The New England journal of medicine*. 2014;370(16):1514-23.
25. Ogurtsova K, da Rocha Fernandes JD, Huang Y, Linnenkamp U, Guariguata L, Cho NH, et al. IDF Diabetes Atlas: Global estimates for the prevalence of diabetes for 2015 and 2040. *Diabetes research and clinical practice*. 2017;128:40-50.
26. Mogensen CE, Christensen CK, Vittinghus E. The stages in diabetic renal disease. With emphasis on the stage of incipient diabetic nephropathy. *Diabetes*. 1983;32 Suppl 2:64-78.
27. Thomas MC, Brownlee M, Susztak K, Sharma K, Jandeleit-Dahm KA, Zoungas S, et al. Diabetic kidney disease. *Nature reviews Disease primers*. 2015;1:15018.
28. Fioretto P, Caramori ML, Mauer M. The kidney in diabetes: dynamic pathways of injury and repair. *The Camillo Golgi Lecture 2007*. *Diabetologia*. 2008;51(8):1347-55.
29. Pugliese G. Updating the natural history of diabetic nephropathy. *Acta diabetologica*. 2014;51(6):905-15.

30. Caramori ML, Kim Y, Huang C, Fish AJ, Rich SS, Miller ME, et al. Cellular Basis of Diabetic Nephropathy. 1 Study Design and Renal Structural-Functional Relationships in Patients With Long-Standing Type 1 Diabetes. 2002;51(2):506-13.
31. Adler AI, Stevens RJ, Manley SE, Bilous RW, Cull CA, Holman RR, et al. Development and progression of nephropathy in type 2 diabetes: The United Kingdom Prospective Diabetes Study (UKPDS 64). *Kidney International*. 2003;63(1):225-32.
32. Klessens CQ, Woutman TD, Veraar KA, Zandbergen M, Valk EJ, Rotmans JI, et al. An autopsy study suggests that diabetic nephropathy is underdiagnosed. *Kidney Int*. 2016;90(1):149-56.
33. Fioretto P, Mauer M. Histopathology of diabetic nephropathy. *Semin Nephrol*. 2007;27(2):195-207.
34. Kanwar YS, Sun L, Xie P, Liu FY, Chen S. A glimpse of various pathogenetic mechanisms of diabetic nephropathy. *Annual review of pathology*. 2011;6:395-423.
35. Checheriță IA, Manda G, Hinescu ME, Peride I, Niculae A, Bîlha Ș, et al. New molecular insights in diabetic nephropathy. *International Urology and Nephrology*. 2016:1-15.
36. Thomas MC. Advanced glycation end products. *Contributions to nephrology*. 2011;170:66-74.
37. Forbes JM, Cooper ME. Glycation in diabetic nephropathy. *Amino acids*. 2012;42(4):1185-92.
38. Lindblom R, Higgins G, Coughlan M, de Haan JB. Targeting Mitochondria and Reactive Oxygen Species-Driven Pathogenesis in Diabetic Nephropathy. *The review of diabetic studies : RDS*. 2015;12(1-2):134-56.
39. Wada J, Makino H. Inflammation and the pathogenesis of diabetic nephropathy. *Clinical science (London, England : 1979)*. 2013;124(3):139-52.
40. Schena FP, Gesualdo L. Pathogenetic mechanisms of diabetic nephropathy. *Journal of the American Society of Nephrology : JASN*. 2005;16 Suppl 1:S30-3.
41. White KE, Bilous RW, Marshall SM, El Nahas M, Remuzzi G, Piras G, et al. Podocyte number in normotensive type 1 diabetic patients with albuminuria. *Diabetes*. 2002;51(10):3083-9.
42. Mauer SM. Structural-functional correlations of diabetic nephropathy. *Kidney Int*. 1994;45(2):612-22.
43. Premaratne E, Verma S, Ekinci EI, Theverkalam G, Jerums G, MacIsaac RJ. The impact of hyperfiltration on the diabetic kidney. *Diabetes Metab*. 2015;41(1):5-17.
44. Forbes JM, Cooper ME. Mechanisms of diabetic complications. *Physiological Reviews*. 2013;93(1):137-88.

45. García-Sánchez O, López-Hernández FJ, López-Novoa JM. An integrative view on the role of TGF-beta in the progressive tubular deletion associated with chronic kidney disease. *Kidney International*. 2010;77(11):950-5.
46. Grande MT, Perez-Barriocanal F, Lopez-Novoa JM. Role of inflammation in tubulo-interstitial damage associated to obstructive nephropathy. *Journal of inflammation (London, England)*. 2010;7:19.
47. Bader R, Bader H, Grund KE, Mackensen-Haen S, Christ H, Bohle A. Structure and function of the kidney in diabetic glomerulosclerosis. Correlations between morphological and functional parameters. *Pathology, research and practice*. 1980;167(2-4):204-16.
48. *Silva's Diagnostic Renal Pathology*. 2 ed. Zhou XJ, Laszik ZG, Nadasdy T, D'Agati VD, editors. Cambridge: Cambridge University Press; 2017.
49. Little MH. Regrow or repair: potential regenerative therapies for the kidney. *Journal of the American Society of Nephrology : JASN*. 2006;17(9):2390-401.
50. Tharaux P-L, Huber T. How many ways can a podocyte die? *Seminars in nephrology*. 2012;32(4):394-404.
51. Schnaper HW. Remnant nephron physiology and the progression of chronic kidney disease. *Pediatric nephrology (Berlin, Germany)*. 2014;29(2):193-202.
52. Go AS, Chertow GM, Fan D, McCulloch CE, Hsu CY. Chronic kidney disease and the risks of death, cardiovascular events, and hospitalization. *The New England journal of medicine*. 2004;351(13):1296-305.
53. Fried LF, Emanuele N, Zhang JH, Brophy M, Conner TA, Duckworth W, et al. Combined angiotensin inhibition for the treatment of diabetic nephropathy. *The New England journal of medicine*. 2013;369(20):1892-903.
54. Perkins BA, Ficociello LH, Silva KH, Finkelstein DM, Warram JH, Krolewski AS. Regression of microalbuminuria in type 1 diabetes. *The New England journal of medicine*. 2003;348(23):2285-93.
55. Amann B, Tinzmann R, Angelkort B. ACE inhibitors improve diabetic nephropathy through suppression of renal MCP-1. *Diabetes care*. 2003;26(8):2421-5.
56. Roscioni SS, Heerspink HJ, de Zeeuw D. The effect of RAAS blockade on the progression of diabetic nephropathy. *Nat Rev Nephrol*. 2014;10(2):77-87.
57. Fioretto P, Steffes MW, Sutherland DE, Goetz FC, Mauer M. Reversal of lesions of diabetic nephropathy after pancreas transplantation. *The New England journal of medicine*. 1998;339(2):69-75.
58. Fioretto P, Sutherland DE, Najafian B, Mauer M. Remodeling of renal interstitial and tubular lesions in pancreas transplant recipients. *Kidney Int*. 2006;69(5):907-12.

59. Strutz F, Zeisberg M. Renal fibroblasts and myofibroblasts in chronic kidney disease. *Journal of the American Society of Nephrology : JASN*. 2006;17(11):2992-8.
60. Grande MT, López-Novoa JM. Fibroblast activation and myofibroblast generation in obstructive nephropathy. *Nature reviews Nephrology*. 2009;5(6):319-28.
61. Liu Y. Renal fibrosis: new insights into the pathogenesis and therapeutics. *Kidney international*. 2006;69(2):213-7.
62. Nath KA. Tubulointerstitial changes as a major determinant in the progression of renal damage. *American journal of kidney diseases : the official journal of the National Kidney Foundation*. 1992;20(1):1-17.
63. Bonventre JV. Can we target tubular damage to prevent renal function decline in diabetes? *Semin Nephrol*. 2012;32(5):452-62.
64. Gilbert RE, Cooper ME. The tubulointerstitium in progressive diabetic kidney disease: More than an aftermath of glomerular injury? *Kidney International*. 1999;56(5):1627-37.
65. Bohle A, Mackensen-Haen S, von Gise H, Grund KE, Wehrmann M, Batz C, et al. The consequences of tubulo-interstitial changes for renal function in glomerulopathies. A morphometric and cytological analysis. *Pathology, research and practice*. 1990;186(1):135-44.
66. Mauer SM, Steffes MW, Ellis EN, Sutherland DE, Brown DM, Goetz FC. Structural-functional relationships in diabetic nephropathy. *J Clin Invest*. 1984;74(4):1143-55.
67. White KE, Bilous RW. Type 2 diabetic patients with nephropathy show structural-functional relationships that are similar to type 1 disease. *Journal of the American Society of Nephrology : JASN*. 2000;11(9):1667-73.
68. Venkatachalam MA, Weinberg JM, Kriz W, Bidani AK. Failed Tubule Recovery, AKI-CKD Transition, and Kidney Disease Progression. *Journal of the American Society of Nephrology : JASN*. 2015;26(8):1765-76.
69. Darby I, Hewitson T. Fibroblast differentiation in wound healing and fibrosis. *Int Rev Cytol*. 2007;257:143-79.
70. Meng XM, Nikolic-Paterson DJ, Lan HY. Inflammatory processes in renal fibrosis. *Nat Rev Nephrol*. 2014;10(9):493-503.
71. Kriz W, LeHir M. Pathways to nephron loss starting from glomerular diseases-insights from animal models. *Kidney Int*. 2005;67(2):404-19.
72. Mack M, Yanagita M. Origin of myofibroblasts and cellular events triggering fibrosis. *Kidney Int*. 2014.
73. Scheinman JI, Tanaka H, Haralson M, Wang SL, Brown O. Specialized collagen mRNA and secreted collagens in human glomerular epithelial, mesangial, and tubular cells. *Journal of the American Society of Nephrology : JASN*. 1992;2(10):1475-83.

74. Essawy M, Soylemezoglu O, Muchaneta-Kubara EC, Shortland J, Brown CB, el Nahas AM. Myofibroblasts and the progression of diabetic nephropathy. *Nephrol Dial Transplant*. 1997;12(1):43-50.
75. Pedagogos E, Hewitson T, Fraser I, Nicholls K, Becker G. Myofibroblasts and arteriolar sclerosis in human diabetic nephropathy. *American journal of kidney diseases : the official journal of the National Kidney Foundation*. 1997;29(6):912-8.
76. Meng X-M, Nikolic-Paterson DJ, Lan HY. TGF-[beta]: the master regulator of fibrosis. *Nat Rev Nephrol*. 2016;advance online publication.
77. Meran S, Steadman R. Fibroblasts and myofibroblasts in renal fibrosis. *International journal of experimental pathology*. 2011;92(3):158-67.
78. LeBleu VS, Taduri G, O'Connell J, Teng Y, Cooke VG, Woda C, et al. Origin and function of myofibroblasts in kidney fibrosis. *Nat Med*. 2013;19(8):1047-53.
79. Chen J, Xia Y, Lin X, Feng X-H, Wang Y. Smad3 signaling activates bone marrow-derived fibroblasts in renal fibrosis. *Laboratory investigation; a journal of technical methods and pathology*. 2014;94(5):545-56.
80. Iwano M, Plieth D, Danoff TM, Xue C, Okada H, Neilson EG. Evidence that fibroblasts derive from epithelium during tissue fibrosis. *J Clin Invest*. 2002;110(3):341-50.
81. Zeisberg EM, Potenta SE, Sugimoto H, Zeisberg M, Kalluri R. Fibroblasts in kidney fibrosis emerge via endothelial-to-mesenchymal transition. *Journal of the American Society of Nephrology : JASN*. 2008;19(12):2282-7.
82. Schrimpf C, Duffield J. Mechanisms of fibrosis: the role of the pericyte. *Current opinion in nephrology and hypertension*. 2011;20(3):297-305.
83. Meng XM, Wang S, Huang XR, Yang C, Xiao J, Zhang Y, et al. Inflammatory macrophages can transdifferentiate into myofibroblasts during renal fibrosis. *Cell death & disease*. 2016;7(12):e2495.
84. Kalluri R, Weinberg R. The basics of epithelial-mesenchymal transition. *The Journal of clinical investigation*. 2009;119(6):1420-8.
85. Floege J, Eitner F, Alpers CE. A new look at platelet-derived growth factor in renal disease. *Journal of the American Society of Nephrology : JASN*. 2008;19(1):12-23.
86. Phanish MK, Winn SK, Dockrell ME. Connective tissue growth factor-(CTGF, CCN2)--a marker, mediator and therapeutic target for renal fibrosis. *Nephron Exp Nephrol*. 2010;114(3):e83-92.
87. Yang F, Chung AC, Huang XR, Lan HY. Angiotensin II induces connective tissue growth factor and collagen I expression via transforming growth factor-beta-dependent and -independent Smad pathways: the role of Smad3. *Hypertension*. 2009;54(4):877-84.

88. Klahr S, Ishidoya S, Morrissey J. Role of angiotensin II in the tubulointerstitial fibrosis of obstructive nephropathy. *American journal of kidney diseases : the official journal of the National Kidney Foundation*. 1995;26(1):141-6.
89. Hinck AP, Mueller TD, Springer TA. Structural Biology and Evolution of the TGF-beta Family. *Cold Spring Harbor perspectives in biology*. 2016;8(12).
90. Goumans MJ, Liu Z, ten Dijke P. TGF-beta signaling in vascular biology and dysfunction. *Cell Res*. 2009;19(1):116-27.
91. Moses HL, Roberts AB, Derynck R. The Discovery and Early Days of TGF-beta: A Historical Perspective. *Cold Spring Harbor perspectives in biology*. 2016;8(7).
92. Ruiz Ortega M, Rodriguez-Vita J, Sanchez Lopez E, Carvajal G, Egido J. TGF-beta signaling in vascular fibrosis. *Cardiovascular research*. 2007;74(2):196-206.
93. Böttinger E. TGF-beta in renal injury and disease. *Seminars in nephrology*. 2007;27(3):309-20.
94. Gordon K, Blobel G. Role of transforming growth factor-beta superfamily signaling pathways in human disease. *Biochimica et biophysica acta*. 2008;1782(4):197-228.
95. Border WA, Noble NA. Transforming growth factor beta in tissue fibrosis. *The New England journal of medicine*. 1994;331(19):1286-92.
96. Border WA, Noble NA. TGF-beta in kidney fibrosis: a target for gene therapy. *Kidney international*. 1997;51(5):1388-96.
97. Yamamoto T, Noble NA, Cohen AH, Nast CC, Hishida A, Gold LI, et al. Expression of transforming growth factor-beta isoforms in human glomerular diseases. *Kidney Int*. 1996;49(2):461-9.
98. Yamamoto T, Nakamura T, Noble NA, Ruoslahti E, Border WA. Expression of transforming growth factor beta is elevated in human and experimental diabetic nephropathy. *Proceedings of the National Academy of Sciences*. 1993;90(5):1814-8.
99. Sanderson N, Factor V, Nagy P, Kopp J, Kondaiah P, Wakefield L, et al. Hepatic expression of mature transforming growth factor beta 1 in transgenic mice results in multiple tissue lesions. *Proc Natl Acad Sci U S A*. 1995;92(7):2572-6.
100. Kopp JB, Factor VM, Mozes M, Nagy P, Sanderson N, Böttinger EP, et al. Transgenic mice with increased plasma levels of TGF-beta 1 develop progressive renal disease. *Laboratory Investigation*. 1996;74(6):991-1003.
101. Mozes MM, Böttinger EP, Jacot TA, Kopp JB. Renal expression of fibrotic matrix proteins and of transforming growth factor-beta (TGF-beta) isoforms in TGF-beta transgenic mice. *Journal of the American Society of Nephrology : JASN*. 1999;10(2):271-80.

102. Koesters R, Kaissling B, Lehir M, Picard N, Theilig F, Gebhardt R, et al. Tubular overexpression of transforming growth factor-beta1 induces autophagy and fibrosis but not mesenchymal transition of renal epithelial cells. *Am J Pathol.* 2010;177(2):632-43.
103. Sonnylal S, Denton CP, Zheng B, Keene DR, He R, Adams HP, et al. Postnatal induction of transforming growth factor beta signaling in fibroblasts of mice recapitulates clinical, histologic, and biochemical features of scleroderma. *Arthritis and rheumatism.* 2007;56(1):334-44.
104. Poncelet AC, de Caestecker MP, Schnaper HW. The transforming growth factor-beta/SMAD signaling pathway is present and functional in human mesangial cells. *Kidney Int.* 1999;56(4):1354-65.
105. Aihara K-I, Ikeda Y, Yagi S, Akaike M, Matsumoto T. Transforming Growth Factor- β 1 as a Common Target Molecule for Development of Cardiovascular Diseases, Renal Insufficiency and Metabolic Syndrome. *Cardiology research and practice.* 2010;2011:175381-.
106. Kitamura M, Suto TS. TGF-beta and glomerulonephritis: anti-inflammatory versus prosclerotic actions. *Nephrol Dial Transplant.* 1997;12(4):669-79.
107. Mason RM, Wahab NA. Extracellular Matrix Metabolism in Diabetic Nephropathy. *Journal of the American Society of Nephrology.* 2003;14(5):1358-73.
108. Fraser D, Wakefield L, Phillips A. Independent regulation of transforming growth factor-beta1 transcription and translation by glucose and platelet-derived growth factor. *Am J Pathol.* 2002;161(3):1039-49.
109. Fraser D, Brunskill N, Ito T, Phillips A. Long-term exposure of proximal tubular epithelial cells to glucose induces transforming growth factor-beta 1 synthesis via an autocrine PDGF loop. *Am J Pathol.* 2003;163(6):2565-74.
110. Weigert C, Sauer U, Brodbeck K, Pfeiffer A, Haring HU, Schleicher ED. AP-1 proteins mediate hyperglycemia-induced activation of the human TGF-beta1 promoter in mesangial cells. *Journal of the American Society of Nephrology : JASN.* 2000;11(11):2007-16.
111. Nath KA, Grande J, Croatt A, Haugen J, Kim Y, Rosenberg ME. Redox regulation of renal DNA synthesis, transforming growth factor-beta1 and collagen gene expression. *Kidney Int.* 1998;53(2):367-81.
112. Phillips AO, Topley N, Steadman R, Morrissey K, Williams JD. Induction of TGF-beta 1 synthesis in D-glucose primed human proximal tubular cells by IL-1 beta and TNF alpha. *Kidney Int.* 1996;50(5):1546-54.
113. Van Obberghen-Schilling E, Roche NS, Flanders KC, Sporn MB, Roberts AB. Transforming growth factor beta 1 positively regulates its own expression in normal and transformed cells. *The Journal of biological chemistry.* 1988;263(16):7741-6.

114. Fukuda K, Yoshitomi K, Yanagida T, Tokumoto M, Hirakata H. Quantification of TGF-beta1 mRNA along rat nephron in obstructive nephropathy. *Am J Physiol Renal Physiol*. 2001;281(3):F513-21.
115. Annes JP, Munger JS, Rifkin DB. Making sense of latent TGFbeta activation. *J Cell Sci*. 2003;116(Pt 2):217-24.
116. Trevillian P, Paul H, Millar E, Hibberd A, Agrez MV. $\alpha\beta 6$ integrin expression in diseased and transplanted kidneys. *Kidney International*. 2004;66(4):1423-33.
117. Yu Q, Stamenkovic I. Cell surface-localized matrix metalloproteinase-9 proteolytically activates TGF-beta and promotes tumor invasion and angiogenesis. *Genes Dev*. 2000;14(2):163-76.
118. Nakao A, Imamura T, Souchelnytskyi S, Kawabata M, Ishisaki A, Oeda E, et al. TGF-beta receptor-mediated signalling through Smad2, Smad3 and Smad4. *The EMBO journal*. 1997;16(17):5353-62.
119. Roberts AB. TGF-beta signaling from receptors to the nucleus. *Microbes and infection*. 1999;1(15):1265-73.
120. Carvajal G, Rodriguez-Vita J, Rodrigues-Dez R, Sanchez-Lpez E, Ruprez M, Cartier C, et al. Angiotensin II activates the Smad pathway during epithelial mesenchymal transdifferentiation. *Kidney international*. 2008;74(5):585-95.
121. Massagué J. How cells read TGF-beta signals. *Nature reviews Molecular cell biology*. 2000;1(3):169-78.
122. Davis BN, Hilyard AC, Lagna G, Hata A. SMAD proteins control DROSHA-mediated microRNA maturation. *Nature*. 2008;454(7200):56-61.
123. Davis BN, Hilyard AC, Nguyen PH, Lagna G, Hata A. Smad proteins bind a conserved RNA sequence to promote microRNA maturation by Drosha. *Mol Cell*. 2010;39(3):373-84.
124. Akhurst R, Hata A. Targeting the TGF β signalling pathway in disease. *Nature reviews Drug discovery*. 2012;11(10):790-811.
125. Lee M, Pardoux Cc, Hall M, Lee P, Warburton D, Qing J, et al. TGF-beta activates Erk MAP kinase signalling through direct phosphorylation of ShcA. *EMBO journal*. 2007;26(17):3957-67.
126. Zhang M, Fraser D, Phillips A. ERK, p38, and Smad signaling pathways differentially regulate transforming growth factor-beta1 autoinduction in proximal tubular epithelial cells. *The American journal of pathology*. 2006;169(4):1282-93.
127. Nakerakanti S, Trojanowska M. The Role of TGF- β Receptors in Fibrosis. *Open Rheumatology Journal*. 2012;6:156-62.
128. Zhang YE. Non-Smad Signaling Pathways of the TGF-beta Family. *Cold Spring Harbor perspectives in biology*. 2017;9(2).

129. von Gersdorff G, Susztak K, Rezvani F, Bitzer M, Liang D, Bottinger EP. Smad3 and Smad4 mediate transcriptional activation of the human Smad7 promoter by transforming growth factor beta. *The Journal of biological chemistry*. 2000;275(15):11320-6.
130. Nakao A, Afrakhte M, Morén A, Nakayama T, Christian JL, Heuchel R, et al. Identification of Smad7, a TGFbeta-inducible antagonist of TGF-beta signalling. *Nature*. 1997;389(6651):631-5.
131. Ebisawa T, Fukuchi M, Murakami G, Chiba T, Tanaka K, Imamura T, et al. Smurf1 Interacts with Transforming Growth Factor- β Type I Receptor through Smad7 and Induces Receptor Degradation. *Journal of Biological Chemistry*. 2001;276(16):12477-80.
132. Kretzschmar M, Doody J, Timokhina I, Massague J. A mechanism of repression of TGFbeta/Smad signaling by oncogenic Ras. *Genes Dev*. 1999;13(7):804-16.
133. Yang J, Zhang X, Li Y, Liu Y. Downregulation of Smad transcriptional corepressors SnoN and Ski in the fibrotic kidney: an amplification mechanism for TGF-beta1 signaling. *Journal of the American Society of Nephrology : JASN*. 2003;14(12):3167-77.
134. Deheuninck J, Luo K. Ski and SnoN, potent negative regulators of TGF- β signaling. *Cell Research*. 2008;19:47.
135. Li JH, Huang XR, Zhu H-J, Oldfield M, Cooper M, Truong LD, et al. Advanced glycation end products activate Smad signaling via TGF- β -dependent and -independent mechanisms: implications for diabetic renal and vascular disease. *The FASEB Journal*. 2003.
136. Hellmich B, Schellner M, Schatz H, Pfeiffer A. Activation of transforming growth factor-beta1 in diabetic kidney disease. *Metabolism: clinical and experimental*. 2000;49(3):353-9.
137. McGowan TA, Dunn SR, Falkner B, Sharma K. Stimulation of urinary TGF-beta and isoprostanes in response to hyperglycemia in humans. *Clinical journal of the American Society of Nephrology : CJASN*. 2006;1(2):263-8.
138. Suthanthiran M, Gerber L, Schwartz J, Sharma V, Medeiros M, Marion R, et al. Circulating transforming growth factor-beta1 levels and the risk for kidney disease in African Americans. *Kidney international*. 2009;76(1):72-80.
139. Hathaway CK, Gasim AM, Grant R, Chang AS, Kim HS, Madden VJ, et al. Low TGFbeta1 expression prevents and high expression exacerbates diabetic nephropathy in mice. *Proc Natl Acad Sci U S A*. 2015;112(18):5815-20.
140. Lopez-Hernandez FJ, Lopez-Novoa JM. Role of TGF-beta in chronic kidney disease: an integration of tubular, glomerular and vascular effects. *Cell Tissue Res*. 2012;347(1):141-54.
141. Dessapt C, Baradez MO, Hayward A, Dei Cas A, Thomas SM, Viberti G, et al. Mechanical forces and TGFbeta1 reduce podocyte adhesion through alpha3beta1 integrin downregulation. *Nephrol Dial Transplant*. 2009;24(9):2645-55.

142. Schiffer M, Bitzer M, Roberts IS, Kopp JB, ten Dijke P, Mundel P, et al. Apoptosis in podocytes induced by TGF-beta and Smad7. *J Clin Invest.* 2001;108(6):807-16.
143. Haberstroh U, Zahner G, Disser M, Thaiss F, Wolf G, Stahl RA. TGF-beta stimulates rat mesangial cell proliferation in culture: role of PDGF beta-receptor expression. *The American journal of physiology.* 1993;264(2 Pt 2):F199-205.
144. Grande JP, Warner GM, Walker HJ, Yusufi AN, Cheng J, Gray CE, et al. TGF-beta1 is an autocrine mediator of renal tubular epithelial cell growth and collagen IV production. *Experimental biology and medicine (Maywood, NJ).* 2002;227(3):171-81.
145. Dai C, Yang J, Liu Y. Transforming growth factor-beta1 potentiates renal tubular epithelial cell death by a mechanism independent of Smad signaling. *The Journal of biological chemistry.* 2003;278(14):12537-45.
146. Ding Y, Kim S, Lee SY, Koo JK, Wang Z, Choi ME. Autophagy regulates TGF-beta expression and suppresses kidney fibrosis induced by unilateral ureteral obstruction. *Journal of the American Society of Nephrology : JASN.* 2014;25(12):2835-46.
147. Xavier S, Vasko R, Matsumoto K, Zullo JA, Chen R, Maizel J, et al. Curtailing endothelial TGF-beta signaling is sufficient to reduce endothelial-mesenchymal transition and fibrosis in CKD. *Journal of the American Society of Nephrology : JASN.* 2015;26(4):817-29.
148. Iglesias-de la Cruz MC, Ziyadeh FN, Isono M, Kouahou M, Han DC, Kalluri R, et al. Effects of high glucose and TGF-beta1 on the expression of collagen IV and vascular endothelial growth factor in mouse podocytes. *Kidney Int.* 2002;62(3):901-13.
149. Inoki K, Haneda M, Maeda S, Koya D, Kikkawa R. TGF-beta 1 stimulates glucose uptake by enhancing GLUT1 expression in mesangial cells. *Kidney Int.* 1999;55(5):1704-12.
150. Tamaki K, Okuda S, Ando T, Iwamoto T, Nakayama M, Fujishima M. TGF-beta 1 in glomerulosclerosis and interstitial fibrosis of adriamycin nephropathy. *Kidney Int.* 1994;45(2):525-36.
151. Verrecchia F, Vindevoghel L, Lechleider RJ, Uitto J, Roberts AB, Mauviel A. Smad3/AP-1 interactions control transcriptional responses to TGF-beta in a promoter-specific manner. *Oncogene.* 2001;20(26):3332-40.
152. Chen SJ, Yuan W, Mori Y, Levenson A, Trojanowska M, Varga J. Stimulation of type I collagen transcription in human skin fibroblasts by TGF-beta: involvement of Smad 3. *The journal of investigative dermatology.* 1999;112(1):49-57.
153. Meng X-M, Chung ACK, Lan H. Role of the TGF- β /BMP-7/Smad pathways in renal diseases. *Clinical science.* 2013;124(4):243-54.
154. Verrecchia F, Chu ML, Mauviel A. Identification of novel TGF-beta /Smad gene targets in dermal fibroblasts using a combined cDNA microarray/promoter transactivation approach. *Journal of biological chemistry.* 2001;276(20):17058-62.

155. Eddy A, López-Guisa J, Okamura D, Yamaguchi I. Investigating mechanisms of chronic kidney disease in mouse models. *Pediatric nephrology*. 2011.
156. Tsuchida K, Cronin B, Sharma K. Novel aspects of transforming growth factor-Beta in diabetic kidney disease. *Nephron*. 2002;92(1):7-21.
157. Dennler S, Itoh S, Vivien D, ten Dijke P, Huet S, Gauthier JM. Direct binding of Smad3 and Smad4 to critical TGF beta-inducible elements in the promoter of human plasminogen activator inhibitor-type 1 gene. *The EMBO journal*. 1998;17(11):3091-100.
158. Chen SJ, Yuan W, Lo S, Trojanowska M, Varga J. Interaction of smad3 with a proximal smad-binding element of the human alpha2(I) procollagen gene promoter required for transcriptional activation by TGF-beta. *J Cell Physiol*. 2000;183(3):381-92.
159. Verrecchia F, Mauviel A. Transforming growth factor-beta signaling through the Smad pathway: role in extracellular matrix gene expression and regulation. *Journal of investigative dermatology*. 2002;118(2):211-5.
160. Kantharidis P, Wang B, Carew RM, Lan HY. Diabetes Complications: The MicroRNA Perspective. *Diabetes*. 2011;60(7):1832-7.
161. McClelland AD, Kantharidis P. microRNA in the development of diabetic complications. *Clinical science (London, England : 1979)*. 2014;126(2):95-110.
162. Zhong X, Chung AC, Chen HY, Meng XM, Lan HY. Smad3-mediated upregulation of miR-21 promotes renal fibrosis. *Journal of the American Society of Nephrology : JASN*. 2011;22(9):1668-81.
163. Pan X, Chen Z, Huang R, Yao Y, Ma G. Transforming growth factor β 1 induces the expression of collagen type I by DNA methylation in cardiac fibroblasts. *PLoS ONE*. 2013;8(4):e60335-e.
164. Baricos WH, Cortez SL, Deboisblanc M, Xin S. Transforming growth factor-beta is a potent inhibitor of extracellular matrix degradation by cultured human mesangial cells. *Journal of the American Society of Nephrology : JASN*. 1999;10(4):790-5.
165. Edwards DR, Murphy G, Reynolds JJ, Whitham SE, Docherty AJ, Angel P, et al. Transforming growth factor beta modulates the expression of collagenase and metalloproteinase inhibitor. *The EMBO journal*. 1987;6(7):1899-904.
166. Yuan W, Varga J. Transforming growth factor-beta repression of matrix metalloproteinase-1 in dermal fibroblasts involves Smad3. *The Journal of biological chemistry*. 2001;276(42):38502-10.
167. Laiho M, Saksela O, Andreassen PA, Keski-Oja J. Enhanced production and extracellular deposition of the endothelial-type plasminogen activator inhibitor in cultured human lung fibroblasts by transforming growth factor-beta. *The Journal of cell biology*. 1986;103(6 Pt 1):2403-10.

168. Overall CM, Wrana JL, Sodek J. Independent regulation of collagenase, 72-kDa progelatinase, and metalloendoproteinase inhibitor expression in human fibroblasts by transforming growth factor-beta. *The Journal of biological chemistry*. 1989;264(3):1860-9.
169. Di Donato A, Ghiggeri GM, Di Duca M, Jivotenko E, Acinni R, Campolo J, et al. Lysyl oxidase expression and collagen cross-linking during chronic adriamycin nephropathy. *Nephron*. 1997;76(2):192-200.
170. Quaggin S, Kapus A. Scar wars: mapping the fate of epithelial-mesenchymal-myofibroblast transition. *Kidney international*. 2011;80(1):41-50.
171. Fan JM, Ng YY, Hill PA, Nikolic-Paterson DJ, Mu W, Atkins RC, et al. Transforming growth factor-beta regulates tubular epithelial-myofibroblast transdifferentiation in vitro. *Kidney Int*. 1999;56(4):1455-67.
172. Hu B, Wu Z, Phan SH. Smad3 mediates transforming growth factor-beta-induced alpha-smooth muscle actin expression. *Am J Respir Cell Mol Biol*. 2003;29(3 Pt 1):397-404.
173. Gentle ME, Shi S, Daehn I, Zhang T, Qi H, Yu L, et al. Epithelial cell TGFbeta signaling induces acute tubular injury and interstitial inflammation. *Journal of the American Society of Nephrology : JASN*. 2013;24(5):787-99.
174. Qi W, Chen X, Polhill TS, Sumual S, Twigg S, Gilbert RE, et al. TGF-beta1 induces IL-8 and MCP-1 through a connective tissue growth factor-independent pathway. *Am J Physiol Renal Physiol*. 2006;290(3):F703-9.
175. Rodriguez-Barbero A, Obreo J, Eleno N, Rodriguez-Pena A, Duwel A, Jerkic M, et al. Endoglin expression in human and rat mesangial cells and its upregulation by TGF-beta1. *Biochemical and biophysical research communications*. 2001;282(1):142-7.
176. Diez-Marques L, Ortega-Velazquez R, Langa C, Rodriguez-Barbero A, Lopez-Novoa JM, Lamas S, et al. Expression of endoglin in human mesangial cells: modulation of extracellular matrix synthesis. *Biochim Biophys Acta*. 2002;1587(1):36-44.
177. Yeh YC, Wei WC, Wang YK, Lin SC, Sung JM, Tang MJ. Transforming growth factor- β 1 induces Smad3-dependent β 1 integrin gene expression in epithelial-to-mesenchymal transition during chronic tubulointerstitial fibrosis. *Am J Pathol*. 2010;177(4):1743-54.
178. Cox T, Erler J. Remodeling and homeostasis of the extracellular matrix: implications for fibrotic diseases and cancer. *Disease models & mechanisms*. 2011;4(2):165-78.
179. Hewitson T. Fibrosis in the kidney: is a problem shared a problem halved? *Fibrogenesis & tissue repair*. 2012;5 Suppl 1:S14-S.
180. Lan H. Diverse roles of TGF- β /Smads in renal fibrosis and inflammation. *International journal of biological sciences*. 2011;7(7):1056-67.

181. Sharma K, Jin Y, Guo J, Ziyadeh FN. Neutralization of TGF- β by anti-TGF- β antibody attenuates kidney hypertrophy and the enhanced extracellular matrix gene expression in STZ-induced diabetic mice. *Diabetes*. 1996;45(4):522-30.
182. Ziyadeh FN, Hoffman BB, Han DC, Iglesias-De La Cruz MC, Hong SW, Isono M, et al. Long-term prevention of renal insufficiency, excess matrix gene expression, and glomerular mesangial matrix expansion by treatment with monoclonal antitransforming growth factor-beta antibody in db/db diabetic mice. *Proc Natl Acad Sci U S A*. 2000;97(14):8015-20.
183. Liang X, Schnaper HW, Matsusaka T, Pastan I, Ledbetter S, Hayashida T. Anti-TGF-beta Antibody, 1D11, Ameliorates Glomerular Fibrosis in Mouse Models after the Onset of Proteinuria. *PLoS One*. 2016;11(5):e0155534.
184. Miyajima A, Chen J, Lawrence C, Ledbetter S, Soslow RA, Stern J, et al. Antibody to transforming growth factor-beta ameliorates tubular apoptosis in unilateral ureteral obstruction. *Kidney Int*. 2000;58(6):2301-13.
185. El Chaar M, Chen J, Seshan S, Jha S, Richardson I, Ledbetter S, et al. Effect of combination therapy with enalapril and the TGF-beta antagonist 1D11 in unilateral ureteral obstruction. *American journal of physiology Renal, fluid and electrolyte physiology*. 2007;292(4):F1291-F301.
186. Trachtman H, Fervenza FC, Gipson DS, Heering P, Jayne DR, Peters H, et al. A phase 1, single-dose study of fresolimumab, an anti-TGF-beta antibody, in treatment-resistant primary focal segmental glomerulosclerosis. *Kidney Int*. 2011;79(11):1236-43.
187. Takakura K, Mizukami K, Mitori H, Noto T, Tomura Y. Antiproteinuric effect of pirfenidone in a rat model of anti-glomerular basement membrane glomerulonephritis. *Eur J Pharmacol*. 2014;737:106-16.
188. RamachandraRao SP, Zhu Y, Ravasi T, McGowan TA, Toh I, Dunn SR, et al. Pirfenidone is renoprotective in diabetic kidney disease. *Journal of the American Society of Nephrology : JASN*. 2009;20(8):1765-75.
189. Li Z, Liu X, Wang B, Nie Y, Wen J, Wang Q, et al. Pirfenidone suppresses MAPK signalling pathway to reverse epithelial-mesenchymal transition and renal fibrosis. *Nephrology (Carlton, Vic)*. 2017;22(8):589-97.
190. Cho ME, Smith DC, Branton MH, Penzak SR, Kopp JB. Pirfenidone slows renal function decline in patients with focal segmental glomerulosclerosis. *Clinical journal of the American Society of Nephrology : CJASN*. 2007;2(5):906-13.
191. Sharma K, Ix JH, Mathew AV, Cho M, Pflueger A, Dunn SR, et al. Pirfenidone for diabetic nephropathy. *Journal of the American Society of Nephrology : JASN*. 2011;22(6):1144-51.

192. Dunker N, Krieglstein K. Targeted mutations of transforming growth factor-beta genes reveal important roles in mouse development and adult homeostasis. *European journal of biochemistry*. 2000;267(24):6982-8.
193. Larsson J, Goumans MJ, Sjostrand LJ, van Rooijen MA, Ward D, Leveen P, et al. Abnormal angiogenesis but intact hematopoietic potential in TGF-beta type I receptor-deficient mice. *The EMBO journal*. 2001;20(7):1663-73.
194. Oshima M, Oshima H, Taketo MM. TGF-beta receptor type II deficiency results in defects of yolk sac hematopoiesis and vasculogenesis. *Dev Biol*. 1996;179(1):297-302.
195. Yaswen L, Kulkarni AB, Fredrickson T, Mittleman B, Schiffman R, Payne S, et al. Autoimmune manifestations in the transforming growth factor-beta 1 knockout mouse. *Blood*. 1996;87(4):1439-45.
196. Leveen P, Larsson J, Ehinger M, Cilio CM, Sundler M, Sjostrand LJ, et al. Induced disruption of the transforming growth factor beta type II receptor gene in mice causes a lethal inflammatory disorder that is transplantable. *Blood*. 2002;100(2):560-8.
197. Yoshimura A, Wakabayashi Y, Mori T. Cellular and molecular basis for the regulation of inflammation by TGF- β . *The Journal of Biochemistry*. 2010;147(6):781-92.
198. Feinberg MW, Watanabe M, Lebedeva MA, Depina AS, Hanai J, Mammoto T, et al. Transforming growth factor-beta1 inhibition of vascular smooth muscle cell activation is mediated via Smad3. *The Journal of biological chemistry*. 2004;279(16):16388-93.
199. Werner F, Jain MK, Feinberg MW, Sibinga NE, Pellacani A, Wiesel P, et al. Transforming growth factor-beta 1 inhibition of macrophage activation is mediated via Smad3. *The Journal of biological chemistry*. 2000;275(47):36653-8.
200. Wang W, Huang XR, Li AG, Liu F, Li JH, Truong LD, et al. Signaling mechanism of TGF-beta1 in prevention of renal inflammation: role of Smad7. *Journal of the American Society of Nephrology : JASN*. 2005;16(5):1371-83.
201. Meng XM, Huang XR, Xiao J, Chung AC, Qin W, Chen HY, et al. Disruption of Smad4 impairs TGF-beta/Smad3 and Smad7 transcriptional regulation during renal inflammation and fibrosis in vivo and in vitro. *Kidney Int*. 2012;81(3):266-79.
202. Chen X, Rateri DL, Howatt DA, Balakrishnan A, Moorleggen JJ, Cassis LA, et al. TGF-beta Neutralization Enhances AngII-Induced Aortic Rupture and Aneurysm in Both Thoracic and Abdominal Regions. *PLoS One*. 2016;11(4):e0153811.
203. Denton CP, Merkel PA, Furst DE, Khanna D, Emery P, Hsu VM, et al. Recombinant human anti-transforming growth factor beta1 antibody therapy in systemic sclerosis: a multicenter, randomized, placebo-controlled phase I/II trial of CAT-192. *Arthritis and rheumatism*. 2007;56(1):323-33.

204. Voelker J, Berg PH, Sheetz M, Duffin K, Shen T, Moser B, et al. Anti-TGF- β 1 Antibody Therapy in Patients with Diabetic Nephropathy. *Journal of the American Society of Nephrology*. 2016.
205. Langham RG, Kelly DJ, Gow RM, Zhang Y, Cordonnier DJ, Pinel N, et al. Transforming growth factor-beta in human diabetic nephropathy: effects of ACE inhibition. *Diabetes care*. 2006;29(12):2670-5.
206. Thallas-Bonke V, Coughlan MT, Bach LA, Cooper ME, Forbes JM. Preservation of kidney function with combined inhibition of NADPH oxidase and angiotensin-converting enzyme in diabetic nephropathy. *Am J Nephrol*. 2010;32(1):73-82.
207. Border WA, Noble NA. Interactions of Transforming Growth Factor- β and Angiotensin II in Renal Fibrosis. *Hypertension*. 1998;31(1):181-8.
208. Sharma K, Eltayeb BO, McGowan TA, Dunn SR, Alzahabi B, Rohde R, et al. Captopril-induced reduction of serum levels of transforming growth factor-beta1 correlates with long-term renoprotection in insulin-dependent diabetic patients. *American journal of kidney diseases : the official journal of the National Kidney Foundation*. 1999;34(5):818-23.
209. Esmatjes E, Flores L, Inigo P, Lario S, Ruilope LM, Campistol JM. Effect of losartan on TGF-beta1 and urinary albumin excretion in patients with type 2 diabetes mellitus and microalbuminuria. *Nephrol Dial Transplant*. 2001;16 Suppl 1:90-3.
210. Piek E, Ju WJ, Heyer J, Escalante Alcalde D, Stewart CL, Weinstein M, et al. Functional characterization of transforming growth factor beta signaling in Smad2- and Smad3-deficient fibroblasts. *Journal of biological chemistry*. 2001;276(23):19945-53.
211. Meng XM, Huang XR, Chung ACK, Qin W, Shao X, Igarashi P, et al. Smad2 Protects against TGF- β /Smad3-Mediated Renal Fibrosis. *Journal of the American Society of Nephrology : JASN*. 2010;21(9):1477-87.
212. Inazaki K, Kanamaru Y, Kojima Y, Sueyoshi N, Okumura K, Kaneko K, et al. Smad3 deficiency attenuates renal fibrosis, inflammation, and apoptosis after unilateral ureteral obstruction. *Kidney Int*. 2004;66(2):597-604.
213. Datto MB, Frederick JP, Pan L, Borton AJ, Zhuang Y, Wang XF. Targeted disruption of Smad3 reveals an essential role in transforming growth factor beta-mediated signal transduction. *Molecular and cellular biology*. 1999;19(4):2495-504.
214. Yang X, Letterio JJ, Lechleider RJ, Chen L, Hayman R, Gu H, et al. Targeted disruption of SMAD3 results in impaired mucosal immunity and diminished T cell responsiveness to TGF-beta. *The EMBO journal*. 1999;18(5):1280-91.
215. Ashcroft GS, Yang X, Glick AB, Weinstein M, Letterio JL, Mizel DE, et al. Mice lacking Smad3 show accelerated wound healing and an impaired local inflammatory response. *Nature Cell Biology*. 1999;1(5):260-6.

216. Sato M, Muragaki Y, Saika S, Roberts A, Ooshima A. Targeted disruption of TGF-beta1/Smad3 signaling protects against renal tubulointerstitial fibrosis induced by unilateral ureteral obstruction. *The Journal of clinical investigation*. 2003;112(10):1486-94.
217. Wang A, Ziyadeh FN, Lee EY, Pyagay PE, Sung SH, Sheardown SA, et al. Interference with TGF-beta signaling by Smad3-knockout in mice limits diabetic glomerulosclerosis without affecting albuminuria. *Am J Physiol Renal Physiol*. 2007;293(5):F1657-65.
218. Nath KA, Croatt AJ, Warner GM, Grande JP. Genetic deficiency of Smad3 protects against murine ischemic acute kidney injury. *Am J Physiol Renal Physiol*. 2011;301(2):F436-42.
219. Benigni A, Zoja C, Campana M, Corna D, Sangalli F, Rottoli D, et al. Beneficial effect of TGFbeta antagonism in treating diabetic nephropathy depends on when treatment is started. *Nephron Exp Nephrol*. 2006;104(4):e158-68.
220. Chen S, Iglesias-de la Cruz MC, Jim B, Hong SW, Isono M, Ziyadeh FN. Reversibility of established diabetic glomerulopathy by anti-TGF-beta antibodies in db/db mice. *Biochemical and biophysical research communications*. 2003;300(1):16-22.
221. Wu CF, Chiang WC, Lai CF, Chang FC, Chen YT, Chou YH, et al. Transforming growth factor beta-1 stimulates profibrotic epithelial signaling to activate pericyte-myofibroblast transition in obstructive kidney fibrosis. *Am J Pathol*. 2013;182(1):118-31.
222. Spurgeon KR, Donohoe DL, Basile DP. Transforming growth factor- β in acute renal failure: receptor expression, effects on proliferation, cellularity, and vascularization after recovery from injury. *American Journal of Physiology - Renal Physiology*. 2005;288(3):F568-F77.
223. Huen SC, Moeckel GW, Cantley LG. Macrophage-specific deletion of transforming growth factor-beta1 does not prevent renal fibrosis after severe ischemia-reperfusion or obstructive injury. *Am J Physiol Renal Physiol*. 2013;305(4):F477-84.
224. Guan Q, Nguan CY, Du C. Expression of transforming growth factor-beta1 limits renal ischemia-reperfusion injury. *Transplantation*. 2010;89(11):1320-7.
225. Isaka Y, Tsujie M, Ando Y, Nakamura H, Kaneda Y, Imai E, et al. Transforming growth factor-beta 1 antisense oligodeoxynucleotides block interstitial fibrosis in unilateral ureteral obstruction. *Kidney Int*. 2000;58(5):1885-92.
226. Petersen M, Thorikay M, Deckers M, van Dinther M, Grygielko ET, Gellibert F, et al. Oral administration of GW788388, an inhibitor of TGF-beta type I and II receptor kinases, decreases renal fibrosis. *Kidney international*. 2008;73(6):705-15.
227. Moon JA, Kim HT, Cho IS, Sheen YY, Kim DK. IN-1130, a novel transforming growth factor-beta type I receptor kinase (ALK5) inhibitor, suppresses renal fibrosis in obstructive nephropathy. *Kidney Int*. 2006;70(7):1234-43.
228. Galarreta CI, Thornhill BA, Forbes MS, Simpkins LN, Kim DK, Chevalier RL. Transforming growth factor-beta1 receptor inhibition preserves glomerulotubular integrity during ureteral

- obstruction in adults but worsens injury in neonatal mice. *Am J Physiol Renal Physiol*. 2013;304(5):F481-90.
229. Gewin L, Vadivelu S, Neelisetty S, Srichai MB, Paueksakon P, Pozzi A, et al. Deleting the TGF-beta receptor attenuates acute proximal tubule injury. *Journal of the American Society of Nephrology : JASN*. 2012;23(12):2001-11.
230. Meng XM, Huang XR, Xiao J, Chen HY, Zhong X, Chung AC, et al. Diverse roles of TGF-beta receptor II in renal fibrosis and inflammation in vivo and in vitro. *J Pathol*. 2012;227(2):175-88.
231. Neelisetty S, Alford C, Reynolds K, Woodbury L, Nlandu-Khodo S, Yang H, et al. Renal fibrosis is not reduced by blocking transforming growth factor-beta signaling in matrix-producing interstitial cells. *Kidney Int*. 2015;88(3):503-14.
232. Zhou L, Fu P, Huang XR, Liu F, Chung AC, Lai KN, et al. Mechanism of chronic aristolochic acid nephropathy: role of Smad3. *Am J Physiol Renal Physiol*. 2010;298(4):F1006-17.
233. Fujimoto M, Maezawa Y, Yokote K, Joh K, Kobayashi K, Kawamura H, et al. Mice lacking Smad3 are protected against streptozotocin-induced diabetic glomerulopathy. *Biochemical and biophysical research communications*. 2003;305(4):1002-7.
234. Li J, Qu X, Yao J, Caruana G, Ricardo SD, Yamamoto Y, et al. Blockade of endothelial-mesenchymal transition by a Smad3 inhibitor delays the early development of streptozotocin-induced diabetic nephropathy. *Diabetes*. 2010;59(10):2612-24.
235. Ai J, Nie J, He J, Guo Q, Li M, Lei Y, et al. GQ5 Hinders Renal Fibrosis in Obstructive Nephropathy by Selectively Inhibiting TGF-beta-Induced Smad3 Phosphorylation. *Journal of the American Society of Nephrology : JASN*. 2015;26(8):1827-38.
236. Chung AC, Huang XR, Zhou L, Heuchel R, Lai KN, Lan HY. Disruption of the Smad7 gene promotes renal fibrosis and inflammation in unilateral ureteral obstruction (UUO) in mice. *Nephrol Dial Transplant*. 2009;24(5):1443-54.
237. Dai XY, Zhou L, Huang XR, Fu P, Lan HY. Smad7 protects against chronic aristolochic acid nephropathy in mice. *Oncotarget*. 2015;6(14):11930-44.
238. Kölling M, Kaucsar T, Schauerte C, Hübner A, Dettling A, Park J-K, et al. Therapeutic miR-21 Silencing Ameliorates Diabetic Kidney Disease in Mice. *Molecular Therapy*. 2017;25(1):165-80.
239. Zhong X, Chung AC, Chen HY, Dong Y, Meng XM, Li R, et al. miR-21 is a key therapeutic target for renal injury in a mouse model of type 2 diabetes. *Diabetologia*. 2013;56(3):663-74.
240. Chau BN, Xin C, Hartner J, Ren S, Castano AP, Linn G, et al. MicroRNA-21 Promotes Fibrosis of the Kidney by Silencing Metabolic Pathways. *Science Translational Medicine*. 2012;4(121):121ra18-ra18.

241. Denby L, Ramdas V, Lu R, Conway BR, Grant JS, Dickinson B, et al. MicroRNA-214 antagonism protects against renal fibrosis. *Journal of the American Society of Nephrology : JASN*. 2014;25(1):65-80.
242. Rodríguez Peña A, Grande M, Eleno NI, Are'valo M, Guerrero C, Santos E, et al. Activation of Erk1/2 and Akt following unilateral ureteral obstruction. *Kidney international*. 2008;74(2):196-209.
243. Jang HS, Han SJ, Kim JI, Lee S, Lipschutz JH, Park KM. Activation of ERK accelerates repair of renal tubular epithelial cells, whereas it inhibits progression of fibrosis following ischemia/reperfusion injury. *Biochim Biophys Acta*. 2013;1832(12):1998-2008.
244. Koya D, Haneda M, Nakagawa H, Isshiki K, Sato H, Maeda S, et al. Amelioration of accelerated diabetic mesangial expansion by treatment with a PKC beta inhibitor in diabetic db/db mice, a rodent model for type 2 diabetes. *FASEB journal : official publication of the Federation of American Societies for Experimental Biology*. 2000;14(3):439-47.
245. Huang X, Chung ACK, Wang X, Lai K, Lan H. Mice overexpressing latent TGF-beta1 are protected against renal fibrosis in obstructive kidney disease. *American journal of physiology Renal, fluid and electrolyte physiology*. 2008;295(1):F118-F27.
246. Huang XR, Chung AC, Zhou L, Wang XJ, Lan HY. Latent TGF-beta1 protects against crescentic glomerulonephritis. *Journal of the American Society of Nephrology : JASN*. 2008;19(2):233-42.
247. Chung AC, Dong Y, Yang W, Zhong X, Li R, Lan HY. Smad7 suppresses renal fibrosis via altering expression of TGF-beta/Smad3-regulated microRNAs. *Molecular therapy : the journal of the American Society of Gene Therapy*. 2013;21(2):388-98.
248. Chai Z, Sarcevic B, Mawson A, Toh BH. SET-related cell division autoantigen-1 (CDA1) arrests cell growth. *Journal of biological chemistry*. 2001;276(36):33665-74.
249. Delbridge ML, Longepied G, Depetris D, Mattei MG, Disteche CM, Marshall Graves JA, et al. TSPY, the candidate gonadoblastoma gene on the human Y chromosome, has a widely expressed homologue on the X - implications for Y chromosome evolution. *Chromosome Research*. 2004;12(4):345-56.
250. Ozbun LL, You L, Kiang S, Angdisen J, Martinez A, Jakowlew SB. Identification of differentially expressed nucleolar TGF-beta1 target (DENTT) in human lung cancer cells that is a new member of the TSPY/SET/NAP-1 superfamily. *Genomics*. 2001;73(2):179-93.
251. Wang G-S, Hong C-J, Yen T-Y, Huang H-Y, Ou Y, Huang T-N, et al. Transcriptional modification by a CASK-interacting nucleosome assembly protein. *Neuron*. 2004;42(1):113-28.

252. Martínez A, Ozbun L, Angdisen J, Jakowlew S. Expression of differentially expressed nucleolar transforming growth factor-beta1 target (DENTT) in adult mouse tissues. *Developmental dynamics*. 2002;224(2):186-99.
253. Ozbun LL, Martinez A, Angdisen J, Umphress S, Kang Y, Wang M, et al. Differentially expressed nucleolar TGF-beta1 target (DENTT) in mouse development. *Dev Dyn*. 2003;226(3):491-511.
254. Ozbun LL, Martínez A, Jakowlew SB. Differentially expressed nucleolar TGF-β1 target (DENTT) shows tissue-specific nuclear and cytoplasmic localization and increases TGF-β1-responsive transcription in primates. *Biochimica et Biophysica Acta - Gene Structure and Expression*. 2005;1728(3):163-80.
255. Tu Y, Wu T, Dai A, Pham Y, Chew P, de Haan J, et al. Cell division autoantigen 1 enhances signaling and the profibrotic effects of transforming growth factor-β in diabetic nephropathy. *Kidney international*. 2011;79(2):199-209.
256. Chai Z, Dai A, Tu Y, Li J, Wu T, Wang Y, et al. Genetic deletion of cell division autoantigen 1 retards diabetes-associated renal injury. *Journal of the American Society of Nephrology*. 2013;24(11):1782-92.
257. Chung W-C, Huang T-N, Hsueh Y-P. Targeted deletion of CASK-interacting nucleosome assembly protein causes higher locomotor and exploratory activities. *NeuroSignals*. 2011;19(3):128-41.
258. Park Y-J, Luger K. Structure and function of nucleosome assembly proteins. *Biochemistry and cell biology*. 2006;84(4):549-58.
259. Tsang KH, Lai SK, Li Q, Yung WH, Liu H, Mak PH, et al. The nucleosome assembly protein TSPYL2 regulates the expression of NMDA receptor subunits GluN2A and GluN2B. *Scientific reports*. 2014;4:3654.
260. Li Y, Zhang DJ, Qiu Y, Kido T, Lau YC. The Y-located proto-oncogene TSPY exacerbates and its X-homologue TSPX inhibits transactivation functions of androgen receptor and its constitutively active variants. *Human molecular genetics*. 2017;26(5):901-12.
261. Kandalaft L, Zudaire E, Portal-Núñez S, Cuttitta F, Jakowlew S. Differentially expressed nucleolar transforming growth factor-beta1 target (DENTT) exhibits an inhibitory role on tumorigenesis. *Carcinogenesis*. 2008;29(6):1282-9.
262. Pham Y, Tu Y, Wu T, Allen TJ, Calkin AC, Watson AM, et al. Cell division autoantigen 1 plays a profibrotic role by modulating downstream signalling of TGF-beta in a murine diabetic model of atherosclerosis. *Diabetologia*. 2010;53(1):170-9.
263. Epping MT, Lunardi A, Nachmani D, Castillo-Martin M, Thin TH, Cordon-Cardo C, et al. TSPYL2 is an essential component of the REST/NRSF transcriptional complex for TGFbeta signaling activation. *Cell death and differentiation*. 2015.

264. Tao K, Fong S, Lu Z, Ching Y, Chan K, Chan S. TSPYL2 is important for G1 checkpoint maintenance upon DNA damage. *PLoS ONE*. 2011;6(6):e21602-e.
265. Polyakova O, Borman S, Grimley R, Vamathevan J, Hayes B, Solari R. Identification of novel interacting partners of Sirtuin6. *PLoS ONE*. 2012;7(12):e51555-e.
266. Li Y, Lau YFC. TSPY and its X-encoded homologue interact with cyclin B but exert contrasting functions on cyclin-dependent kinase 1 activities. *Oncogene*. 2008;27(47):6141-50.
267. Kido T, Ou JH, Lau YF. The X-linked tumor suppressor TSPX interacts and promotes degradation of the hepatitis B viral protein HBx via the proteasome pathway. *PLoS One*. 2011;6(7):e22979.
268. Sun G, Yuen Chan S, Yuan Y, Wang Chan K, Qiu G, Sun K, et al. Isolation of differentially expressed genes in human heart tissues. *Biochimica et Biophysica Acta (BBA) - Molecular Basis of Disease*. 2002;1588(3):241-6.
269. Kido T, Lo RCI, Li Y, Lee J, Tabatabai ZL, Ng IOI, et al. The potential contributions of a Y-located protooncogene and its X homologue in sexual dimorphisms in hepatocellular carcinoma. *Human Pathology*. 2014.
270. Li J, Huynh P, Dai A, Wu T, Tu Y, Chow B, et al. Diabetes Reduces Severity of Aortic Aneurysms Depending on the Presence of Cell Division Autoantigen 1 (CDA1). *Diabetes*. 2018;67(4):755-68.
271. Eyler CE, Wu Q, Yan K, MacSwords JM, Chandler-Militello D, Misuraca KL, et al. Glioma stem cell proliferation and tumor growth are promoted by nitric oxide synthase-2. *Cell*. 2011;146(1):53-66.
272. Tu Y, Wu W, Wu T, Cao Z, Wilkins R, Toh B-H, et al. Antiproliferative autoantigen CDA1 transcriptionally up-regulates p21(Waf1/Cip1) by activating p53 and MEK/ERK1/2 MAPK pathways. *Journal of biological chemistry*. 2007;282(16):11722-31.
273. Lassila M, Seah K, Allen T, Thallas V, Thomas M, Candido R, et al. Accelerated nephropathy in diabetic apolipoprotein e-knockout mouse: role of advanced glycation end products. *Journal of the American Society of Nephrology*. 2004;15(8):2125-38.
274. Sievers F, Wilm A, Dineen D, Gibson TJ, Karplus K, Li W, et al. Fast, scalable generation of high-quality protein multiple sequence alignments using Clustal Omega. *Molecular systems biology*. 2011;7:539.
275. Waterhouse AM, Procter JB, Martin DM, Clamp M, Barton GJ. Jalview Version 2--a multiple sequence alignment editor and analysis workbench. *Bioinformatics (Oxford, England)*. 2009;25(9):1189-91.
276. Tesch GH, Allen TJ. Rodent models of streptozotocin-induced diabetic nephropathy (methods in renal research). *Nephrology*. 2007;12(3):261-6.

277. Watson AM, Li J, Schumacher C, de Gasparo M, Feng B, Thomas MC, et al. The endothelin receptor antagonist avosentan ameliorates nephropathy and atherosclerosis in diabetic apolipoprotein E knockout mice. *Diabetologia*. 2010;53(1):192-203.
278. Tikellis C, Koh P, Burns W, Kantharidis P. Quantitative gene expression analysis in kidney tissues. *Methods in molecular biology (Clifton, NJ)*. 2009;466:83-107.
279. Kantharidis P, Hagiwara S, Brennan E, McClelland AD. Study of microRNA in diabetic nephropathy: isolation, quantification and biological function. *Nephrology (Carlton, Vic)*. 2015;20(3):132-9.
280. Schmittgen TD, Livak KJ. Analyzing real-time PCR data by the comparative C(T) method. *Nature protocols*. 2008;3(6):1101-8.
281. Gorres KL, Raines RT. Prolyl 4-hydroxylase. *Critical reviews in biochemistry and molecular biology*. 2010;45(2):106-24.
282. Samuel C. Determination of collagen content, concentration, and sub-types in kidney tissue. *Methods in molecular biology*. 2009;466:223-35.
283. Chai O-H, Song C-H, Park S-K, Kim W, Cho E-S. Molecular regulation of kidney development. *Anatomy & cell biology*. 2013;46(1):19-31.
284. Hayashi S, McMahon AP. Efficient recombination in diverse tissues by a tamoxifen-inducible form of Cre: A tool for temporally regulated gene activation/inactivation in the mouse. *Developmental Biology*. 2002;244(2):305-18.
285. Yokoi H, Kasahara M, Mukoyama M, Mori K, Kuwahara K, Fujikura J, et al. Podocyte-specific expression of tamoxifen-inducible Cre recombinase in mice. *Nephrology, Dialysis, Transplantation*. 2010;25(7):2120-4.
286. Olorunniji FJ, Rosser SJ, Stark WM. Site-specific recombinases: molecular machines for the Genetic Revolution. *The Biochemical journal*. 2016;473(6):673-84.
287. Feil S, Valtcheva N, Feil R. Inducible Cre mice. *Methods in molecular biology (Clifton, NJ)*. 2009;530:343-63.
288. Ma F, Tesch G, Ozols E, Xie M, Schneider M, Nikolic Paterson D. TGF- β 1-activated kinase-1 regulates inflammation and fibrosis in the obstructed kidney. *American journal of physiology Renal physiology*. 2011;300(6):F1410-F21.
289. Pitzonka L, Wang X, Ullas S, Wolff DW, Wang Y, Goodrich DW. The THO ribonucleoprotein complex is required for stem cell homeostasis in the adult mouse small intestine. *Molecular and cellular biology*. 2013;33(17):3505-14.
290. Zhong ZA, Sun W, Chen H, Zhang H, Lay YA, Lane NE, et al. Optimizing tamoxifen-inducible Cre/loxP system to reduce tamoxifen effect on bone turnover in long bones of young mice. *Bone*. 2015;81:614-9.

291. Jelinsky SA, Harris HA, Brown EL, Flanagan K, Zhang X, Tunkey C, et al. Global Transcription Profiling of Estrogen Activity: Estrogen Receptor α Regulates Gene Expression in the Kidney. *Endocrinology*. 2003;144(2):701-10.
292. Falke LL, Broekhuizen R, Huitema A, Maarseveen E, Nguyen TQ, Goldschmeding R. Tamoxifen for induction of Cre-recombination may confound fibrosis studies in female mice. *J Cell Commun Signal*. 2017;11(2):205-11.
293. Dellê H, Rocha JRC, Cavaglieri RC, Vieira JM, Malheiros DMAC, Noronha IL. Antifibrotic Effect of Tamoxifen in a Model of Progressive Renal Disease. *Journal of the American Society of Nephrology*. 2012;23(1):37-48.
294. Cohen AM, Rosenmann E. Effect of the Estrogen Antagonist, Tamoxifen, on Development of Glomerulosclerosis in the Cohen Diabetic Rat. *Diabetes*. 1985;34(7):634-8.
295. Mao S, Xu H, Zou L, Xu G, Wu Z, Ding Q, et al. Estrogen preserves split renal function in a chronic complete unilateral ureteral obstruction animal model. *Experimental and therapeutic medicine*. 2014;7(6):1555-62.
296. Kim D, Lee AS, Jung YJ, Yang KH, Lee S, Park SK, et al. Tamoxifen ameliorates renal tubulointerstitial fibrosis by modulation of estrogen receptor alpha-mediated transforming growth factor-beta1/Smad signaling pathway. *Nephrol Dial Transplant*. 2014;29(11):2043-53.
297. Babelova A, Avaniadi D, Jung O, Fork C, Beckmann J, Kosowski J, et al. Role of Nox4 in murine models of kidney disease. *Free radical biology & medicine*. 2012;53(4):842-53.
298. Ma X, Ding J, Min H, Wen Y, Gao Q. Protective role of low-dose TGF-beta1 in early diabetic nephropathy induced by streptozotocin. *International immunopharmacology*. 2013;17(3):752-8.
299. Qi Z, Fujita H, Jin J, Davis LS, Wang Y, Fogo AB, et al. Characterization of susceptibility of inbred mouse strains to diabetic nephropathy. *Diabetes*. 2005;54(9):2628-37.
300. Kitada M, Ogura Y, Koya D. Rodent models of diabetic nephropathy: their utility and limitations. *International journal of nephrology and renovascular disease*. 2016;9:279-90.
301. Kher A, Meldrum KK, Wang M, Tsai BM, Pitcher JM, Meldrum DR. Cellular and molecular mechanisms of sex differences in renal ischemia-reperfusion injury. *Cardiovasc Res*. 2005;67(4):594-603.
302. Ucero A, Benito Martin A, Izquierdo M, Sanchez Niño M, Sanz A, Ramos A, et al. Unilateral ureteral obstruction: beyond obstruction. *International Urology and Nephrology*. 2013.
303. Wei Q, Dong Z. Mouse model of ischemic acute kidney injury: technical notes and tricks. *Am J Physiol Renal Physiol*. 2012;303(11):F1487-94.
304. Chevalier R, Forbes M, Thornhill B. Ureteral obstruction as a model of renal interstitial fibrosis and obstructive nephropathy. *Kidney international*. 2009;75(11):1145-52.

305. Zager RA, Johnson AC, Becker K. Acute unilateral ischemic renal injury induces progressive renal inflammation, lipid accumulation, histone modification, and "end-stage" kidney disease. *Am J Physiol Renal Physiol*. 2011;301(6):F1334-45.
306. El Sabbahy M, Vaidya V. Ischemic kidney injury and mechanisms of tissue repair. Wiley interdisciplinary reviews Systems biology and medicine. 2010.
307. Little MH, Kairath P. Does Renal Repair Recapitulate Kidney Development? *Journal of the American Society of Nephrology*. 2016.
308. Le Clef N, Verhulst A, D'Haese PC, Vervaeet BA. Unilateral Renal Ischemia-Reperfusion as a Robust Model for Acute to Chronic Kidney Injury in Mice. *PLoS One*. 2016;11(3):e0152153.
309. Wang Y, Jia L, Hu Z, Entman ML, Mitch WE, Wang Y. AMP-activated protein kinase/myocardin-related transcription factor-A signaling regulates fibroblast activation and renal fibrosis. *Kidney Int*. 2017.
310. Hewitson T, Mookerjee I, Masterson R, Zhao C, Tregear G, Becker G, et al. Endogenous relaxin is a naturally occurring modulator of experimental renal tubulointerstitial fibrosis. *Endocrinology*. 2007;148(2):660-9.
311. Mookerjee I, Hewitson T, Halls M, Summers R, Mathai M, Bathgate RAD, et al. Relaxin inhibits renal myofibroblast differentiation via RXFP1, the nitric oxide pathway, and Smad2. *The FASEB journal*. 2009;23(4):1219-29.
312. Ko GJ, Grigoryev DN, Linfert D, Jang HR, Watkins T, Cheadle C, et al. Transcriptional analysis of kidneys during repair from AKI reveals possible roles for NGAL and KIM-1 as biomarkers of AKI-to-CKD transition. *Am J Physiol Renal Physiol*. 2010;298(6):F1472-83.
313. Danobeitia JS, Ziemelis M, Ma X, Zitur LJ, Zens T, Chlebeck PJ, et al. Complement inhibition attenuates acute kidney injury after ischemia-reperfusion and limits progression to renal fibrosis in mice. *PLoS One*. 2017;12(8):e0183701.
314. Jain S, Bicknell GR, Nicholson ML. Molecular changes in extracellular matrix turnover after renal ischaemia-reperfusion injury. *The British journal of surgery*. 2000;87(9):1188-92.
315. Cook-Mills JM, Marchese ME, Abdala-Valencia H. Vascular Cell Adhesion Molecule-1 Expression and Signaling During Disease: Regulation by Reactive Oxygen Species and Antioxidants. *Antioxidants & Redox Signaling*. 2011;15(6):1607-38.
316. Gahmberg CG, Tolvanen M, Kotovuori P. Leukocyte adhesion--structure and function of human leukocyte beta2-integrins and their cellular ligands. *European journal of biochemistry*. 1997;245(2):215-32.
317. Kelly KJ, Williams WW, Jr., Colvin RB, Meehan SM, Springer TA, Gutierrez-Ramos JC, et al. Intercellular adhesion molecule-1-deficient mice are protected against ischemic renal injury. *J Clin Invest*. 1996;97(4):1056-63.

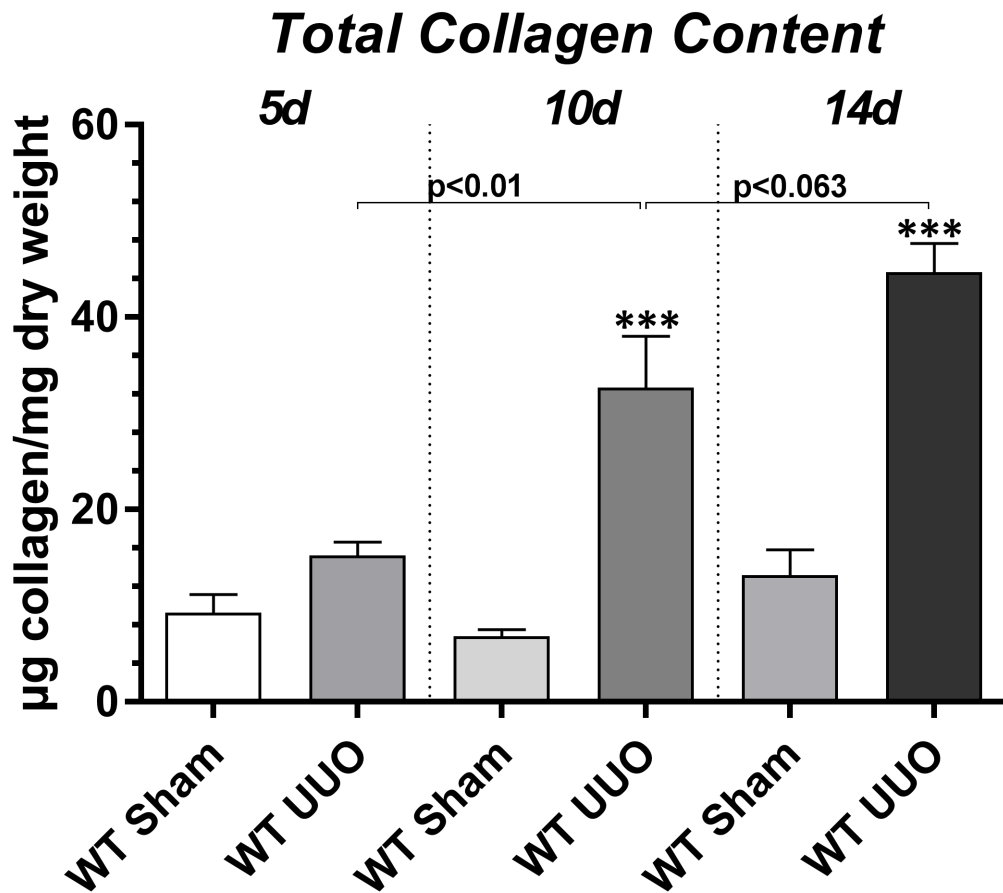
318. Kelly KJ, Williams WW, Jr., Colvin RB, Bonventre JV. Antibody to intercellular adhesion molecule 1 protects the kidney against ischemic injury. *Proc Natl Acad Sci U S A*. 1994;91(2):812-6.
319. Rabb H, Mendiola CC, Saba SR, Dietz JR, Smith CW, Bonventre JV, et al. Antibodies to ICAM-1 Protect Kidneys in Severe Ischemic Reperfusion Injury. *Biochemical and biophysical research communications*. 1995;211(1):67-73.
320. Cheng Q-L, Chen X-M, Li F, Lin H-L, Ye Y-Z, Fu B. Effects of ICAM-1 antisense oligonucleotide on the tubulointerstitium in mice with unilateral ureteral obstruction. *Kidney International*. 2000;57(1):183-90.
321. Park JG, Ryu SY, Jung IH, Lee YH, Kang KJ, Lee MR, et al. Evaluation of VCAM-1 antibodies as therapeutic agent for atherosclerosis in apolipoprotein E-deficient mice. *Atherosclerosis*. 2013;226(2):356-63.
322. Ricardo SD, van Goor H, Eddy AA. Macrophage diversity in renal injury and repair. *J Clin Invest*. 2008;118(11):3522-30.
323. Kushiyama T, Oda T, Yamada M, Higashi K, Yamamoto K, Sakurai Y, et al. Alteration in the phenotype of macrophages in the repair of renal interstitial fibrosis in mice. *Nephrology (Carlton, Vic)*. 2011;16(5):522-35.
324. Chatterjee PK, Patel NSA, Kvale EO, Cuzzocrea S, Brown PAJ, Stewart KN, et al. Inhibition of inducible nitric oxide synthase reduces renal ischemia/reperfusion injury. *Kidney International*. 2002;61(3):862-71.
325. Vodovotz Y, Geiser AG, Chesler L, Letterio JJ, Campbell A, Lucia MS, et al. Spontaneously increased production of nitric oxide and aberrant expression of the inducible nitric oxide synthase in vivo in the transforming growth factor beta 1 null mouse. *J Exp Med*. 1996;183(5):2337-42.
326. Sugiyama Y, Kakoi K, Kimura A, Takada I, Kashiwagi I, Wakabayashi Y, et al. Smad2 and Smad3 are redundantly essential for the suppression of iNOS synthesis in macrophages by regulating IRF3 and STAT1 pathways. *International Immunology*. 2012;24(4):253-65.
327. Tan CK, Tan EH, Luo B, Huang CL, Loo JS, Choong C, et al. SMAD3 Deficiency Promotes Inflammatory Aortic Aneurysms in Angiotensin II-Infused Mice Via Activation of iNOS. *Journal of the American Heart Association: Cardiovascular and Cerebrovascular Disease*. 2013;2(3):e000269.
328. Li Y, Cai M, Sun Q, Liu Z, Cardounel AJ, Swartz HM, et al. Hyperoxia and transforming growth factor β 1 signaling in the post-ischemic mouse heart. *Life sciences*. 2013;92(10):547-54.

329. Saura M, Zaragoza C, Herranz B, Griera M, Diez-Marques L, Rodriguez-Puyol D, et al. Nitric oxide regulates transforming growth factor-beta signaling in endothelial cells. *Circ Res*. 2005;97(11):1115-23.
330. Hochberg D, Johnson CW, Chen J, Cohen D, Stern J, Vaughan ED, Jr., et al. Interstitial fibrosis of unilateral ureteral obstruction is exacerbated in kidneys of mice lacking the gene for inducible nitric oxide synthase. *Laboratory investigation; a journal of technical methods and pathology*. 2000;80(11):1721-8.
331. Miyajima A, Chen J, Poppas DP, Vaughan ED, Jr., Felsen D. Role of nitric oxide in renal tubular apoptosis of unilateral ureteral obstruction. *Kidney International*. 2001;59(4):1290-303.
332. Chatterjee PK, Patel NS, Sivarajah A, Kvale EO, Dugo L, Cuzzocrea S, et al. GW274150, a potent and highly selective inhibitor of iNOS, reduces experimental renal ischemia/reperfusion injury. *Kidney Int*. 2003;63(3):853-65.
333. Yang L, Besschetnova T, Brooks C, Shah J, Bonventre J. Epithelial cell cycle arrest in G2/M mediates kidney fibrosis after injury. *Nature medicine*. 2010;16(5):535-43, 1p following 143.
334. Canaud G, Bonventre JV. Cell cycle arrest and the evolution of chronic kidney disease from acute kidney injury. *Nephrol Dial Transplant*. 2015;30(4):575-83.
335. Hesketh EE, Czopek A, Clay M, Borthwick G, Ferenbach D, Kluth D, et al. Renal ischaemia reperfusion injury: a mouse model of injury and regeneration. *Journal of visualized experiments : JoVE*. 2014(88).
336. Adamopoulos C, Mihailidou C, Grivaki C, Papavassiliou KA, Kiaris H, Piperi C, et al. Systemic effects of AGEs in ER stress induction in vivo. *Glycoconjugate journal*. 2016;33(4):537-44.
337. Dou L, Poitevin S, Sallee M, Addi T, Gondouin B, McKay N, et al. Aryl hydrocarbon receptor is activated in patients and mice with chronic kidney disease. *Kidney Int*. 2018.
338. Kakiuchi C, Ishiwata M, Hayashi A, Kato T. XBP1 induces WFS1 through an endoplasmic reticulum stress response element-like motif in SH-SY5Y cells. *Journal of neurochemistry*. 2006;97(2):545-55.
339. Ito T, Tsukumo S, Suzuki N, Motohashi H, Yamamoto M, Fujii-Kuriyama Y, et al. A constitutively active arylhydrocarbon receptor induces growth inhibition of jurkat T cells through changes in the expression of genes related to apoptosis and cell cycle arrest. *The Journal of biological chemistry*. 2004;279(24):25204-10.
340. Hu PP-c, Shen X, Huang D, Liu Y, Counter C, Wang X-F. The MEK Pathway Is Required for Stimulation of p21WAF1/CIP1 by Transforming Growth Factor- β . *Journal of Biological Chemistry*. 1999;274(50):35381-7.

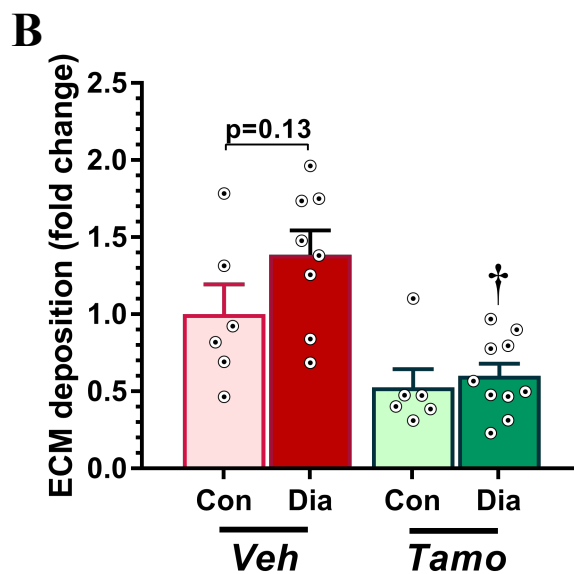
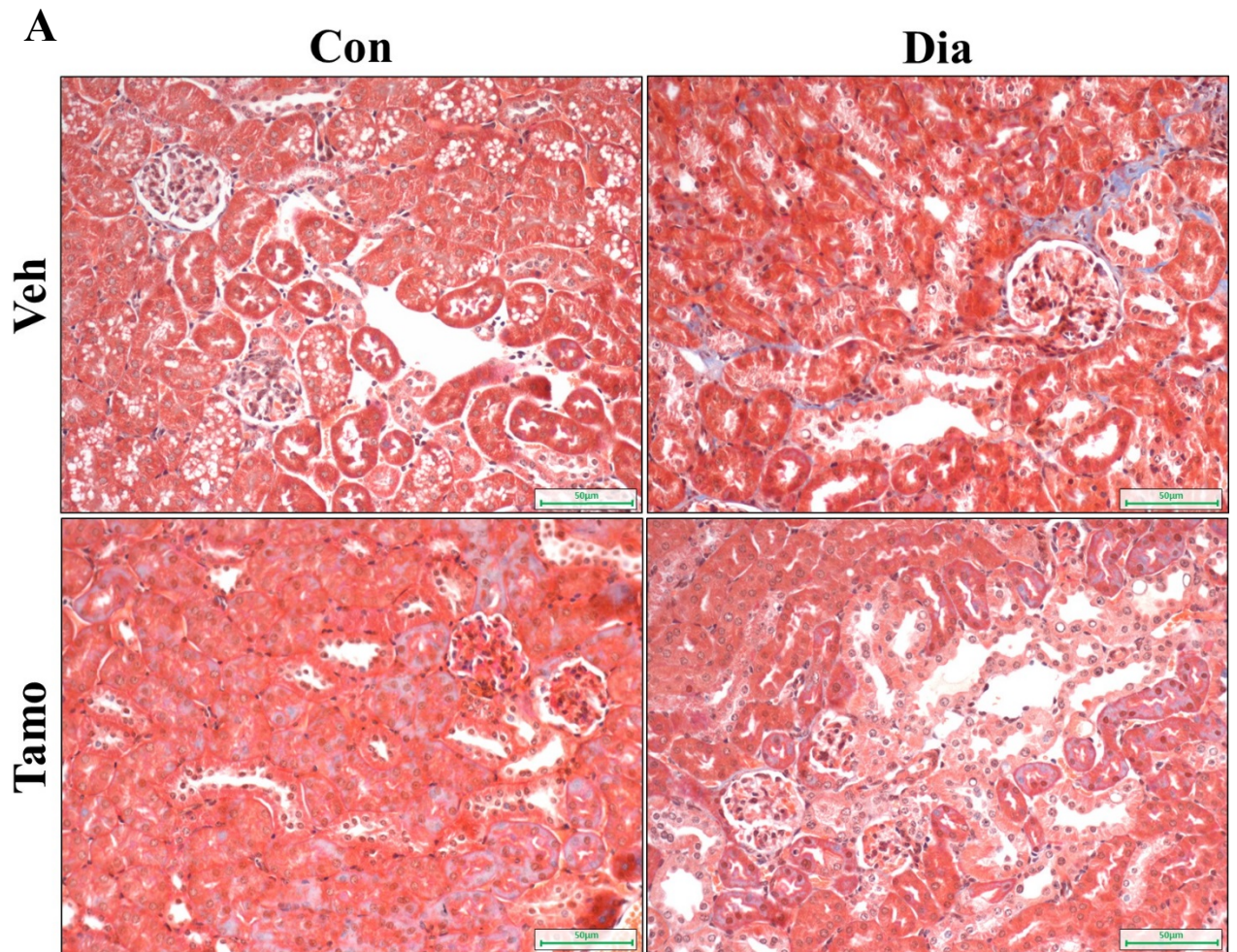
341. Datto MB, Li Y, Panus JF, Howe DJ, Xiong Y, Wang XF. Transforming growth factor β induces the cyclin-dependent kinase inhibitor p21 through a p53-independent mechanism. *Proceedings of the National Academy of Sciences of the United States of America*. 1995;92(12):5545-9.

Appendix

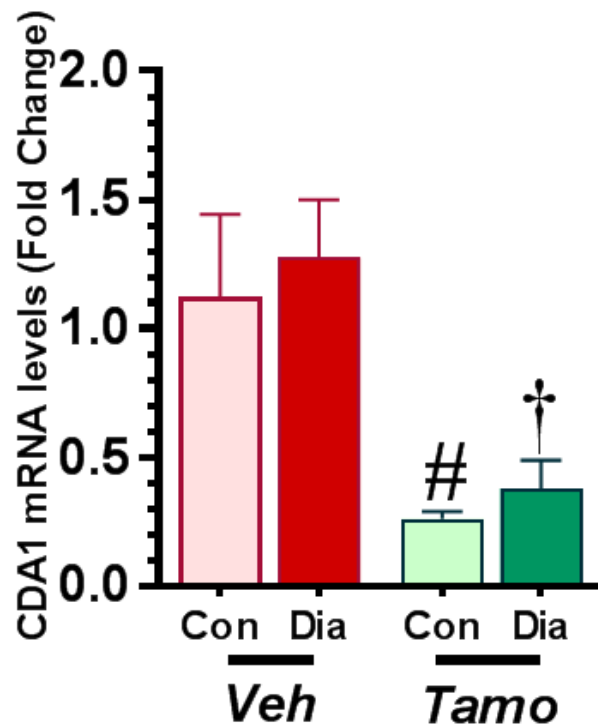
Supplementary Figures



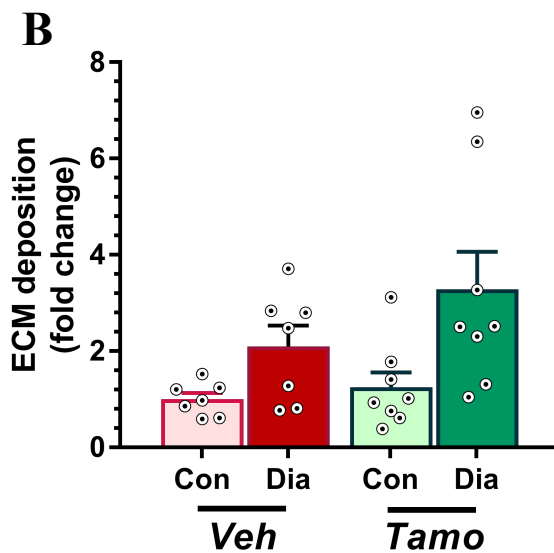
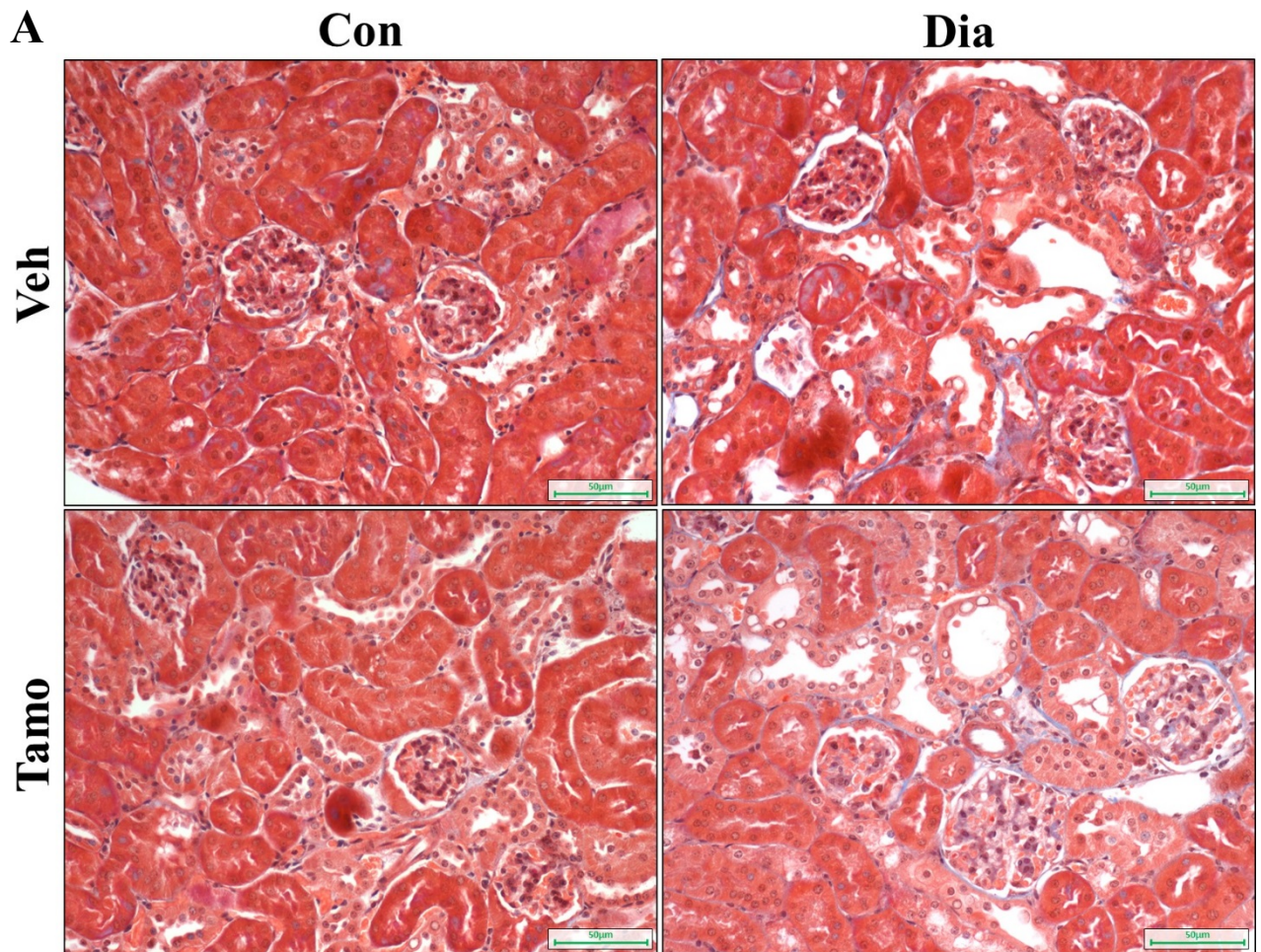
Supplementary Figure 1. Total collagen content progressively increases with time in the UVO model. Obstructed kidneys from CDA1 WT mice were analysed using hydroxyproline content to examine total collagen content in all timepoints examined. Data are shown as mean±SE (n=5 for sham, n=9 for UVO). ***p<0.001 vs corresponding Sham control.



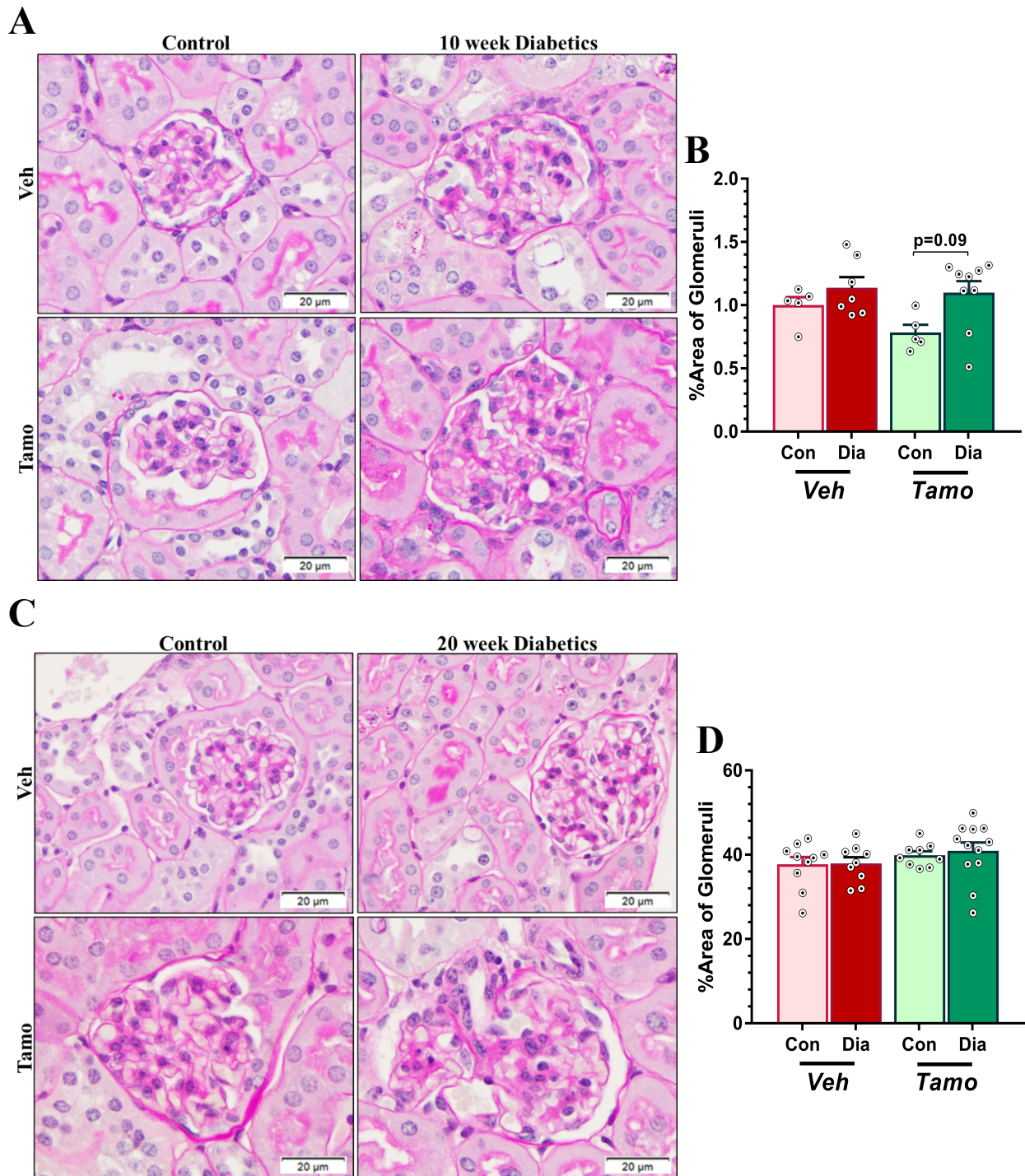
Supplementary Figure 2. Induced genetic deletion of CDA1 attenuates diabetes-associated ECM accumulation in mice. Masson's Trichrome staining for renal ECM accumulation in 10-week non-diabetic (Con) and diabetic (Dia) CDA1^{flox}/ERCre mice treated with Tamo or Veh is shown in blue (A, magnification 200x), and quantification of staining (B). Fold changes are shown as mean±SE (n=6-7 for Con, >7 for Dia). †††p<0.001 vs Veh Dia.



Supplementary Figure 3. Tamoxifen administration induces genetic deletion of CDA1 in aortic tissue of CDA1^{flx}/ERCre mice. Male CDA1^{flx} and CDA1^{flx}/ERCre mice were rendered diabetic (Dia) with STZ injections, (or buffer alone to serve as non-diabetic controls (Con)) at 6-8 weeks of age and were injected with tamoxifen (Tamo) or vehicle to delete the CDA1 gene in CDA1^{flx}/ERCre mice at 10 weeks of diabetes. Aortas were collected at 20 weeks of diabetes. Aortic CDA1 mRNA levels are expressed as mean±SE (n=3-4). #p<0.05 vs Veh Con, †p<0.05 vs Veh Dia.

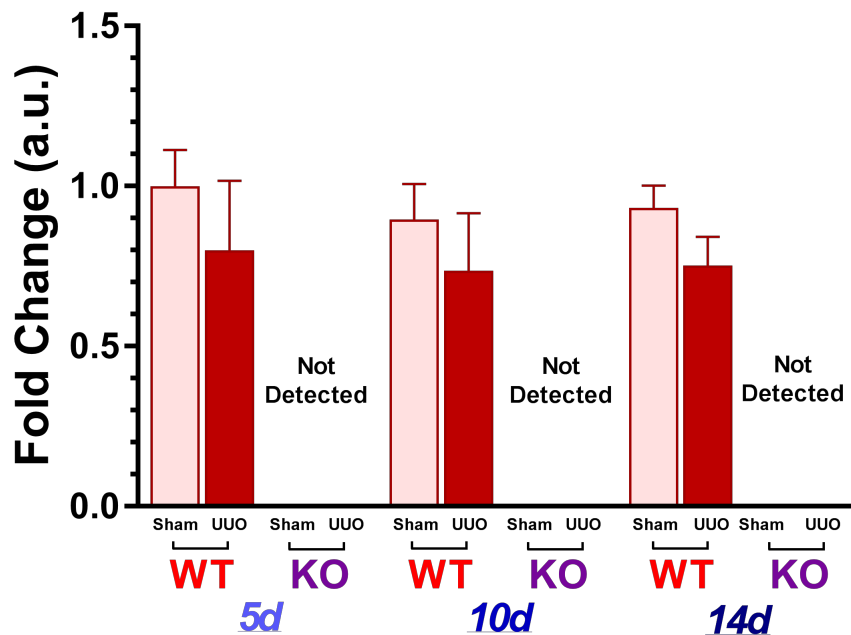


Supplementary Figure 4. Delayed CDA1 genetic knockout does not attenuate diabetes-associated ECM deposition. Masson's Trichrome staining for renal ECM accumulation in 20-week Con and Dia CDA1^{flox}/ERCre mice treated with Tamo or Veh is shown in blue (A, magnification 200x), and quantification of staining (B). Fold changes are shown as mean±SE (n=6-7 for Con, >7 for Dia).

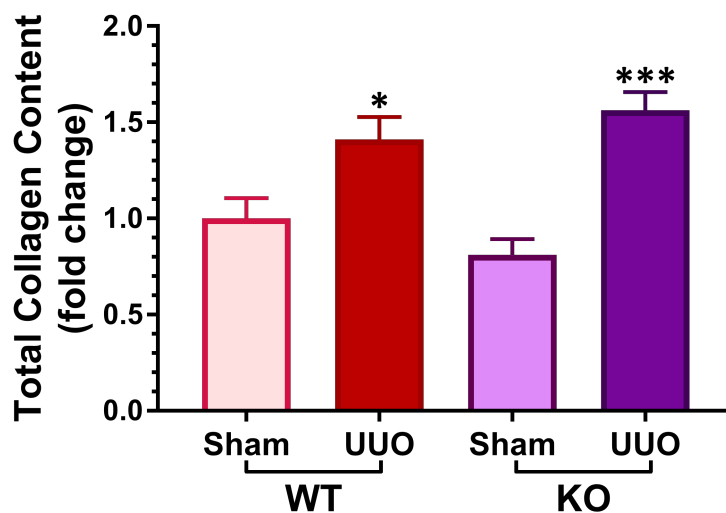


Supplementary Figure 5. Mesangial expansion is not significantly increased in STZ-induced diabetic mice. Representative images of PAS images from the 10 and 20-week CDA1^{flox}/ERCre mice receiving vehicle or treated with tamoxifen (**A** and **C**, respectively. Magnification 200x), and quantification of staining (**B** and **D**, respectively). Fold changes are shown as mean±SE (n=5-7 for Con, >7 for Dia).

CDA1KO



Supplementary Figure 6. Confirmation of genetic deletion of CDA1 in UUO study. Genetic deletion of CDA1 in KO mice was confirmed by genotyping as well as qRT-PCR using primers specific for the region of CDA1 gene which was deleted in KO mice. Data shown as mean±SE (n>5 for sham, n>6 for UUO).



Supplementary Figure 7. UUO-associated collagen content in mice is not affected by CDA1 deficiency. Total collagen content as measured by hydroxyproline assay of renal cortex CDA1 WT and KO mice 14 days post-UUO. *p<0.05, ***p<0.001 vs corresponding Sham control (n>7).

Publications during enrolment

Li, J.,* **Huynh, P.**,* Dai, A.,* Wu, T., Tu, Y., Chow, B., Kiriazis, H., Du, XJ., Bach, LA., Wilkinson-Berka, JL., Biro, E., Walker, P., Nataatmadja, M., West, M., Golledge, J., Allen, TJ., Cooper, ME., and Chai, Z. ***Diabetes Reduces Severity of Aortic Aneurysms Depending on the Presence of Cell Division Autoantigen 1 (CDA1)***. *Diabetes*. 2018;67(4):755-68.

*These authors contributed equally to this work.

In this attached paper, *Cell Division Autoantigen 1 (CDA1)* has been implicated to play a role in increasing diabetes-associated fibrosis in the vasculature via its ability to enhance TGF β signalling activity. Indeed, the actions of CDA1 in diabetes-associated atherosclerosis appears to lead to accumulation of extracellular matrix in the vascular wall, thereby strengthening it. This role of CDA1 in the vasculature in diabetes appears to explain the long-term puzzling clinical observation that diabetic subjects are less likely to develop aortic aneurysms. The findings in this paper are consistent with my hypothesis, as well as my observations from the early intervention study, whereby the absence or inhibition of CDA1 activity results in the attenuation of TGF β -mediated profibrotic processes.



Diabetes Reduces Severity of Aortic Aneurysms Depending on the Presence of Cell Division Autoantigen 1 (CDA1)

Jiaze Li,^{1,2,3} Pacific Huynh,^{1,2,3} Aozhi Dai,^{1,3} Tieqiao Wu,^{1,3} Yugang Tu,³ Bryna Chow,^{1,3} Helen Kiriazis,⁴ Xiao-Jun Du,⁴ Leon A. Bach,^{5,6} Jennifer L. Wilkinson-Berka,¹ Erik Birocs,⁷ Philip Walker,^{8†} Maria Nataatmadja,^{7,8} Malcolm West,^{7,8} Jonathan Golledge,^{7,8,9} Terri J. Allen,^{1,3} Mark E. Cooper,^{1,2,3} and Zhonglin Chai^{1,2,3}

Diabetes 2018;67:755–768 | <https://doi.org/10.2337/db17-0134>

Diabetes is a negative risk factor for aortic aneurysm, but the underlying explanation for this phenomenon is unknown. We have previously demonstrated that cell division autoantigen 1 (CDA1), which enhances transforming growth factor- β signaling, is upregulated in diabetes. We hypothesized that CDA1 plays a key role in conferring the protective effect of diabetes against aortic aneurysms. Male wild-type, CDA1 knockout (KO), apolipoprotein E (ApoE) KO, and CDA1/ApoE double-KO (dKO) mice were rendered diabetic. Whereas aneurysms were not observed in diabetic ApoE KO and wild-type mice, 40% of diabetic dKO mice developed aortic aneurysms. These aneurysms were associated with attenuated aortic transforming growth factor- β signaling, reduced expression of various collagens, and increased aortic macrophage infiltration and matrix metalloproteinase 12 expression. In the well-characterized model of angiotensin II-induced aneurysm formation, concomitant diabetes reduced fatal aortic rupture and attenuated suprarenal aortic expansion, changes not seen in dKO mice.

Furthermore, aortic CDA1 expression was downregulated \sim 70% within biopsies from human abdominal aortic aneurysms. The identification that diabetes is associated with upregulation of vascular CDA1 and that CDA1 deletion in diabetic mice promotes aneurysm formation provides evidence that CDA1 plays a role in diabetes to reduce susceptibility to aneurysm formation.

Aortic aneurysm is a major cause of mortality in older adults (1). Interestingly, although diabetes is associated with an increased incidence of cardiovascular disease, specifically related to atherosclerosis, the incidence of aortic aneurysms has been reported to be reduced in diabetes (2–5). The underlying mechanisms for this puzzling clinical observation are poorly understood (2,6). Diabetic complications are considered to be closely linked to enhanced transforming growth factor- β (TGF- β) signaling (7–11). Aneurysm formation is thought to occur as a result of altered

¹Department of Diabetes, Central Clinical School, Monash University, Melbourne, Australia

²Department of Immunology, Central Clinical School, Monash University, Melbourne, Australia

³Diabetes Division, Baker IDI Heart and Diabetes Institute, Melbourne, Australia

⁴Experimental Cardiology Laboratory, Baker IDI Heart and Diabetes Institute, Melbourne, Australia

⁵Department of Medicine, Central Clinical School, Monash University, Melbourne, Australia

⁶Department of Endocrinology and Diabetes, Alfred Hospital, Melbourne, Australia

⁷Vascular Biology Unit, Queensland Research Centre for Peripheral Vascular Disease, James Cook University, Townsville, Australia

⁸University of Queensland, Brisbane, Australia

⁹Department of Vascular and Endovascular Surgery, Townsville Hospital, Townsville, Australia

Corresponding authors: Zhonglin Chai, zhonglin.chai@monash.edu, and Jonathan Golledge, jonathan.golledge@jcu.edu.au.

Received 31 January 2017 and accepted 1 January 2018.

This article contains Supplementary Data online at <http://diabetes.diabetesjournals.org/lookup/suppl/doi:10.2337/db17-0134/-/DC1>.

J.L., P.H., and A.D. contributed equally to this work.

P.H., A.D., T.W., B.C., T.J.A., M.E.C., and Z.C. are currently affiliated with the Department of Diabetes, Central Clinical School, Monash University, Melbourne, Australia.

†Deceased.

© 2018 by the American Diabetes Association. Readers may use this article as long as the work is properly cited, the use is educational and not for profit, and the work is not altered. More information is available at <http://www.diabetesjournals.org/content/license>.

TGF- β signaling, enhanced inflammation, and activation of matrix metalloproteinases (MMPs), which leads to increased degradation of extracellular matrix (ECM) and weakening of the vessel wall (12,13). Genetic mutations and impaired functions of genes involved in the TGF- β signaling pathway have been demonstrated to play a causal role in aortic aneurysm formation (14–22). We have previously shown that cell division autoantigen 1 (CDA1) is upregulated in diabetes and enhances TGF- β signaling, including in the vasculature (23–25). Based on these findings, we postulated a role for CDA1 in promoting resistance to aneurysm formation in diabetes. In the current study, we have directly examined if CDA1 contributes to the relative protection from aortic aneurysm associated with diabetes using various models of aneurysm formation in the setting of concurrent streptozotocin-induced diabetes in mice with and without deletion of CDA1, a molecule implicated in TGF- β signaling.

RESEARCH DESIGN AND METHODS

Mice With and Without Diabetes

The CDA1 knockout (KO) and the CDA1/apolipoprotein E (ApoE) double-KO (dKO) mouse strains, both on a C57BL/6 background, have been previously described (25). In this study, male wild-type (WT), CDA1 KO, and ApoE KO and dKO mice were rendered diabetic by five consecutive daily injections with streptozotocin (55 mg/kg) or injected with buffer alone to serve as nondiabetic controls. Animals were euthanized 20 weeks later for analysis of aortic tissues and metabolic parameters as previously described (23–25). The animal studies were approved by the Alfred Medical Research and Education Precinct Animal Ethics Committee.

Morphometric Determination of Aortic Size and Histological and Biochemical Analyses

Aortas were dissected and placed in cold 0.9% sodium chloride and photographed. A subset of aortas was either fixed in 10% neutral buffered formalin for histological analysis or snap frozen in liquid nitrogen for later extraction of total RNA. The maximum diameters of the ascending, descending, and abdominal aortas were determined by analysis of the photographed images as previously described (26). Measurements were taken in duplicate in a blinded fashion.

Assessment of Aortic Aneurysm

Aortic aneurysms were assessed by three techniques in different experiments. Firstly, isolated aortas were photographed and morphometrically examined (see above). Secondly, aortas were examined histologically for areas of balloon-like bulges under the microscope at a magnification $\times 10$. Histological features of aneurysm such as medial elastin lamella breaks, adventitial structural damage, and macrophage infiltration were sought (27). Thirdly, aortas were examined in vivo using ultrasound imaging, and the maximum aortic diameters were determined at the suprarenal region (see below).

Analysis of Aortic Elastin Lamella and Collagen Fibril Structure

Paraffin-embedded aortic sections (4- μ m thick) were stained in orcein solution and counterstained by hematoxylin and eosin (H&E) as previously described (28). The degree of elastin lamella fragmentation was graded by an observer blinded to the mouse group using a scoring system (scores 0–4) previously used (29,30). Examples of each grade are illustrated in Supplementary Fig. 1. Elastin lamella thickness of each sample was randomly measured at 10 random locations using Photoshop CS4 software (Adobe Systems). Aortic collagen staining using picosirius red (31) and confocal microscopy examination of the collagen fiber network (32) have been previously described. Picosirius red-stained collagen fiber images were analyzed for fiber anisotropy using the Fibriltool plugin in ImageJ software (National Institutes of Health) as described previously (33).

Immunohistochemical Staining

Paraffin-embedded aortic sections were immunohistochemically stained for various fibrotic and inflammatory proteins, and the staining signals were quantified as previously described (24,25). For phospho-Smad3 staining, the percentage of cells with positively stained nuclei among cells examined were quantified. Antibodies to collagen III (ab7778), phospho-Smad3 (ab52903), and F4/80 (ab16911) were purchased from Abcam (Cambridge, U.K.), and antibody to collagen IV (GWB-5A65E0) was from GenWay Biotech (San Diego, CA). Negative control with no primary antibody and isotype control antibodies (Supplementary Fig. 2) was performed to confirm the specificity of the immunohistochemical staining.

Determination of mRNA Levels in Mouse Aortas

Gene-specific mRNA levels were determined by real-time RT-PCR as previously described (24,25). RT-PCR was carried out on the cDNA templates using TaqMan Fast Universal PCR Master Mix (Applied Biosystems, Foster City, CA) with β -actin gene used as an internal control. The sequences of primers and probes are shown in Supplementary Table 1.

Angiotensin II Infusion in Nondiabetic and Diabetic Mice

To further explore the role of diabetes and CDA1 expression, a well-characterized model of aortic aneurysm formation was studied, involving angiotensin II (AngII) infusion (34). Male mice were rendered diabetic by streptozotocin as described above. Ten weeks later, both nondiabetic and diabetic mice were implanted with an Alzet osmotic minipump (model 1004; Alzet, Cupertino, CA) subcutaneously, which released AngII at a dose of 1 μ g/min/kg for 4 weeks. Animals found dead were autopsied in order to identify any evidence of aortic aneurysm rupture as well as the rupture site. Animals found to be severely sick, which had to be killed according to the animal welfare guidelines, were included as censored in the survival curve comparison analysis. Animals were killed after 4 weeks' AngII infusion, and their aortas were examined for the assessment of aortic aneurysms. Isolated aortas were photographed before being

either fixed in formalin for subsequent histology or frozen for further analysis.

Measurement of Inner Diameter of the Suprarenal Aorta in Live Animals

Ultrasound imaging examination was performed on animals receiving AngII infusion in order to analyze the size of the abdominal aorta (35). Animals were examined on the same day or <2 days before AngII infusion started in order to measure the baseline diameter as well as at weeks 1 and 2 after AngII infusion in order to detect the changes in aortic diameter. High-resolution anterior–posterior images of motion-mode of aortas in isoflurane-anesthetized animals were recorded using the Vevo 2100 Imaging System with a 40-MHz probe (VisualSonics, Toronto, Ontario, Canada). The maximum inner wall to inner wall diameter of the suprarenal region of the aorta during systole was measured using the Vevo 2100 1.6.0 software.

Data Analysis

All of the data collected from the animal studies were analyzed by two-way ANOVA, and pairwise comparisons between experimental groups were performed using the Newman-Keuls test or by Fisher exact test. The D'Agostino-Pearson omnibus normality test was performed to check if the data were normally distributed. Survival curves were analyzed by Kaplan-Meier analysis and log-rank test. Any difference with $P < 0.05$ was defined as statistically significant.

Determination of Aortic CDA1 Gene Expression Levels in Human Abdominal Aortic Aneurysm Samples

In order to explore the role of CDA1 in human aneurysm formation, expression of the CDA1 gene was measured in human abdominal aortic aneurysm (AAA) biopsy samples. Ethics approval for the human sample work was obtained from the Townsville and the Royal Brisbane and Women's Hospitals' committees. Patients provided written informed consent. Abdominal aortic specimens were obtained from 15 patients undergoing open surgery to treat AAA and six organ donors. The maximum infrarenal aortic diameter was assessed in patients with AAA from axial computed tomography angiography images using the viewer function on a Philips workstation (MxView Visualization Workstation Software; Philips Electronics, Amsterdam, the Netherlands) as previously reported (36,37). The definitions of risk factors such as dyslipidemia, hypertension, diabetes, coronary heart disease, and smoking were as previously described (38). Full-thickness aortic wall biopsies were collected in RNAlater solution (Ambion, Waltham, MA) and stored at -80°C until assayed. The QuantiTect SYBR Green one-step RT-PCR Kit (Qiagen, Hilden, Germany) was used according to the manufacturer's instructions with 40 ng total RNA as template. All reactions were independently repeated in duplicate. QT00024353 and QT00095431 QuantiTect Primer Assays (Qiagen) were used to determine CDA1 and β -actin mRNA, respectively. CDA1 mRNA levels were calculated by using the concentration–threshold cycle standard curve method and normalized against the average expression

of β -actin. The Mann–Whitney U test was performed to identify differences in CDA1 mRNA levels between AAA and control biopsies. Statistical significance was defined at the conventional 5% level.

RESULTS

Diabetic dKO Mice Were Prone to Aortic Aneurysm Formation

Metabolic parameters at 20 weeks after streptozotocin injections showed diabetes-associated changes in these mice as expected (Supplementary Table 2). No aneurysms were seen in diabetic WT or ApoE KO mice, but interestingly, aortic aneurysms were identified in 40% (10 out of 25) of diabetic dKO mice. Eight mice had solitary AAAs, and two mice had multiple aneurysms within the descending and abdominal aortas. Examples of these aneurysms are shown in Fig. 1A. Histological examination on five of the aortas with aneurysms demonstrated medial elastin lamellae fragmentation and macrophage infiltration in these aortas. No such bulges or histological features of aneurysm were observed in the diabetic ApoE KO mice ($n = 27$) (Fig. 1B) or in other groups (WT control, $n = 15$; WT diabetic, $n = 16$; CDA1 KO control, $n = 13$; CDA1 KO diabetic, $n = 17$; ApoE KO control, $n = 26$; dKO control, $n = 14$; $P < 0.003$ vs. diabetic dKO, Fisher exact test).

Diabetic dKO Mice Had Increased Aortic Diameters

A moderate increase in aortic diameter determined by the morphometric method was observed in the ascending (1.31 ± 0.02 vs. 1.20 ± 0.02 mm; $P < 0.002$) and descending (1.10 ± 0.12 vs. 0.84 ± 0.03 mm; $P = 0.036$) aortas of the diabetic dKO mice compared with the diabetic ApoE KO mice (Fig. 1C and D). A tendency toward an increase in the aortic diameter in the abdominal region (1.03 ± 0.10 vs. 0.88 ± 0.03 mm; $P = 0.13$) was also observed, although this difference was not statistically significant (Fig. 1E). Furthermore, WT and CDA1 KO mice on the C57BL/6 background, including both nondiabetic and diabetic groups, had no difference in aortic diameter (Supplementary Fig. 3).

Extensive Elastin Lamella Breakages at the Sites of Aortic Aneurysms

Histological examination of orcein- and H&E-stained aortic sections showed extensive breakage of the elastin lamella at the aneurysm site in diabetic dKO mice (Fig. 2). Diabetic ApoE KO mice developed atherosclerotic plaques within the intima (Fig. 2A). The diabetic dKO mice developed plaques invading into the media and adventitia, associated with breakage of elastin lamella at the affected site (Fig. 2A). An approximately twofold increase in the aortic elastin fragmentation in ApoE KO and dKO mice was observed when compared with WT and CDA1 KO mice (Fig. 2B). The diabetic dKO group had an $\sim 30\%$ greater elastin fragmentation compared with the diabetic ApoE KO group (Fig. 2B). The elastin lamella was thicker in diabetic ApoE KO mice. This parameter was significantly attenuated in the diabetic dKO mice (Fig. 2C).

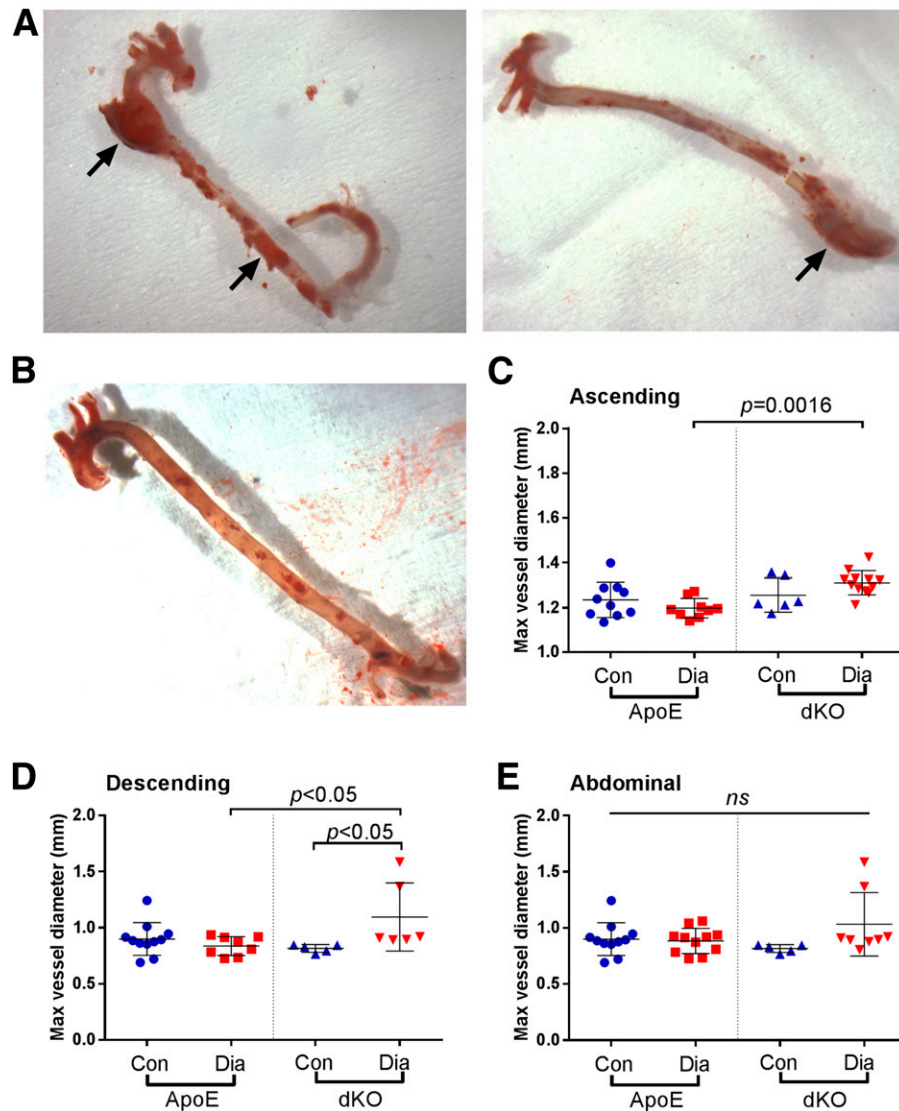


Figure 1—Aneurysms develop in diabetic dKO mice after 20 weeks of diabetes. *A*: Representative aortas from diabetic dKO mice show multiple aneurysms (arrows) at thoracic (left) and abdominal (right) sites. *B*: A representative aorta from a diabetic ApoE KO (ApoE) mouse shows no aneurysms. Aortic sizes (diameter) at ascending (*C*), descending (*D*), and abdominal (*E*) regions from control (Con) and diabetic (Dia) ApoE KO and diabetic dKO groups are shown as univariate scatterplots with mean \pm SD and *P* value between specified groups.

CDA1 Deficiency Attenuated Diabetes-Associated Vascular Expression of ECM Genes Leading to Vascular ECM Remodeling

Aortic mRNA levels for collagens I and III were increased in diabetic ApoE KO mice compared with nondiabetic controls. Both of these parameters were significantly attenuated in the diabetic dKO mice (Fig. 3*A*). Immunohistochemical staining showed that aortic accumulation of collagens III (Fig. 3*B* and *C*) and IV (Fig. 3*D* and *E*) was greater in diabetic ApoE KO compared with nondiabetic mice, albeit the difference in quantification of collagen III staining failed to reach statistical significance. This effect of diabetes was significantly attenuated in the dKO mice. Picrosirius red staining showed that diabetic dKO mice aortas had lost the well-knitted collagen fiber structure within the aortic adventitia around the aneurysms (Fig. 4*A*). Collagen fiber

structure within the medial layer of aortic aneurysms within the diabetic dKO mice was disorganized. This was consistent with the collagen fibril anisotropy finding, as assessed using ImageJ software (National Institutes of Health). A higher level of collagen fibril disarray at the lesion sites in the diabetic dKO mice has been observed, when compared with the diabetic ApoE KO mice (Fig. 4*B*). Confocal stacking images confirmed the disorganized collagen fiber network around the aneurysms in diabetic dKO mice (Fig. 4*C*).

TGF- β /Smad3 Signaling Was Attenuated in the Aortas of Diabetic dKO Mice

Nuclear staining of phospho-Smad3 in aortic sections by immunohistochemistry (Fig. 5*A*) showed a greater positive staining rate in diabetic ApoE KO mice compared with nondiabetic mice (>30 vs. \sim 13%; $P < 0.0001$). This parameter

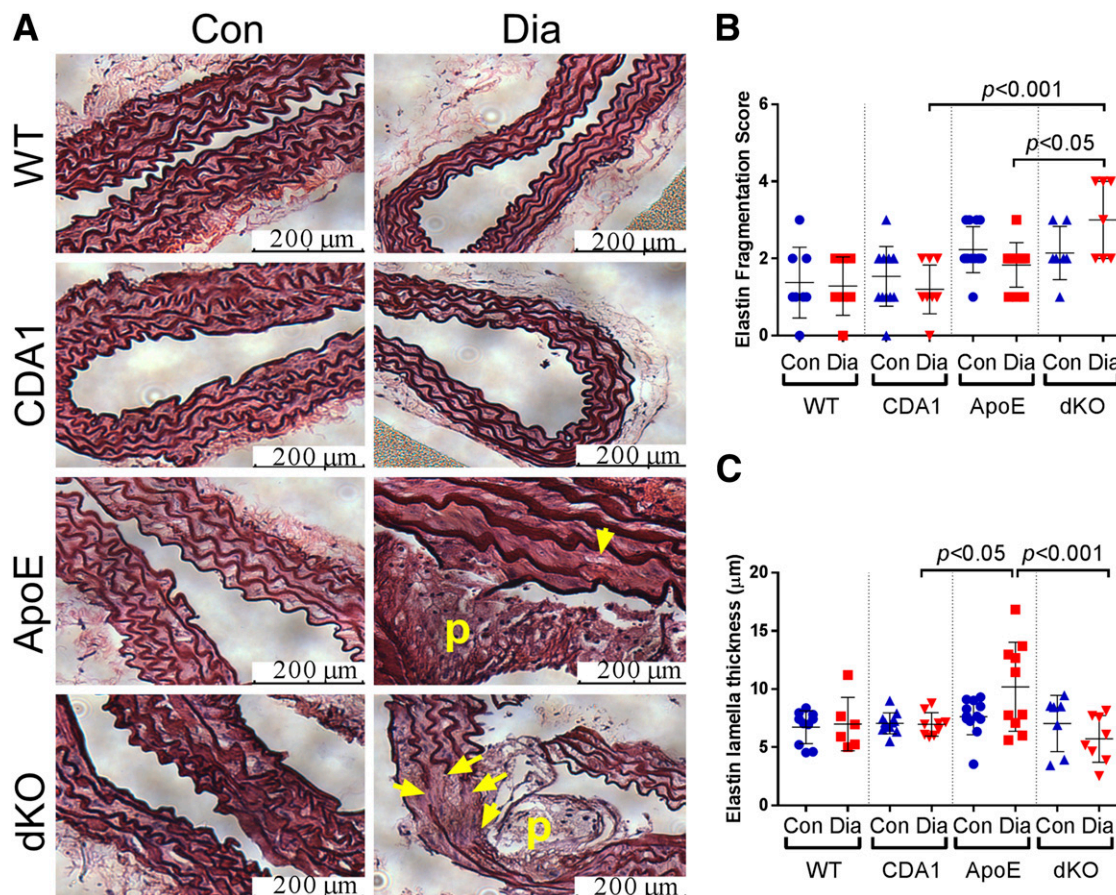


Figure 2—Extensive elastin lamella breaks at the aneurysm site. **A:** Ocein/H&E staining of aorta sections from 20-week diabetic (Dia) and age-matched nondiabetic control (Con) WT, CDA1 KO (CDA1), ApoE KO (ApoE), and CDA1/ApoE dKO (dKO) mice show elastin lamellae. Yellow arrows indicate the elastin lamella breaks. The atherosclerotic plaques are labeled (yellow “p”). Elastin fragmentation scores (**B**) and elastin lamella thickness (**C**) are shown as univariate scatterplots with mean ± SD and *P* value between specified groups.

was attenuated in diabetic dKO mice (~20%; *P* < 0.0001) (Fig. 5B). The effect of CDA1 on aortic phospho-Smad3 levels is further confirmed by Western blotting in 14-week diabetic and nondiabetic WT and CDA1 KO mice (Supplementary Fig. 4).

Diabetes and ApoE Deficiency Are Associated With Increased Aortic Macrophage Infiltration and MMP12 Expression

Mature macrophage marker, F4/80, was stained in aortas from diabetic ApoE KO (Fig. 6A) and dKO (Fig. 6B) mice with a twofold greater staining area observed in diabetic ApoE KO mice compared with controls (Fig. 6C, left panel). There was no statistically significant difference in F4/80 staining area between diabetic dKO and diabetic ApoE KO groups. Macrophages mainly accumulated within the atherosclerotic plaques in the intima of diabetic ApoE KO mice (Fig. 6A), whereas macrophages were abundantly present within the media as well as in the adventitia in the diabetic dKO mice at sites of aneurysms (Fig. 6B). When analyzing the macrophage staining distribution across the sectional layers of the aortic wall containing a plaque, the F4/80 immunohistochemical staining area in the medial-adventitial

layers was approximately fivefold more than that seen in the intima in diabetic dKO mice, whereas there was more staining in the intima in the diabetic ApoE mice (Fig. 6C, right panel). The macrophage is known to be the main source of MMP12 within the vasculature, which is responsible for elastin degradation (39). Minimal MMP12 gene expression was detected in the WT and CDA1 KO groups. ApoE deficiency was associated with a >100-fold increase in aortic MMP12 mRNA levels in ApoE KO and dKO mice (*P* < 0.05) (Fig. 6D). Diabetes further increased the MMP12 mRNA levels in both strains of ApoE-deficient mice. MMP12 mRNA levels within macrophages isolated from the peritoneal cavity of ApoE KO and dKO mice were approximately fourfold higher than those of WT and CDA1 KO mice (Fig. 6E). These findings suggest that the infiltrating macrophages in the aorta of ApoE-deficient mice contributed to the increased activities of MMP12, leading to elastin degradation in the aortic wall.

Protective Effect of Diabetes in AngII-Induced Aneurysm in ApoE KO Mice Is CDA1 Dependent

Male ApoE KO and dKO mice injected with streptozotocin, monitored weekly, demonstrated blood glucose levels

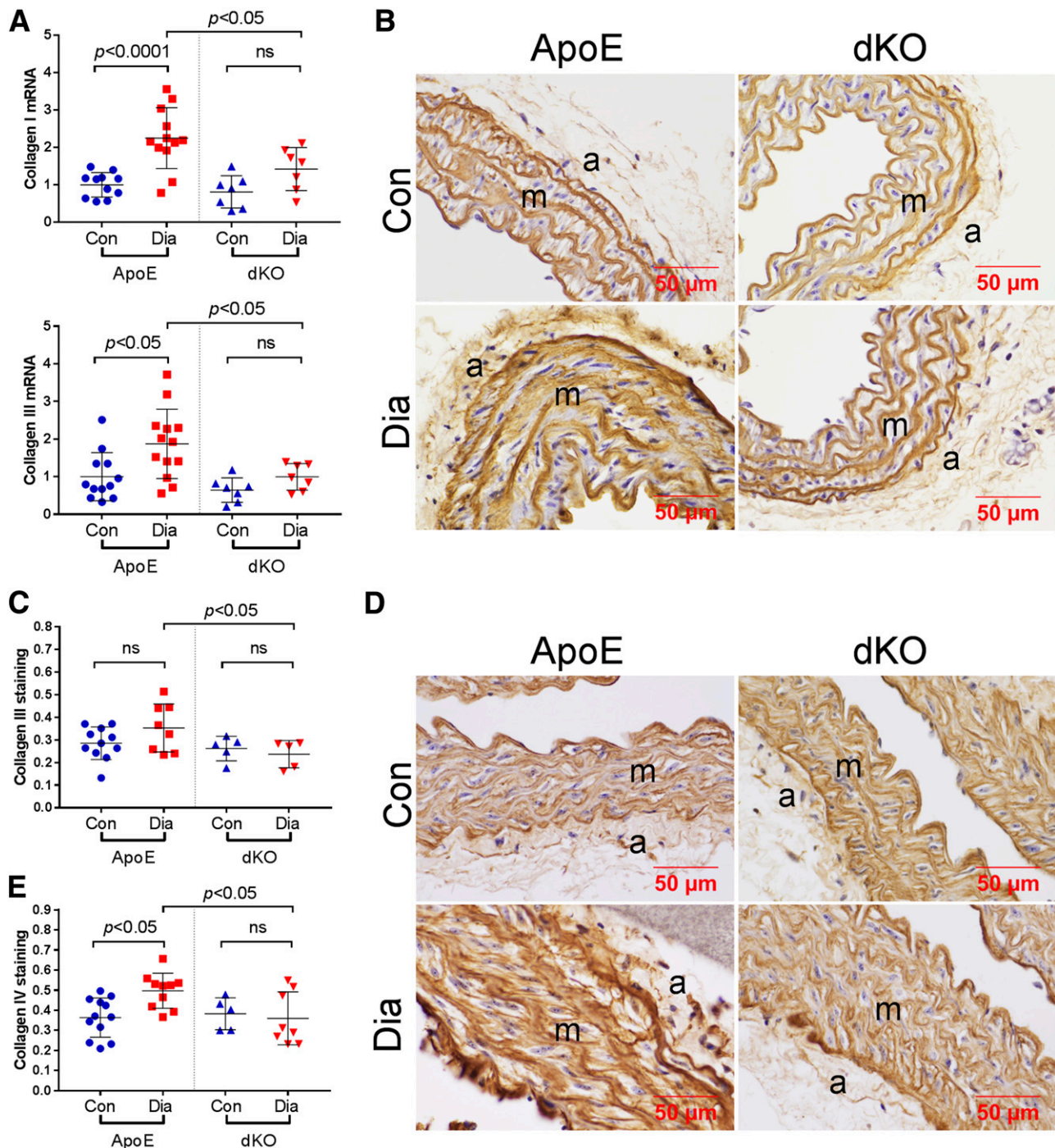


Figure 3—CDA1 deficiency attenuates diabetes-associated increases in aortic expression of collagens I, III, and IV. **A**: Aortic mRNA levels for collagens I and III in control (Con) and 20-week diabetic (Dia) ApoE KO (ApoE) and dKO groups are shown as univariate scatterplots with mean \pm SD and *P* value between specified groups. **B–E**: Representative immunohistochemical staining for aortic collagens III (**B**) and IV (**D**) of these mice is shown. The quantification of the immunohistochemical staining for collagens III (**C**) and IV (**E**) is shown as individual value, mean \pm SD, and *P* value between specified groups. a, adventitia; m, media.

>20 mmol/L, whereas mice injected with buffer alone had blood glucose levels of \sim 10 mmol/L. Ten weeks after streptozotocin injections, diabetic mice had lower body weight than controls (Supplementary Table 3). Both diabetic and control mice were given an AngII infusion for 4 weeks with the AngII dosage adjusted according to the

body weight of individual mouse. The elevated HbA_{1c} levels seen in the diabetic mice and the blood pressure levels in all groups were not affected by the AngII infusion (Supplementary Table 3). Approximately 53% (9 out of 17) of nondiabetic ApoE KO mice died of aortic aneurysm rupture, occurring on days 3–13 during the AngII infusion,

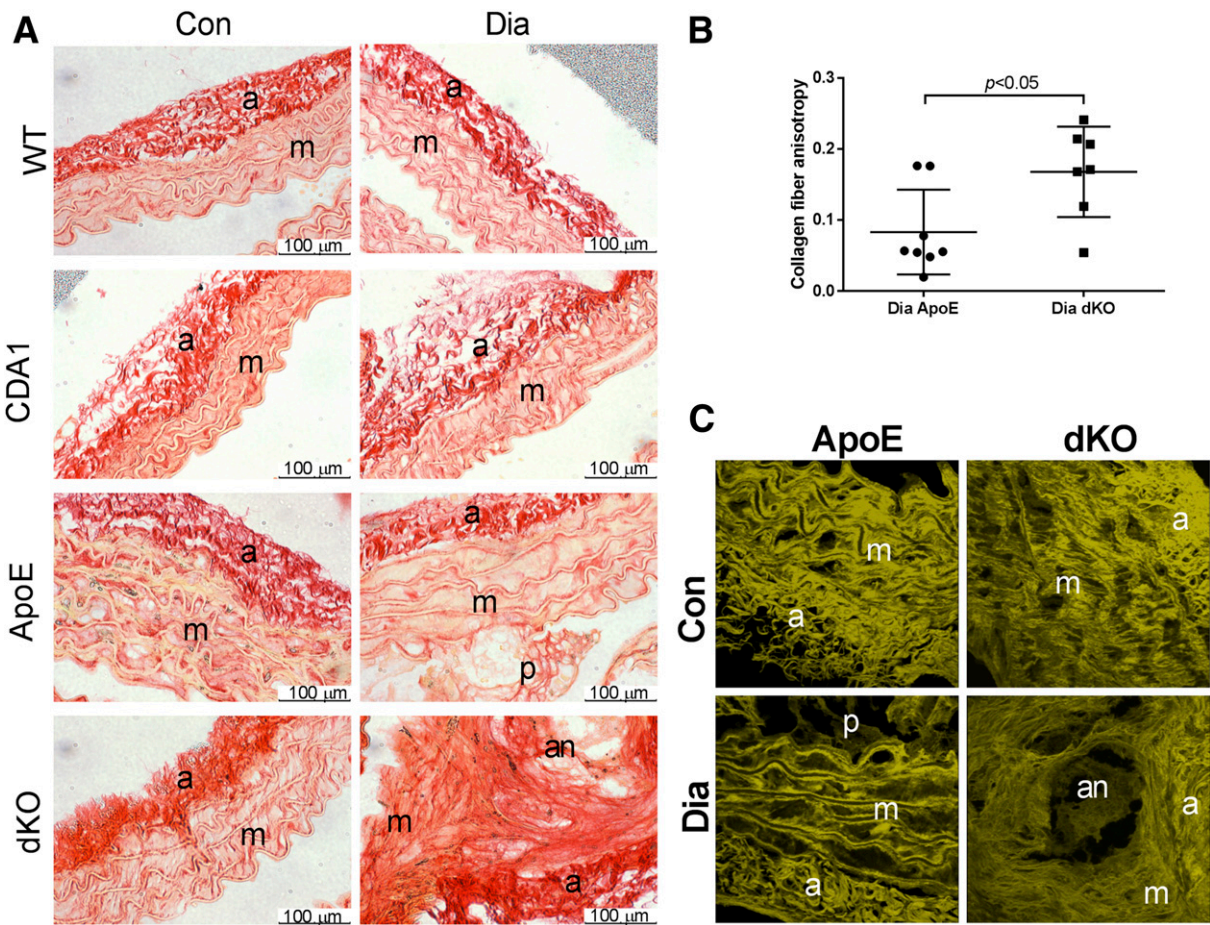


Figure 4—Picosirius red–stained aortic sections examined by light microscopy show disorganized collagen fiber structures in the medial and adventitial layers of diabetic (Dia) dKO mouse aortas, particularly at the aneurysm sites in comparison with WT, CDA1 KO (CDA1), and ApoE KO (ApoE) groups (A). The collagen fiber orientation anisotropy quantitation at the sites of lesion in diabetic ApoE and dKO mice as determined using ImageJ software (National Institutes of Health) is shown (B). Collagen fiber organization, reconstructed from the backscatter confocal images of aortas from diabetic dKO mice, shows more disorganization than that from ApoE KO mice (C). a, adventitia; an, aneurysm site; Con, control; m, media; p, plaque.

whereas diabetic ApoE KO mice had a lower fatal rupture rate of 19% (4 out of 21) occurring on days 5, 7, 22, and 25 ($P < 0.05$) (Fig. 7A). This diabetes-associated protective effect on aneurysm-related mortality was not observed in AngII-infused dKO mice in which CDA1 had been deleted, with similar survival curves for both nondiabetic and diabetic dKO mice (Fig. 7B). Kaplan-Meier analysis of all four groups confirmed these findings. Nondiabetic ApoE KO mice had shorter estimated mean survival of 17.0 days [95% CI 12.0–22.1] than diabetic mice (25.3 days [95% CI 22.4–28.2]; $P = 0.029$, log-rank pairwise comparison), whereas nondiabetic and diabetic dKO mice had similar survivals (21.7 days [95% CI 17.4–26.0] vs. 24.7 days [95% CI 20.5–28.9]; $P = 0.39$). Comparison of nondiabetic ApoE KO and dKO groups showed no clear difference, which was confirmed by log-rank analysis of these groups alone ($P = 0.18$). These findings demonstrate that diabetes was associated with reduced severity of aortic aneurysms induced by an AngII infusion in ApoE KO mice and, importantly, that this phenomenon was CDA1 dependent.

In this model, most of the fatal aneurysm rupture occurred in the abdominal aorta with blood clot seen in the abdomen (Supplementary Figs. 5 and 6). Furthermore, there was a significantly enlarged diameter in the suprarenal region of aortas in these mice (Supplementary Figs. 5 and 6). Aneurysms were identified by the presence of aortic enlargement in 82% (14 out of 17) of nondiabetic and 60% (12 out of 20) of diabetic ApoE KO mice and similarly in 81% (17 out of 21) of nondiabetic dKO and 62% (8 out of 13) of diabetic dKO mice (Supplementary Figs. 5 and 6). These observations and the mortality data suggest that CDA1 does not affect the onset but rather the severity of aneurysm in this model.

AngII infusion caused suprarenal aortic expansion in both nondiabetic and diabetic ApoE KO mice (Fig. 7C), with aortic diameter determined by ultrasound (Supplementary Fig. 7). Baseline suprarenal aortic diameters had low individual variation within either nondiabetic or diabetic ApoE KO mice. Diabetic ApoE KO mice had a larger mean diameter at baseline than nondiabetic controls

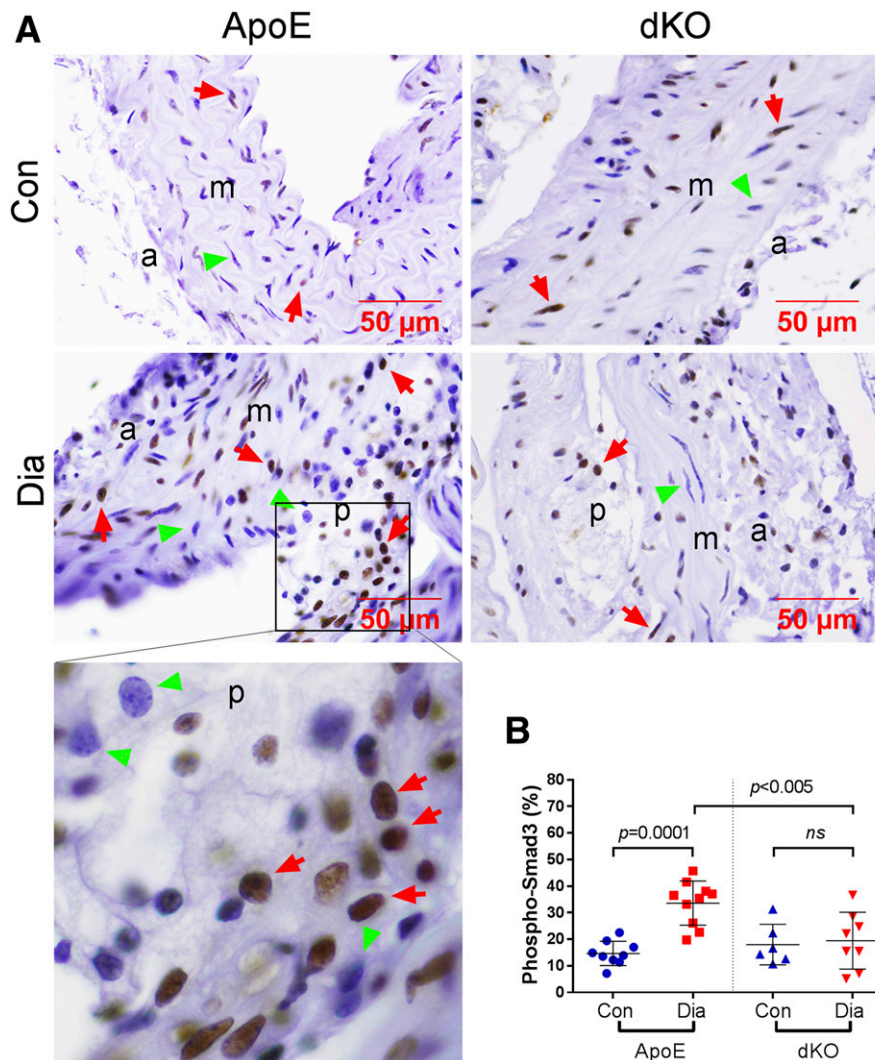


Figure 5—Aortic nuclear phospho-Smad3 staining is increased by diabetes in ApoE KO mice and is attenuated in diabetic dKO mice. Nuclear staining of phospho-Smad3 (Ser^{433/435}) detected by immunohistochemical staining (brown color) is shown in aortas from nondiabetic (Con) and 20-week diabetic (Dia) ApoE KO (ApoE) and dKO mice (A). A part of the ApoE Dia section (boxed) is shown as an enlarged image. Red arrows indicate positive staining; green arrowheads indicate negative staining. B: The phospho-Smad3 nuclear stained positive cells (%) are quantified and shown as univariate scatterplots with mean \pm SD and *P* value between specified groups. a, adventitia; m, media; p, plaque.

(1.17 ± 0.03 vs. 1.03 ± 0.02 mm; $P < 0.05$) (Fig. 7C). After 1 week of AngII infusion, the mean diameters of both groups were significantly increased ($P < 0.001$) (Fig. 7C). All of the mice in the nondiabetic ApoE KO group had an enlarged aortic size, whereas some mice in the diabetic group had no change in aortic diameter (Fig. 7C). The aortic expansion rate at week 1 in response to AngII infusion was 161 ± 11 and $130 \pm 7\%$ ($P < 0.05$) in nondiabetic and diabetic ApoE KO mice, respectively (Fig. 7E).

At baseline, the suprarenal aortic diameter was larger in dKO mice with CDA1 deleted (1.29 ± 0.03 mm) than in ApoE KO mice (1.03 ± 0.02 mm) ($P < 0.001$) or diabetic dKO mice (1.1 ± 0.06 mm) ($P < 0.05$) (Fig. 7D). After 1 week of AngII infusion, mean suprarenal aortic diameters increased relative to those at baseline in both nondiabetic and diabetic dKO groups ($P < 0.05$) (Fig. 7D). Unlike ApoE

KO mice, there was no difference in the aortic expansion rates between nondiabetic and diabetic dKO mice (126 ± 10 vs. $125 \pm 11\%$) (Fig. 7F), demonstrating that the inhibitory effect of diabetes on aortic expansion in response to AngII, as observed in ApoE KO mice, was CDA1 dependent. This finding complements the aortic aneurysm rupture data (Fig. 7A and B) and indeed suggests that CDA1 per se mediates the protective effect of diabetes in reducing the severity of AngII-induced aneurysms in this model.

CDA1 Expression Was Downregulated in Human Subjects With AAA

In order to explore the clinical relevance of our primary findings from the preclinical studies, we examined the mRNA levels of CDA1 in 15 biopsy samples from human patients with AAA and 6 nonaneurysm control samples.

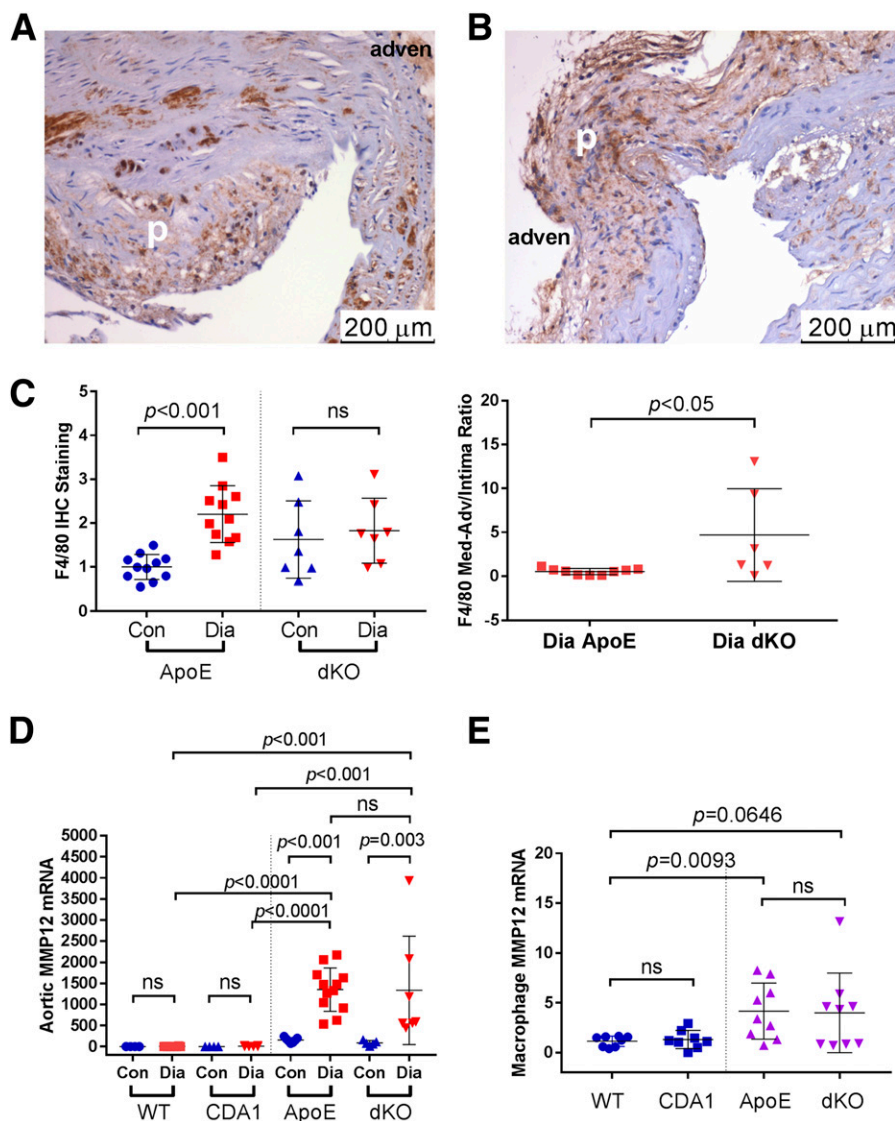


Figure 6—Macrophage infiltration and MMP12 expression are increased in 20-week diabetic mice with ApoE deficiency. A–C: Immunohistochemical (IHC) staining of the macrophage marker, F4/80, is shown in the aortic sections of diabetic ApoE KO (A) and dKO (B) mice. Atherosclerotic plaque (p) and adventitial side (adven) of aortic wall are indicated. Quantification of the staining is shown for control (Con) and diabetic (Dia) ApoE KO (ApoE) and dKO mice (C, left panel). The ratio of the medial-adventitial (Med-Adv) F4/80 staining to the intima staining at sites containing a plaque in Dia ApoE and dKO mice is also shown (C, right panel). MMP12 mRNA levels in aortas from Con and 20-week Dia WT, CDA1 KO (CDA1), ApoE, and dKO mice (D) as well as in macrophages (E) isolated from peritoneal cavity, using the method previously described (55), of ~12-week-old male WT, CDA1 KO, ApoE KO, and dKO mice were determined by RT-PCR. Data (C–E) are shown as univariate scatterplots with mean \pm SD and *P* value between specified groups.

The majority of the patients with AAA were male (80%) and had dyslipidemia (73%). One-third of the patients with AAA were diabetic (33%). Their average maximum infrarenal aortic diameter was 58.9 ± 2.8 mm (mean \pm SEM), with a trend toward a smaller diameter in subjects with diabetes ($n = 5$) than in subjects without diabetes (51.8 ± 5.1 mm [$n = 5$] vs. 62.5 ± 2.9 mm [$n = 10$]; $P = 0.072$). The average age of the AAA group was greater than that of the control samples from younger organ donors ($P < 0.001$), reflecting the fact that AAA is an age-related disease (Supplementary Table 4). As shown in Fig. 8, CDA1 gene expression

in the AAA samples was downregulated ~70% when compared with the control subjects ($P = 0.006$). In patients with AAA, there was no difference in CDA1 expression levels between participants with diabetes and without diabetes (Fig. 8).

DISCUSSION

The current study reveals a potential molecular mechanism to explain, at least in part, the resistance to aneurysm formation in diabetes, a puzzling and previously poorly understood observation. Numerous studies have revealed

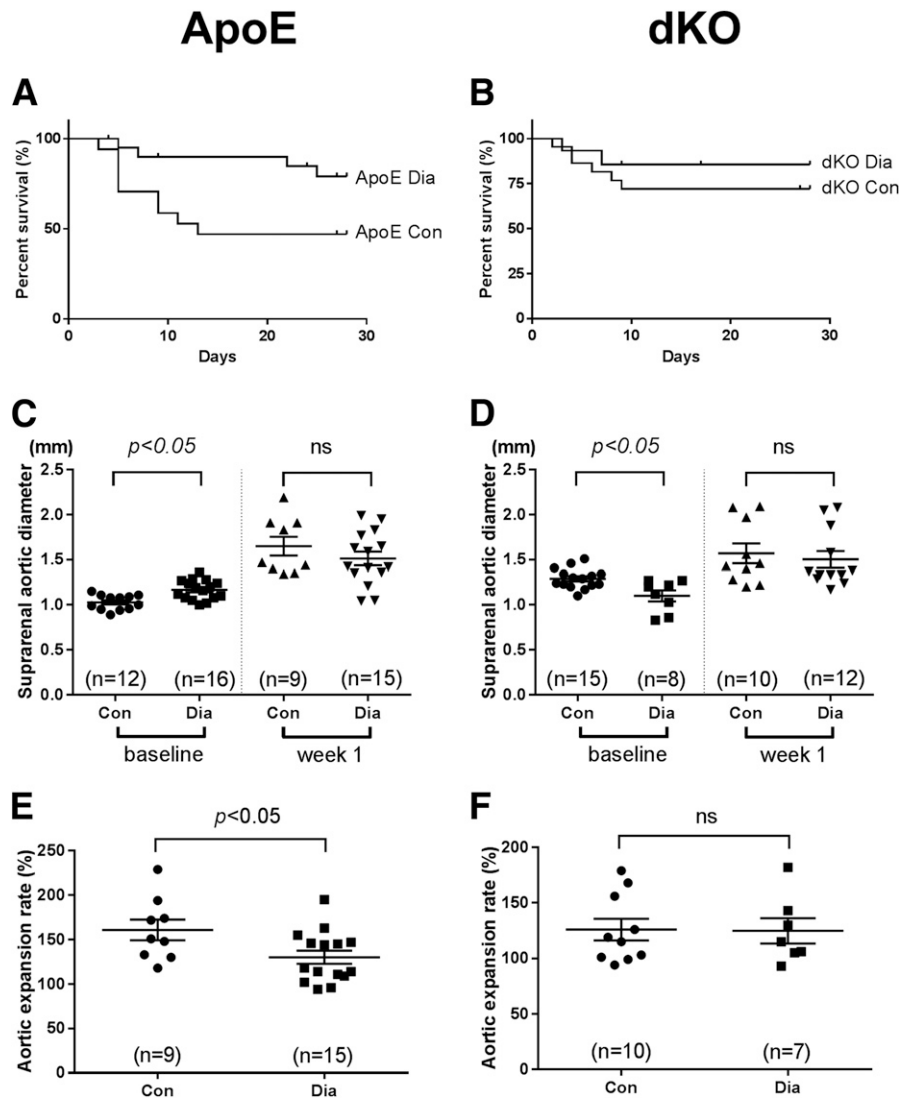


Figure 7—Diabetes reduces fatal aortic aneurysm rupture and aortic expansion in AngII-infused ApoE KO mice, which are CDA1 dependent. Percent survival (%) curves of control (Con) and diabetic (Dia) ApoE KO (A) and dKO (B) mice are shown with respect to days of AngII infusion. Animals killed for animal welfare reasons, including three diabetic ApoE KO, one nondiabetic dKO, and six diabetic dKO mice, were included in the survival curve (censored). Inner diameters of supragenital aortas determined by ultrasound imaging at baseline and week 1 after AngII infusion are shown for Con and Dia ApoE KO (C) and dKO (D) mice. Supragenital aortic expansion rates (%) at week 1 relative to the baseline are shown for Con and Dia ApoE KO (E) and dKO (F) mice. Individual value, group mean \pm SEM, group size (*n*), and *P* value between specified groups are shown (C–F).

a decreased incidence of aneurysms in subjects with diabetes, as summarized in a recent meta-analysis (2). Interestingly, metformin, a widely used diabetes medication, has been observed to be associated with reduced AAA growth in patients who have diabetes (40,41). Whether this association is due to metformin alone or the effect of diabetes plus metformin is not clear and requires a randomized trial to resolve. In the current study, in which metformin was not administered, diabetic ApoE KO mice had less severe aneurysms than their nondiabetic controls. It appears likely that there are multiple mechanisms by which diabetes slows AAA growth, including the mechanisms highlighted in this study.

Diabetes is a state of enhanced fibrosis with increased ECM accumulation in the vasculature (7,23). We have previously shown increased renal and vascular expression of CDA1 in diabetes, which enhances TGF- β /Smad signaling, leading to increased ECM accumulation (23–25). Increased ECM accumulation presumably contributes to the relative protection against aneurysm formation in subjects with diabetes, although it is possible that multiple mechanisms are involved (2,6,12,42). It has been reported that subjects with diabetes with chronic complications are less likely to develop aortic aneurysms than patients with diabetes without complications (43). In this and in our previous studies (7,23), diabetic ApoE KO mice did not develop any

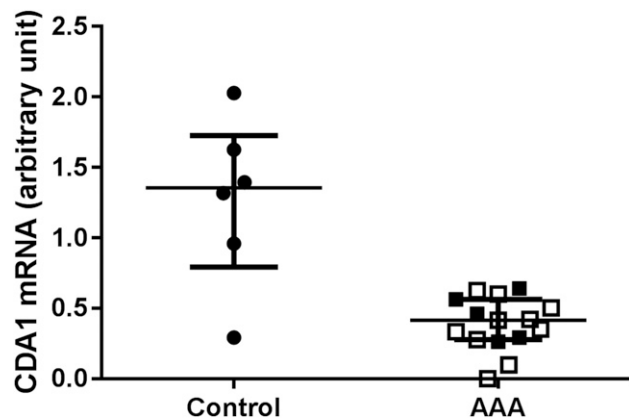


Figure 8—CDA1 mRNA levels are decreased in AAAs in humans. Aortas from 15 subjects with AAA and 6 organ donors as control subjects were examined for CDA1 mRNA levels by RT-PCR using β -actin as a housekeeping gene control. β -Actin was chosen as the housekeeping gene because analyses showed that its expression was similar in aortic biopsies from patients and organ donors. Individual results (relative value) are shown as dots in groups as well as the group median value with the interquartile range. Open squares represent 10 subjects without diabetes, and black squares represent 5 subjects with diabetes and AAA. Control group median is 1.356 (interquartile range 0.792–1.726) and AAA group median is 0.415 (interquartile range 0.279–0.564). $P = 0.006$.

aneurysms in the absence of classic stimuli of aneurysm formation, such as AngII infusion, and were found to have greater aortic phospho-Smad3 levels; greater accumulation of collagens I, III, and IV; and greater thickness of elastin lamella, which could reflect an increase in strength of the aortic wall. We have previously shown that aortic mRNA levels of CDA1 (the *Tsypyl2* gene) are increased by approximately twofold at 10 weeks after diabetes induction in ApoE KO mice, which are further increased to greater than sixfold at 20 weeks after diabetes induction with concurrent increases in aortic CDA1 protein staining, TGF- β expression, and ECM accumulation (23). We have previously reported that CDA1 overexpression and CDA1 knock-down or genetic deletion of CDA1 enhances and attenuates TGF- β signaling, respectively, as reflected by changes in TGF- β -stimulated phosphorylation of Smad3 and TGF- β -responsive promoter luciferase reporter activities. This effect of CDA1 on TGF- β signaling is probably at least in part via influencing expression of TGF- β type I receptor (23–25). In this study, diabetic dKO mice in the absence of CDA1 showed attenuated TGF- β signaling, breakage of elastin lamella, and reduced ECM accumulation, which presumably would contribute to aneurysm formation (44,45). The effect of CDA1 on TGF- β signaling in the vascular smooth muscle cells has been previously described (23). Indeed, this finding is consistent with a recent report that impaired TGF- β signaling in the vascular smooth muscle cells causes aortic aneurysm formation in mice (22). This increase in aneurysm formation is reflected by the increased aortic diameter in diabetic dKO mice. This is potentially clinically relevant because TGF- β and other TGF-

β -dependent molecules such as connective tissue growth factor remain targets for reducing other diabetic complications such as nephropathy in subjects with diabetes (11,46). The current study highlights the possibility that aggressive approaches to interrupt the TGF- β axis could lead to increased susceptibility to aneurysms.

As outlined earlier, numerous clinical studies, recently summarized in a meta-analysis (2), have demonstrated reduced aneurysms in subjects with type 2 diabetes (T2D). Indeed, our preclinical experiments are consistent with the clinical studies with reduced severity of aortic dilation in response to the proaneurysm stimulus, AngII, in diabetic mice. Although these studies have focused on an insulin-deficient model of diabetes, because aneurysms occur in the older population in whom T2D is more prevalent, it is worth considering subsequent studies in relevant models of T2D.

Runt-related transcription factor 2 (Runx2) is known to be upregulated by TGF- β (47) and is involved in calcification in the vasculature. Furthermore, recently, Runx2 was found to be upregulated in aortas of diabetic *db/db* mice in association with increased aortic fibrosis and stiffness (48). Whether CDA1 plays a role in affecting Runx2 in the vascular calcification and vascular fibrosis due to its ability to influence TGF- β signaling requires further investigation, although our experiments failed to show this phenomenon in our model (data not shown), which displays prominent aneurysm development rather than vascular calcification.

Macrophage activation and infiltration from the adventitia are common features observed in aneurysms (39,49). Macrophages were mainly located within the atherosclerotic plaque specifically within the intimal layer of the aorta in the diabetic ApoE KO mice. By contrast, in diabetic dKO mice, macrophages infiltrated into the medial and adventitial layers with associated increased elastin breakage in the medial layer and collagen structural damage in both medial and adventitial layers. This finding is consistent with the macrophage distribution pattern previously reported in other models of aneurysm formation (50,51), which is associated with increased elastin fiber digestion and aneurysm or dissection formation (34,39,49,52). The mechanisms responsible for the differential distribution patterns of macrophages within the aortas in diabetic ApoE KO and diabetic dKO mice are still unclear. It is yet to be determined whether CDA1 deficiency-related ECM remodeling is responsible for the aortic wall becoming more prone to the widespread macrophage infiltration into the media and adventitial layers.

Therefore, this study suggests the importance of inflammation and the attenuation of profibrotic pathways in the pathogenesis of aortic aneurysm. Deletion of CDA1, a molecule closely linked to the TGF- β axis, led to enhanced aneurysm formation in the context of the generally profibrotic milieu of diabetes. The role of the TGF- β axis in aneurysm formation has been extensively explored, with a large body of experimental and clinical data (14–21,53) emphasizing

that dysregulation of this pathway, both enhanced and reduced TGF- β signaling, is associated with aneurysm formation.

Based on the results of our studies, part of the protective role of diabetes in the pathogenesis of aneurysms is postulated to be mediated by CDA1. Indeed, AngII infusion caused development of severe AAA mainly in the suprarenal region of aortas in ApoE KO and dKO mice, as reflected by rapid death due to aortic aneurysm rupture within a few days and significant expansion of the suprarenal aorta in response to AngII. These parameters were significantly attenuated in the diabetic ApoE KO mice. By contrast, diabetic CDA1-deficient dKO mice failed to show attenuation of these parameters when compared with their non-diabetic dKO counterparts. Thus, these findings clearly demonstrate a role for CDA1 in mediating the protective effect of diabetes on aneurysms. Because the occurrence rate of aneurysm was similar in both ApoE KO and dKO mice, it appears that CDA1 reduces aneurysm severity, but not the formation of aneurysms in this model. This is consistent with the notion that CDA1 promotes the TGF- β /Smad/ECM pathway, leading to increased accumulation of ECMs in the vasculature in diabetes (23), hence limiting the growth of the aneurysms induced by AngII.

In this study, the two mouse strains (ApoE KO and dKO) appeared to differ in response to the AngII infusion, as reflected by a trend toward higher survival and less aortic expansion in dKO mice, albeit these differences are not statistically significant, probably due to a small group size. A comparison between the nondiabetic and diabetic littermates of ApoE KO mice showed a diabetes-associated protection in the AngII infusion groups with respect to fatality and aortic expansion (Fig. 7A and E). This phenomenon of diabetes-associated protection of aneurysm development was not seen in the dKO groups (Fig. 7B and F). Use of a CDA1-transgenic mouse strain to overexpress CDA1 in relevant vascular cells or a pharmacological enhancer of CDA1, if available, would be very useful to confirm the role of CDA1 in protecting aneurysm development in this animal model.

The potential clinical relevance of these preclinical findings was explored, and CDA1 expression was found to be reduced \sim 70% in human AAA samples when compared with control subjects without AAA. These AAA samples have been previously shown to have reduced expression of the TGF- β type II receptor (21). This is consistent with our previous experimental results that CDA1 deficiency was associated with decreased TGF- β signaling (23–25). This finding in humans supports the potential likelihood that CDA1 plays a protective role in human aneurysms. We have previously described that CDA1 expression is increased in experimental atherosclerosis in a model without aneurysms (23) and found that CDA1 was strongly stained in human atherosclerotic plaques (A. Dai, Z. Chai, unpublished observation). These findings may reflect distinct roles for CDA1 in vascular ECM remodeling and the obviously different pathogenic factors involved in the development of atherosclerosis and aneurysms (54). In this study, subjects

with diabetes with AAA had reduced CDA1 gene expression consistent with CDA1 playing a key protective role in aneurysm formation in those individuals who are susceptible to this condition. With limited availability of appropriate human aneurysmal tissue, protein levels of CDA1 could not be measured, and this is a limitation of this study.

In conclusion, this study demonstrated that CDA1-deficient mice with concurrent diabetes developed aneurysms, but diabetic mice in the presence of CDA1 were protected from severe aneurysms. With evidence of reduced CDA1 expression in human AAA, these findings are consistent with the postulate that CDA1 may play a protective role against aneurysm formation. Our findings suggest that CDA1 may be a therapeutic target to prevent or retard the progression of human aneurysms and that this protein may play a key role in explaining the clinical observation that subjects with diabetes are less susceptible to aneurysm formation.

Acknowledgments. The authors thank Samantha Sacca (Baker IDI Heart and Diabetes Institute) for assistance with animal studies. Organ donors and next of kin (Donate Life in Queensland) are gratefully acknowledged. Sadly, Philip Walker died during the final preparation of the manuscript, and the authors are indebted to his untiring work and leadership on this and other vascular research.

Funding. This study was supported by the National Health and Medical Research Council (NHMRC) and the National Heart Foundation of Australia. M.E.C. is an NHMRC Senior Principal Research Fellow, X.-J.D. is an NHMRC senior research fellow, and J.G. is a Practitioner Fellow. J.G. holds a Senior Clinical Research Fellowship from the Health and Medical Research Office, Queensland, Australia. M.N. is supported by the Prince Charles Hospital Foundation, Brisbane, Queensland, Australia.

Duality of Interest. No potential conflicts of interest relevant to this article were reported.

Author Contributions. J.L. performed the 20-week diabetes animal study. J.L. and Z.C. wrote the manuscript. P.H., A.D., and T.W. performed the AngII infusion animal study. Y.T. and B.C. were involved in animal tissue collection and analysis. H.K. and X.-J.D. carried out ultrasound imaging. X.-J.D., L.A.B., J.L.W.-B., J.G., T.J.A., and M.E.C. read and critically edited the manuscript. L.A.B. analyzed survival curve data. E.B. performed analysis of human biopsy samples. P.W., M.N., M.W., and J.G. organized collection of human samples and data. Z.C. designed and initiated the experiments. Z.C. is the guarantor of this work and, as such, had full access to all of the data in the study and takes responsibility for the integrity of the data and the accuracy of the data analysis.

References

1. Moxon JV, Parr A, Emeto TI, Walker P, Norman PE, Gollidge J. Diagnosis and monitoring of abdominal aortic aneurysm: current status and future prospects. *Curr Probl Cardiol* 2010;35:512–548
2. Shantikumar S, Ajjan R, Porter KE, Scott DJ. Diabetes and the abdominal aortic aneurysm. *Eur J Vasc Endovasc Surg* 2010;39:200–207
3. Lederle FA, Johnson GR, Wilson SE, et al.; Aneurysm Detection and Management (ADAM) Veterans Affairs Cooperative Study Group. Prevalence and associations of abdominal aortic aneurysm detected through screening. *Ann Intern Med* 1997;126:441–449
4. Blanchard JF, Armenian HK, Friesen PP. Risk factors for abdominal aortic aneurysm: results of a case-control study. *Am J Epidemiol* 2000;151:575–583
5. Karanjia PN, Madden KP, Lobner S. Coexistence of abdominal aortic aneurysm in patients with carotid stenosis. *Stroke* 1994;25:627–630
6. Gollidge J, Karan M, Moran CS, et al. Reduced expansion rate of abdominal aortic aneurysms in patients with diabetes may be related to aberrant monocyte-matrix interactions. *Eur Heart J* 2008;29:665–672

7. Candido R, Jandeleit-Dahm KA, Cao Z, et al. Prevention of accelerated atherosclerosis by angiotensin-converting enzyme inhibition in diabetic apolipoprotein E-deficient mice. *Circulation* 2002;106:246–253
8. Ruiz-Ortega M, Rodríguez-Vita J, Sanchez-Lopez E, Carvajal G, Egido J. TGF-beta signaling in vascular fibrosis. *Cardiovasc Res* 2007;74:196–206
9. Ziyadeh FN, Hoffman BB, Han DC, et al. Long-term prevention of renal insufficiency, excess matrix gene expression, and glomerular mesangial matrix expansion by treatment with monoclonal antitransforming growth factor-beta antibody in db/db diabetic mice. *Proc Natl Acad Sci U S A* 2000;97:8015–8020
10. Petersen M, Thorikay M, Deckers M, et al. Oral administration of GW788388, an inhibitor of TGF-beta type I and II receptor kinases, decreases renal fibrosis. *Kidney Int* 2008;73:705–715
11. McGowan TA, Zhu Y, Sharma K. Transforming growth factor-beta: a clinical target for the treatment of diabetic nephropathy. *Curr Diab Rep* 2004;4:447–454
12. Norman PE, Davis TM, Le MT, Golledge J. Matrix biology of abdominal aortic aneurysms in diabetes: mechanisms underlying the negative association. *Connect Tissue Res* 2007;48:125–131
13. Didangelos A, Yin X, Mandal K, et al. Extracellular matrix composition and remodeling in human abdominal aortic aneurysms: a proteomics approach. *Mol Cell Proteomics* 2011;10:M111.008128
14. Boileau C, Guo DC, Hanna N, et al.; National Heart, Lung, and Blood Institute (NHLBI) Go Exome Sequencing Project. TGFβ2 mutations cause familial thoracic aortic aneurysms and dissections associated with mild systemic features of Marfan syndrome. *Nat Genet* 2012;44:916–921
15. Lindsay ME, Schepers D, Bolar NA, et al. Loss-of-function mutations in TGFβ2 cause a syndromic presentation of thoracic aortic aneurysm. *Nat Genet* 2012;44:922–927
16. Pannu H, Fadulu VT, Chang J, et al. Mutations in transforming growth factor-beta receptor type II cause familial thoracic aortic aneurysms and dissections. *Circulation* 2005;112:513–520
17. Loeys BL, Schwarze U, Holm T, et al. Aneurysm syndromes caused by mutations in the TGF-beta receptor. *N Engl J Med* 2006;355:788–798
18. van de Laar IM, Oldenburg RA, Pals G, et al. Mutations in SMAD3 cause a syndromic form of aortic aneurysms and dissections with early-onset osteoarthritis. *Nat Genet* 2011;43:121–126
19. Holm TM, Habashi JP, Doyle JJ, et al. Noncanonical TGFβ signaling contributes to aortic aneurysm progression in Marfan syndrome mice. *Science* 2011;332:358–361
20. Loeys BL, Chen J, Neptune ER, et al. A syndrome of altered cardiovascular, craniofacial, neurocognitive and skeletal development caused by mutations in TGFBR1 or TGFBR2. *Nat Genet* 2005;37:275–281
21. Biros E, Walker PJ, Nataatmadja M, West M, Golledge J. Downregulation of transforming growth factor, beta receptor 2 and Notch signaling pathway in human abdominal aortic aneurysm. *Atherosclerosis* 2012;221:383–386
22. Zhang P, Hou S, Chen J, et al. Smad4 deficiency in smooth muscle cells initiates the formation of aortic aneurysm. *Circ Res* 2016;118:388–399
23. Pham Y, Tu Y, Wu T, et al. Cell division autoantigen 1 plays a profibrotic role by modulating downstream signalling of TGF-beta in a murine diabetic model of atherosclerosis. *Diabetologia* 2010;53:170–179
24. Tu Y, Wu T, Dai A, et al. Cell division autoantigen 1 enhances signaling and the profibrotic effects of transforming growth factor-β in diabetic nephropathy. *Kidney Int* 2011;79:199–209
25. Chai Z, Dai A, Tu Y, et al. Genetic deletion of cell division autoantigen 1 retards diabetes-associated renal injury. *J Am Soc Nephrol* 2013;24:1782–1792
26. Rush C, Nyara M, Moxon JV, Trollope A, Cullen B, Golledge J. Whole genome expression analysis within the angiotensin II-apolipoprotein E deficient mouse model of abdominal aortic aneurysm. *BMC Genomics* 2009;10:298
27. Daugherty A, Cassis LA. Mouse models of abdominal aortic aneurysms. *Arterioscler Thromb Vasc Biol* 2004;24:429–434
28. Xu Q, Chakravorty A, Bathgate RA, Dart AM, Du XJ. Relaxin therapy reverses large artery remodeling and improves arterial compliance in senescent spontaneously hypertensive rats. *Hypertension* 2010;55:1260–1266
29. Xiao J, Angsana J, Wen J, et al. Syndecan-1 displays a protective role in aortic aneurysm formation by modulating T cell-mediated responses. *Arterioscler Thromb Vasc Biol* 2012;32:386–396
30. Sun J, Sukhova GK, Yang M, et al. Mast cells modulate the pathogenesis of elastase-induced abdominal aortic aneurysms in mice. *J Clin Invest* 2007;117:3359–3368
31. Soro-Paavonen A, Watson AM, Li J, et al. Receptor for advanced glycation end products (RAGE) deficiency attenuates the development of atherosclerosis in diabetes. *Diabetes* 2008;57:2461–2469
32. Dolber PC, Spach MS. Conventional and confocal fluorescence microscopy of collagen fibers in the heart. *J Histochem Cytochem* 1993;41:465–469
33. Boudaoud A, Burian A, Borowska-Wykręć D, et al. FibrilTool, an ImageJ plug-in to quantify fibrillar structures in raw microscopy images. *Nat Protoc* 2014;9:457–463
34. Daugherty A, Manning MW, Cassis LA. Angiotensin II promotes atherosclerotic lesions and aneurysms in apolipoprotein E-deficient mice. *J Clin Invest* 2000;105:1605–1612
35. Barisione C, Charnigo R, Howatt DA, Moorleghen JJ, Rateri DL, Daugherty A. Rapid dilation of the abdominal aorta during infusion of angiotensin II detected by noninvasive high-frequency ultrasonography. *J Vasc Surg* 2006;44:372–376
36. Parr A, Buttner P, Shahzad A, Golledge J. Relation of infra-renal abdominal aortic calcific deposits and cardiovascular events in patients with peripheral artery disease. *Am J Cardiol* 2010;105:895–899
37. Parr A, McCann M, Bradshaw B, Shahzad A, Buttner P, Golledge J. Thrombus volume is associated with cardiovascular events and aneurysm growth in patients who have abdominal aortic aneurysms. *J Vasc Surg* 2011;53:28–35
38. Golledge J, Clancy P, Jamrozik K, Norman PE. Obesity, adipokines, and abdominal aortic aneurysm: Health in Men study. *Circulation* 2007;116:2275–2279
39. Curci JA, Liao S, Huffman MD, Shapiro SD, Thompson RW. Expression and localization of macrophage elastase (matrix metalloproteinase-12) in abdominal aortic aneurysms. *J Clin Invest* 1998;102:1900–1910
40. Fujimura N, Xiong J, Kettler EB, et al. Metformin treatment status and abdominal aortic aneurysm disease progression. *J Vasc Surg* 2016;64:46–54.e8
41. Golledge J, Moxon J, Pinchbeck J, et al. Association between metformin prescription and growth rates of abdominal aortic aneurysms. *Br J Surg* 2017;104:1486–1493
42. Torsney E, Pirianov G, Cockerill GW. Diabetes as a negative risk factor for abdominal aortic aneurysm - does the disease aetiology or the treatment provide the mechanism of protection? *Curr Vasc Pharmacol* 2013;11:293–298
43. Prakash SK, Pedroza C, Khalil YA, Milewicz DM. Diabetes and reduced risk for thoracic aortic aneurysms and dissections: a nationwide case-control study. *J Am Heart Assoc* 2012;1:e000323
44. Wang Y, Ait-Oufella H, Herbin O, et al. TGF-beta activity protects against inflammatory aortic aneurysm progression and complications in angiotensin II-infused mice. *J Clin Invest* 2010;120:422–432
45. Campa JS, Greenhalgh RM, Powell JT. Elastin degradation in abdominal aortic aneurysms. *Atherosclerosis* 1987;65:13–21
46. Yanagita M. Inhibitors/antagonists of TGF-β system in kidney fibrosis. *Nephrol Dial Transplant* 2012;27:3686–3691
47. Lee KS, Hong SH, Bae SC. Both the Smad and p38 MAPK pathways play a crucial role in Runx2 expression following induction by transforming growth factor-beta and bone morphogenetic protein. *Oncogene* 2002;21:7156–7163
48. Raaz U, Schellinger IN, Chernogubova E, et al. Transcription factor Runx2 promotes aortic fibrosis and stiffness in Type 2 diabetes mellitus. *Circ Res* 2015;117:513–524
49. Shipley JM, Wesselschmidt RL, Kobayashi DK, Ley TJ, Shapiro SD. Metalloelastase is required for macrophage-mediated proteolysis and matrix invasion in mice. *Proc Natl Acad Sci USA* 1996;93:3942–3946
50. Saraff K, Babamusta F, Cassis LA, Daugherty A. Aortic dissection precedes formation of aneurysms and atherosclerosis in angiotensin II-infused, apolipoprotein E-deficient mice. *Arterioscler Thromb Vasc Biol* 2003;23:1621–1626
51. Rateri DL, Howatt DA, Moorleghen JJ, Charnigo R, Cassis LA, Daugherty A. Prolonged infusion of angiotensin II in apoE(-/-) mice promotes macrophage

recruitment with continued expansion of abdominal aortic aneurysm. *Am J Pathol* 2011;179:1542–1548

52. Daugherty A, Manning MW, Cassis LA. Antagonism of AT2 receptors augments angiotensin II-induced abdominal aortic aneurysms and atherosclerosis. *Br J Pharmacol* 2001;134:865–870

53. Nataatmadja M, West M, West J, et al. Abnormal extracellular matrix protein transport associated with increased apoptosis of vascular smooth muscle cells in

marfan syndrome and bicuspid aortic valve thoracic aortic aneurysm. *Circulation* 2003;108(Suppl. 1):II329–II334

54. Golledge J, Norman PE. Atherosclerosis and abdominal aortic aneurysm: cause, response, or common risk factors? *Arterioscler Thromb Vasc Biol* 2010;30:1075–1077

55. Zhang X, Goncalves R, Mosser DM. The isolation and characterization of murine macrophages. *Curr Protoc Immunol* 2008;Chapter 14:Unit 14.1

SUPPLEMENTARY DATA

Supplementary Table 1. Sequence of real-time qRT-PCR probes and primers

Gene	Species	Sequence
CDA1	Human	Probe: (FAM)-5'-TTCCTGCGTCTCAAGC -3'-(TAMARA) Forward primer: 5'-AACATCAAGGCAGGCAAAGC – 3' Reverse primer: 5'-GAAGGGTCTTCGCATCTGGAT – 3'
CDA1	Mouse	Probe: (FAM)-5'-CTTGGGCCAGCCTG'-3'-(TAMARA) Forward primer: 5'-TGCTGCCGGTCCCAA – 3' Reverse primer: 5'-TGTTTATCCGATCTTCCCTTTCTT – 3'
Col I	Mouse	Probe: (FAM)-5'-ATCGACCCTAACCAAG-3'-(TAMARA) Forward primer: 5'-GACTGGAAGAGCGGAGAGTACTG – 3' Reverse primer: 5'-CCTTGATGGCGTCCAGGTT – 3'
Col III	Mouse	Probe: (FAM)-5'-AATATCAAACACGCAAGGC-3'-(TAMARA) Forward primer: 5'-GGGAATGGAGCAAGACAGTCTT-3' Reverse primer: 5'-TGCGATATCTATGATGGGTAGTCTCA -3'
Col IV	Mouse	Probe: (FAM)-5'-CAGTGCCCTAACGGT-3'-(TAMARA) Forward primer: 5'-GGCGGTACACAGTCAGACCAT-3' Reverse primer: 5'-GGAATAGCCGATCCACAGTGA-3'
MMP12	Mouse	Probe: (FAM)-5'-CCAAGCTGATTTCCA-3'-(TAMARA) Forward primer: 5'-TGAGGCAGGAGCTCATGGA-3' Reverse primer: 5'-GGCTTGATTCTGGGAAGTG-3'

SUPPLEMENTARY DATA

Supplementary Table 2. Metabolic data of control and diabetic WT, CDA1 knockout, ApoE knockout and dKO mice

Genotype:	WT		CDA1		ApoE		dKO	
	Control	Diabetic	Control	Diabetic	Control	Diabetic	Control	Diabetic
Group:	(n=15)	(n=12)	(n=15)	(n=12)	(n=25)	(n=27)	(n=14)	(n=16)
BW (g)	33.3±0.9	25.7±0.5 [†]	31.2±0.5 [‡]	26.8±0.6 [†]	30.6±0.6 [‡]	23.2±0.7 ^{†, #}	32.8±0.8 [‡]	24.1±0.8 [†]
Glucose (mM)	13.5±0.9	28.6±1.1 [†]	11.2±0.6	27.4±1.7 [†]	14.0±0.7	28.4±1.2 [†]	13.6±0.9	27.1±1.0 [†]
HbA1c (%)	4.3±0.1	11.7±0.5 [†]	4.8±0.3	11.5±0.8 [†]	4.1±0.1	15.4±0.7 ^{†, #}	4.2±0.1	13.5±1.3 [†]
	(n=12)	(n=10)	(n=10)	(n=7)	(n=11)	(n=12)	(n=10)	(n=7)
Cholesterol (mM)	1.4±0.05	1.4±0.1	1.5±0.1	1.4±0.1	8.9±0.9 [§]	19.7±1.3 ^{†, **}	10.4±0.8 [§]	22.3±2.5 ^{†, **}
HDL (mM)	0.85±0.04	0.6±0.07 [*]	1.0±0.1	0.6±0.08 [*]	2.2±0.3 [§]	3.9±0.3 ^{†, **}	2.6±0.2 [§]	4.5±0.5 ^{*, **}
LDL (mM)	0.5±0.02	0.6±0.05 [*]	0.4±0.03	0.7±0.05 [*]	6.3±0.6 [§]	14.9±1.0 ^{†, **}	7.3±0.5 [§]	16.3±1.9 ^{†, **}
LDL/HDL ratio	0.57±0.04	1.1±0.2 [*]	0.5±0.10	1.5±0.5 [*]	3.1±0.4 [§]	4.0±0.2 ^{*, **}	2.9±0.2 [§]	3.6±0.1 ^{*, **}
TG (mM)	0.1±0.00	0.3±0.00 [†]	0.2±0.05	0.3±0.00 [#]	0.8±0.2 [§]	2.0±0.4 ^{*, #}	1.3±0.2 [§]	3.3±0.8 ^{*, **}

* $p < 0.05$, [†] $p < 0.001$ vs control of the same genotype; [‡] $p < 0.05$, [§] $p < 0.001$ vs WT control; ^{||} $p < 0.05$ vs ApoE control; [#] $p < 0.05$, ^{**} $p < 0.001$ vs WT diabetic; Values are mean ± s.e (n=7-27).

Metabolic data for all mouse groups collected at 20 weeks after the last streptozotocin (diabetic) or buffer (non-diabetic) injection: Body weight (BW) of diabetic groups was lower than their non-diabetic control counterparts. Plasma glucose and HbA1c levels were higher in diabetic mice. There was no difference in the severity of hyperglycemia in the diabetic groups amongst the various genotypes, except for a higher HbA1c in the diabetic ApoE knockout compared to the diabetic WT mice ($p < 0.05$). ApoE deficiency resulted in significant higher plasma levels of lipids, such as HDL, LDL and tryglycerides (TG). Diabetes was associated with lower HDL levels and increased LDL levels, LDL/HDL ratio and TG levels in WT and CDA1 KO mice. In ApoE KO mice diabetes was associated with increased levels of HDL, LDL, LDL/HDL ratio and TG. Importantly, CDA1 deficiency did not change any of these parameters.

SUPPLEMENTARY DATA

Supplementary Table 3. Metabolic data of angiotensin infused mice

Genotype:	ApoE		dKO	
	Control	Diabetic	Control	Diabetic
BW (g) (Prior AngII infusion)	30.4±0.6 (n=17)	27.1±0.6* (n=20)	31.9±0.6 (n=15)	25.4±0.9* (n=15)
HbA1c (%) (Endpoint)	4.7±0.1 (n=5)	10.8±0.9* (n=12)	4.3±0.1 (n=10)	10.0±1.2* (n=7)
BP (Systolic, mmHg) (Baseline)	104±1 (n=17)	103±1 (n=16)	103±2 (n=5)	106±1 (n=8)
BP (Systolic, mmHg) (Week 1)	104±1 (n=9)	104±1 (n=12)	106±1 (n=8)	104±1 (n=7)
BP (Systolic, mmHg) (Week 2)	106±1 (n=8)	104±1 (n=12)	104±3 (n=3)	104±1 (n=8)

* $p < 0.001$ vs control of the same genotype; Values are mean ± s.e. n: group size; BW: body weight at the time when AngII minipump was inserted; BP: blood pressure determined by tail cuff plethysmography in conscious and pre-warmed mice (Krege JH, Hodgin JB, Haganan JR, Smithies O: A noninvasive computerized tail-cuff system for measuring blood pressure in mice. Hypertension 1995;25:1111-1115); Baseline: BP measured before AngII infusion; Week 1 and Week 2: BP measured at week 1 and 2, respectively, after AngII infusion.

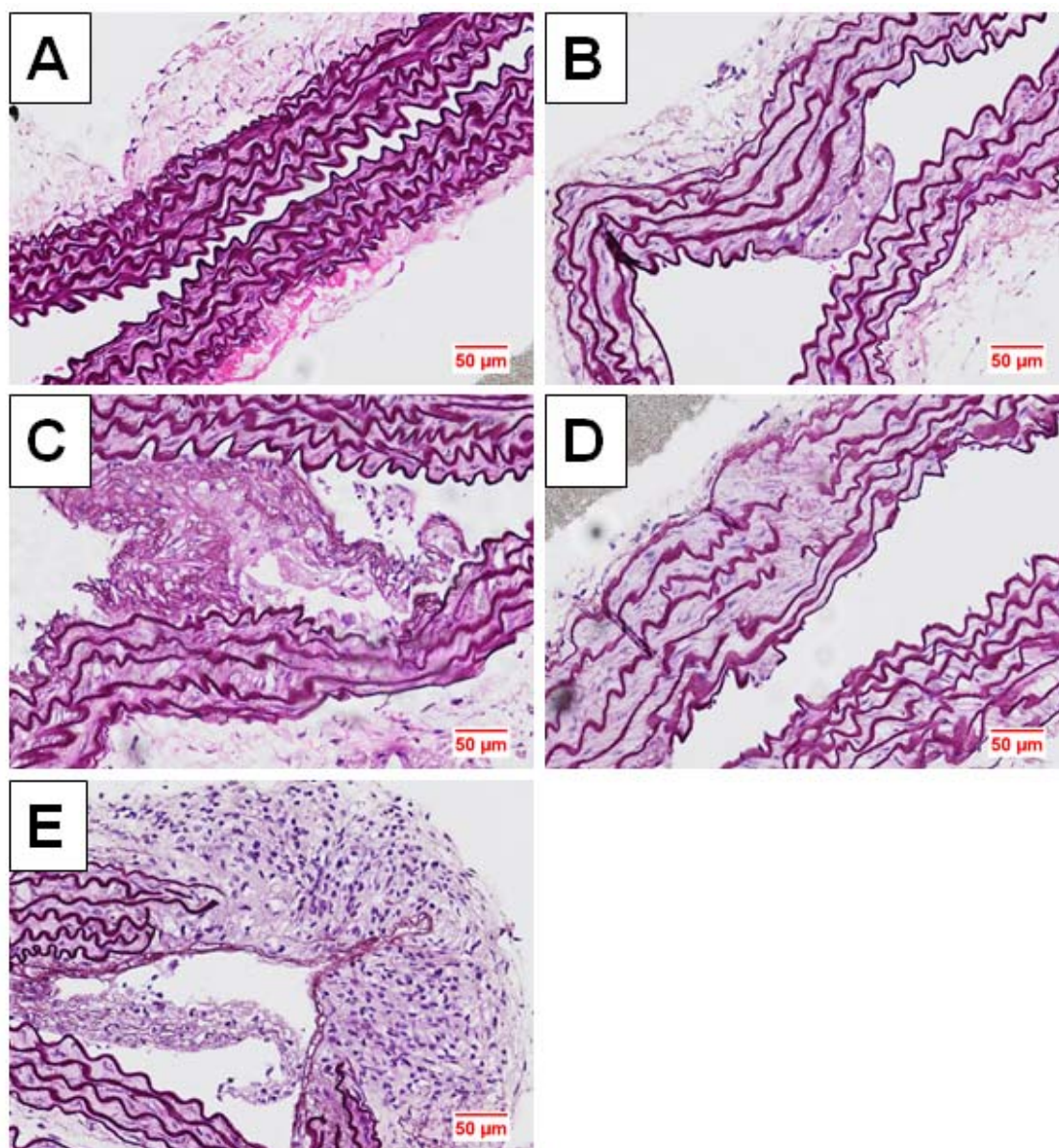
SUPPLEMENTARY DATA

Supplementary Table 4. Characteristics of subjects included in this study

Characteristic	AAA	Controls	P
Number	15	6	
Gender (M/F)	(12/3)	(4/2)	0.565
Aortic diameter (mm)	58.9±10.9	-	
Age (years)	70.7±6.4	42.7±12.5	<0.001
Peripheral arterial disease	0 (0%)	-	
Hypertension	10 (67%)-		
Diabetes mellitus	5 (33%)	-	
Dyslipidemia	11 (73%)-		
Coronary heart disease	9 (60%)	-	
Ever smoker	10 (67%)-		

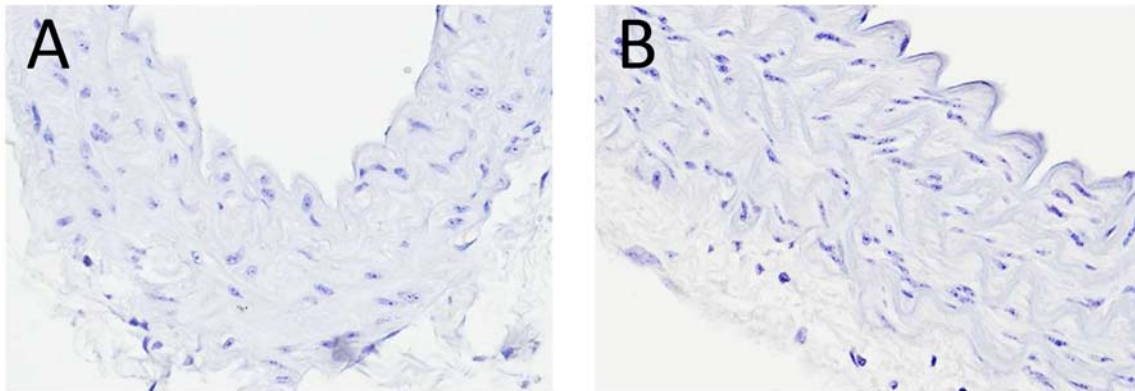
SUPPLEMENTARY DATA

Supplementary Figure 1. Representative images of aortic elastin lamella fragmentation with grading scores 0 (A), 1 (B), 2 (C), 3 (D) and 4 (E).

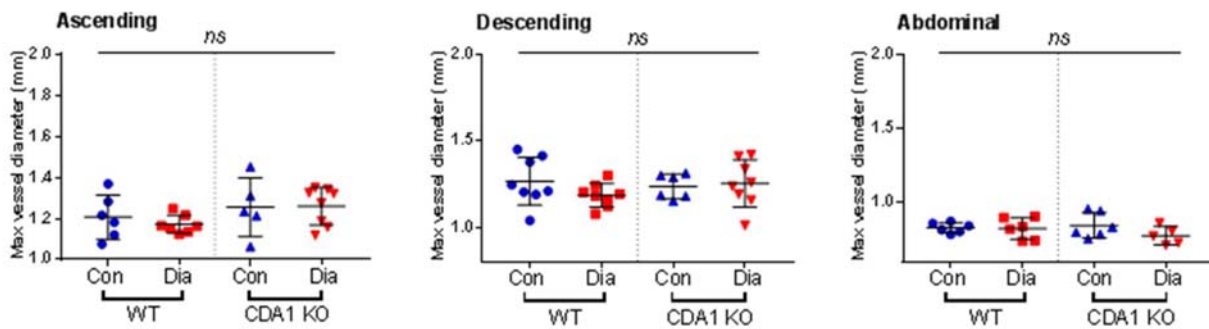


SUPPLEMENTARY DATA

Supplementary Figure 2. Negative control of immunohistochemical staining shows no background staining on mouse aorta sections. Representative pictures of immunohistochemical staining with either no primary antibody on a Non-diabetic (A) or with control rabbit IgG (1 $\mu\text{g}/\text{mL}$) on a diabetic (B) ApoE knockout mouse aorta section is shown.

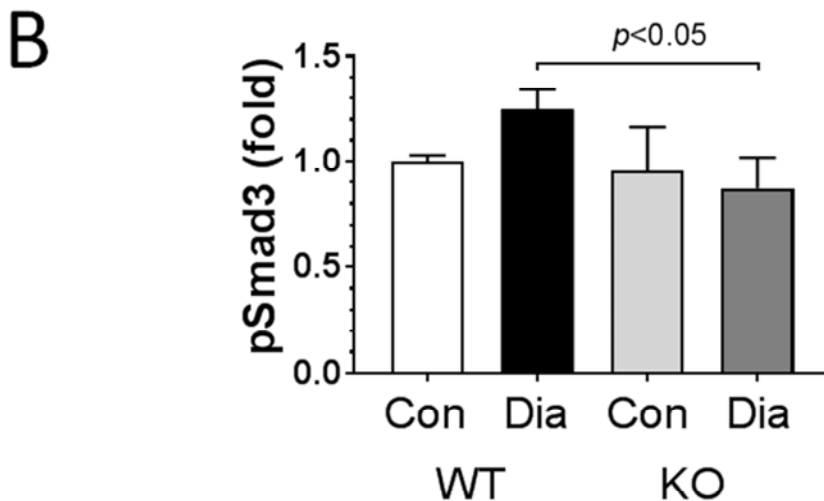
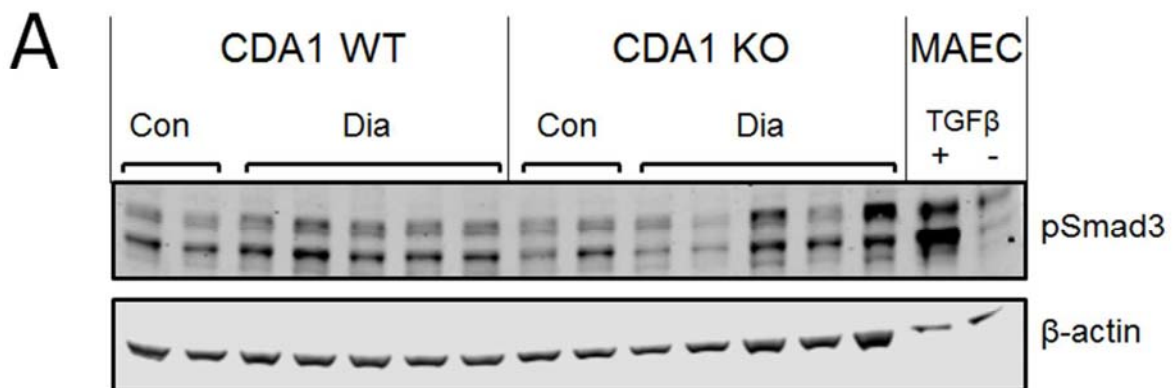


Supplementary Figure 3. Aortic size (diameter) of WT and CDA1 knockout mice are not changed with induced diabetes for 20 weeks. Ascending, descending and abdominal regions of aortas from control (Con) and diabetic (Dia) Wt and CDA1 knockout (KO) are shown as univariate scatter plots with mean \pm SD. There is no statistically significant difference among groups (*ns*) analyzed by ANOVA.



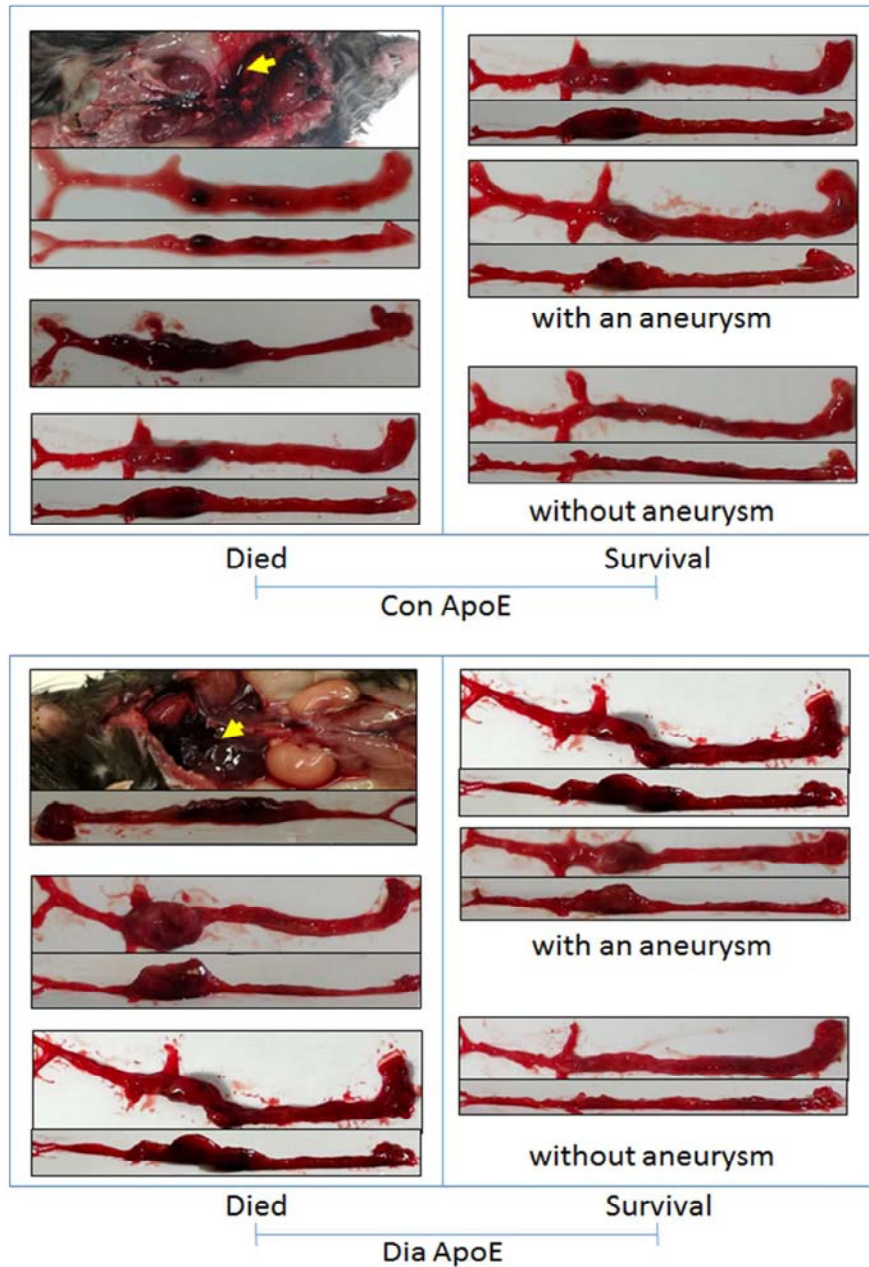
SUPPLEMENTARY DATA

Supplementary Figure 4. Aortic phospho-Smad3 expression levels are attenuated in diabetic CDA1 knockout mice. **A:** Aortas from 14-week streptozotocin induced diabetic (Dia) and age-matched non-diabetic control (Con) mice were homogenized for protein extraction. Estimated 20 $\mu\text{g}/\text{lane}$ protein was loaded for Western blotting. Phospho-Smad3 (pSmad3) was detected by anti-phospho-Smad3 antibody ($\text{S}^{423}/\text{S}^{425}$) (Abcam, Cat#: ab52903, 1:500 dilution). β -actin was re-probed and is shown as a loading control. Protein extracts ($5\mu\text{g}/\text{lane}$) from primary mouse aortic endothelial cells (passage 12-13) (MAEC) treated with TGF- β (2.5 ng/mL) for 30 min (+) and without TGF- β treatment (-) were used as positive and negative controls, respectively. **B:** The WB bands of aortic samples were quantified and pSmad3 level of each sample was normalized by β -actin. The pSmad3 levels (fold) relative to Con WT group (mean \pm SEM) are shown in a bar graph. Data were analyzed using one-way ANOVA with a least significant difference post hoc test for multiple comparisons of the means. A statistically significant difference between Dia WT and Dia KO groups is indicated by $P<0.05$ ($n=5$).



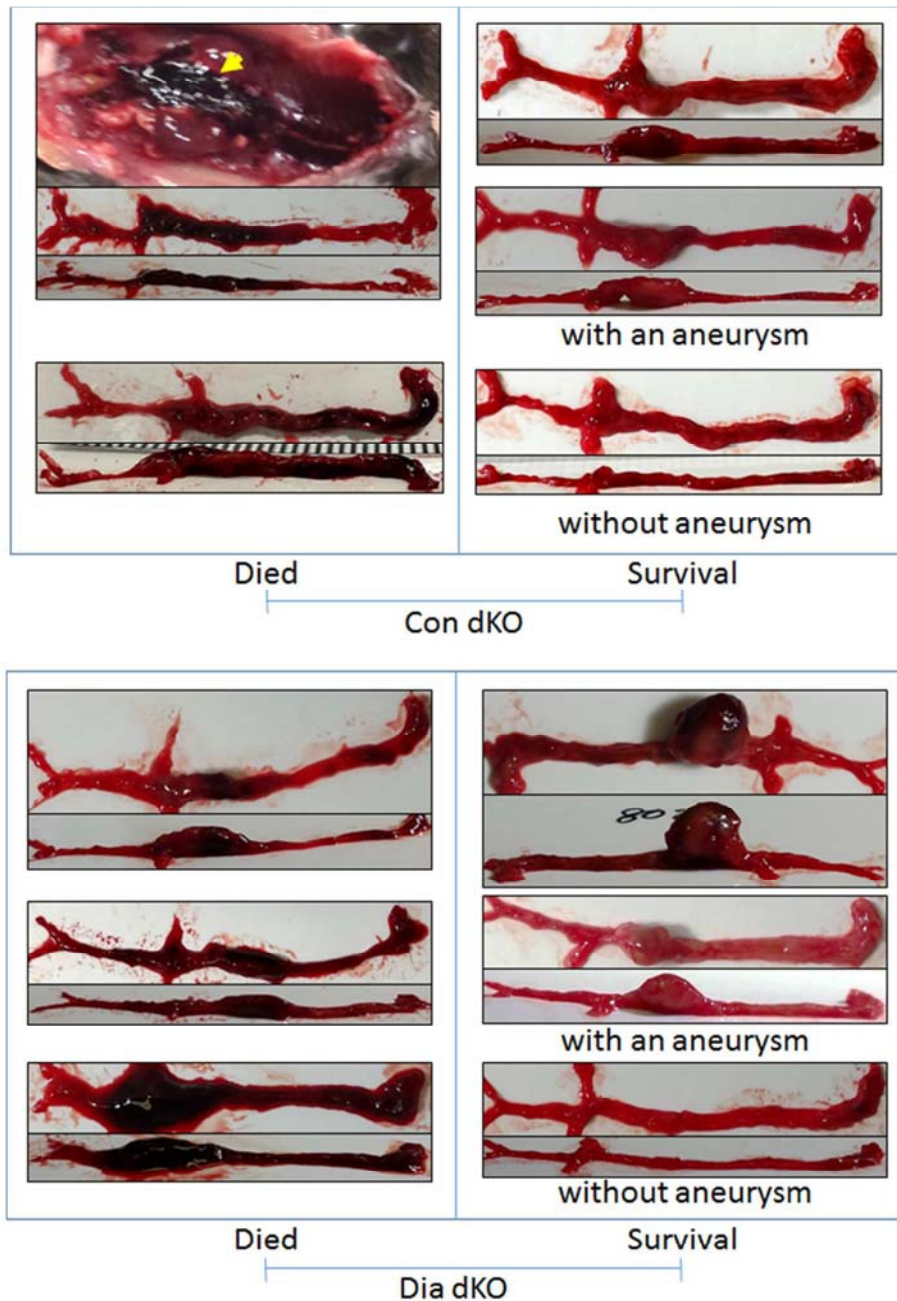
SUPPLEMENTARY DATA

Supplementary Figure 5. Top (upper) and side (lower) views of representative aortas isolated from ApoE KO mice are shown. All animals that received an AngII infusion via an Alzet minipump either died early (Died) or were killed at the endpoint of the 4-week infusion (Survival). Non-diabetic control (Con ApoE) and diabetic ApoE KO (Dia ApoE) mice that died from aortic aneurysm rupture, mostly at the suprarenal region of aorta, showed evidence of blood clot (yellow arrow) in the abdomen. Surviving animals either developed significant aneurysms (with an aneurysm) or did not develop aneurysms (without aneurysm)



SUPPLEMENTARY DATA

Supplementary Figure 6. Top (upper) and side (lower) views of representative aortas isolated from dKO mice are shown. All animals that received an AngII infusion via an Alzet minipump either died early (Died) or were killed at the endpoint of the 4-week infusion (Survival). Non-diabetic control (Con dKO) and diabetic (Dia dKO) dKO mice that died from aortic aneurysm/rupture, mostly at the suprarenal region of aorta, showed evidence of blood clot (yellow arrow) in the abdomen. Surviving animals either developed significant aneurysms (with an aneurysm) or did not develop aneurysms (without aneurysm).



SUPPLEMENTARY DATA

Supplementary Figure 7. Ultrasound images of the abdominal aorta from a mouse at baseline (Baseline) and 1 week after AngII infusion (Week 1). From the B-mode long-axis ultrasound image of the abdominal aorta (A, *upper panel*), the suprarenal region of aorta was selected (yellow dashed line) to generate a motion-mode (M-mode) image over time (*lower panel*). The aortic diameter was measured as the distance between the upper (anterior) and lower (posterior) aortic inner walls at the systolic phase (green arrows). Please note regional aortic dilation is evident after AngII infusion (See Diameter, week 1 vs baseline).

